MoDOT

Research, Development and Technology

FHWA/HNTB

RDT 05-004

Wind Induced Vibration of Stay Cables

Interim Final Report

RI 98-034

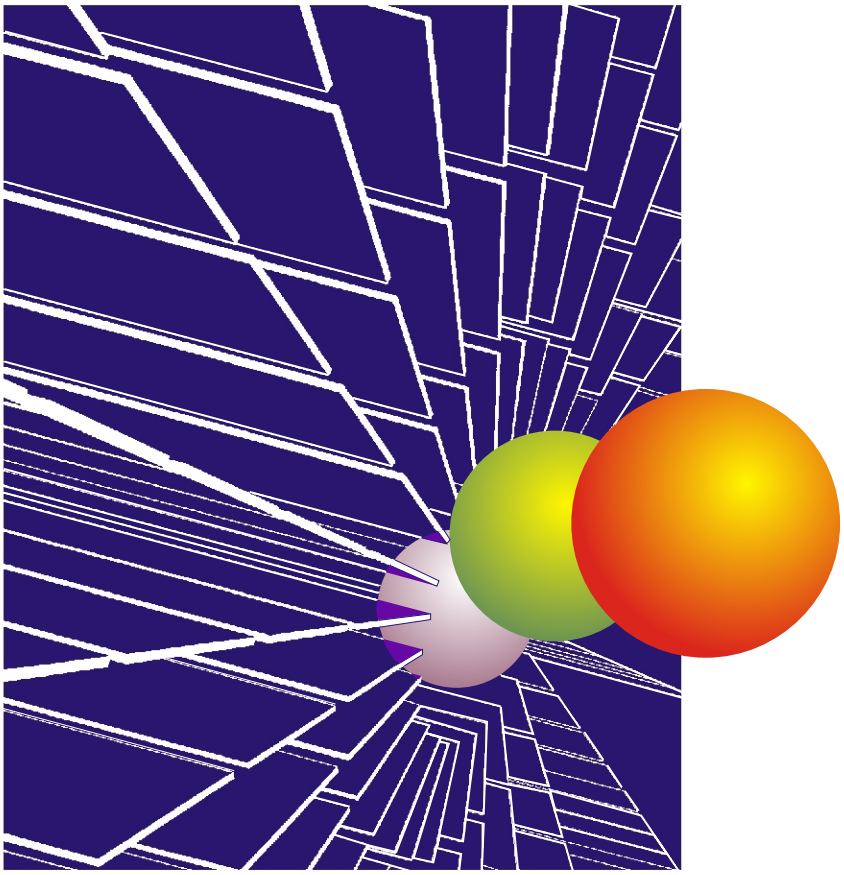

February, 2005

TECHNICAL REPORT DOCUMENTATION PAGE

1. Report No. **RI98-034 RDT05-004**	**2. Government Accession No.**	**3. Recipient's Catalog No.**
4. Title and Subtitle Wind Induced Vibration of Stay Cables		**5. Report Date** February 2005 **6. Performing Organization Code**
7. Author(s) Sena Kumarasena, Nicholas P. Jones, Peter Irwin, Peter Taylor		**8. Performing Organization Report No.**
9. Performing Organization Name and Address Primary Consultant: HNTB Corporation 75 State St., Boston MA 02109 In association with: John Hopkins University Dept. of Civil Engineering, Baltimore, MD 21218-2686 Rowan Williams Davies & Irwin, Inc. 650 Woodlawn Road West, Guelph, Ontario N1K 1B8 Buckland and Taylor, Ltd. Suite 101, 788 Harborside Drive, North Vancouver, BC V7P3R7		**10. Work Unit No.** **11. Contract or Grant No.** DTFH61-99-C-00095
12. Sponsoring Agency Name and Address Office of Infrastructure R&D Federal Highway Administration 6300 Georgetown Pike McLean, VA 22101-2296		**13. Type of Report and Period Covered** Interim Final Report **14. Sponsoring Agency Code**

15. Supplementary Notes
Contracting Officer's Technical Representative (COTR) – Harold Bosch. This interim final report is being printed by the Missouri Department of Transportation at the request of the Cable Stay Bridge Pooled Fund Technical Committee. FHWA will publish the final report.

16. Abstract Cable-stayed bridges have become the form of choice over the past several decades for bridges in the medium to long span range. In come cases serviceability problems involving large amplitude vibrations of stay cables under certain wind and rain conditions have been observed. This study was conducted in order to develop a set of consistent design guidelines for mitigation of excess cable vibration on cable-stay bridges.

In order to accomplish this objective the Project Team started with a thorough review of existing literature to determine the state of knowledge and identify any gaps that must be filled in order to enable the formation of a consistent set of design recommendations. This review indicated that while the rain/wind problem is known in sufficient detail, galloping of dry inclined cables was the most critical wind-induced vibration mechanism in need of further experimental research. A series of wind-tunnel tests was performed to study this mechanism. Analytical and experimental research was performed to study mitigation methods, covering a range of linear and non –linear dampers and cross-ties. The study also included brief studies on live load induced vibration and establishing driver/pedestrian comfort criteria.

Based on the above, design guidelines for mitigation of wind-induced vibrations of stay cables were developed.

17. Key Words Cable-stayed bridge, cables, vibrations, wind, rain, dampers, cross ties	**18. Distribution Statement** No restrictions. This document is available to the public through National Technical Information Center, Springfield, Virginia 22161

19. Security Classification (of this report) Unclassified	**20. Security Classification (of this page)** Unclassified	**21. No. of Pages** 260	**22. Price**

Form DOT F 1700.7 (06/98) Reproduction of completed pages authorized

SI* (MODERN METRIC) CONVERSION FACTORS

APPROXIMATE CONVERSIONS TO SI UNITS

Symbol	When You Know	Multiply By	To Find	Symbol
		LENGTH		
in	inches	25.4	millimeters	mm
ft	feet	0.305	meters	m
yd	yards	0.914	meters	m
mi	miles	1.61	kilometers	km
		AREA		
in^2	square inches	645.2	square millimeters	mm^2
ft^2	square feet	0.093	square meters	m^2
yd^2	square yard	0.836	square meters	m^2
ac	acres	0.405	hectares	ha
mi^2	square miles	2.59	square kilometers	km^2
		VOLUME		
fl oz	fluid ounces	29.57	milliliters	mL
gal	gallons	3.785	liters	L
ft^3	cubic feet	0.028	cubic meters	m^3
yd^3	cubic yards	0.765	cubic meters	m^3
NOTE: volumes greater than 1000 L shall be shown in m^3				
		MASS		
oz	ounces	28.35	grams	g
lb	pounds	0.454	kilograms	kg
T	short tons (2000 lb)	0.907	megagrams (or "metric ton")	Mg (or "t")
		TEMPERATURE (exact degrees)		
°F	Fahrenheit	5 (F-32)/9 or (F-32)/1.8	Celsius	°C
		ILLUMINATION		
fc	foot-candles	10.76	lux	lx
fl	foot-Lamberts	3.426	candela/m^2	cd/m^2
		FORCE and PRESSURE or STRESS		
lbf	poundforce	4.45	newtons	N
lbf/in^2	poundforce per square inch	6.89	kilopascals	kPa

APPROXIMATE CONVERSIONS FROM SI UNITS

Symbol	When You Know	Multiply By	To Find	Symbol
		LENGTH		
mm	millimeters	0.039	inches	in
m	meters	3.28	feet	ft
m	meters	1.09	yards	yd
km	kilometers	0.621	miles	mi
		AREA		
mm^2	square millimeters	0.0016	square inches	in^2
m^2	square meters	10.764	square feet	ft^2
m^2	square meters	1.195	square yards	yd^2
ha	hectares	2.47	acres	ac
km^2	square kilometers	0.386	square miles	mi^2
		VOLUME		
mL	milliliters	0.034	fluid ounces	fl oz
L	liters	0.264	gallons	gal
m^3	cubic meters	35.314	cubic feet	ft^3
m^3	cubic meters	1.307	cubic yards	yd^3
		MASS		
g	grams	0.035	ounces	oz
kg	kilograms	2.202	pounds	lb
Mg (or "t")	megagrams (or "metric ton")	1.103	short tons (2000 lb)	T
		TEMPERATURE (exact degrees)		
°C	Celsius	1.8C+32	Fahrenheit	°F
		ILLUMINATION		
lx	lux	0.0929	foot-candles	fc
cd/m^2	candela/m^2	0.2919	foot-Lamberts	fl
		FORCE and PRESSURE or STRESS		
N	newtons	0.225	poundforce	lbf
kPa	kilopascals	0.145	poundforce per square inch	lbf/in^2

*SI is the symbol for the International System of Units. Appropriate rounding should be made to comply with Section 4 of ASTM E380. (Revised March 2002)

TABLE OF CONTENTS

EXECUTIVE SUMMARY 1
1 INTRODUCTION 3
1.1 BACKGROUND 3
1.2 PROJECT OBJECTIVES AND TASKS 6

2 COMPILATION OF EXISTING INFORMATION 7
2.1 REFERENCE MATERIALS 7
2.2 INVENTORY OF U.S. CABLE-STAYED BRIDGES 7

3 ANALYSIS, EVALUATION, AND TESTING 9
3.1 MECHANICS OF WIND-INDUCED VIBRATIONS 9
3.2 WIND-TUNNEL TESTING OF DRY INCLINED CABLES 15
3.3 OTHER EXCITATION MECHANISMS 19
3.4 STUDY OF MITIGATION METHODS 22
3.5 FIELD MEASUREMENTS OF STAY CABLE DAMPING 35
3.6 BRIDGE USER TOLERANCE LIMITS ON STAY CABLE VIBRATION 40

4 DESIGN GUIDELINES 43
4.1 NEW CABLE-STAYED BRIDGES 43
4.2 RETROFIT OF EXISTING BRIDGES 46
4.3 WORKED EXAMPLE 47

5 RECOMMENDATIONS FOR FUTURE RESEARCH AND DEVELOPMENT 53

APPENDIX A: DATABASES

APPENDIX A1: DATABASE OF REFERENCE MATERIALS 59
APPENDIX A2: INVENTORY OF U.S. CABLE-STAYED BRIDGES 79

APPENDIX B: INCLINED CABLE AERODYNAMICS

APPENDIX B1: WIND-INDUCED CABLE VIBRATIONS 85
B1.1 MECHANICS OF WIND-INDUCED VIBRATIONS 85
B1.2 MITIGATING MEASURES 95

APPENDIX B2: WIND-TUNNEL TESTING OF STAY CABLES 99
EXECUTIVE SUMMARY 99
B2.1 INTRODUCTION.....100
B2.2 MODEL DESIGN 102
B2.3 WIND TUNNEL TESTS 105
B2.4 RESULTS AND DISCUSSION 116

APPENDIX C: RESEARCH ON MITIGATION METHODS

APPENDIX C1: LIST OF TECHNICAL PAPERS 151

APPENDIX C2: ANALYTICAL AND FIELD INVESTIGATIONS.....153
C2.1 OUTLINE OF RESEARCH AREAS 153
C2.2 ADDITION OF LINEAR AND NONLINEAR DAMPERS.....153
C2.3 CROSS TYING OF STAY CABLES.....169
C2.4 DAMPERS IN COMBINATION WITH CROSS-TIES 179
C2.5 FIELD ASSESSMENT OF DAMPER AND CROSS-TIE PERFORMANCE.....184
C2.6 DETAILED STUDY OF DAMPER PERFORMANCE 193

APPENDIX D: ADDITIONAL STUDIES

APPENDIX D1: INTRODUCTION TO MECHANICS OF INCLINED CABLES 207
D1.1 STAY CABLE STATIC PROPERTIES.....207
D1.2 STAY CABLE DYNAMIC PROPERTIES 211

APPENDIX D2: LIVE LOAD INDUCED VIBRATION STUDY 217
D2.1 INTRODUCTION 217
D2.2 FREE VIBRATION ANALYSIS 219
D2.3 STATIC LIVE LOAD ANALYSIS.....231
D2.4 DYNAMIC LIVE LOAD ANALYSIS.....235
D2.5 CONCLUSIONS.....247

APPENDIX D3: STUDY OF USER COMFORT 249

REFERENCES 253

LIST OF FIGURES

Figure Page

Figure 1: Comparison of wind velocity-damping relation of inclined dry cable.....18
Figure 2: Cable M26, Tension vs. Time. Transit train speed 50 mph (80km/hr). 19
Figure 3: Time history and power spectral density (PSD) of the first 2-Hz for deck at mid-span (vertical direction).....20
Figure 4: Time history and power spectral density (PSD) of the first 2-Hz for cable at AS24 (in-plane direction) deck level wind speed.. 20
Figure 5: Deck level wind speed.....21
Figure 6: Damper at cable anchorage. 22
Figure 7: Taut cable with a linear damper. 23
Figure 8: Normalized Damping Ratio versus Normalized Damper Coefficient: Linear Damper. 24
Figure 9: Normalized Damping Ratio versus Normalized Damper Coefficient: β=0.5 24
Figure 10: Fred Hartman Bridge.....25
Figure 11: Cable cross-tie systems. 27
Figure 12: Dames Point Bridge.....28
Figure 13: General problem formulation. 29
Figure 14: General problem formulation (original configuration). 29
Figure 15: Eigenfunctions of the network equivalent to Fred Hartman Bridge; modes 1 and 5. 30
Figure 16: Comparative analysis of network vibration characteristics and individual-cable behavior; Fred Hartman Bridge. 31
Figure 17: Fred Hartman Bridge, field performance testing arrangement.....32
Figure 18: Types of cable surface treatments. 34
Figure 19: Example of test data for spiral bead cable surface treatment. 34
Figure 20: Leonard P. Zakim Bunker Hill Bridge 35
Figure 21: Sample decay: No damping and no cross-ties.....36
Figure 22: Sample decay: With damping and no cross-ties.....37
Figure 23: Sample decay: With damping and cross-ties.....37
Figure 24: Sunshine Skyway Bridge.....38
Figure 25: Stay and damper brace configuration 38
Figure 26: Reference database search page. 59
Figure 27: Reference database search results page.....60
Figure 28: U.S. cable-stayed bridge database - Switchboard. 80
Figure 29: U.S. cable-stayed bridge database - General bridge information.....81
Figure 30: U.S. cable-stayed bridge database - Cable data.....82
Figure 31: U.S. cable-stayed bridge database - Wind data. 83
Figure 32: Galloping of inclined cables.....90
Figure 33: Aerodynamic devices. 92
Figure 34: Cable cross-ties.....96
Figure 35: Viscous damping 97
Figure 36: Material damping. 97
Figure 37: Angle relationships between stay cables and natural wind 102

Figure Page

Figure 38: Cable supporting rig. 103
Figure 39: Longitudinal section of the "Propulsion" wind tunnel. 105
Figure 40: Cross-section of the working section of "Propulsion" wind tunnel. 106
Figure 41: Data acquisition system. 107
Figure 42: Airpot damper. 109
Figure 43: Cross-section of airpot damper. 109
Figure 44: Elastic bands on the spring coils 110
Figure 45: Side view of Setups 1B and 1C. 112
Figure 46: Side view of Setups 2A and 2C. 113
Figure 47: Side view of Setups 3A and 3C. 114
Figure 48: Cable set up in wind tunnel for testing. 115
Figure 49: Amplitude-dependent damping with Setup 2C (smooth surface, low damping). 122
Figure 50: Divergent Response of Inclined Dry Cable
(Setup 2C, smooth surface, low damping). 123
Figure 51a: Lower end X-motion, time history of Setup 2C at U=32 m/s. 123
Figure 51b: Top end X-motion, time history of Setup 2C at U=32 m/s. 124
Figure 51c: Lower end Y-motion, time history of Setup 2C at U=32 m/s. 124
Figure 51d: Top end Y-motion, time history of Setup 2C at U=32 m/s. 125
Figure 52: Trajectory of Setup 2C at U=32 m/s. 125
Figure 53a: Lower end X-motion, time history of Setup 2A at U=18 m/s
in the first 5 minutes. 126
Figure 53b: Top end X-motion, time history of Setup 2A at U=18 m/s
in the first 5 minutes. 126
Figure 53c: Lower end Y-motion, time history of Setup 2A at U=18 m/s
in the first 5 minutes. 127
Figure 53d: Top end Y-motion, time history of Setup 2A at U=18 m/s
in the first 5 minutes. 127
Figure 54a: Lower end X-motion, time history of Setup 2A at U=18 m/s
in second 5 minutes. 128
Figure 54b: Top end X-motion, time history of Setup 2A at U=18 m/s
in second 5 minutes. 128
Figure 54c: Lower end Y-motion, time history of Setup 2A at U=18 m/s
in second 5 minutes. 129
Figure 54d: Top end Y-motion, time history of Setup 2A at U=18 m/s
in second 5 minutes. 129
Figure 55a: Lower end X-motion, time history of Setup 2A at U=19 m/s. 130
Figure 55b: Top end X-motion, time history of Setup 2A at U=19 m/s. 130
Figure 55c: Lower end Y-motion, time history of Setup 2A at U=19 m/s. 131
Figure 55d: Top end Y-motion, time history of Setup 2A at U=19 m/s. 131
Figure 56a: Lower end X-motion, time history of Setup 1B at U=24 m/s. 132
Figure 56b: Top end X-motion, time history of Setup 1B at U=24 m/s. 132
Figure 56c: Lower end Y-motion, time history of Setup 1B at U=24 m/s. 133
Figure 56d: Top end Y-motion, time history of Setup 1B at U=24 m/s. 133

Figure Page

Figure 57a: Lower end X-motion, time history of Setup 1C at U=36 m/s. 134
Figure 57b: Top end X-motion, time history of Setup 1C at U=36 m/s. 134
Figure 57c: Lower end Y-motion, time history of Setup 1C at U=36 m/s. 135
Figure 57d: Top end Y-motion, time history of Setup 1C at U=36 m/s. 135
Figure 58a: Lower end X-motion, time history of Setup 3A at U=22 m/s. 136
Figure 58b: Top end X-motion, time history of Setup 3A at U=22 m/s. 136
Figure 58c: Lower end Y-motion, time history of Setup 3A at U=22 m/s. 137
Figure 58d: Top end Y-motion, time history of Setup 3A at U=22 m/s. 137
Figure 59a: Trajectory of Setup 2A at U=18 m/s, first 5 minutes. 138
Figure 59b: Trajectory of Setup 2A at U=18 m/s, second 5 minutes. 138
Figure 59c: Trajectory of Setup 2A at U=19 m/s. 139
Figure 60: Trajectory of Setup 1B at U=24 m/s. 140
Figure 61: Trajectory of Setup 1C at U=36 m/s. 140
Figure 62: Trajectory of Setup 3A at U=22 m/s 141
Figure 63: Wind-induced response of inclined dry cable (Setup 2A) 142
Figure 64: Wind-induced response of inclined dry cable (Setup 1B).....142
Figure 65: Wind-induced response of inclined dry cable (Setup 1C).....143
Figure 66: Wind-induced response of inclined dry cable (Setup 3A) 143
Figure 67: Wind-induced response of inclined dry cable (Setup 3B).....144
Figure 68: Critical Reynolds number of circular cylinder (from Scruton, 1981) 144
Figure 69: Damping trace of four different levels of damping (Setup 1B) 145
Figure 70: Effect of structural damping on the wind response of inclined cable (Setup 1B).....145
Figure 71: Surface roughness effect on wind-induced response
of dry inclined cable (Setup 3A).....146
Figure 72: Surface roughness effect on wind-induced response
of dry inclined cable (Setup 1B) 146
Figure 73: Surface roughness effect on wind-induced response
of dry inclined cable (Setup 2A). 147
Figure 74a: Amplitude-dependent damping in the X-direction with Set-up 2A. 148
Figure 74b: Amplitude-dependent damping in the Y-direction with Set-up 2A. 148
Figure 75a: Wind-induced response of inclined cable in the X-direction with Set-up 2A.....149
Figure 75b: Wind-induced response of inclined cable in the Y-direction with Set-up 2A.....149
Figure 76: Comparison of wind velocity-damping relation of inclined dry cable.....150
Figure 77: Taut cable with linear damper. 155
Figure 78: Normalized Damping Ratio versus Normalized Damper Coefficient.....157
Figure 79a: Cable with Attached Friction/Viscous Damper.....159
Figure 79b: Force-Velocity Curve for Friction/Viscous Damper.....159
Figure 80a: Normalized Damping Ratio vs. "Clamping Ratio". 160
Figure 80b: Normalized Viscous Damper Coefficient vs. "Clamping Ratio".....160
Figure 81: Relationship between Nondimensional Parameters μ and κ with
Different Values of the Clamping Ratio Θ_{ci} for a Friction/Viscous Damper. 163
Figure 82: Normalized Damping Ratio vs. κ with varying μ.....164
Figure 83: Normalized Damping Ratio versus Normalized Damper Coefficient: β=0.5. 166

Figure Page

Figure 84a: Normalized Damping Ratio versus Mode Ratio (β=1).....167
Figure 84b: Normalized Damping Ratio versus Amplitude Ratio (β=0.5).....167
Figure 84c: Normalized Damping Ratio versus Mode-Amplitude Ratio (β=0). 167
Figure 85: General problem formulation. 170
Figure 86: General problem formulation (original configuration). 173
Figure 87: Eigenfunctions of the network equivalent to Fred Hartman Bridge; 1st – 8th modes. 175
Figure 88: Comparative analysis of network vibration characteristics and individual-cable behavior; Fred Hartman Bridge. 176
Figure 89: Generalized cable network configuration.....179
Figure 90: Twin cable with variable position connector. 181
Figure 91a: Twin cable system, with connector location ξ = 0.35, example of frequency solution for linear spring model.....182
Figure 91b: Typical solution curves of the complex frequency for the dash-pot. 182
Figure 91c: Intermediate segments of specific cables only. 182
Figure 92a: Fred Hartman Bridge ("A-line") 3D network.....182
Figure 92b: Equivalent model.....182
Figure 93a: Frequency solutions (1st mode) for the damped cable network ("A"-line). 183
Figure 93b: Complex modal form (1st mode) for the optimized system "M1[uo]".....183
Figure 94: Damping vs. mode number for Hartman stays A16 and A23 185
Figure 95: Stay vibration and damper force characteristics; Stay A16. 188
Figure 96: Stay vibration and damper force characteristics; Stay A23. 189
Figure 97: In-plane vs. lateral RMS displacement for AS16 and AS23.....194
Figure 98: Sample Lissajous plots of displacement for two records from AS16. 195
Figure 99: Power spectral density of displacement of two records from AS16 195
Figure 100: Sample Lissajous plots of displacement for two records from AS23 196
Figure 101: Power spectral density of displacement of two records from AS23 196
Figure 102: In-plane vs. lateral RMS displacement for AS16 and AS23 after damper installation.....197
Figure 103: Lissajous and power spectral density plots of displacement for record A. 198
Figure 104: Modal frequencies of stay AS16 and AS23 199
Figure 105: Second-mode frequency vs. RMS displacement for stay AS16.....200
Figure 106: Estimated modal damping of Stay AS16 showing effect of damper. 201
Figure 107: Histogram of estimated damping for mode 2 of AS16 and mode 3 of AS23. 201
Figure 108: Dependence of modal damping on damper force.....202
Figure 109: RMS damper force vs. RMS displacements for AS16 and AS23.....203
Figure 110: Damper force vs. displacement and velocity for a segment of a sample record. 204
Figure 111: Displacement and damper force time histories of a sample record.....205
Figure 112: Incline stay cable properties.....207
Figure 113: Definition diagram for a horizontal cable (taut string), compared to the definition diagram for an inclined cable. 211
Figure 114: Cable $\sqrt{\ /\ }$ vs. Cable Unstressed Length, summary of Alex Fraser, Maysville, and Owensboro Bridges.....215

Figure Page

Figure 115: Cable Frequency vs Cable Unstressed Length, Summary of Alex Fraser, Maysville, and Owensboro Bridges. 216
Figure 116: RAMA 8 Bridge - Artistic Rendering. 217
Figure 117: RAMA 8 Bridge computer model; XY, YZ & ZX views. 218
Figure 118: Independent Cable M26 discretization-10 segment model- XZ view. 220
Figure 119: Cable catenary. 221
Figure 120: Cable modes; XZ, YZ, and XY views. 222
Figure 121: Inextensible cable mode 1 - In-plane; XY, YX & XZ views. 224
Figure 122: Cable M26 discretization - 10-segment model. View: Isometric. Only cables M26 are shown. Other cables not shown for clarity. 225
Figure 123: Cable M26 discretization - 10-segment model -XZ view. Other cables not shown for clarity. 225
Figure 124: Fundamental bridge modes. 227
Figure 125: Additional bridge modes. 228
Figure 126: Four 'first' modes of the cables; XY, YZ & XZ views. 229
Figure 127: Four ‘second' modes of the cables; XY, YZ & XZ views. 229
Figure 128: Four ‘third’ modes of the cables; XY, YZ & XZ views. 230
Figure 129: Nodes, members, and cables for comparison of results. 231
Figure 130: RAMA 8 Bridge Model Damping vs. Frequency. 235
Figure 131: Vertical Displacements, Velocities, and Accelerations of Node 427 vs. Time. Train speed 80 km/h. 237
Figure 132: Member 1211; Bending Moment vs. Time. Train speed 80km/h. 238
Figure 133: Cable M26, Tension vs. Time. Train speed 80 km/hr. 238
Figure 134: Difference in cable tension for cable M26 between the dynamic train load case and static train load case vs. Time. Train speed 80 km/h. 239
Figure 135: Cable M26 Tension Spectra. Train speed 80 km/h. 239
Figure 136: Global Coordinate Displacements of Cable M26 Nodes [mm] vs. Time. Train speed 80 km/hr. 241
Figure 137: Transformation from global coordinates to coordinates along the cable 242
Figure 138: Local Coordinate Displacements of nodes of cable M26 [mm]. Displacements are shown for 3 nodes of the cable: at 1/4 span (closer to the tower), 1/2 span and 3/4 span (closer to the deck). Train speed 80 km/h. 243
Figure 139: Spectra for movements of cable M26 nodes: at ¼ span (closer to the tower), ½ span, and ¾ span (closer to the deck). Frequency range 0 – 2 Hz, train speed 80 km/h. 244
Figure 140: Deck rotations and cable end rotations for cable M26 -dynamic (train speed 80 km/h) and static 246
Figure 141: Deck rotations and cable end rotations for cable M21 -dynamic (train speed 80 km/h) and static 246
Figure 142: Effect of mode (constant amplitude and velocity). 250
Figure 143: Effect of velocity (constant amplitude). 250
Figure 144: Effect of amplitude (constant velocity). 251

LIST OF TABLES

Table Page

Table 1: Dry inclined cable testing - Model setup. 16
Table 2: Dry inclined cable testing - Damping levels....16
Table 3: Dry inclined cable testing - Surface condition 16
Table 4: Stay and damper properties 26
Table 5: Cable network modes (0-4 Hz) predicted by the model. 32
Table 6: Preliminary cable damping measurements - Leonard P. Zakim Bunker Hill Bridge 36
Table 7: Preliminary cable damping measurements from the Sunshine Skyway Bridge 39
Table 8: Cable stayed bridge inventory. 79
Table 9: Bridges reporting cable vibration and mitigating measures. 98
Table 10: Model setup. 111
Table 11: Different damping levels of the model. 111
Table 12: Surface condition. 111
Table 13: Limited-amplitude motion. 117
Table 10: Geometrical and structural characteristics of the Fred Hartman system. 173
Table 11: Individual cable frequencies (0-4 Hz) of the A-line side span stays of the Fred Hartman Bridge (direct measurement). 191
Table 12: Cable network modes (0-4 Hz) predicted by the model (A-line system). 191
Table 13: Stay cable property comparison. 215
Table 14: Free independent extensible cable vibration vs. theoretical inextensible. 221
Table 15: Free independent inextensible cable vibration periods – theoretical values and values obtained by analysis. 223
Table 16: Cable vibration period and frequencies – Theoretical values and values obtained by analysis. 226
Table 17: Vertical displacements due to live load. 232
Table 18: Bending moments due to live load. 232
Table 19: Cable forces due to live load. 233
Table 20: Cable end rotations and deck rotations. 234

EXECUTIVE SUMMARY

Cable-stayed bridges have become the structural form of choice for medium to long span bridges over the past several decades. With their increasingly widespread use, some cases of serviceability problems with large amplitude vibrations of stay cables due to environmental conditions have surfaced. A significant correlation had been observed between the occurrence of these large amplitude vibrations and occurrences of rain combined with wind, leading to the adoption of the term "rain/wind vibrations." However, a few instances of large amplitude vibrations have also been reported (in the literature) without rain.

In 1999, the Federal Highway Administration (FHWA) commissioned a study team led by HNTB Corporation and three subconsultants, Johns Hopkins University, Rowan Williams Davies & Irwin, Inc. (RWDI), and Buckland and Taylor, Ltd. to investigate wind-induced vibration of stay cables. The Project Team represented expertise in cable-stayed bridge design, academia, and wind engineering.

By this time, a substantial amount of research on this subject had already been conducted by researchers and cable suppliers in the U.S. and abroad. This work has firmly established the water rivulet formation and its interaction with the wind flow as the root cause of the rain/wind vibrations. With this understanding, various surface modifications had been proposed and tested with the aim of disrupting this water rivulet formation. Recently developed mitigation measures such as "double helix" surface modifications as well as traditional measures such as external dampers and cable cross-ties have been provided to many of the newer bridges. However, the lack of a uniform criteria or a consensus in some of the other key areas such as large amplitude galloping of dry cables has made the practical and consistent application of the known mitigation methods difficult.

The objective of this FHWA sponsored study was to develop a set of uniform design guidelines for vibration mitigation for stay cables on cable-stayed bridges. The project was subdivided into the following distinct tasks:

- Task A: Develop electronic database of reference materials
- Task B: Develop electronic database of inventory of U.S. cable-stayed bridges
- Task C: Analysis, evaluation and testing
- Task D: Assessment of mitigation
- Task F: Project documentation

The initial phase of the study consisted of a collection of available literature on stay cable vibration. Due to the large volume of existing literature, the information was entered into two electronic databases. These databases were developed to be user friendly, have search capabilities, and also facilitate entering of new information as it becomes available. The databases have been turned over to FHWA for future maintenance. It is expected that these will be deployed over the internet for use by the engineering community.

The Project Team conducted a thorough review of the existing literature to determine the state of knowledge and identify any gaps that must be filled to enable the formation of a consistent set of design recommendations. This review indicated that while the rain/wind problem is known in sufficient detail, galloping of dry inclined cables was the most critical wind-induced vibration

mechanism in need of further experimental research. A series of wind-tunnel tests was conducted at the University of Ottawa propulsion wind tunnel to study this mechanism. This tunnel had a test section 10-ft (3-m) wide, 20-ft (6-m) high, and 39-ft (12-m) long, and could reach 87-mph (39-m/s) maximum wind speed. With a removable roof section, this tunnel was ideal for the high speed galloping tests of inclined full-scale cable segments.

The results of the Project Team's dry inclined cable testing have significant implications for the design criteria of cable-stayed bridges. The 2001 PTI Recommendations for Stay Cable Design, Testing, and Installation indicates that the level of damping required for each cable is controlled by the inclined galloping provision, which is more stringent than the provision to suppress rain/wind vibrations. This testing, however, suggests that if even a low amount of structural damping is provided to the cable system, inclined cable galloping vibrations are not significant. This damping corresponds to a Scruton number of 3, which is less than the minimum of 10 established for suppression of rain/wind vibrations. Therefore if enough damping is provided to mitigate rain/wind vibrations, then dry cable instability should also be suppressed.

The Project Team obtained matching funds from Canada's National Engineering and Sciences Research Council (NSERC) for the testing at the University of Ottawa, effectively doubling the FHWA's funding for the wind tunnel testing task. The Project Team also supplemented the study by incorporating work of its key team members on other ongoing, related projects at no cost to the FHWA.

Analytical research was also performed covering a wide spectrum of related issues, such as the behavior of linear and nonlinear dampers and cable cross-ties. The research also included brief studies on parametric excitation and establishing driver/pedestrian comfort criteria with respect to stay cable oscillation.

Based on the above, design guidelines for mitigation of wind-induced vibrations of stay cables were developed. These are presented with two worked examples that illustrate their application. It must be noted that this is the first time such design guidelines have been proposed. They are meant to provide a level of satisfactory performance for stay cables with respect to recurring large amplitude stay oscillations due to common causes that have been identified to date, and are not intended to eliminate stay cable oscillations altogether (as this would be impractical).

It is expected that these guidelines can be suitably refined based on future observations on actual performance of stay cables in bridges around the world as well as developments in stay-cable technology. With the widespread recognition of the mitigation of stay cable vibration as an important design issue among long-span bridge designers, all new cable-stayed bridges are more than likely to incorporate some form of mitigation discussed in this document. This would provide ample future opportunity to measure real life performance of bridges against the design guidelines contained herein.

As a precautionary note, the state of the art in mitigation of stay cable vibration is not an exact science. These new guidelines are only intended for use by professionals with experience in cable-stayed bridge design, analysis, and wind engineering, and should only be applied with engineering judgement and due consideration of special conditions surrounding each project.

1 INTRODUCTION

1.1 BACKGROUND

Cable-stayed bridges are a relatively new structural form made feasible with the combination of advances in manufacturing of materials, construction technology, and analytical capabilities that took place largely within the last few decades.

The first modern cable-stayed bridge was the Stromsund Bridge built in the 1950's in Sweden with a main span of 600-ft (183-m) and two symmetrical back spans of 245-ft (75-m) each. It had only two cables on each side of the tower, anchored to steel I edge girders.

Today, cable-stayed bridges have firmly established their unrivalled position as the most efficient and cost effective structural form in the 500-ft (150-m) to 1500-ft (460-m) span range. The cost efficiency and the general satisfaction with their aesthetic aspects has propelled this span range in either direction, with both increasingly shorter and increasingly longer spans being designed and constructed at the present time. The record span built to date is the Tatara Bridge connecting the islands of Honshu and Shikoku in Japan, with its 2920-ft (890-m) long main span. The planned Stonecutters Bridge in Hong Kong has a 3280-ft (1000-m) long main span. The early engineering approach to the stay cables was essentially derived and hybridized from the already established engineering experience with suspension cables and post-tensioning technology.

The stay cables are laterally flexible structural members with very low fundamental frequency (first natural mode). Due to the range of different cable lengths (thus the range of frequencies) the collection of stay cables on a cable stayed bridge has practically a continuum of fundamental and higher mode frequencies. Thus, any excitation mechanism with any arbitrary frequency is likely to find one or more cables with either a fundamental or higher mode frequency sympathetic to the excitation. Cables also have very little inherent damping and are therefore not able to dissipate much of the excitation energy, making them susceptible to large amplitude build-up. For this reason, the stay cables can be somewhat lively by nature and have been known to be susceptible to excitations, especially during construction, wind, and rain/wind conditions.

Recognition of this susceptibility of stay cables has led to the incorporation of some mitigation measures on several of the earlier structures. These included cable cross-ties that effectively reduce the free length of cables (increasing their frequency) and external dampers that increase cable damping. Perhaps due to the lack of widespread recognition of the stay cable issues by the engineering community and the supplier organizations, the application of these mitigation measures on early bridges appear to have been fairly sporadic. However, those incorporating cable cross-ties or external dampers have generally performed well.

Field observation programs have provided the basis for characterization of stay cable vibrations and the environmental factors that induce them (Wianecki, 1979; Hikami & Shiraishi, 1988; Matsumoto et al. 1997). Peak-to-peak amplitudes up to 6 ft (2 m) have been reported, with typical values of around 2 ft (60 cm). Vibrations have been observed primarily in the lower cable modes, with frequencies ranging approximately from 1 to 3 Hz. Early reports described the

vibrations simply as transverse in the vertical plane, but detailed observations suggest a more complicated elliptical loci.

High-amplitude vibrations have been observed over a limited range of wind speeds. At several bridges in Japan the observed vibrations were restricted to a wind velocity range from 13 mph to 38 mph (6 to 17 m/s) (Matsumoto et al., 1993). More recent field measurements revealed large-amplitude vibrations at around 90 mph (40 m/s). The wind speed did not reach values sufficiently high to determine whether these vibrations were also velocity-restricted (Matsumoto et al., 1997).

The stays of the Brotonne Bridge in France were observed to vibrate only when the wind direction was 20°-30° relative to the bridge longitudinal axis (Wianecki, 1979). On the Meiko-Nishi Bridge in Japan, vibrations were observed with wind direction greater than 45° from the deck only on cables that declined in the direction of the wind (Hikami & Shiraishi, 1988). However, instances have also been reported subsequently of simultaneous vibration of stays with opposite inclinations to the wind (Matsumoto et al., 1990).

From field observations it became evident that these large oscillation episodes occurred under moderate rain combined with moderate wind conditions, and hence were referred to as "rain/wind vibrations" (Hikami & Shiraishi, 1988). Extensive research studies at many leading institutions over the world have undoubtedly confirmed the occurrence of rain/wind induced vibrations. Totally unknown prior to its manifestation on cable-stayed bridges, the mechanisms leading to rain/wind vibrations have been identified. The formation of a so-called water rivulet along the upper side of the cable under moderate rain conditions and its interaction with wind flow have been solidly established as the cause through many recent studies and wind-tunnel tests (Hikami & Shiraishi, 1988; Matsumoto et al., 1992; Flamand, 1994; Verwiebe & Ruscheweyh, 1997).

Based on this understanding, exterior cable surface modifications that interfere with the water rivulet formation have been tried and proven to be very effective in the mitigation of the rain/wind vibrations. Particularly popular (and shown to be effective through experimental studies) are the double spiral bead formations affixed to the outer surface of the cable pipes (Flamand, 1994). Cable exterior pipes with such surface modifications are available with all major cable suppliers with test data applicable to the particular system. This type of spiral bead surface modification has been applied on many cable-stayed bridges both with and without other mitigation measures such as external dampers and cable ties. From the observations available to date, the bridges incorporating stay-cables with effective surface modifications appear to be generally free of rain/wind vibrations.

At the time of the present investigation, it was evident that the rain/wind problem had been essentially solved, at least for practical provisions for its mitigation. The Scruton number, identified later in the report, is generally accepted as the key parameter describing susceptibility of a given cable to rain/wind vibrations. Raising the Scruton number by increasing damping or, alternatively, use of cable cross-ties has been recognized as the standard solution for the mitigation of rain/wind vibrations. Generally these are applied in combination with a proven surface modification.

However, no such clarity existed with respect to other potential sources of cable vibration. High speed galloping of inclined cables (discussed later) was the single most issue that limited the designer's options. The only effective method available for satisfying the existed criterion on galloping was to raise the natural frequency of cables through the use of cable cross-ties. However, the inclined dry cable galloping criteria being used was postulated on such a limited set of data that its application was frequently brought into question.

Thus, to meet the project objective of formulating design guidelines, some further experimental and analytical work was needed to supplement the existing knowledge base on stay cable vibration issues.

1.2 PROJECT OBJECTIVES AND TASKS

The charter of the Project Team, established early in the development of the program, consisted of the following objectives with regards to "Wind Induced Vibration of Stay Cables":

- Identify gaps in current knowledge base
- Conduct analytical and experimental research in critical areas
- Study performance of existing cable-stayed bridges
- Study current mitigation methods
- Develop procedures for aerodynamic performance assessment
- Develop design and retrofit guidelines for stay cable vibration mitigation

Overall project goals were translated into a series of Tasks A through F:

Task A: Synthesize Available Information

Reference Database (Appendix A1, Section 2.1)
Descriptions of Wind-Induced Cable Vibrations (Appendix B1, Section 3.1)

Task B: Inventory of U.S. Cable-Stayed Bridges

Inventory Database (Appendix A2, Section 2.2)

Task C: Perform Analysis/Evaluation/Testing

Wind-Tunnel Testing of Dry Inclined Cables (Appendix B2, Section 3.2)
Study of Mitigation Methods (Appendix C1, Appendix C2, Section 3.4)
Study of Other Excitation Mechanisms (Appendix D2, Section 3.3)
Field Measurements of Stay Cable Damping (Section 3.5)
Study of User Comfort (Appendix D3, Section 3.6)
Calculations on Mechanics of Inclined Cables (Appendix D1)

Task D: Develop Guidelines for Design and Retrofit (Section 4.0)

Task E: Formulate Recommendations for Future Research (Section 5.0)

Task F: Project Documentation

2 COMPILATION OF EXISTING INFORMATION

2.1 REFERENCE MATERIALS

An extensive literature survey was initially performed to form a baseline for the current study. An on-line database of references was created so that all members of the Project Team could add or extract information as necessary. The database has 198 references and includes the article titles, authors, reference information, and abstracts when attainable and has built-in search capabilities. Examples of search pages and a full listing of the references in this database are included in Appendix A1.

2.2 INVENTORY OF U.S. CABLE-STAYED BRIDGES

An inventory of cable-stayed bridges in the United States was created to organize and share existing records with the entire Project Team. This database includes information on geometry, cable properties, cable anchorages, aerodynamic detailing, site conditions, and observed responses to wind for 26 cable-stayed bridges. The inventory is stored in Microsoft Access (Microsoft Office) database format, which allows for easy data entry and retrieval. Complete descriptions, examples of data forms, and a full list of bridges in the database are given in Appendix A2.

This electronic database of U.S. cable-stayed bridges, along with the reference database, has been turned over to FHWA. They are expected to be launched over the internet for use by the engineering community.

3 ANALYSIS, EVALUATION, AND TESTING

3.1 MECHANICS OF WIND-INDUCED VIBRATIONS

There are a number of mechanisms that can potentially lead to vibrations of stay cables. Some of these types of excitation are more critical or probable than others but all are listed here for completeness:

- Vortex excitation of an isolated cable or groups of cables
- Rain/wind induced vibrations of cables
- Wake galloping of groups of cables
- Galloping of single cables inclined to the wind
- Galloping of cables with ice accumulations
- Aerodynamic excitation of overall bridge modes of vibration involving cable motion
- Motions due to buffeting by wind turbulence
- Motion due to fluctuating cable tensions

All of these mechanisms are discussed in detail in Appendix B1. Vortex excitation, rain/wind, wake galloping of groups of cables, and galloping of single dry inclined cables all require careful consideration by the designer and are described in summary form later in this section.

The following parameters are relevant to these wind-induced vibrations:

Reynolds Number

A key parameter in the description of compressible fluid flow around objects (such as wind around stay cables) is the Reynolds number. The Reynolds number is a measure of the ratio of the inertial forces of wind to the viscous forces (Simiu & Scanlan, 1996) and is given by the following:

$$\mathrm{Re} = \frac{\rho V D}{\mu} \tag{1}$$

ρ = air density (lbf/ft^3, kg/m^3)
V = wind velocity (ft/sec, m/sec)
D = cable diameter (ft, m)
μ = viscosity of air (lbf/ft-sec, g/m-sec)

Strouhal Number

The Strouhal number is a dimensionless parameter relevant to vortex excitation:

$$S = \frac{N_s D}{V} \tag{2}$$

N_s = frequency of vortex excitation

The Strouhal number remains constant over extended ranges of wind velocity. For circular cross-section cables in the Reynolds number range $1x10^4$ to $3x10^5$, S is about 0.2.

Scruton Number

The Scruton number is an important parameter when considering vortex excitation, rain/wind induced vibrations, wake galloping, and dry inclined cable galloping.

$$S_c = \frac{m\zeta}{\rho D^2} \tag{3}$$

m	= mass of cable per unit length (lbf/ft, kg/m)
ζ	= damping as ratio of critical damping
ρ	= air density (lbf/ft^3, kg/m^3)
D	= cable diameter (ft, m)

This relationship shows that increasing the mass density and damping of the cables increases the Scruton number. Most types of wind-induced oscillation tend to be mitigated by increasing the Scruton number.

Vortex Excitation of an Isolated Cable and Groups of Cables

Vortex excitation is probably the most classical type of wind-induced vibrations. It is characterized by limited-amplitude vibrations at relatively low wind speeds. Vortex excitation of a single isolated cable is caused by the alternate shedding of vortices from the two sides of the cable when the wind is approximately perpendicular to the cable axis. The wind velocity at which the vortex excitation frequency matches the natural frequency (N_r) is found by using the Strouhal number S:

$$V = \frac{N_r D}{S} \tag{4}$$

The amplitude of the cable oscillations is inversely proportional to the Scruton number S_c. Increasing the mass and damping of the cables increases the Scruton number and therefore reduces oscillation amplitudes.

Inherent cable damping ratios can range anywhere from 0.0005 to 0.01, and an accurate value is difficult to predict. The lower end of this range is typical of very long cable stays without any grout infill, while the upper end of this range is more typical of shorter cable-stays with grouting and perhaps some external damping. A realistic estimate of inherent cable damping ratios on in-service bridges is in the range from 0.001 to 0.005. (See Section 3.5 for field measurements.)

For example, a cable consisting of steel strands grouted inside the cable pipe and with a damping ratio (ζ) of 0.005 has a Scruton number of about 12, and the amplitude of oscillation is only

about one half of a percent of the cable diameter. During construction and prior to grouting, the damping ratio of stay cables can be extremely low, e.g. 0.001, and the amplitude could conceivably increase to about 4% of the cable diameter, which is still small. Therefore, vortex shedding from the cables is unlikely to be a major vibration problem for cable-stayed bridges. By adding a small amount of damping, vortex excitation will be effectively suppressed.

Rain/Wind Induced Vibrations

The combination of rain and moderate wind speeds can cause high amplitude cable vibrations at low frequencies. This phenomenon has been observed on many cable-stayed bridges and has been researched in detail.

Rain/wind induced vibrations were first identified by Hikami and Shiraishi (1987) on the Meiko-Nishi cable stayed bridge. Since then, these vibrations have been observed on other cable-stayed bridges, including the Fred Hartman Bridge in Texas, the Sidney Lanier Bridge in Georgia, the Cochrane Bridge in Alabama, the Talmadge Memorial Bridge in Georgia, the Faroe Bridge in Denmark, the Aratsu Bridge in Japan, the Tempohzan Bridge in Japan, the Erasmus Bridge in Holland, and the Nanpu and Yangpu Bridges in China. These vibrations occurred typically when there was rain and moderate wind speeds (18-34 mph, 8-15 m/s) in the direction angled 20° to 60° to the cable plane with the cable declined in the direction of the wind. The frequencies were low, typically less than 3 Hz. The peak amplitudes were very high, in the range of 10-in to 3-ft (0.25-m to 1.0-m), with violent movements resulting in clashing of adjacent cables observed in several cases.

Wind tunnel tests have shown that rivulets of water running down the upper and lower surfaces of the cable in rainy weather were the essential component of this aeroelastic instability (Hikami & Shiraishi, 1987; Matsumoto et al., 1989). The water rivulets changed the effective shape of the cable, and moved as the cable oscillated causing cyclical changes in the aerodynamic forces which led to the wind feeding energy into oscillations. The wind direction causing the excitation was approximately 45° to the cable plane. The particular range of wind velocities that caused the oscillations appears to be that which maintained the upper rivulet within a critical zone on the upper surface of the cable.

It is noteworthy that some of the rain/wind vibrations that have been observed on cable-stayed bridges have occurred during construction when both the damping and mass of the cable system are likely to have been lower than in the completed state, resulting in a low Scruton number. For the Meiko-Nishi Bridge, the Scruton number was estimated at 1.7. The grouting of the cables adds both mass and damping, and often sleeves of visco-elastic material are added to the cable end regions which further raises the damping. The available circumstantial evidence indicates that the rain/wind type of vibration primarily arises as a result of some cables having exceptionally low damping, down in the $\zeta = 0.001$ range.

Since some bridges have been built without experiencing problems from rain/wind vibration of cables it appears probable that in some cases the level of damping naturally present is sufficient to avoid the problem. The rig test data of Saito et al. (1994), obtained using realistic cable mass

and damping values, are useful in helping to define the boundary of instability for rain/wind oscillations. Based on their results it appears that rain wind oscillations can be reduced to a harmless level using the following criteria for the Scruton number (PTI, 2001):

$$\frac{m\zeta}{\rho D^2} > 10 \qquad (5)$$

This criterion can be used to specify the amount of damping that must be added to the cable to mitigate rain/wind vibrations.

Since the rain/wind oscillations are due to the formation of rivulets on the cable surface, it is probable that the instability is sensitive to the surface roughness. Several researchers have tried using small protrusions on the cable surface to solve the problem. Flamand (1994) has used helical fillets 1/16 inch (1.5 mm) high on the cables of the Normandie Bridge. This technique has proven successful, with a minimal increase in drag coefficient. This type of cable surface treatment is becoming a popular design feature for new cable-stayed bridges, including the Leonard P. Zakim Bunker Hill Bridge (MA), U.S. Grant Bridge (OH), Greenville Bridge (MS), William Natcher Bridge (KY), Maysville-Aberdeen Bridge (KY), and the Cape Girardeau Bridge (MO).

Wake Galloping for Groups of Cables

Wake galloping is the elliptical movement caused by variations in drag and across-wind forces for cables in the wake of other elements, such as towers or other cables. This occurs at high wind speeds and leads to large amplitude oscillations. These oscillations have been found to cause fatigue of the outer strands of bridge hangers at end clamps on suspension and arch bridges. Similar fatigue problems are a theoretical possibility on cable-stayed bridges, but to date none have been documented.

The Scruton number is an important parameter with regard to wake galloping effects. An approximate equation for the minimum wind velocity U_{CRIT} above which instability can be expected due to wake galloping effects has been proposed (Irwin, 1997; Cooper, c.1985; PTI, 2001). It is given by:

$$U_{CRIT} = c\, f\, D\sqrt{S_c} \qquad (6)$$

c = constant
f = natural frequency
D = cable diameter
S_c = Scruton Number

For circular sections, the constant c has an approximate median value of 40. For cable-stayed bridges, this constant depends on the clear spacing between cables, and the following range of values based on the cable spacing are commonly used:

c = 25 for closely spaced cables (2D to 6D spacing)
c = 80 for normally spaced cables (generally 10D and higher)

Due to the level of uncertainty associated with practical applications, it is recommended that these values be applied conservatively, exercising engineering judgement.

The critical wind velocity may be low enough to occur commonly during the life of the bridge. Wake galloping therefore has the potential to cause serviceability problems. The equation for U_{CRIT} suggests several possibilities for mitigation. By increasing the Scruton number or natural frequency, the cables will be stable up to a higher wind velocity. However, increasing the frequency is far more effective in raising U_{CRIT} due to the square root manifestation of Sc in the above expression. The Scruton number increases with additional damping. The natural frequency may be increased by installing spacers or cross-ties along the cables to shorten the effective length of cable for the vibration mode of concern.

It should be noted that wake galloping is not a major design concern for normal well separated cable arrangements. For unusual cases, however, it is recommended that some attention be paid to the possibility of wake galloping.

Galloping of Dry Inclined Cables

Galloping of single dry, inclined cables is a theoretical possibility. Results from one experimental study (Saito et al., 1994) seem to suggest that this could be a concern for cable-stayed bridges. Theoretical formulations predict that this galloping may occur at high wind speeds with possible large-amplitude vibrations and that many existing cable-stayed bridges are susceptible, but there is no evidence of their occurrence in the field.

Single cables of circular cross-section do not gallop when they are aligned normal to the wind. However, when the wind velocity has a component that is not normal to the cable axis, an instability with the same characteristics as galloping has been observed. For a single inclined cable the wind acts on an elliptical cross-section of cable. An ellipticity of 2.5, corresponding to an angle of inclination of the cable of approximately 25°, can occur in the outer-most cables of long-span bridges. (Ellipticity is defined as the maximum width divided by the minimum width - e.g., a circle has an ellipticity of 1.0.) There is the potential for galloping instability if the level of structural damping in these cables is very low.

Saito et al. (1994) conducted a series of wind tunnel experiments on a section of bridge cable mounted on a spring suspension system. Their data suggest an instability criterion given approximately by the following (this general relation was given in a different form in Equation 6 for wake galloping, with c = 40):

$$(U/f\mathrm{D})_{\mathrm{CRIT}} = 40\sqrt{\mathrm{S_c}} \qquad (7)$$

This data was for cases where the angle between the cable axis and wind direction was 30° to 60°. The above criterion is a difficult condition to satisfy, particularly for the longer cables of cable-stayed bridges with a typical diameter of 6 to 8-in (150 to 200-mm). Further experimental research was necessary to confirm the results of Saito et al. (1994) and to extend the range of conditions studied. All of their experiments used low levels of damping, so it was important to

investigate whether galloping of an inclined cable is possible at damping ratios of 0.005 and higher.

Based on existing information, it was apparent that galloping of dry inclined cables presented the biggest concern and biggest unknown for wind-induced vibration mitigation. The Project Team therefore focused the wind-tunnel test program on this subject, as described in Section 3.2 of this report.

3.2 WIND-TUNNEL TESTING OF DRY INCLINED CABLES

Introduction

From the information reported on the various types of cable vibrations due to wind loads, it was determined that galloping of dry inclined cables was the most critical issue requiring further experimental research. The wind tunnel data of Saito et al. (1994) showed evidence of dry inclined cable oscillations with some of the characteristics of galloping, and stability criteria were suggested in their paper. However, based on their criteria, many existing cable-stayed bridges would have shown more evidence of dry cable galloping than has actually been observed. In order to clarify the dry cable galloping phenomenon and evaluate the stability criteria proposed by Saito et al. (1994), the Research Team conducted a series of wind tunnel tests of a full-size 2D sectional model of an inclined cable in the "Propulsion" wind tunnel at the Montreal Road campus of the Institute of Aerospace Research, National Research Council Canada (IAR/NRCC). A full description of the testing is included in Appendix B2.

The objectives of this study were to:

- Investigate the existence of dry inclined cable galloping
- Clarify the mechanisms of this type of vibration
- Determine the effects of the following parameters – wind speed, structural damping, surface roughness, and wind direction
- Refine the stability criterion proposed by Saito et al. (1994)

The following section summarizes the test program and its results.

Testing

The model was developed to be similar to that used in the test carried out by Saito et al. (1994). A 22-ft (6.7-m) long cable consisted of an inner steel pipe covered with a smooth polyethylene tube with an outside diameter of 6.3-in (160 mm). The effective mass per cable length was 40.9 lb/ft (60.8 kg/m). The end supports at the upwind end were maintained out of the wind flow above the wind tunnel, and at least 19.2-ft (5.9-m) of the 22-ft (6.7-m) length of the cable was directly exposed to the wind tunnel flow.

Testing was performed for various levels of structural damping, cable frequency ratios, surface roughness and at various angles of wind flow. The cable model orientation was changed against the mean wind flow direction for several configurations. The model was supported in the wind tunnel with the angles Φ and α being adjustable to represent different θ and β combinations. Figure 37 of Appendix B2 shows the relationship of these angles to the cable and wind direction. Similar to the Japanese studies (Saito et al., 1994), θ and β represent respectively the angle between the horizontal plane and the cable, and the yaw angle between the wind direction and the longitudinal bridge axis. The orientation of the two degree of freedom springs (perpendicular to the cable longitudinal axis) could be rotated about the cable axis through an angle α. Φ is the angle between the wind tunnel floor and the cable. The angle is only important when the vertical and horizontal frequencies of the cable are tuned to different frequencies. In the wind tunnel

this led to testing with an adjustable virtual ground plane. The relationship between the cable and the mean wind direction is represented by Equations 8 and 9:

$$\cos \Phi = \cos \beta \cos \theta \tag{8}$$

$$\tan \alpha = \tan \beta / \sin \theta \tag{9}$$

The aerodynamic behavior of the inclined cable model was investigated with different combinations of model setup, damping level and surface roughness as described in the following tables:

Table 1: Dry inclined cable testing - Model setup.

Full Scale Cable Angles Tested			Model Test Cable/Pipe Angles	
Model Setup	θ^o	β^o	Φ^o	α^o
1B	45	0	45	0
1C	30	35.3	45	54.7
2A	60	0	60	0
2C	45	45	60	54.7
3A	35	0	35	0
3B	20	29.4	35	58.7

Table 2: Dry inclined cable testing - Damping levels.

Damping Description	Dampers Used	Approximate Damping Range (% of critical) damping is amplitude dependent
Low damping	No damper added	0.03 to 0.09
Intermediate damping	16 elastic bands per sway spring	0.05 to 0.10
High damping	28 elastic bands per sway spring	0.15 to 0.25
Very high damping	Airpot damper with 1 1/4 dial turns	0.30 to 1.00

Table 3: Dry inclined cable testing - Surface condition.

Smooth Surface	Polyethylene (PE) Pipe with clean surface
Rough Surface	Polyethylene (PE) Pipe with glue sprayed on the windward side of the cable

Results Summary

Limited-amplitude oscillations were observed under a variety of conditions. The limited-amplitude vibrations occurred within narrow wind speed ranges only, which is characteristic of vortex excitation of the high speed type described by Matsumoto (1998). For the typical cable diameters and wind speeds of concern on cable-stayed bridges the Reynolds number (defined in Section 3.1) is in the critical range where large changes in the airflow patterns around the cables occur for relatively small changes in Reynolds number. The excitation mechanism is thus likely to be linked with these changes. The maximum amplitude of the response depended on the orientation angle of the cable. For wind blowing along the cable, for cables with a vertical inclination angle $\theta \sim 45°$, the increase of surface roughness made the unstable range shift to lower wind speeds.

The results of this testing showed a deviation from the criteria described in the introduction. While significant oscillations of the cable occurred (double amplitudes up to 1D), it is not conclusive that this was dry inclined cable galloping. In fact, as indicated above they had similar characteristics to Matsumoto's (1998) high speed vortex excitation. Divergent oscillations only occurred for one test setup at very low damping, and the vibrations had to be suppressed since the setup only allowed for amplitudes of 1D. Large vibrations were only found at the lowest damping ratios ($\zeta<0.001$). Above a damping ratio of 0.003, no significant vibrations (> 0.4-in ; >10-mm) were observed.

Figure 1 shows the results of this experiment as compared to the instability line determined by Saito et al. (1994). The graph presents Reduced Wind Velocity Ur vs. the Scruton number, where:

$$Ur = U_{CRIT} / (f D) \qquad (10)$$

U_{CRIT} = critical wind velocity at which instability occurs
f = natural frequency
D = cable diameter

The bold points indicate cable motions with amplitudes from ±0.4-in (10-mm) to ± 3.1-in (80-mm). Note the test rig would not allow for motions greater than ± 3.1-in (80-mm). However, only one test case reached this limit and is denoted by the triangular point. One point from Miyata et al. (1994) is also shown.

Conditions with oscillations less than ±0.4-in (10-mm) are denoted with an open circle. Many of these points lie in the region denoted as Unstable based on the Instability Line of Saito et al. (1994). It is suggested that this line can be redefined based on the dashed line denoted as FHWA Instability Line.

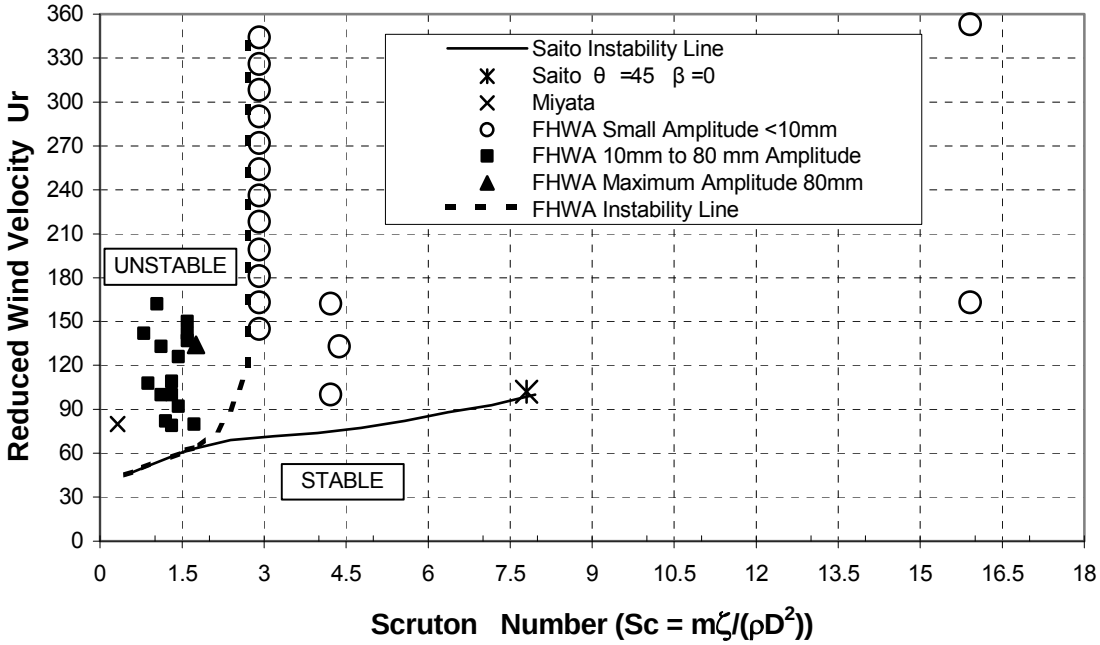

Figure 1: Comparison of wind velocity-damping relation of inclined dry cable.

This testing suggests that if even a low amount of structural damping is provided (ζ>0.003), then vortex shedding and inclined cable galloping vibrations are not significant. This damping corresponds to a Scruton number of approximately 3, which is less than the minimum of 10 established for suppression of rain/wind vibrations (discussed in Section 3.1). Therefore dry cable instability should be suppressed by default if enough damping is provided to mitigate rain/wind vibrations. A complete report of the wind-tunnel testing by the Project Team on dry inclined cables is given in Appendix B2.

A second phase of testing was conducted on a static model to verify the findings of the initial study, using the same orientations where the large amplitude oscillations occurred. Pressure taps were added to record aerodynamic force measurements. The objectives of this phase were to clarify the mechanism of dry inclined cable galloping and investigate the differences between galloping and high-speed vortex shedding. The test report was not available as of the production of this document.

3.3 OTHER EXCITATION MECHANISMS

Effects Due to Live Load

This study was carried out by the Project Team to assess the amount of vibration caused by live loading and determine if this movement is significant as compared to wind vibration. To address this problem a computer model of a real bridge was subjected to a moving train load, and the vibrations of an individual cable were analyzed. A moving train has a greater effect on cables than passing trucks or random traffic. The cable tensions, displacements and anchorage rotations obtained from the dynamic time history analysis were compared to an analysis ignoring all dynamic effects as well as the results obtained from influence line calculations which are normally carried out during design. A summary of this work is given in this section, and the complete report is included in Appendix D2.

A 3D computer model of the Rama 8 Bridge in Bangkok, Thailand, was created for this analysis. The bridge has a single tower and a 984-ft (300-m) main span. The third longest cable (M26), with an unstressed length of 981-ft (299.1-m), was studied to determine the effects of live loading.

A static live load analysis was first conducted as a baseline using a 5-car transit train, neglecting dynamic properties of the train. Influence line analyses were performed to determine the maximum and minimum effects due to live load. For dynamic analysis, the transit train was modeled as a mass on damped springs and moved across the bridge at a speed of 50 mph (80 km/hr), taking into account the dynamic interaction between the train and the structure. The tension in Cable M26 is plotted in Figure 2 to compare the dynamic effects to the static effect. Note that the increase in maximum cable tension due to dynamic effects is less than 10%.

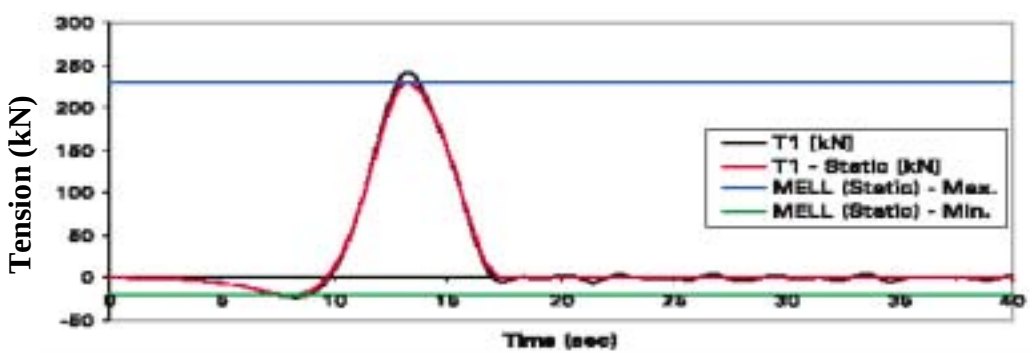

Figure 2: Cable M26, Tension vs. Time. Transit train speed 50 mph (80km/hr).

The results of this study indicated the following:

- A stay cable which is discretized with twenty elements accurately predicts the free vibration characteristics of a stay cable.
- Once the cable is modeled as part of the real structure with the tower and the deck providing realistic end conditions, the cable frequencies only change slightly but the mode shapes become spatial rather than being purely in-plane or out of plane.

- The cable tensions, displacements and end rotations are dominated by the 'static' deformation response associated with the passing of the moving load. Subsequent dynamic oscillations are typically an order of magnitude smaller than the static maximum.
- It appears that the dynamic response of the cable, during the train passage and in the subsequent free vibration phase, is driven by the vibration of the bridge deck.

Deck-Stay Interaction Due to Wind

Measurements of both deck and stay movements were taken at the Fred Hartman Bridge during the passage of a storm. For this specific record, Figures 3 and 4 show the time-histories (first 5 minutes) and power spectral densities (PSDs) of vertical deck acceleration at midspan and of the adjacent stay cable AS24, respectively. Cable AS24 has a length of 650-ft (198-m) and a natural frequency of approximately 0.59Hz. Figure 5 shows the wind speed at deck level.

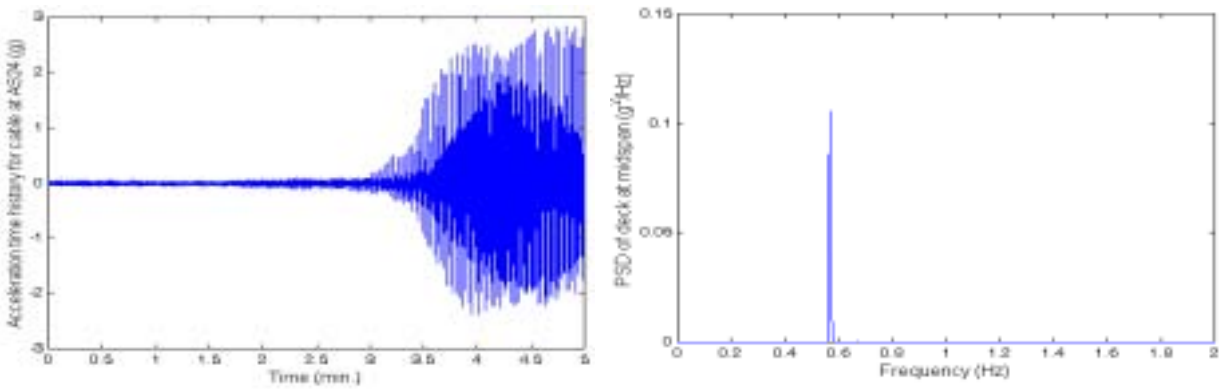

Figure 3: Time history and power spectral density (PSD) of the first 2-Hz for deck at mid-span (vertical direction).

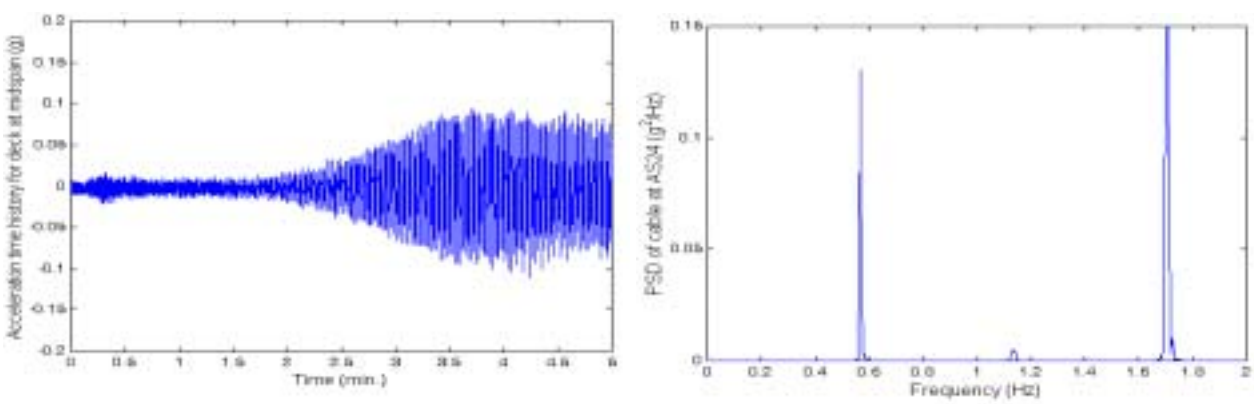

Figure 4: Time history and power spectral density (PSD) of the first 2-Hz for cable at AS24 (in-plane direction) deck level wind speed.

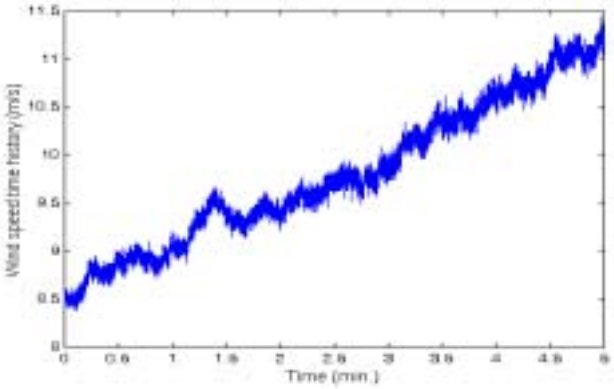

Figure 5: Deck level wind speed.

Figures 3 and 4 show a dominant frequency of vibration at approximately 0.58 Hz. It is important to note that this frequency corresponds quite closely to the third symmetric vertical mode of the superstructure, and is also close to the first mode of the stay cable AS24. This is an interesting and important observation since the first-mode vibrations of a cable at this level of acceleration are generally associated with large displacements. In fact, by integrating the acceleration time-history, the displacement amplitude (peak to peak) was estimated to be approximately 3-ft (1-m).

Furthermore, by observing the time-histories it can be seen that the significant vibrations are initially observed at the deck instead of the cable. This observation, as well as the similarity of modal frequencies, suggests that the deck is driving the cable to vibrate with large amplitude in its fundamental mode. Vortex-induced vibration of the deck is thought to be the driving mechanism for this motion. Further studies are continuing to identify additional occurrences of this behavior for corroboration, and to better understand the underlying mechanisms their consequences. These findings are not complete at the time of production of this report.

It is emphasized that this appears to be a rare event; very few occurrences of this nature have been identified.

3.4 STUDY OF MITIGATION METHODS

Development of recommended design approaches was based on previous and current research focusing on cable aerodynamics, dampers, and cross-ties. Theories on the behavior of linear and nonlinear dampers and cross-tie systems were developed and compared to field measurements on the Fred Hartman Bridge, Leonard P. Zakim Bunker Hill Bridge, Sunshine Skyway Bridge, and Veterans Memorial Bridge. Basic findings are discussed below, and more detailed discussions are found in Appendix C2 and in the technical papers listed in Appendix C1.

Linear and non-Linear Dampers

To suppress the problematic vibrations of stay cables, dampers are often added to the stays near the anchorages (due to practical limitations of installation). Although the mechanisms that induce the observed vibrations may still not be completely understood, dampers have had relatively widespread use, and their effectiveness has been demonstrated. However, criteria for damper design are not well established. Current recommendations for required damping levels to suppress rain/wind vibrations were developed using relatively simplified wind-tunnel models (PTI, 2001), and it is not clear whether these guidelines are adequate or appropriate for vibration suppression in the field. In addition, it is important to note that vibrations can occur in more than one mode of the cable, and little has been done to address the question of required damping levels for each mode. The anticipated widespread application of dampers for cable vibration suppression justifies further research aimed at better understanding the resulting dynamic system and refinement of design guidelines. An example of a damper provided to a cable anchorage is shown in Figure 6.

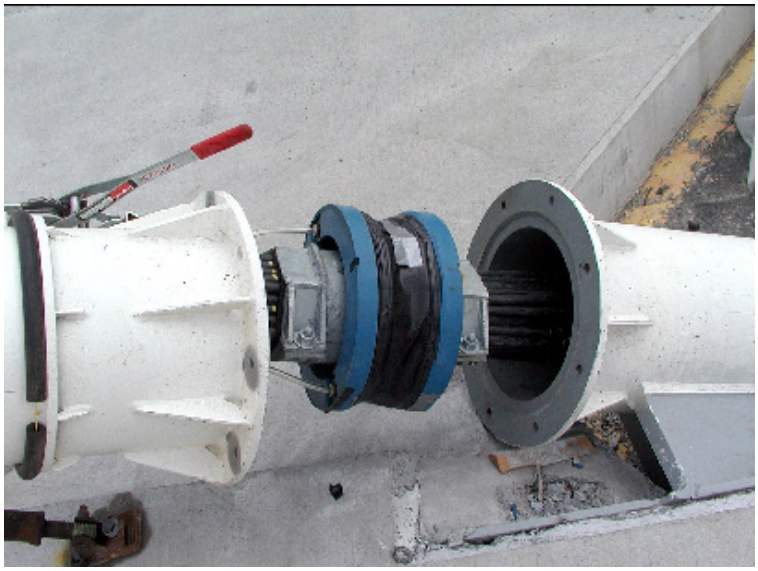

Figure 6: Damper at cable anchorage.

Linear dampers

Free vibrations of a taut cable with an attached linear viscous damper were investigated in detail. In designing a damper for cable vibration suppression, it is necessary to determine the levels of supplemental damping provided in the first several modes of vibration for different values of the damper coefficient and different damper locations. Previous investigations of linear dampers have focused on vibrations in the first few modes for damper locations near the end of the cable. However, damper performance in the higher modes is of particular interest, as full-scale measurements indicate that vibrations of moderate amplitude can occur over a wide range of cable modes. This study investigates the dynamics of a taut cable-damper system in higher modes and without restriction on the damper location (see Figure 7).

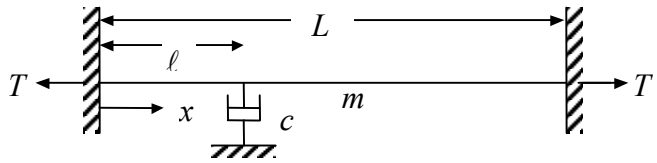

Figure 7: Taut cable with linear damper.

An analytical formulation of the complex eigenvalue problem for free vibration was used to derive an equation for the eigenvalues that is independent of the damper coefficient. This "phase equation" reveals the attainable modal damping ratios ζ_i and corresponding oscillation frequencies for a given damper location ℓ/L, affording an improved understanding of the solution characteristics and revealing the important role of damper-induced frequency shifts in characterizing the response of the system. For damper locations, such as near the end of the stay, resulting in small frequency shifts, the following relationship can be derived:

$$\frac{\zeta_i}{(\ell/L)} \cong \frac{\pi^2\kappa}{(\pi^2\kappa)^2+1} \quad ; \quad \kappa \equiv \frac{c}{mL\omega_{o1}} i \frac{\ell}{L} \qquad \text{(11a, b)}$$

i	=	mode of vibration
c	=	damping coefficient
m	=	mass per unit length
ω_{o1}	=	fundamental circular frequency
ℓ/L	=	normalized damper location

In Figure 8, the normalized damping ratio $\zeta/(\ell/L)$ has been plotted against the nondimensional damping parameter, κ, for the first five modes for a damper location of ℓ/L=0.02, and it is evident that the five curves collapse very nearly onto a single curve in good agreement with the theoretical approximation.

It is important to note that because the mode number is incorporated in the nondimensional damping parameter κ, the optimal damping ratio can be achieved in only one mode of vibration. This is a potential limitation for linear dampers, because it is currently unclear how to specify, a priori, the mode in which optimal performance should be achieved for effective suppression of stay-cable vibration, and designing a damper for optimal performance in a particular mode may potentially leave the cable susceptible to vibrations in other modes.

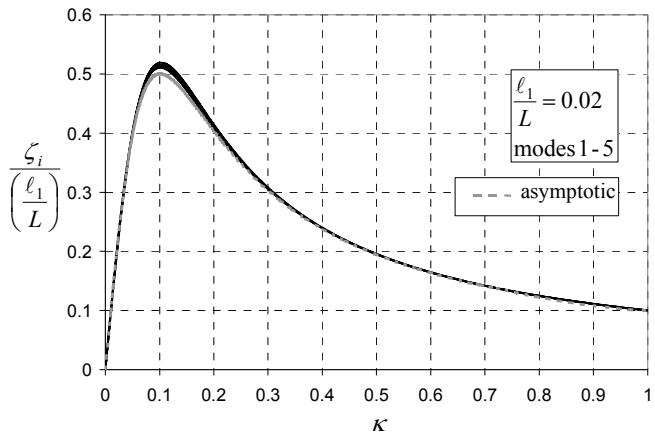

Figure 8: Normalized Damping Ratio versus Normalized Damper Coefficient: Linear Damper.

Non-linear Dampers

The dynamic behavior of a taut cable with a passive, nonlinear, power-law damper attached at an intermediate point was investigated. Recent investigations indicated that a nonlinear damper may potentially overcome the limitation in performance of a linear damper whereby optimal damping performance can only be achieved in one mode of vibration.

The exact formulation of the complex eigenvalue problem for a taut cable with a linear damper was extended to develop a single-mode approximation for the amplitude-dependent effective damping ratios for the power-law damper. An asymptotic approximate solution revealed a nondimensional grouping of parameters κ, that was used to extend the universal estimation curve for the linear damper to the case of a nonlinear damper. For a damping exponent of β=1 (linear damper), the expression for κ is the same as the previous equation derived for a linear damper. The shape of the curve is slightly different for each value of damping exponent, β, but for a given damping exponent the curve is nearly invariant with damper location and mode number over the same range of parameters as the universal estimation curve for the linear case (Figure 9).

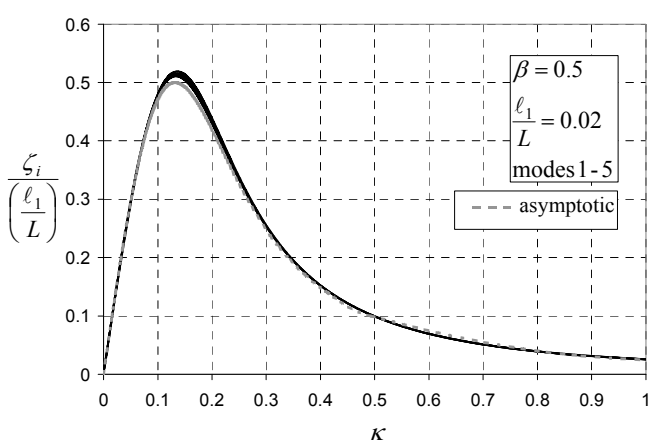

Figure 9: Normalized Damping Ratio versus Normalized Damper Coefficient: β=0.5

Because the nondimensional damping parameter κ depends on both the amplitude and mode number of oscillation, the optimal damping performance will be achieved, in general, at different amplitudes of vibration in each mode. An "optimal" value for the damper coefficient can be determined by specifying a design amplitude of oscillation in a given mode at which the optimal performance is desired. Therefore a non-linear damper has the potential to allow optimal damping performance over a wider range of modes than for a linear damper.

In the special case of β=0.5 (a square-root damper), it was observed that the damping performance is independent of mode number and depends only on the amplitude of vibration. In designing a square-root damper it is sufficient to specify only the amplitude, A_{opt}, and the optimal damping performance is achieved at the same amplitude in each mode. These features suggest that nonlinear dampers may offer some advantages over linear dampers for cable vibration suppression, while retaining the advantages of economy and reliability offered by a passive mitigation strategy.

Field Performance of Dampers

This investigation seeks to evaluate the effectiveness of passive linear dampers installed on two stays on a cable-stayed bridge by comparing response statistics before and after the damper installation and by investigating in detail the damper performance in a few selected records corresponding to different types of excitation.

Viscous dampers (dash-pot type) were installed on two stays (A16 and A23) on the main-span of the Fred Hartman Bridge (Figure 10), a twin-deck cable-stayed bridge over the Houston Ship channel, with central span of 1250 ft (380m) and side spans of 482 ft (147m). The deck is composed of precast concrete slabs on steel girders with four lanes of traffic, carried by a total of 192 cables in four inclined planes, spaced at 50 ft (15m) intervals.

Figure 10: Fred Hartman Bridge.

Properties of the two stays and the dampers that have been installed on these stays are given in Table 4. Commercially available dampers were selected for the application.

Table 4: Stay and damper properties.

	Stay Properties			Damper Properties		
	Length	Outside Diameter	Mass	Natural Frequency	Location	Damping Constant
Stay name	L ft (m)	D in (mm)	m lbf/ft (kg/m)	f_{o1} Hz	ℓ/L	c lbf-s/ft (kN-s/m)
AS16	285 (87.0)	5.5 (140)	32.2 (47.9)	1.24	.045	4800 (70.0)
AS23	599 (182)	6.3 (160)	50.0 (75.9)	0.64	.037	12000 (175.1)

Data have been collected for almost three years after the damper installation. The dampers were designed for optimal performance in the fundamental mode of vibration, which should provide adequate damping in the first several modes to suppress rain/wind vibration. Wind speed is reported at deck level. Wind direction is measured in degrees clockwise from the bridge axis, with zero degrees corresponding to wind approximately from the north, directly along the bridge axis. Acceleration data are reported from transducers installed on the stays usually about 20-ft (6-m) vertically above deck level.

Results before damper installation show patterns that are consistent with other field and wind tunnel observations (see Appendix C2 for additional details):

- A high density of points is seen near the abscissa, which generally corresponds to vortex-induced vibration in a variety of modes and low-level buffeting response of the stay to random excitations.
- Multiple points over a wide range of wind speeds are of high amplitude (RMS acceleration > 0.5g), indicating the characteristic signature of rain/wind oscillation.
- One-minute mean wind speeds at deck level reached 34 mph (15 m/s) before the dampers were installed, and almost 40 mph (18 m/s) in the period after installation. This latter value corresponds to a one-minute average wind speed of 60 mph (27 m/s) at the top of the tower, recorded during a thunderstorm.
- The dependence on wind direction is also clear, with A16 showing its peak responses between 90° and 160°, and A23 over a narrower range between 90° and 135°.

Results after installation of the dampers suggest the following:

- Amplitudes are significantly reduced across all recorded wind speeds [up to 40 mph (18 m/s) at deck level] with maximum RMS acceleration amplitudes of around 0.5g.
- The dependence on wind direction has been altered significantly, with the largest responses now nearer to a 90° angle of incidence.
- Based on the measured forces in the dampers, they are functioning and providing dissipative force to the stays as intended.

In conclusion, the benefits of adding dampers are evident. Dampers can potentially be attached unobtrusively near the stay anchorage at the deck or tower, and thus detract minimally from the aesthetics of the structure.

Cross-Tie Systems

One possible method to counteract undesired oscillations is to increase the in-plane stiffness of stays by connecting them together with a set of transverse secondary cables, defined as cross-ties. From a dynamic perspective, the properties of the single cables are modified by the presence of the lateral constraints that influence their oscillation characteristics. Similarly, a connection of simple suspended elements is transformed into a more complex cable network. Figure 11 shows an example of cable cross-tie systems applied to a bridge.

Figure 11: Cable cross-tie system.

It is evident that detailed studies of cross-ties and interconnected cable systems are not well reported and most of the recommendations that are currently followed seem to be linked to practice or previous experience. A fundamental study to better understand the behavior was therefore necessary.

This has shown that cross-ties potentially work by increasing the generalized mass and therefore Scruton number in the lower modes, and by raising frequencies and localizing the vibration in higher modes. They are also likely to increase the effective damping of a cable through the friction at cross-tie connections and also by providing a mechanism to transfer energy from one cable to another. However, these are difficult to quantify reliably using analytical methods.

The Dames Point Bridge (Figure 12) in Jacksonville, Florida, is an example of the effective use of cross-ties on an older bridge designed prior to the discovery of rain/wind vibrations. Although some wind-induced oscillations were observed during construction prior to grouting and cross-tie installation, no problematic cable vibrations have been reported on this bridge since it was completed in 1989.

Figure 12: Dames Point Bridge.

There is also the potential to combine cable cross-ties and dampers into a single device (Kumarasena, 1999). This could provide an efficient system where a damper at one location provides damping to a system of cables through the cross-ties. This method could be highly effective, as the damping would be provided at a point significantly into the cable length. The issues of aesthetics and serviceability need to be further addressed.

Analysis

An alternative analytical method was developed to examine cable cross-tie networks, and was used to study the Fred Hartman Bridge cable system.

Limited study of in-plane vibrations of complex cable networks has usually been performed by means of finite element methods due to the number of cable elements that are involved and the variability of the global characteristics of the system. An analytical method and efficient numerical procedure was developed that models the behavior of a set of interconnected cables. The analytical method is an alternative procedure for the derivation of the equation of motion (free-vibration problem) of a network, based on the taut-cable theory. This approach offers a number of advantages over the finite element method and provides a tool that is useful in the design and optimization of such systems for practical application.

The initial problem formulation is depicted in Figure 13. The example shows a simplified network, defined by a set of two taut cables, connected by means of a vertical rigid rod (to be relaxed later). See Appendix C2 for the formulation of the analytical method for this system.

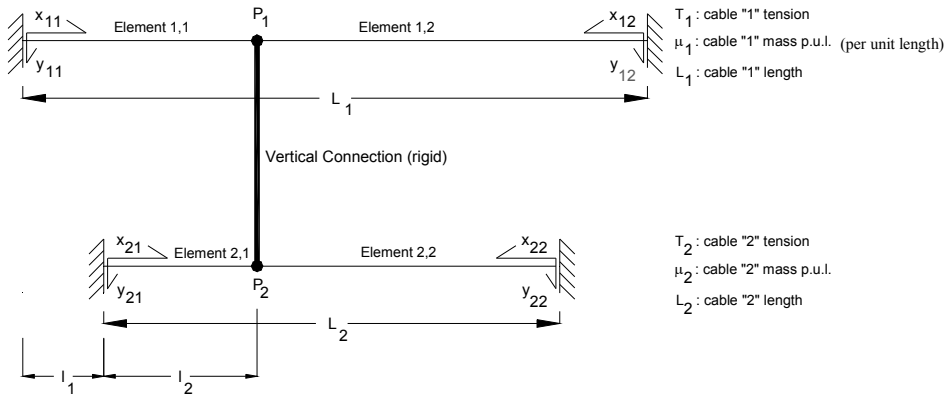

Figure 13: General problem formulation.

The free-vibration analysis method was applied to the study of a cable network that was modeled after the Fred Hartman Bridge. The investigated system corresponds to the south-tower central-span portion, a set of twelve stays with a three-dimensional arrangement (Figure 14). Stay "24S" is assumed as a reference element; all other stay quantities are normalized with respect to this element.

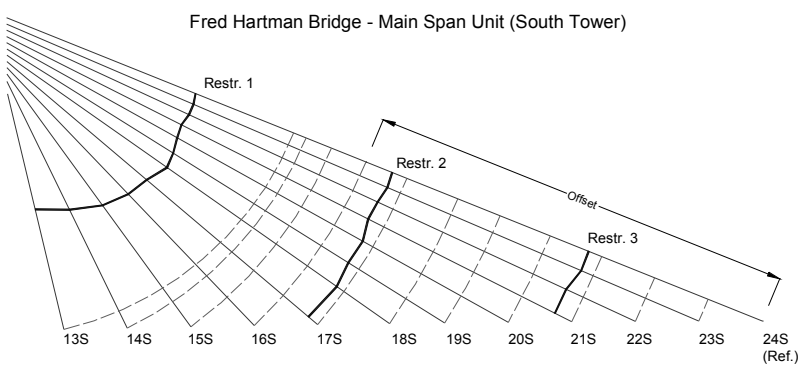

Figure 14: General problem formulation (original configuration).

The transverse connectors, an "eight-loop" steel wire rope system, are located in accordance with the existing system. The three-dimensional cable network was reduced to an equivalent two-dimensional problem. The definition of the modal frequencies and mode shapes of the network (free-vibration analysis) was performed through the study of the roots of the determinant of the system matrix as a function of the reduced frequency of the structure.

Figure 15 depicts the eigenfunctions for Modes 1 and 5 of the model, normalized so that the resulting modal mass of the network is unitary. A careful study of the solution patterns showed two categories of roots:

> Global modes, where the whole set of cables is involved in the oscillation. (ex., Mode 1)
>
> Local modes, where the maximum amplitudes are located in the intermediate segments of specific cables. The overall characteristics of these modal forms can be different from the solution for individual cables, and influenced by the presence and the location of the transverse connectors. The wavelength of these modes is essentially governed by the distance between two consecutive connectors. (ex., Mode 5)

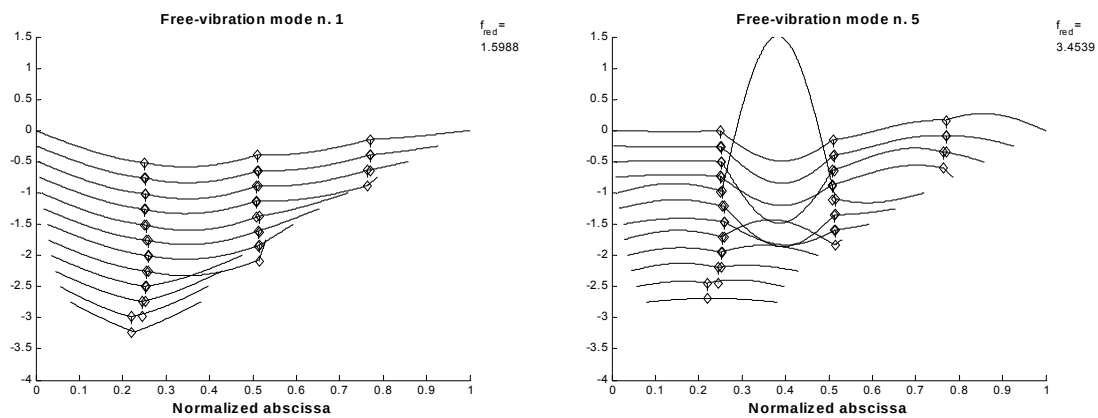

Figure 15: Eigenfunctions of the network equivalent to Fred Hartman Bridge; modes 1 and 5.

In Figure 16, the natural frequencies (Hz) are plotted as a function of the mode number and compared to the individual cable behavior. Solutions are shown for three comparative cases (NET_3C, original configuration; NET_3RC perfectly rigid transverse links; NET_3CG modified non-rigid configuration with ground restrainers). For practical purposes, the connectors in the original configuration can be considered as effectively rigid, since the two graphics (NET_3C, NET_3RC) essentially overlap.

From Figure 16, it can be seen that the sequence of fundamental global modes is followed by a high-density solution pattern, corresponding to the localized modes. An upper and lower limit frequency can be detected, in this case 1.9 and 2.7 Hz, respectively. Both limits are connected by the frequency of anti-symmetric second modes in the individual stays. The upper value is directly related to the frequency of shorter cables, while the lower value is influenced by a combination of the stays in the central part of the structure (presence of pseudo-symmetric components). The high density of frequencies suggests a potential sensitivity to forced oscillations, exciting the network within this range, in which the dynamics can be influenced by a combination of these modal forms. Beyond this upper limit the situation reverts to a set of higher network modes and thereafter, a second plateau appears in the frequency range coincident with high-order antisymmetric individual segment modes. This pattern of consecutive “steps” defines a typical pattern for the behavior.

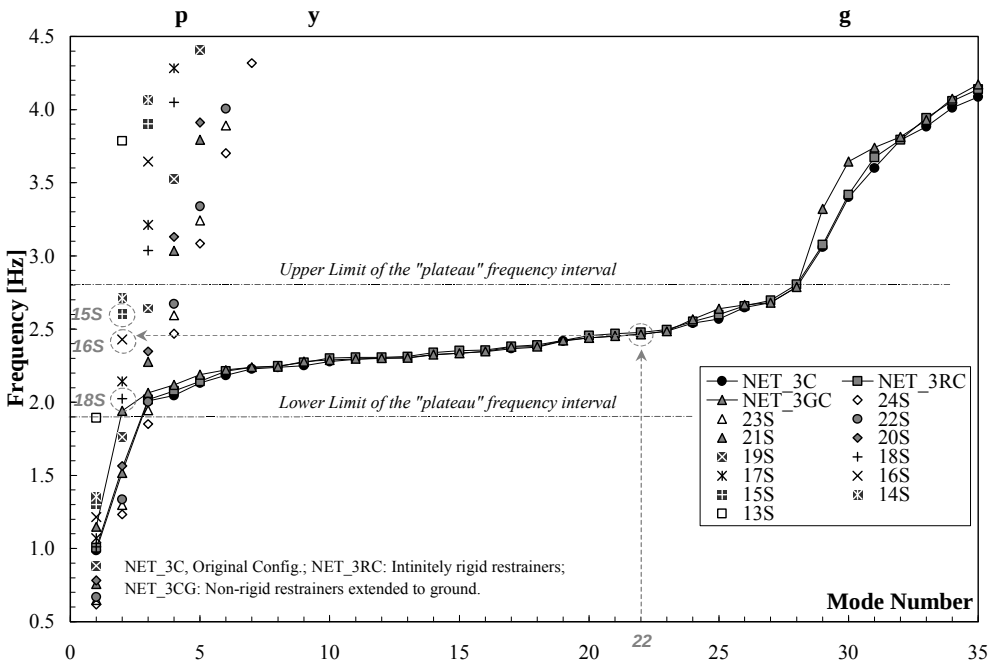

Figure 16: Comparative analysis of network vibration characteristics and individual-cable behavior; Fred Hartman Bridge.

Field Performance

Field measurements of the Fred Hartman Bridge were compared to analysis results to validate the analysis approach for cross-tied systems. A long-term ambient vibration survey was conducted to monitor stay-cable vibration and to better understand the overall performance of the structure and its modal characteristics. More than ten thousand trigger files were recorded during a period of three years and continued thereafter. An algorithm was designed for the automatic processing of the records.

The methodology was applied to the study of the side-span unit of the south tower of the bridge (see Figure 17). The cable network is configured by means of three transverse restrainers. The data set was extracted from the records of four in-plane and out-of-plane accelerometers, placed along stays AS1, AS3, AS5 and AS9 at a height of approximately 22 ft (7m) from the deck level. The correspondence between the predicted modal characteristics and the real behavior was carried out by simultaneous spectral analysis of the in-plane acceleration record database of the four locations. The analysis was founded on the simultaneous identification of the same dominant in-plane frequency on all the four investigated cables.

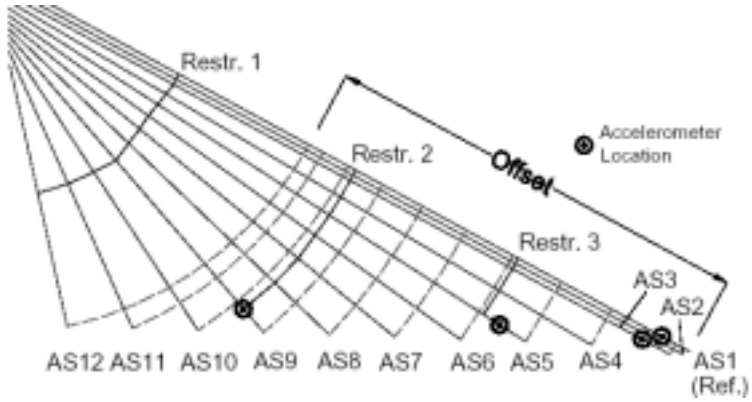

Figure 17: Fred Hartman Bridge, field performance testing arrangement.

The investigation considered the presence of cable network behavior along with individual cable and, eventually, global (deck) structure modes. The fundamental frequencies of each stay were identified through field measurements, and were adopted as input data in the numerical procedure to allow for a consistent comparison of the results with the real situation. The results of the simulation are summarized in Table 5, in which the frequencies of the modes between 0 and 4 Hz are indicated. The subdivision into global and local network modes is indicated along with information about the general characteristics of the modal shape.

The computed frequency of NM1 (0.926 Hz) is close to the 10th bending mode of the bridge (0.924 Hz), which suggests a potential susceptibility to interaction of the deck-stay system in this range. Low-density values of frequency can be seen up to 2.4 Hz (NM5) and beyond 3 Hz (NM30). The plateau behavior was detected between 2.4 and 3.0 Hz, associated the local behavior and a high density of solutions (NM5-NM29).

Table 5: Cable network modes (0-4 Hz) predicted by the model.

Mode N.	NM1	NM2	NM3	NM4	NM5	NM6	NM7	NM8	NM9	NM10	NM11	NM12	NM13	NM14	NM15	NM16	NM17	NM18
Frequency [Hz]	0.926	1.458	2.043	2.332	2.368	2.406	2.430	2.448	2.467	2.472	2.500	2.556	2.582	2.600	2.631	2.644	2.662	2.677
Mode type	G-S	G-AS	G-S	L	L	L	L	L	L	L	L	L	L	L	L	L	L	L

Mode N.	NM19	NM20	NM21	NM22	NM23	NM24	NM25	NM26	NM27	NM28	NM29	NM30	NM31	NM32	NM33	NM34	NM35	NM36
Frequency [Hz]	2.689	2.697	2.720	2.747	2.765	2.797	2.819	2.862	2.956	2.994	3.018	3.217	3.347	3.417	3.456	3.689	3.948	4.077
Mode type	L	L	L	L	L	L	L	L	L	L	L	G-S	G-S	G-S	L	G-AS	L	L

G = Global Network mode; L= Local Network mode; S = symmetric; AS = antisymmetic

The results of the field data analysis showed consistent similarities with the predicted values. They also indicated the potential presence of some of the "new" modal forms in frequency ranges in which modal characteristics from other sources (individual stays, global structure, etc.) were often excluded. NM1 was clearly identified in one occasion only for a continuous time interval of about fifteen minutes, corresponding to an extremely rare occurrence in terms of ambient-induced vibration. This event was mainly driven by the high-amplitude motion of the deck due to vortex shedding and related to a strong wind with direction almost perpendicular to the bridge axis.

Considerations for Cross-Tie Systems

This analysis shows that careful consideration must be given for the design of cross-ties. The general frequency increment in the fundamental modes that is usually attained by the introduction of transverse connectors must be balanced with the potential undesirable behavior of the local modes. A set of considerations for the improvement of the response of a cable network is proposed:

1. Keep the location of the first plateau as high as possible, distant from the fundamental modes, in order that the antisymmetric individual-cable modes (2nd mode) that mostly contribute to the network modal shape are those of the shorter cables. Symmetric configurations of the restrainers with respect to intermediate-length cables is preferred to increase the frequency interval (lower limit in particular) corresponding to local modes, since they minimize the longest segment length.

2. Relative stiffness of the transverse restrainers does not seem to play a significant role in the definition of the modal characteristics. Rather, the frequency ratio among different stays (related to the reference cable frequency) seems to be responsible for the network mode sequence. A good compromise between small frequency ratios (shorter stays) and high values (longer stays) is preferred for the optimization of the system. Unfortunately this aspect is not connected to the cross-tied configuration but to the existing setup of the bridge.

3. A cable network cannot be designed to withstand all possible excitations; the best thing that can be done is to select some sources of vibrations and "tune" the network not to respond to them, since the behavior becomes complex due to the presence of the plateau. Localized modes are practically unmanageable since they mainly concern internal elements of the system, although in these cases the vibration is confined to a selected portion of the structure and the potential implications for long-term structural sensitivity (fatigue damage) are less relevant.

4. A network combined with additional mechanical dampers, connected to the deck at specific locations, might be seen as an efficient way of vibration reduction. The presence of pseudo-symmetric behavior should be carefully assessed: it generates "non-dampable" modes (half of the structure is at rest). This behavior is enhanced by the presence of ground connectors. It might be possible to use a ground-restrainer in the proximity of the shortest cable, close to the tower in combination with dampers on the segments on the right side of the longest cables closest to the deck. In fact the first pseudo-symmetric modes, in this model, are those related to the unconstrained regions of the network and the presence of a damper in this position might become efficient. This opportunity must be balanced with the fact that, when the addition of these devices is necessary, the high inclination of the short cables might make them difficult to install.

5. It should be noted that cross-ties may be less effective at controlling out-of-plane oscillations. This further suggests the importance of using dampers in coordination with cross-tie systems.

6. Finally the optimal design of a network should be based not only on structural performance considerations but also on cost provisions (installation, maintenance). In this way the preferred solution should be suggested perhaps through a more extended optimization technique.

Cable Surface Treatment

The effectiveness of different surface modifications are determined from wind tunnel tests. No accepted methodology exists for the design of these elements. All major cable suppliers provide cable pipes that include surface modifications to mitigate rain/wind vibrations. Several types of cable surface treatments are shown in Figure 18. Extensive research has been done in the past and these surface treatments have been shown to be effective for mitigation of rain/wind vibration.

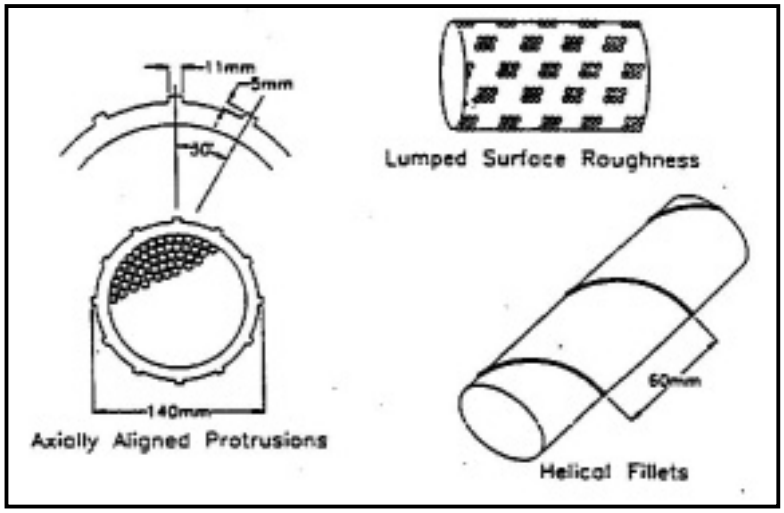

Figure 18: Types of cable surface treatments.

The double helix spiral bead formations are the most common on new bridges, such as the Leonard P. Zakim Bunker Hill Bridge (MA), U.S. Grant Bridge (OH), Greenville Bridge (MS), William Natcher Bridge (KY), Maysville-Aberdeen Bridge (KY), and Cape Girardeau Bridge (MO). As a manufacturer proprietary item, test data demonstrating their effectiveness is generally available from the cable suppliers (Figure 19).

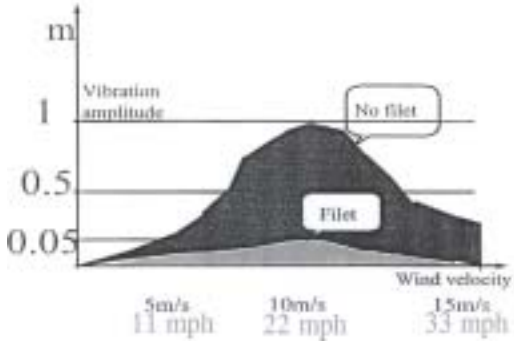

Figure 19: Example of test data for spiral bead cable surface treatment.

3.5 FIELD MEASUREMENTS OF STAY CABLE DAMPING

Leonard P. Zakim Bunker Hill Bridge (over Charles River in Boston, MA)

FHWA performed measurements during construction of the Leonard P. Zakim Bunker Hill Bridge (Figure 20), a cable-stayed bridge with inverted-Y shaped towers and a main span of 745-ft (227-m). The bridge is 183-ft (56-m) wide with 10 lanes (2 cantilevered lanes). The cables are ungrouted and arranged in a single plane for the back spans and two inclined planes for the main span. External visco-elastic dampers at the roadway level, cable cross-ties, and a double helical fillet cable surface treatment were applied to mitigate cable vibrations. Measurements were taken before and after installation of dampers and cross-ties.

Figure 20: Leonard P. Zakim Bunker Hill Bridge.

Preliminary results available as of this writing (private communication – reported data has not been independently verified by the study team) demonstrate the effectiveness of these mitigation methods. Table 6 shows the fundamental frequencies and damping ratios for the longest cables of the bridge before and after damper installation. In general, results show that the addition of dampers increases the frequency (by about 10%) and significantly increases the damping of the cables. Further evaluation of the measurements may be necessary, particularly since the data indicate that a few cables have smaller damping ratios after addition of dampers. In general, the damping ratio of ungrouted cables without external dampers appear to vary from 0.10% to 0.36% with an average of 0.20%. The external dampers raise the cable damping to an average of 0.37%.

Figures 21, 22, and 23 show the time histories of decay of manually excited cables before installation of dampers and cross-ties, after damper installation, and after cross-tie installation, respectively. The preliminary results demonstrate the effectiveness of not only the dampers, but also the cable cross-ties in raising the level of effective damping of the cable system. As the test method consisted of exciting one cable and recording the decay of its oscillations, some energy transferred from the excited cable to the adjoining cables through the cross-ties. Thus the reported damping with cross-ties may reflect values higher than the actual damping in the global system.

Table 6: Preliminary cable damping measurements - Leonard P. Zakim Bunker Hill Bridge.

Cable	Length (ft)	No Dampers Freq. (Hz)	No Dampers Damping Ratio	After Damper Installation Freq. (Hz)	After Damper Installation Damping Ratio
C1N	336	1.11	0.23%	1.21	0.46%
C2N	321	1.16	0.24%	1.27	0.37%
C3N	306	1.29	0.20%	1.42	0.44%
C32NE	397	0.96	0.20%	1.09	0.11%
C32NW	397	0.93	0.34%	1.14	0.34%
C33NE	417	0.89	0.14%	1.04	0.33%
C33NW	417	0.90	0.36%	1.04	0.44%
C34NE	438	0.86	0.10%	1.04	NA
C34NW	438	0.86	0.17%	0.97	0.38%
C34SW	422	0.89	0.14%	1.01	0.35%
C34SE	422	0.85	0.20%	1.05	0.14%
C33SW	402	0.91	0.28%	1.04	0.38%
C33SE	402	0.94	0.11%	1.10	0.34%
C32SW	383	1.01	0.12%	1.14	0.60%
C32SE	383	0.99	0.16%	1.14	0.40%
C3S	315	1.21	0.21%	1.33	0.36%
C2S	331	1.11	0.18%	1.22	0.58%
C1S	346	1.08	0.14%	1.16	0.27%
AVERAGE	382	1.00	0.20%	1.13	0.37%

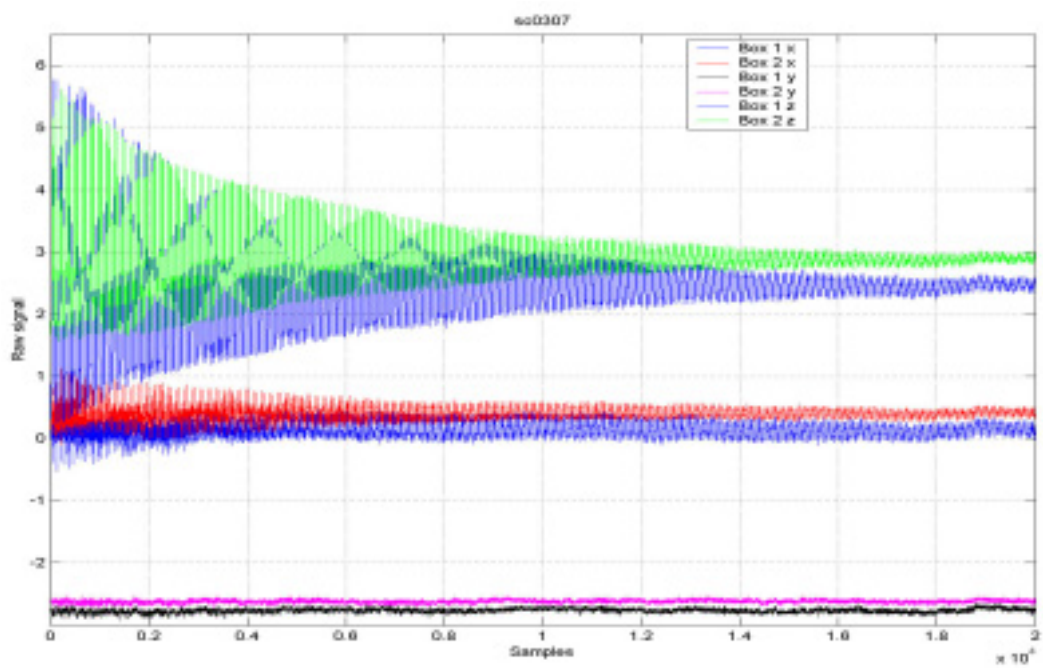

Figure 21: Sample decay: No damping and no cross-ties.

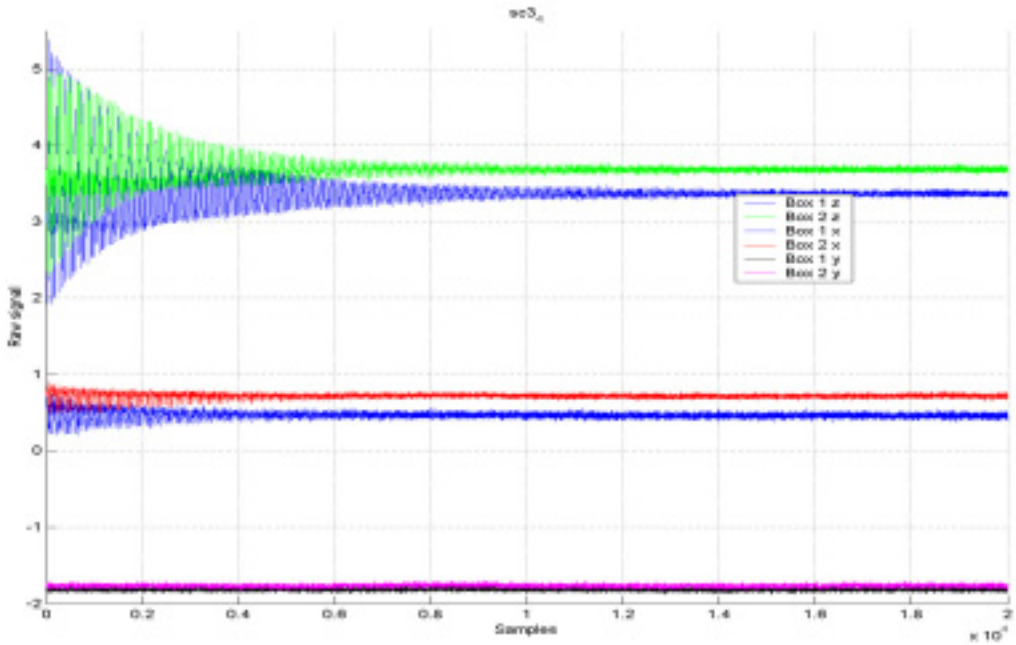

Figure 22: Sample decay: With damping and no cross-ties.

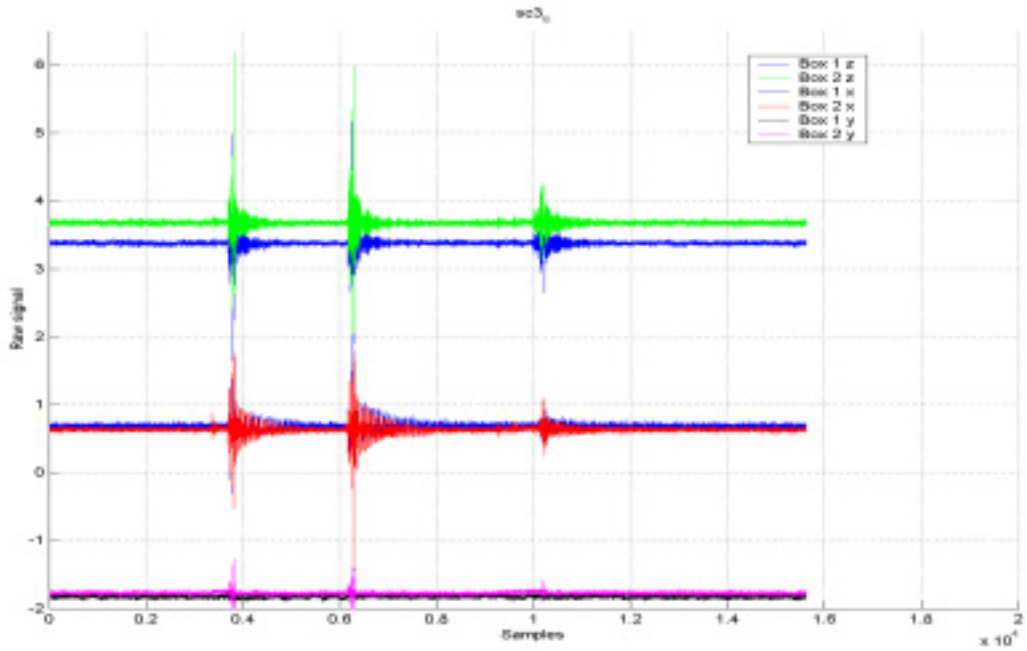

Figure 23: Sample decay: With damping and cross-ties.

Sunshine Skyway Bridge (St. Petersburg, FL)

The Sunshine Skyway Bridge (Figure 24) has been in service since 1982 and has not had reported problems with cable vibrations. The bridge has a main span of 1200-ft (366-m) between two single-mast towers and 84 cables in a single cable plane. The cables are provided with external viscous dampers (Figure 25), but no cross-ties or surface treatment.

Figure 24: Sunshine Skyway Bridge.

Figure 25: Stay and damper brace configuration.

Field measurements on the cables of the Sunshine Skyway Bridge were taken to study damping in multiple modes of vibration. This data provides a baseline for comparison of future measurements to evaluate cable damping performance of other cable-stayed bridges. Table 7 contains preliminary frequency and damping estimates from the ambient data (private communication).

What also makes this set of data interesting is that the cables on the Sunshine Skyway Bridge are all installed with two inclined struts that are each connected to three viscous dampers. This type of configuration enables the dampers to provide supplemental damping in two directions, unlike the case of the dampers on the Fred Hartman Bridge, which are oriented in the in-plane direction only. In fact, no excessive cable vibrations have been reported for the Sunshine Skyway Bridge, even though it is located in a region full of frequent wind and rain, while for the cables of the Fred Hartman Bridge there were still cases of some reported large-amplitude vibrations in the lateral direction that could not be suppressed by the damper.

Table 7: Preliminary cable damping measurements from the Sunshine Skyway Bridge.

Cable	Mode 1		Mode 2		Mode 3	
	Frequency (Hz.)	Damping (%)	Frequency (Hz.)	Damping (%)	Frequency (Hz.)	Damping (%)
N01	2.92	0.30%	5.87	0.10%	8.88	0.13%
N03	2.24	0.47%	4.52	0.24%	6.80	0.11%
N05	1.66	0.48%	3.32	0.19%	N/A	N/A
N07	1.41	0.36%	2.82	0.19%	4.24	0.13%
N09	1.19	0.48%	2.37	0.36%	3.57	0.22%
N10	1.08	1.05%	2.21	0.38%	3.33	0.30%
N11	1.02	0.69%	2.00	N/A	3.07	0.24%
N12	0.97	1.12%	1.92	0.48%	2.89	0.30%
N13	0.92	0.70%	N/A	N/A	N/A	N/A
N15	0.83	0.40%	1.64	0.53%	2.46	0.27%
N18	0.73	0.50%	1.44	0.35%	N/A	N/A
N20	0.62	N/A	1.25	0.37%	1.89	0.56%
N21	0.61	N/A	1.20	0.37%	N/A	N/A
N22	0.61	N/A	1.21	0.70%	1.82	0.36%
N23	0.65	N/A	1.29	N/A	1.93	0.24%
N24	0.68	N/A	1.34	N/A	N/A	N/A
N25	0.72	0.37%	1.43	0.29%	2.15	0.28%
N26	0.77	1.53%	1.52	0.55%	2.28	0.42%
N28	0.81	0.61%	1.60	0.43%	N/A	N/A
N30	0.89	0.65%	1.77	0.37%	2.67	0.28%
N32	1.00	0.79%	2.00	0.25%	3.01	0.20%
N34	1.12	N/A	2.24	N/A	3.40	0.16%
N36	1.34	0.69%	2.66	0.33%	3.99	0.21%
MIN	0.61	0.30%	1.2	0.10%	1.82	0.11%
MAX	2.92	1.53%	5.87	0.70%	8.88	0.56%
AVERAGE	1.08	0.66%	2.16	0.36%	3.43	0.26%

3.6 BRIDGE USER TOLERANCE LIMITS ON STAY CABLE VIBRATION

Field records from the large amplitude cable vibrations typical of rain/wind vibration episodes have noted that such vibrations can have the effect of alarming bridge users and general observers on the safety of the structure. In reality however, even for extreme cases, such vibrations have only produced limited damage to non-structural cable anchorage components. In closer examination, even these failures of the secondary elements can generally be traced to fatigue prone or other unsuitable details. There is little field evidence to indicate permanent structural damage to the cables or other primary load carrying members as a result of rain/wind vibrations on the affected bridges. A detailed examination of the level of stress generated in the primary elements due to these oscillations may generally indicate that the amplitude of dynamic stresses are not high enough to be a serious fatigue issue for cable strands or other bridge components either.

While the design displacements based on fatigue (or other design criteria) can be readily obtained through proper engineering calculations, there is little information in the literature to determine what level of cable oscillations can be permitted based on user tolerance to such displacements. In some cases, it can be expected that the displacement limits based on user acceptance may govern over those based on direct stress evaluation. The user acceptability threshold for a rural high level crossing where the observer is the motorist could be much less critical than that for an urban bridge where the public may be able to observe the bridge in close proximity. Detailed determinations of such limits are both complex and somewhat subjective. Thus, at least a preliminary identification of these human comfort thresholds was deemed important in developing design guidelines.

A design criteria set forth by these factors would be independent of those required by the structural effects involved, similar in nature to existing codes limiting deflection in bridges or drift in tall buildings. The human mechanism of perception of stay cable vibration is quite different from, say, the perception of building or floor movement by an occupant. The former is purely visual where as the latter is mostly physical feel. If a building occupant is near a window, some visual aspects of building movement with respect to fixed features of the landscape may become apparent. However, buildings rarely may exhibit such levels of movement and it is likely that other design criteria may prohibit a building design this flexible. Building occupant comfort is typically ensured by limiting acceleration and jerk (rate of change of acceleration). For torsional movements of tall buildings however, there are some limits based on visual perception that may have some level of similarity to the case under study. The parameters may be:

- User Proximity (Rural setting vs. urban)
- Cable diameter
- Cable displacement
- Mode shape
- Cable length
- Velocity

Focusing on typical cable sizes and typical vibration frequencies applicable to practical situations can further condense these parameters.

The study of user tolerance limits described in Appendix D3 was an attempt to establish some preliminary criteria on user perception of stay cable vibrations. In this study, user perception was determined with vibration mode-shape, velocity, and vibration amplitude as variables.

The two most important factors affecting user comfort were found to be the amplitude of the vibration and the velocity. As the frequency range is somewhat limited, it would stand to reason that the comfort criteria could be based on the amplitude. The study indicated that a reasonable recommendation of a limit on vibration amplitude (single) would be 1 cable diameter. Ideally, further reducing this to 0.5 diameters or below has the effect of making the vibrations virtually unnoticeable.

This study is preliminary and based on a relatively small sample size. Therefore, further investigation should be performed to refine any design criteria based on user comfort.

4 DESIGN GUIDELINES

4.1 NEW CABLE-STAYED BRIDGES

1. General:

A sufficiently detailed cable vibration analysis (including modal analysis of the cable system) must be performed as part of the bridge design to identify the potential for cable vibration. The following factors must be examined: the dynamic properties of the cables, dynamics of the structural system, geometry of the cable layout, cable spacing, exposure conditions, and estimated Scruton Numbers (S_c).

2. Mitigation of Rain/Wind Mechanism:

At a minimum, providing an effective surface treatment for cable pipes to mitigate rain/wind vibrations is highly recommended. One common method is the use of double-helical beads. The effectiveness of the surface treatment must be based on the tests applicable to the specific system, provided by the manufacturer.

3. Additional Mitigation:

Depending on the outcome of the vibration study (Item 1), the provision of at least one of the following major cable vibration mitigation measures (in addition to surface treatment) is recommended:

- Additional damping (using external dampers)
- Cable cross-ties

4. Minimum Scruton Number

Following are minimum desired Scruton Numbers (S_c):

$m\zeta / \rho D^2 > 10$	for regular cable arrangements
$m\zeta / \rho D^2 > 5$	for cable pipes with effective surface treatment suppressing rain/wind vibrations (see note below)

Note: Limited tests (Larose & Smitt, 1999) on cables with double-helix surface treatments have suggested that $m\zeta / \rho D^2 > 5$ may be acceptable. However, it is felt that such reductions should be made only for regularly spaced single cable arrangements. In general it is recommended to keep the Scruton Number as high as possible by providing external dampers and/or cross-ties. For unusual geometry or double stay arrangements where parallel stays are placed within close proximity to one another, careful case-by-case evaluation of these limits are recommended.

5. External Dampers:

Manufacturer warranties should be provided for all damping devices. Most dampers used in bridges are proprietary items and design details should be provided by the manufacturer.

A damper can be tuned to yield optimal damping in any one selected mode (see Figure 8). For other modes the level of damping will be less than this optimal value. Rain/wind vibrations occur predominantly in mode 2. Therefore, if a damper is to be tuned to a particular mode to mitigate rain/wind vibrations, it appears logical to select mode 2.

There are many types and designs of dampers, and linear dampers have been shown to be effective through their widespread use in the past. However, recent analytical studies show that non-linear dampers can be used to provide a more optimal condition than linear dampers, as these are effective over a larger range of modes. In particular, the damping performance of square-root dampers (β=0.5) is independent of the mode number and is only affected by the amplitude of vibration.

With some dampers (such as dash-pot type), an initial static friction force must be overcome before engaging of the viscous element. Field experiments have shown the presence of this stick-move-stick-move behavior associated with such dampers. This may effectively provide a fixed node instead of the intended damping for the cable at low amplitude oscillations, and should be considered. The visco-elastic type dampers where an elastomeric element is permanently engaged between the cable and the supporting elements, theoretically, are free of such initial frictional thresholds. On the other hand, there are also damper designs that rely on friction as the energy dissipation mechanism and the static friction threshold for such dampers may be higher than for the other types.

Another factor needing consideration is the directionality of the damper. The cable vibrations observed in the field indicate both vertical and horizontal components of motion. Some damper designs are antisymmetric and provide damping against cable motion in any direction. Other dampers (e.g. dash-pot types) provide damping against motion only along the axis of the damper. It is possible to arrange two or more such dampers so that the combination is effective in all directions. As the majority of the observed motion due to rain/wind vibrations is in the vertical direction, it may be sufficient to provide damping against only the vertical motion. However, this has not been clearly established. It is recommended that damping be made effective against cable movement in any direction.

Damper mounting details may transfer lateral forces due to damper action onto components of the cable anchorage. Such forces must be considered in the design of the cable anchorages.

6. Cable Cross-ties:

If used, provide clear and mandatory specifications for cable cross-ties. Experience shows that cross-ties, when properly detailed and installed, can be an effective method for suppressing undesirable levels of cable vibrations. Reported failures of cross-ties have been generally traced to improper details and material selection.

The use of cross-ties creates local modes, which must be considered in design. The frequency of the first plateau of local modes (see Section 3.4) should be kept as high as possible. Symmetric configurations of the restrainers with respect to intermediate-length cables is preferred to increase the frequency interval (lower limit in particular) corresponding to local modes, since they minimize the longest segment length.

Cable cross-ties must be provided with initial tension sufficient to prevent slack of the cross-ties during design wind events. The level of tension depends on the dynamic properties of the cable system and the design wind event. The initial cross-tie tensions must be established based on rational engineering analysis. Also, the tie to cable connection must be carefully designed and detailed for the transfer of the design forces.

7. User Tolerance Limits:

A preliminary survey (see Appendix D3) on sensitivity of bridge users to stay cable vibrations has indicated that the comfort criteria for cable displacement can be described using the following maximums (within 0.5 to 2.0 Hz range):

- 0.5 D (Preferred)
- 1.0 D (Recommended)
- 2.0 D (Not to Exceed)

While this aspect may need further study, the above can be used as a guide when such displacements can be computed and/or needed as input for design of such elements as dampers and cross-ties. The displacement limits need not be considered for extreme events.

4.2 RETROFIT OF EXISTING BRIDGES

If an existing bridge is found or suspected to exhibit episodes of excessive stay cable vibration, an initial field survey and inspection of the cable system should be performed to assemble the following information:

- Eye-witness accounts, video footage of episodes
- Condition of the stay cable anchorages and related components, noting any visible damage and/or loose, displaced components

A brief field instrumentation and measurement program can be used to obtain such parameters as the existing damping levels of the cables. Instrumentation of cables to record the vibration episodes, wind direction, wind velocity, and rain intensity during their occurrences could also provide some confirmation of the nature of cable vibrations.

The mitigation methods available for retrofit of existing bridges follow closely those provided for the new bridges. However, the application of surface treatment may be difficult, not practical, or cost prohibitive on existing structures. The addition of cross-ties and/or dampers is recommended.

A split-pipe with surface modifications can be installed over the existing cable pipe if this is found to be practical and cost effective. In many of the older bridges for cables using polyethylene (PE) pipes, ultraviolet (UV) protection to cable pipes is provided by wrapping the PE pipe with Tedlar tape. These cables require periodic re-wrapping as part of routine maintenance. The newer high-density polyethylene (HDPE) cable pipes are manufactured with a co-extruded outer shell that provides the needed UV resistance, thus providing a split-pipe as a secondary outer pipe has the added benefit of eliminating the need for future Tedlar taping for the UV protection.

In addition, any damaged cable anchorage hardware must be properly retrofitted or replaced. It is recommended that the original cable supplier be contacted to ensure the replacement of cable anchorage components and that the addition of mitigative devices are compatible with the original design of the stay anchorage area.

4.3 WORKED EXAMPLES

EXAMPLE 1

The following application shows how the information presented in this report can be used to assess the vulnerability of a given cable and provide mitigation measures.

Properties:

Assume the following has been established based on the site meteorological data:

Wind velocity for structural design : 90 mph (100 year return)
Wind velocity for stability design : 130 mph (10,000 year return)

Cable C1: Total length = 350 ft.
Exterior Diameter = 11 in.
Mass = 127 lb/ft
Tension = 1485 kips (under dead load)

As the live load cable tension under normal service is only a small fraction of the dead load, the cable vibration evaluations typically ignore the live load.

Under dead load, the modal frequencies of the cable are computed to be:

f_1 = 0.875 Hz
f_2 = 1.750 Hz
f_3 = 2.625 Hz

Rain/Wind:

Design for $S_c = m\zeta / \rho D^2 \geq 10$, as established in the design guidelines
Note that typical damping inherent in cables are in the range of 0.1 to 0.2%.

For $S_c = m\zeta / \rho D^2 \geq 10$, using $\rho = 0.0765$ lb/ft^3,
the minimum damping required for $S_c \geq 10$ is $\zeta \geq 0.005$ (0.5%).

Galloping:

(Note that the present investigation has shown that galloping is not a major issue for normally spaced cable stays. However this is included in this example to demonstrate its application.)

The critical wind velocity for onset of galloping was given in Equation 6: $U_{CRIT} = c\, f\, D\sqrt{S_c}$

The numerical value of the constant c is typically taken as:

for wake galloping, c = 25 for closely spaced cables (2 to 6D)
c = 80 for normally spaced cables (10 to 20D)

for inclined dry cable galloping, c = 35*

As galloping leads to divergent oscillations, it is considered a stability issue and the critical wind speed for onset of galloping is desired to be over 130 mph.

For $U_{CRIT} = c\, f\, D\sqrt{S_c} \geq 130$ mph (190.7 ft/sec),

$$f \geq \frac{U_{CRIT}}{cD\sqrt{S_c}} = \frac{65.8}{c}$$

Assuming $S_c \geq 10$, $f \geq$ 2.63 Hz for c = 25 (closely spaced cables)
0.82 Hz for c = 80 (normally spaced cables)
1.88 Hz for c = 35*

Design Options:

A) If the cable geometry falls within normal cable spacing and ignoring dry inclined galloping*:

Galloping: The requirement for mitigation of wake galloping is automatically met (f_1 = 0.875 Hz $> f$ = 0.82 Hz). Thus cable cross-ties are not required to raise the natural frequency of the cable.

Rain/Wind: For rain wind, two options exist – (i) damping and (ii) cross-ties

i) provide damping such that $\zeta \geq 0.005$ (0.5%, corresponding to $S_c = 10$)

Assuming $\zeta \geq 0.005$ is to be achieved in the 1st mode and the damper is to be located 11'-8" from the lower anchorage of the cable,

$$\frac{\zeta_i}{l/L} = \frac{0.005}{11.67\text{ft} / 350\text{ft}} = 0.15$$

*Note that the wind tunnel tests conducted in the current study indicate that this can be ignored for normally spaced cables with damping ratios exceeding about 0.3%.

From Figure 8 and Equation 11a, $\kappa = \frac{c}{mL\omega_{ol}} i \frac{l}{L} = 0.0125$

Therefore $c = 0.0125 \frac{mL\omega_{ol}}{i} \frac{L}{l} = 0.0125 \frac{(127\text{lb/ft})(350\text{ft})(2\pi * 0.875/\text{sec})}{i * 0.0333} * \frac{\text{slugs}}{32.2\text{lb}}$

$$c = \frac{2850}{i} \frac{\text{slugs}}{\text{sec}} = \frac{2850}{i} \frac{\text{lbf sec}}{\text{ft}}$$

Rain/wind vibrations generally involve the first 3 modes of cable vibration, mode 2 being the most predominant.

Provide $\zeta_1 = 0.005$ (1st mode damping ratio 0.5%)

This requires a damper with a damping constant

$c = \frac{2850}{i}$ lbf-sec/ft = 2850 lbf-sec/ft

Compute damping ratio in 2nd and 3rd modes:

2nd mode (i=2): $\kappa = \frac{c}{mL\omega_{ol}} 2 \frac{l}{L} = 0.0250$

From Figure 8, $\frac{\zeta_2}{l/L} = 0.23$, therefore $\zeta_2 = 0.0077$ (>0.005 OK)

3rd mode (i=3): $\kappa = \frac{c}{mL\omega_{ol}} 3 \frac{l}{L} = 0.0375$

From Figure 8, $\frac{\zeta_3}{l/L} = 0.36$, therefore $\zeta_3 = 0.0120$ (>0.005 OK)

Therefore, a damper with a damping coefficient of c = 2850 lbf-sec/ft at 11'8" from the lower end anchorage provides the following damping ratios for the first 3 modes.

Mode 1	$\zeta_1 = 0.0050$ (0.50%)	and	$S_c = 10.0$
Mode 2	$\zeta_2 = 0.0077$ (0.73%)	and	$S_c = 15.2$
Mode 3	$\zeta_3 = 0.0120$ (1.17%)	and	$S_c = 23.7$

These are considered sufficient to mitigate rain/wind vibrations based on the Scruton number criterion. Note that the above computation ignores the natural damping present in the cable. Hence the actual Scruton numbers, including the inherent damping, will be larger than those computed, making the design somewhat conservative.

ii) provide cable cross-ties

Note that by providing two cable cross-ties at the 1/3 points cable modes 1 and 2 are eliminated, raising the natural frequency of the cable net to about 2.63 Hz. The cable cross-ties also raise damping of the cable system considerably, as demonstrated by the preliminary vibration measurements taken from the Leonard P. Zakim Bunker Hill Bridge (Section 3.4).

B) If the cables are spaced closer together, using

$$U_{CRIT} = 25\, f\, D\sqrt{S_c} \geq 130 \text{ mph}, \quad f = 2.63 \text{ Hz}$$

It is noted that providing two cable cross-ties at the 1/3 points would raise the natural frequency to 2.63 Hz. This is out of range for rain/wind vibrations. It is generally believed that additional dampers can be neglected as the cable cross-ties are more than likely to raise the damping ratio beyond the 0.5% needed for mitigating rain/wind vibrations

Summary:

Thus the cable vibration mitigation following recommendations of the current study would consist of:

a) For normal cable arrangements : Either a damper with c = 2850 lbf-sec/ft mounted 11'8" from the end anchorage **or** cable cross-ties at 1/3 points

b)For closely spaced cable arrangements : Cable cross-ties at 1/3 points. The designer can consider providing additional damping depending on the details of the project, careful analysis of the specifics, and engineering judgement and expertise.

In all cases an effective surface treatment such as the double helix spiral beads provided by leading cable manufacturers is recommended for normal cable spacings. Limited tests show that the damper size may be reduced by as much as 50% with an effective surface treatment. Note that the elimination of dry inclined cable galloping as a design consideration for normal cable arrangements makes it possible to provide a mitigation design using only dampers, without the use of cross-ties.

EXAMPLE 2

Example 1 demonstrated the use of the design guide in sizing the dampers so that the minimum Scruton number criteria is met for the 1st and higher modes. Example 2 is based on data provided in Table 4, and is an illustration of providing maximum possible damping in mode 1.

Data from Table 4

	Stay Properties			Damper Properties		
	Length	Outside Diameter	Mass	Natural Frequency	Location	Damping Constant
Stay name	L ft (m)	D in (mm)	m lbf/ft (kg/m)	f_{o1} Hz	ℓ/L	c lbf-s/ft (kN-s/m)
AS16	285 (87.0)	5.5 (140)	32.2 (47.9)	1.24	.045	4800 (70.0)
AS23	599 (182)	6.3 (160)	50.0 (75.9)	0.64	.037	12000 (175.1)

Cable AS16:

Equation 11a: $\kappa = \frac{c}{mL\omega_{ol}} i \frac{l}{L} = \frac{(4800\text{lbf sec/ ft})(0.045)}{(32.2\text{lb/ ft})(285\text{ft})(2\pi * 1.24/\text{sec})} * (32.2 \frac{\text{lb}}{\text{slug}}) * i = 0.0973 * i$

Equation 11b: $\frac{\zeta_i}{l/L} = \frac{\pi^2 \kappa}{(\pi^2 \kappa)^2 + 1}$

Mode 1 $\kappa = 0.0973$, $\frac{\zeta_1}{l/L} = 0.500$, $\zeta_1 = 0.045*0.500 = 0.0225$ (2.3%), Sc = 45.1

Mode 2 $\kappa = 0.1946$, $\frac{\zeta_2}{l/L} = 0.410$, $\zeta_2 = 0.045*0.410 = 0.0184$ (1.8%), Sc = 36.9

Mode 3 $\kappa = 0.2919$, $\frac{\zeta_3}{l/L} = 0.310$, $\zeta_3 = 0.045*0.310 = 0.0140$ (1.4%), Sc = 28.1

Cable AS23:

Equation 11a: $\kappa = \frac{c}{mL\omega_{ol}} i \frac{l}{L} = \frac{(12000\text{lbf sec/ ft})(0.037)}{(50.0\text{lb/ ft})(599\text{ft})(2\pi * 0.64/\text{sec})} * (32.2 \frac{\text{lb}}{\text{slug}}) * i = 0.1187 * i$

Mode 1 $\kappa = 0.1187$, $\frac{\zeta_1}{l/L} = 0.494$, $\zeta_1 = 0.037*0.494 = 0.0183$ (1.8%), Sc = 43.4

Mode 2 $\kappa = 0.2374$, $\frac{\zeta_2}{l/L} = 0.361$, $\zeta_2 = 0.037*0.361 = 0.0134$ (1.3%), Sc = 31.8

Mode 3 $\kappa = 0.3561$, $\frac{\zeta_3}{l/L} = 0.263$, $\zeta_3 = 0.037*0.263 = 0.0097$ (0.97%), Sc = 23.0

Note that the optimum value of $\zeta/(l/L)$ for linear dampers near the end of the stay is approximately 0.50, as is evident from Figure 8. For cables AS16 and AS23, the damping provided in the 1st mode is very close to this optimum, with damping in higher modes falling below the optimal level. The damper coefficients for the dampers used here are very large compared to the value obtained in Example 1, and the Scruton Numbers for modes 1-3 are much greater than the minimum of 10 recommended for suppression of rain/wind vibrations.

5 RECOMMENDATIONS FOR FUTURE RESEARCH AND DEVELOPMENT

The design guidelines provide a concise approach to suppress wind-induced vibrations in cable-stayed bridges, and are based on the existing knowledge base and further investigations performed through this project. While the design recommendations are empirical, the mitigation methods discussed (dampers, cable cross-ties, and surface modification) are proven to be effective through both past experience and research. Future research in the following areas clarifying some of the remaining key issues would strengthen the design guidelines.

This is the first time a set of design guidelines have been proposed for the mitigation of stay cable vibration. It is expected that future adjustments based on actual cable performance and advances in cable technology may require further refinements to the design guidelines.

1. Wind-tunnel testing of dry inclined cables.

Galloping of dry inclined cables was investigated using wind-tunnel testing in the current study and was found to be less critical than previously believed. However, further research would be valuable to confirm the findings and to study the effects additional parameters. Future wind-tunnel testing could include :

- More data points to validate the first 2 phases
- Study the effect of cable frequencies, which are potentially important for the aerodynamic behavior of the inclined dry cable
- Further study of the Reynolds number effect, resulting from the model surface condition and the orientation angle

2. Deck-induced vibration of stay cables.

Deck-induced vibration of stay cables has been observed in a few instances in the field-measured data, occurring in the fundamental mode of a stay with quite large amplitudes. Further investigation of this potential source of excitation would be beneficial, and may include comparison of analytical predictions and field measurements and analytical modeling of the influence of attached dampers. Effort needs to be made to identify more records in which interaction is evident between vibrations of the bridge deck and stays. As more and more newer bridge superstructure sections are aerodynamically refined to mitigate vortex-induced oscillations of the roadway as a user comfort criteria, the deck-stay interaction may become primarily an issue for older bridges.

3. Mechanics of rain/wind induced vibrations.

Rain/wind vibrations appear to be the most problematic of the measured vibrations, with their large amplitudes and relatively frequent occurrence, and are among the most significant considerations in the design of mitigation measures for stay cables. One of the primary components of future research could be to develop a more in-depth understanding of the underlying mechanics of rain/wind induced stay-cable vibration. This effort would have a focus somewhat different from that adopted in this study, where the objective was simply to develop a

sufficient understanding to be able to arrest the practical occurrence of objectionable levels of stay cable vibrations. It is believed that such an in-depth study could build upon the findings from this and other recent projects, and include continued detailed analysis of the wealth of full-scale data collected (data on U.S. bridges as well as large-scale data from Japan as available) and a critical review of existing proposed mechanisms.

This effort may include the following two components: identification of key observed characteristics and evaluation of proposed mechanisms. Further analysis of the measured vibration records both before and after the damper installation could provide additional insight into the nature of the rain/wind excitation mechanism and clarify which types of proposed mechanisms are more appropriate. A good start on this task has already been made, but there are more data that need to be carefully analyzed that were outside the present project scope. Some of the more interesting observations need further detailed investigation using the diverse data sets.

Many of the proposed mechanisms were postulated based on wind tunnel investigations. While useful, some caution must be taken in interpretation of these data as field conditions may contain three-dimensionality of the flows that the wind tunnel testing cannot replicate.

4. Develop a mechanics-based model for stay-cable vibration enabling the prediction of anticipated vibration characteristics.

In designing effective and economical dampers for rain/wind vibration suppression, it would be of great assistance to have a model with the capability to predict, for an arbitrary stay cable, the following characteristics of rain/wind vibration:

- Preferred Mode: The full-scale measurements have indicated that rain/wind vibrations tend to occur in a preferred mode over a fairly wide range of wind speeds; for a given stay, which mode(s) will be preferred?
- Wind Speed and Direction: Over what range of wind speeds and wind directions will the problematic vibrations occur? (This question is actually not of significant concern in the design of dampers.)
- Damping Levels: How much damping is necessary to adequately suppress vibrations?
- Amplitudes, Forces, and Power: What will be the steady-state amplitudes as a function of damping ratio? What levels of force may be expected in the damper, and what will be the power dissipation demands?

It is likely that rain/wind vibrations can be modeled in a manner similar to vortex-induced vibrations: as a nonlinear oscillator characterized by a negative-damping type instability at small amplitudes, and a limit cycle at large amplitudes. Such a model could be developed using the following steps:

- Obtain reliable estimates of inherent mechanical damping in the undamped stays, as inherent damping is expected to be a critically important parameter in estimating oscillation amplitudes.
- Identify records from various stays corresponding to the onset of rain/wind vibration, and characterize the energy input as a function of amplitude.

- For each stay, from the records collected previously, identify an election of "worst-case" time histories corresponding to the maximum energy input under the ideal wind conditions for rain/wind vibration.
- Using parameters such as inherent mechanical damping; stay length, diameter, tension, and mass/length; wind speed and air density, obtain the best possible normalization of the "worst-case" energy-input versus amplitude curves so that the curves from various stays can collapse (almost) onto a single curve.
- Identify a nonlinear oscillator model that can capture the measured energy input versus amplitude curves, and use the field-measured data to estimate the model parameters.
- Investigate the dependence of the model parameters on wind speed and wind direction for the various stays, and identify appropriate normalizations of these parameters to allow comparison among stays.

There are strong indications that a nonlinear negative damping model may be a promising approach. This is based upon observation of what appears to be a negative-damping type of instability for small amplitudes, causing the amplitude to increase until a limit cycle is reached. Vibrations occur over a fairly narrow range of wind directions, and occur in one or two preferred modes over a fairly wide range of wind speeds. These observations and potential model can be used to carefully evaluate proposed mechanisms for consistency and reasonableness.

While ultimately the model resulting from the proposed work may take the form of an analytical formulation, in which equations of motion for cable vibration are expressed mathematically, it may also be an empirical model which seeks to obtain a good fit to the field measurements from different stays, it may simply take the form of general conclusions achieved from a statistical analysis of the measured vibrations, or it may represent a combination of the three approaches.

Such a model will enable a much more comprehensive treatment of the problem both in terms of when such vibrations are likely to occur, and what (quantitatively) will be the effect of various mitigation approaches: dampers, cross-ties, and aerodynamic treatments. The ability to do such analysis presently does not exist.

5. Predict the performance of stay cables after mitigation using the model.

The most practical application of such a model would be to be able to predict the level of stay oscillations after the application of mitigation methods. This would also enable the combination of important observations from the modeling of the field-measured vibrations and from the analysis of the restrained system in order to predict performance after vibration mitigation efforts (specifically dampers and cross-ties). Special attention again could be devoted to a discussion of the mitigation of rain/wind induced vibration. Mitigation of other types of vibration, such as vortex-induced vibrations, particularly in the higher modes and deck-stay interaction could also be evaluated. More in-depth analysis of field measurements of damper performance can also be performed in order to compare measured and predicted oscillation amplitudes after mitigation.

6. Perform a detailed quantitative assessment of various alternative mitigation strategies.

As has been demonstrated in this report, dampers are not the only method available for mitigation of stay-cable vibration. Other potentially suitable solutions include the provision of additional damping by other means, such as redesigned anchorages, cross-ties, and aerodynamic treatments. It is considered important to assess their relative performance using the model. It is noted that we have data from stays with cross-ties from the Fred Hartman Bridge, and stays with aerodynamic treatments (rings) from the Veterans Memorial Bridge. In addition, efficient analytical/numerical tools for the prediction of the dynamic response of two-dimensional cable "networks" (representing cross-tied stay systems) have been developed using this project.

Using the results of the predictions (Item 5), the performance of these approaches can be compared and this information used to evaluate the suitability of the various methods. Important economic assessments must also be considered.

7. Improved understanding of inherent damping in stays and that provided by external devices.

The inherent damping in a cable, generally accepted to be fairly low, is not readily quantifiable, and there are very few reported measurements. A better understanding of damping in cables (both with and without external dampers) could have some benefit in practical applications from extensive field measurements, so as to facilitate more effective and rational mitigation of stay cable vibrations. Substantial progress has been made towards this goal by analyzing the full-scale measurement data collected at the Fred Hartman Bridge and by preliminarily estimating modal frequencies and damping ratios for two cables on the bridge as described in this report. By comparing the amplitudes of vibrations before and after damper installation, dampers were found to be generally successful in mitigating the vibrations. In a few cases, when the vibrations were primarily in the lateral direction and the dampers were oriented in the in-plane direction, there is evidence that the dampers were not effective at suppressing them.

Frequency shifts caused by the dampers were also clearly identified and the discovered relationship between modal frequency and vibration amplitude seems to be in agreement with the actual configuration of the cable-damper system in the field. Compared to frequency estimation, results from damping estimation are more complicated: modal damping ratios estimated from different records are usually scattered and the relationship between these estimated damping ratios and the characteristics of the vibrations is still not very clear. Nonetheless, the results do suggest that the level of inherent damping in the cables is indeed very low and that the rain/wind mechanism introduces some kind of negative damping into the system, consequently making the vibration amplitude large.

Relationships between the modal damping ratios and such quantities as modal displacement and modal damper force need to be investigated. Testing of an actual damper is also deemed as beneficial. The damper should be driven by either force or displacement with different periods. Numerical simulation can also be used for this purpose and force-displacement curves thus obtained can be compared to field measurement data. It will be helpful to separate the part of the vibration when the damper is evidently engaged from the rest of the vibration when it is not

engaged e.g., by using wavelet transforms. Energy methods can also be applied to the part of the vibration when the damper is engaged to estimate the effective damping during that period of time.

Research so far has been concentrated on full-scale measurement data from two cables of the Fred Hartman Bridge. Data from other instrumented cables of this bridge and some cables of the Veterans Memorials Bridge, which were instrumented during the same period of time, are also available for analysis. In addition, forced vibration tests and short-term ambient tests have been conducted on some cables of the Sunshine Skyway Bridge in Tampa, Florida. Data collected from these tests are of special interest because cable damping can be estimated from the forced vibration tests using the logarithmic decrement method and compared with the values estimated from the ambient tests. No excessive cable vibration has been reported for the Sunshine Skyway Bridge so far, even though it is located in a region full of frequent wind and rain. More detailed analysis of the full-scale data from this bridge will help understand the reasons for these observations.

8. Improved understanding of cross-tie solutions.

As pointed out in the report, cross-ties combined with dampers seem to offer the possibility of enhanced performance over their component counterparts. Application of such a combined system has been previously discussed (Kumarasena, 1999). It is considered important to extend the modeling developed herein to better study and understand these characteristics, and to provide a tool for designers. The ability to optimize cross-tie configurations also seems to be an important area for future research.

9. Refine recommendations for effective and economical design of stay-cable vibration mitigation strategies for future bridges.

While the design recommendations proposed are believed to be sufficient as minimum criteria for practical mitigation of unacceptable levels of stay vibrations, these efforts could help by addressing quantitatively the following issues:

- How much supplemental damping should be provided in each mode for vibration suppression?
- Which type of nonlinear damper (including the case of linear) is most appropriate for cable vibration mitigation?
- For which mode of vibration should the damper performance be optimized?
- For what force levels and energy dissipation capacity should the damper be designed?

This project has been successful in producing a set of guidelines and recommendations for stay-cable vibration mitigation based on information available at the time of its conclusion. While this does include information based on a review of the literature and a significant amount of research on the characterization of field measurements and damper performance, the guidelines may be improved through the future research items proposed.

APPENDIX A1: DATABASE OF REFERENCE MATERIALS

An extensive amount of research was initially performed to form a baseline for the current study. An on-line database of references was created so that all members of the Research Team could add or extract information as necessary. The database includes the article titles, authors, reference information, and abstracts when attainable. There are 198 references in the database, including 89 with abstracts.

Search capability is also provided, with options to search by key word, author, source, and date. The search page is shown in Figure 26, and a search results page is shown in Figure 27. A full listing of the references in this database is included at the end of this appendix.

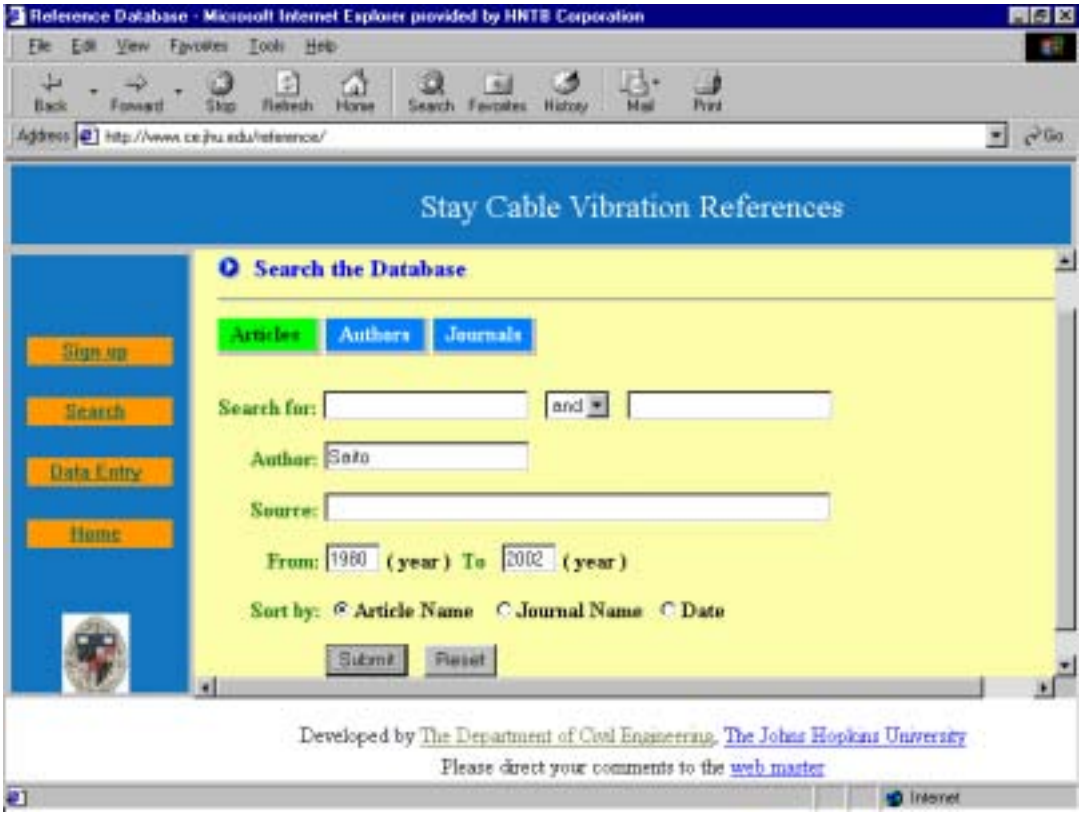

Figure 26: Reference database search page.

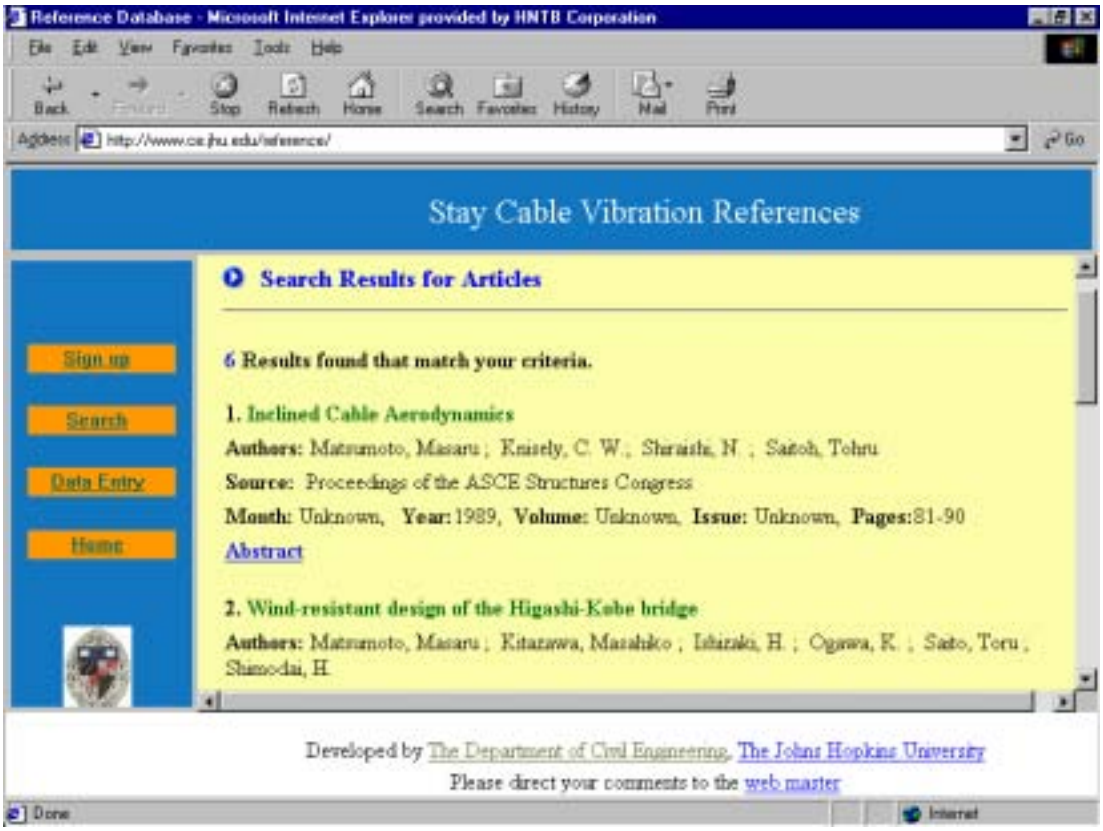

Figure 27: Reference database search results page.

List of References Included in Database

1. On the Parametric Excitation of a Dynamic System Having Multiple Degrees of Freedom
Authors: Fang, J.
Source: Journal of Applied Mechanics
Month: Sep, Year:1963, Volume: N/A, Issue: N/A, Pages: N/A
Abstract: N/A

2. On the Parametric Excitation of a Dynamics System Having Multiple Degrees of Freedom
Authors: Hsu., C. S.
Source: Journal of Applied Mechanics
Month: Sep, Year:1963, Volume: N/A, Issue: N/A, Pages: N/A
Abstract: N/A

3. Classic Normal Modes in Damped Linear Dynamic Systems
Authors: McConnell, Kenneth G.; Uhrig, A.
Source: Journal of Applied Mechanics
Month: Sep, Year:1965, Volume: N/A, Issue: N/A, Pages: N/A
Abstract: N/A

4. Mathematical analysis of transmission line vibration
Authors: Claren, R. ; Diana, G.
Source: IEEE Trans. on Power Apparatus and Systems
Month: N/A, Year:1969, Volume:Pas-88, Issue:12, Pages:1741-71
Abstract: N/A

5. Mechanisms and Alleviation of Wind Induced Structural Vibrations
Authors: Cooper, K. R.; Wardlaw, R. L.
Source: Proceedings of Second Symposium on Applications of Solid Mechanics
Month: N/A, Year:1974, Volume: N/A, Issue: N/A, Pages:369-99
Abstract: N/A

6. Steady State Response of a Dynamical System Under Combined Parametric and Forcing Excitations
Authors: Fang, J. ; Lyons, G. J.
Source: Journal of Applied Mechanics
Month: Jun, Year:1974, Volume: N/A, Issue: N/A, Pages: N/A
Abstract: N/A

7. Steady-State Response of a Dynamical System Under Combined Parametric and Forcing Excitations
Authors: Hsu., C. S.; Cheng, W. H.
Source: Journal of Applied Mechanics
Month: Jun, Year:1974, Volume: N/A, Issue: N/A, Pages: N/A
Abstract: N/A

8. The vortex induced oscillation of elastic structural elements
Authors: Iwan, W. D.
Source: Journal of Applied Mechanics
Month: N/A, Year:1975, Volume: N/A, Issue: N/A, Pages:1378-82
Abstract: N/A

9. Flow-induced vibration
Authors: Blevins, R. D.
Source: Van Nostrand Reinhold Company, New York
Month: N/A, Year:1977, Volume: N/A, Issue: N/A, Pages: N/A
Abstract: N/A

10. Harmonically Forced, Finite Amplitude Vibration of a String
Authors: Tgata, G.
Source: Journal of Sound and Vibration
Month: N/A, Year:1977, Volume:51, Issue:4, Pages: N/A
Abstract: N/A

11. The Generalized Harmonic Balance Method For Determining the Combination Resonance in the Parametric Dynamic Systems
Authors: Szemplinska-Stupnicka, W.
Source: Journal of Sound and Vibration
Month: N/A, Year:1978, Volume:58, Issue:3, Pages: N/A
Abstract: N/A

12. Cables wind excited vibrations of cable-stayed bridge
Authors: Wianecki, J.
Source: Proceedings of 5th International Conference of Wind Engineering, Colorado
Month: N/A, Year:1979, Volume: N/A, Issue: N/A, Pages:1381-93
Abstract: Available

List of References Included in Database (cont.)

13. Cable Structures
Authors: Irvine, H. Max
Source: MIT Press, Cambridge, Massachusetts
Month: N/A, Year:1981, Volume: N/A, Issue: N/A, Pages: N/A
Abstract: N/A

14. The Natural Frequencies and Mode Shapes of Cables with Attached Masses
Authors: Sergev, S. S.; Iwan, W. D.
Source: Journal of Energy Resources Technology - Transactions of the ASME
Month: Sep, Year:1981, Volume:103, Issue: N/A, Pages: N/A
Abstract: N/A

15. Modal damping of flexural oscillation in suspended cables
Authors: Yamaguchi, H. ; Fujino, Yozo
Source: Transactions. JSCE
Month: N/A, Year:1982, Volume: N/A, Issue: N/A, Pages: N/A
Abstract: N/A

16. Control of wind-induced vibrations of cable-stayed bridges
Authors: Aschrafi, M. ; Hirsch, Gerhard
Source: Proceedings of the 6th International Conference on Wind Engineering Gold Coast, Australia
Month: N/A, Year:1983, Volume: N/A, Issue: N/A, Pages: N/A
Abstract: N/A

17. The fatigue performance of socketed terminations to structural strands
Authors: Hobbs, R. E.; Smith, H. Allison
Source: Proceedings of ICE, Part 2
Month: N/A, Year:1983, Volume:25, Issue: N/A, Pages:35-48
Abstract: N/A

18. Weak-wind induced vibration of transmission lines
Authors: Working-Group on Weak-Wind Induced Vibration,
Source: Technical Report of Electrical Society (in Japanese)
Month: N/A, Year:1983, Volume:129, Issue: N/A, Pages: N/A
Abstract: N/A

19. Dynamic and aeroelastic action of guy cables
Authors: Karna, T.
Source: Publication 18 Espoo, Finland
Month: N/A, Year:1984, Volume: N/A, Issue: N/A, Pages: N/A
Abstract: N/A

20. Hysteresis in bridge strand
Authors: Hobbs, R. E.; Raoof, Mohammed
Source: Proceedings of ICE, Part 2
Month: N/A, Year:1984, Volume:77, Issue: N/A, Pages:445-64
Abstract: Available

21. The dynamics of taut inclined cables
Authors: Triantafyllou, M. S.
Source: Quarterly Journal of Mechanics and Applied Mathematics
Month: N/A, Year:1984, Volume:37, Issue: N/A, Pages:421-440
Abstract: Available

22. The nonlinear dynamics of long, slender cylinders
Authors: Kim, Y. C.; Triantafyllou, M. S.
Source: Journal of Energy Resources Technology - Transactions of the ASME
Month: N/A, Year:1984, Volume:106, Issue:2, Pages:250-256
Abstract: N/A

23. The bending of spiral strand and armoured cables close to terminations
Authors: Raoof, Mohammed ; Hobbs, R. E.
Source: Journal of Energy Resources Technology - Transactions of the ASME
Month: N/A, Year:1984, Volume:106, Issue: N/A, Pages:394-355?
Abstract: N/A

24. Rain vibration of cables on cable-stayed bridge
Authors: Hikami, Y.
Source: Journal of Japan Association of Wind Engineering No. 27
Month: N/A, Year:1986, Volume:27, Issue: N/A, Pages: N/A
Abstract: N/A

25. Natural frequencies and modes of inclined cables
Authors: Triantafyllou, M. S.; Grinfogel, L.
Source: Journal of Structural Engineering
Month: N/A, Year:1986, Volume:112, Issue:1, Pages:139-148
Abstract: Available

List of References Included in Database (cont.)

26. Condition of Steel Cable after Period of Service
Authors: Phoenix, S. L.; Johnson, H. H.; McGuire, W.
Source: Journal of Structural Engineering
Month: Jun, Year:1986, Volume:112, Issue:6, Pages: N/A
Abstract: N/A

27. Cable-stayed bridges
Authors: Kanok-Nukulchai, W.
Source: Proceedings of the International Conference on Cable-Stayed Bridges, Bangkok
Month: N/A, Year:1987, Volume: N/A, Issue: N/A, Pages: N/A
Abstract: N/A

28. Experimental study on Ajikawa Bridge cable vibration
Authors: Miyasaka, K. ; Ohshima, K. ; Nakabayashi, S.
Source: Hanshin Express-way Public Corp. Eng. Report no. 7
Month: N/A, Year:1987, Volume: N/A, Issue: N/A, Pages: N/A
Abstract: N/A

29. Generating mechanisms for cable-stay oscillations at the Far0 Bridges
Authors: Langso, H. E.; Larsen, O. D.
Source: Proceedings of the International Conference on Cable-Stayed Bridges, Bangkok
Month: N/A, Year:1987, Volume: N/A, Issue: N/A, Pages:1023-1033
Abstract: N/A

30. Tuned mass damper for supressing wind effects on cable-stayed bridges
Authors: Malhorta, P. K.; Wieland, M.
Source: Proceedings Conference Bangkok Thailand
Month: N/A, Year:1987, Volume: N/A, Issue: N/A, Pages: N/A
Abstract: N/A

31. Vibrations and vibration control of stay cables in cable-stayed bridge
Authors: Wieland, M. ; Shrestha, P.
Source: AIT Publ.
Month: N/A, Year:1987, Volume: N/A, Issue: N/A, Pages: N/A
Abstract: N/A

32. Aerodynamic stability of the cables of a cable-stayed bridge subject to rain (A case study of the Aji River Bridge)
Authors: Ohshima, K. ; Nanjo, M.
Source: Proceedings of the 3rd U.S.--Japan Bridge workshop
Month: N/A, Year:1987, Volume: N/A, Issue: N/A, Pages:324-335
Abstract: Available

33. On the Vortex-Induced Oscillation of Long Structural Elements
Authors: Jones, Nicholas P.
Source: Journal of Energy Resources Technology - Transactions of the ASME
Month: Dec, Year:1987, Volume:109, Issue: N/A, Pages: N/A
Abstract: N/A

34. On the Vortex-Induced Oscillation of Long Structural Elemets
Authors: Iwan, W. D.; Jones, Nicholas P.
Source: Journal of Energy Resources Technology - Transactions of the ASME
Month: Dec, Year:1987, Volume:109, Issue: N/A, Pages: N/A
Abstract: N/A

35. Full dynamic testing of the Annacis bridge
Authors: Stiemer, S. F.; Taylor, P. ; Vincent, D.
Source: IABSE Proc.
Month: N/A, Year:1988, Volume: N/A, Issue: N/A, Pages: N/A
Abstract: N/A

36. Performance of bridge cables
Authors: Tilly, G. P.
Source: 1st Oleg Kerensky Memorial Conference Session 4, London, Institution of Structural Engineers
Month: N/A, Year:1988, Volume: N/A, Issue: N/A, Pages: N/A
Abstract: N/A

37. Properties of wire rope under various fatigue loadings
Authors: Strzemiecki, J. ; Hobbs, R. E.
Source: CESLC Report SC6, Department of Civil Engineering, Imperial College, London, U.K.
Month: N/A, Year:1988, Volume: N/A, Issue: N/A, Pages: N/A
Abstract: N/A

List of References Included in Database (cont.)

38. Rain-wind induced vibration of the cables of the Aratsu Bridge
Authors: Yoshimura, T. ; Tanaka, T. ; Sasaki, N. ; Nakatani, S.
Source: Proceedings of the 10th National Conference on Wind Engineering, Tokyo
Month: N/A, Year:1988, Volume: N/A, Issue: N/A, Pages:127-132
Abstract: N/A

39. Unstable Aerodynamic Vibrations and Prevention Methods for Cables in Cable-stayed Bridges
Authors: Miyazaki, Miyazaki
Source: Proceedings of the 10th Wind Engineering Symposium
Month: N/A, Year:1988, Volume: N/A, Issue: N/A, Pages: N/A
Abstract: N/A

40. Analytical study on Growth Mechanism of Rain Vibration of Cables
Authors: Yamaguchi, H.
Source: Journal of Wind Engineering
Month: N/A, Year:1988, Volume:33, Issue: N/A, Pages:73-80
Abstract: Available

41. Rain-wind induced vibrations of cables in cable stayed bridges
Authors: Hikami, Y. ; Shiraishi, N.
Source: Journal of Wind Engineering and Industrial Aerodynamics
Month: N/A, Year:1988, Volume:29, Issue: N/A, Pages:409-418
Abstract: Available

42. The elastic frequencies of cables
Authors: Burgess, J. J.; Triantafyllou, M. S.
Source: Journal of Sound and Vibration
Month: N/A, Year:1988, Volume:120, Issue:1, Pages:153-165
Abstract: Available

43. Active structural control in civil engineering (State-of-the-art)
Authors: Soong, T. T.
Source: Engineering Structures
Month: N/A, Year:1988, Volume: N/A, Issue: N/A, Pages: N/A
Abstract: Available

44. Cables in trouble
Authors: Watson, S. C.; Stafford, D.
Source: Civil Engineering ASCE
Month: N/A, Year:1988, Volume:58, Issue: N/A, Pages:38
Abstract: Available

45. Rain-wind induced vibrations of cables in cable stayed bridges
Authors: Hirsch, Gerhard ; Shiraishi, N.
Source: Journal of Wind Engineering and Industrial Aerodynamics
Month: N/A, Year:1988, Volume:29, Issue: N/A, Pages:409-418
Abstract: Available

46. Torsion Tests on large spiral strands
Authors: Raoof, Mohammed ; Hobbs, R. E.
Source: Journal of Strain Analysis
Month: N/A, Year:1988, Volume:23, Issue:2, Pages:97-104
Abstract: N/A

47. Cable stayed bridges
Authors: Walther, R. ; Houriet, B. ; Isler, W. ; Moia, P.
Source: T. Telford, London
Month: N/A, Year:1988, Volume: N/A, Issue: N/A, Pages: N/A
Abstract: N/A

48. Free bending tests on large spiral strands
Authors: Raoof, Mohammed
Source: Proceedings of ICE, Part 2
Month: N/A, Year:1989, Volume:87, Issue: N/A, Pages:605-626
Abstract: Available

49. Wind-induced cable vibration of cable-stayed bridges in Japan
Authors: Matsumoto, Masaru ; Yokoyama, K. ; Miyata, Toshio
Source: Proceedings of Canada-Japan Workshop on Bridge Aerodynamics, Ottawa
Month: N/A, Year:1989, Volume: N/A, Issue: N/A, Pages:101-110
Abstract: N/A

List of References Included in Database (cont.)

50. A study on the aerodynamic stability of the Aratsu Bridge
Authors: Yoshimura, T. ; Inoue, A. ; Kaji, K., K. ; Savage, M. S.
Source: Proceedings of Canada-Japan Workshop on Bridge Aerodynamics, Ottawa
Month: N/A, Year:1989, Volume: N/A, Issue: N/A, Pages:41-50
Abstract: Available

51. Damping stay cables with ties
Authors: Ehsan, Fazl ; Scanlan, Robert H.
Source: Proceedings of the 5th U.S. Japan Workshop on Bridge Engineering
Month: N/A, Year:1989, Volume: N/A, Issue: N/A, Pages:203-217
Abstract: Available

52. Inclined Cable Aerodynamics
Authors: Matsumoto, Masaru ; Knisely, C. W.; Shiraishi, N. ; Saitoh, Tohru
Source: Proceedings of the ASCE Structures Congress
Month: N/A, Year:1989, Volume: N/A, Issue: N/A, Pages:81-90
Abstract: Available

53. Wind analysis questioned.
Authors: Reina, Peter
Source: ENR
Month: N/A, Year:1989, Volume:223, Issue: N/A, Pages:21
Abstract: N/A

54. Approximate Explicit Formulas for Complex Modes of Two Degree-of-Freedom (2DOF) System
Authors: Pacheco, Benito M.
Source: Structural Engineering/Earthquake Engineering, JSCE
Month: Apr, Year:1989, Volume:6, Issue:1, Pages: N/A
Abstract: N/A

55. Perturbation Technique to Approximate the Effect of Damping Nonproportionality in Modal Damping Analysis
Authors: Pacheco, Benito M.
Source: Structural Engineering/Earthquake Engineering, JSCE
Month: Apr, Year:1989, Volume:6, Issue:1, Pages: N/A
Abstract: N/A

56. Damping Effects of Viscous Shearing Damper Newly Developed for Suppression of Vibration
Authors: Yoneda, M. ; Maeda, K.
Source: Proceedings of the 11th Wind Engineering Symposium
Month: N/A, Year:1990, Volume: N/A, Issue: N/A, Pages: N/A
Abstract: N/A

57. Dynamic strain measurements in cables of a cable-stayed bridge in Bangkok
Authors: Wieland, M. ; Lukkunaprasit, P.
Source: Report (unpublished) of Chulalongkorn University Bangkok
Month: N/A, Year:1990, Volume: N/A, Issue: N/A, Pages: N/A
Abstract: N/A

58. Aerodynamic behavior of inclined circular cylinders - cable aerodynamics
Authors: Matsumoto, Masaru ; Shiraishi, N. ; Bearman, P. W.; Knisely, C.
Source: Journal of Wind Engineering
Month: N/A, Year:1990, Volume:33, Issue: N/A, Pages:63-72
Abstract: Available

59. Non-linear cable response and model testing in water
Authors: Papazoglou, V. J.; Mavrakos, S.A. ; Triantafyllou, M. S.
Source: Journal of Sound and Vibration
Month: N/A, Year:1990, Volume:140, Issue:1, Pages:103-115
Abstract: Available

60. Aeroelastic analysis of cable-stayed bridges.
Authors: Scanlan, Robert H.; Jones, Nicholas P.
Source: Journal of Structural Engineering
Month: N/A, Year:1990, Volume:116, Issue: N/A, Pages:279-97
Abstract: Available

61. Free bending of spiral strands
Authors: Raoof, Mohammed
Source: Journal of Engineering Mechanics
Month: N/A, Year:1990, Volume:116, Issue:3, Pages:512-30
Abstract: Available

List of References Included in Database (cont.)

62. Chaotic dynamics
Authors: Baker, G. L.; Gollub, J. P.
Source: Cambridge University press
Month: N/A, Year:1990, Volume: N/A, Issue: N/A, Pages: N/A
Abstract: N/A

63. A simple method of designing cable vibration dampers of cable-stayed bridges
Authors: Uno, K. ; Kitagawa, S. ; Tsutsumi, H. ; Inoue, A.
Source: J. Struct. Engrg., Japan Society of Civil Engineering, Tokyo, Japan
Month: N/A, Year:1991, Volume:37A, Issue: N/A, Pages:789-798
Abstract: N/A

64. Analytical estimation of structural damping in cable structures
Authors: Yamaguchi, H. ; Jayawardena, L.
Source: Proceedings of the 8th International conference on Wind Engineering London, Ontario
Month: N/A, Year:1991, Volume: N/A, Issue: N/A, Pages: N/A
Abstract: Available

65. Dynamic Response and structural health monitoring of long-span cable-supported bridges
Authors: Abdel-Ghaffar, Ahmed M.; Masri, S. F.
Source: Workshop Infrastructure '91Hong-Kong
Month: N/A, Year:1991, Volume: N/A, Issue: N/A, Pages: N/A
Abstract: N/A

66. Progress in Wind Engineering
Authors: Davenport, A. G.
Source: Proceedings of the 8th International conference on Wind Engineering London, Ontario
Month: N/A, Year:1991, Volume: N/A, Issue: N/A, Pages: N/A
Abstract: N/A

67. Recent advances in control of wind-induced vibrations of guyed masts
Authors: Hirsch, Gerhard
Source: Proceedings of the 8th International conference on Wind Engineering London, Ontario
Month: N/A, Year:1991, Volume: N/A, Issue: N/A, Pages: N/A
Abstract: N/A

68. Importance of cable vibration in dynamics of cable-stayed bridges
Authors: Abdel-Ghaffar, Ahmed M.; Khalifa, M. A.
Source: Journal of Engineering Mechanics
Month: N/A, Year:1991, Volume:117 No. 11, Issue: N/A, Pages:2571
Abstract: Available

69. Ambient vibration measurements on a cable-stayed bridge.
Authors: Wilson, John C.; Liu, Tao
Source: Earthquake Engineering and Structural Dynamics
Month: N/A, Year:1991, Volume:20, Issue: N/A, Pages:423-47
Abstract: Available

70. Dynamic structural properties of cable-stayed Tampico bridge.
Authors: Muria-Vila, D. ; Gomez, R. ; King, C.
Source: Journal of Structural Engineering
Month: N/A, Year:1991, Volume:117, Issue: N/A, Pages:3396-416
Abstract: Available

71. Modelling of a cable-stayed bridge for dynamic analysis.
Authors: Wilson, John C.; Gravelle, Wayne
Source: Earthquake Engineering and Structural Dynamics
Month: N/A, Year:1991, Volume:20, Issue: N/A, Pages:707-21
Abstract: Available

72. Wind-resistant design of the Higashi-Kobe bridge
Authors: Matsumoto, Masaru ; Kitazawa, Masahiko ; Ishizaki, H. ; Ogawa, K. ; Saito, Toru ; Shimodai, H.
Source: Bridge and Foundation Engineering
Month: N/A, Year:1991, Volume: N/A, Issue: N/A, Pages: N/A
Abstract: N/A

73. Upper-Bound Prediction of Cable Damping Under Cyclic Bending
Authors: Huang, Y. P.
Source: Journal of Engineering Mechanics
Month: Dec, Year:1991, Volume:117, Issue:12, Pages: N/A
Abstract: N/A

List of References Included in Database (cont.)

74. Dynamic Stiffness Matrix of Sagging Cable
Authors: Starossek, Uwe
Source: Journal of Engineering Mechanics
Month: Dec, Year:1991, Volume:117, Issue:12, Pages: N/A
Abstract: N/A

75. Dynamic Stability of Cables Subjected to an Axial Periodic Load
Authors: Takahashi, K.
Source: Journal of Sound and Vibration
Month: N/A, Year:1991, Volume:144, Issue:2, Pages: N/A
Abstract: N/A

76. Rain-wind aeroelastic instability of the inclined hangers of a suspension bridge
Authors: Zasso, A. ; Bocciolone, M. ; Brownjohn, J.
Source: Preprints of Inaugural Conference of the Wind Engineering Society UK
Month: N/A, Year:1992, Volume: N/A, Issue: N/A, Pages: N/A
Abstract: N/A

77. The effects of three-dimensional imposed disturbances on bluff body near wake flow
Authors: Bearman, P. W.; Tombazis, N.
Source: Preprints of the Second BBAA
Month: N/A, Year:1992, Volume: N/A, Issue: N/A, Pages: N/A
Abstract: N/A

78. Discussion of Dynamic stability of cables subjected to an axial periodic load
Authors: Perkins, N. C.
Source: Journal of Sound and Vibration
Month: N/A, Year:1992, Volume:156, Iss 2, Issue: N/A, Pages:361-65
Abstract: Available

79. Modal interactions in the nonlinear response of elastic cables under parametric external excitation
Authors: Perkins, N. C.
Source: International Journal of Non-Linear Mechanics
Month: N/A, Year:1992, Volume:27, Iss 2, Issue: N/A, Pages:233-50
Abstract: Available

80. Rain-wind induced vibration of cables of cable-stayed bridges
Authors: Matsumoto, Masaru ; Shiraishi, N. ; Shirato, H.
Source: Proceedings of the 8th International conference on Wind Engineering London, Ontario
Month: N/A, Year:1992, Volume:44, Issue: N/A, Pages:2011-22
Abstract: Available

81. Dynamic characteristics of the Sunshine Skyway Bridge
Authors: Jones, Nicholas P.; Thompson, J. M.
Source: Proceedings of U.S.--Japan Bridge Workshop
Month: N/A, Year:1992, Volume: N/A, Issue: N/A, Pages: N/A
Abstract: N/A

82. Aerodynamic stability of a cable-stayed bridge with girder, tower and cables
Authors: Ogawa, K. ; Shimodai, H. ; Ishizaki, H.
Source: Proceedings of the 10th International Conference on Wind Engineering, Copenhagen, 1999
Month: N/A, Year:1992, Volume:42, Issue:1, Pages:1227-38
Abstract: Available

83. Analytical Aerodynamic Investigation of Cable Stayed Helgeland Bridge
Authors: Kovacs, I. ; Svensson, H. S.; Jordet, E.
Source: Journal of Structural Engineering
Month: N/A, Year:1992, Volume:110, Issue:1, Pages:147-60
Abstract: N/A

84. Bridge engineering and aerodynamics
Authors: Ostenfield, K. H.; Larsen, A.
Source: Proceedings of the1st International Symposium Large Bridges, Balkema
Month: N/A, Year:1992, Volume: N/A, Issue: N/A, Pages: N/A
Abstract: N/A

85. Cable-stayed bridge vibration due to road surface roughness.
Authors: Wang, Ton-Lo ; Huang, Dongzhou
Source: Journal of Structural Engineering
Month: N/A, Year:1992, Volume:118, Issue: N/A, Pages:1354-74
Abstract: Available

List of References Included in Database (cont.)

86. Closed form vibration analysis of sagged cable mass suspensions
Authors: Chang, S. P.; Perkins, N. C.
Source: Journal of Applied Mechanics Transactions of the ASME
Month: N/A, Year:1992, Volume:57, Issue:4, Pages:923-28
Abstract: N/A

87. Damping Phenomena in a wire rope vibration isolation system
Authors: Tinker, M. L.; Cutchins, M. A.
Source: Journal of Sound and Vibration
Month: N/A, Year:1992, Volume:157, Issue:1, Pages: 7-10
Abstract: Available

88. Dynamic stability of cables subjected to an axial periodic load
Authors: Perkins, N. C.
Source: Journal of Sound and Vibration
Month: N/A, Year:1992, Volume:156, Issue:2, Pages:361-65
Abstract: N/A

89. Experimental investigation of dynamics of transverse impoulse wave propagation and dispersion in steel wire ropes
Authors: Kwun, H, ; Durkhardt, S. L.
Source: Journal of the Acoustical Society of America
Month: N/A, Year:1992, Volume:92, Issue:4, Pages:1973-80
Abstract: N/A

90. Experimental Study on Cable Response to Vortex-induced Vibrations
Authors: Yokoyama, K. ; Kusakabe, ; Fujiwara, T. ; Hojo, Tetsuo
Source: Proceedings of the 12th Wind Engineering Symposium
Month: N/A, Year:1992, Volume: N/A, Issue: N/A, Pages: N/A
Abstract: N/A

91. Fatigue resistance of large diameter cable for cable stayed bridges
Authors: Takena, K. ; Miki, C. ; Shimokawa, H. ; Sakamoto, K.
Source: Journal of Structural Engineering
Month: N/A, Year:1992, Volume:110, Issue:3, Pages:701-15
Abstract: Available

92. Free bending fatigue life estimation for cables close to points of fixity
Authors: Raoof, Mohammed
Source: Journal of Engineering Mechanics
Month: N/A, Year:1992, Volume:118, Issue:9, Pages:1747-64
Abstract: Available

93. Free bending fatigue of axially preloaded spiral strands
Authors: Raoof, Mohammed
Source: Journal of Strain Analysis
Month: N/A, Year:1992, Volume:27, Issue:3, Pages:127-36
Abstract: N/A

94. Free vibration of a sagged cable supporting a discrete mass
Authors: Cheng, S. P.; Perkins, N. C.
Source: Journal of the Acoustical Society of America
Month: N/A, Year:1992, Volume:91, Issue:5, Pages:2654-62
Abstract: N/A

95. Wire stress calculations in helical strands undergoing bending
Authors: Raoof, Mohammed ; Huang, Y. P.
Source: Journal of Offshore Mechanics and Arctic Engineering
Month: N/A, Year:1992, Volume:114, Issue:3, Pages:212-19
Abstract: Available

96. Development of viscous damper to control the wind-induced vibration of cables
Authors: Yoneda, M. ; Maeda, K. ; Izaki, H. ; Shimoda, I.
Source: Journal of JSME (in Japanese)
Month: N/A, Year:1992, Volume:58, Issue:555, Pages: N/A
Abstract: N/A

97. Lateral vibrations of steel cables including structural damping
Authors: Raoof, Mohammed ; Huang, Y. P.
Source: Proceedings of Inst. Civ. Engrs Structs of Bldgs
Month: N/A, Year:1993, Volume:99, Issue: N/A, Pages:123-33
Abstract: Available

List of References Included in Database (cont.)

98. Structural Control
Authors: Housner, G. W.; Masri, S. F.
Source: Workshop Honolulu 1993
Month: N/A, Year:1993, Volume: N/A, Issue: N/A, Pages: N/A
Abstract: N/A

99. Active stiffness control of cable vibration
Authors: Fujino, Yozo ; Warnitchai, P. ; Pacheco, D. M.
Source: Journal of Applied Mechanics Transactions of the ASME
Month: N/A, Year:1993, Volume:60, Iss 4, Issue: N/A, Pages:948-950
Abstract: Available

100. Estimation curve for modal damping in stay cables with viscous damper
Authors: Pacheco, Benito M.; Fujino, Yozo ; Sulekh, Ajai
Source: Journal of Structural Engineering
Month: N/A, Year:1993, Volume:119, Iss 6, Issue: N/A, Pages:1961-79
Abstract: Available

101. Vortex induced vibrations of a long flexible circular cylinder
Authors: Brika, D. ; Laneville, A.
Source: Journal of Fluid Mechanics
Month: N/A, Year:1993, Volume:250, Issue: N/A, Pages:481-508
Abstract: Available

102. Ambient Vibration Survey: Sunshine Skyway Bridge
Authors: Jones, Nicholas P.; Thompson, J. M.
Source: Proceedings of Structures Congress
Month: N/A, Year:1993, Volume: N/A, Issue: N/A, Pages: N/A
Abstract: Available

103. A device for suppressing wake galloping of stay cables for cable-stayed bridges
Authors: Yoshimura, T. ; Savage, M. S.; Tanaka,, H. ; Wakasa, T.
Source: Journal of Wind Engineering and Industrial Aerodynamics
Month: N/A, Year:1993, Volume:49, Issue:3-Jan, Pages:497-505
Abstract: Available

104. Active modal control of vortex-induced vibrations of a flexible cylinder
Authors: Daz, A. ; Kim, M.
Source: Journal of Sound and Vibration
Month: N/A, Year:1993, Volume:165, Issue:1, Pages:69-84
Abstract: Available

105. An experimental study on active tendon control of cable stayed bridges
Authors: Warnitchai, P. ; Fujino, Yozo ; Pacheco, D. M.; Agret, R.
Source: Earthquake Engineering and Structural Dynamics
Month: N/A, Year:1993, Volume:22, Issue:2, Pages:93-111
Abstract: Available

106. Damping and response measurement on a small-scale model of a cable-stayed bridge.
Authors: Garevski, Mihail A.; Severn, Roy T.
Source: Earthquake Engineering and Structural Dynamics
Month: N/A, Year:1993, Volume:22, Issue: N/A, Pages:13-29
Abstract: Available

107. Design of steel cables against free-bending fatigue at terminations
Authors: Raoof, Mohammed
Source: The Structural Engineer
Month: N/A, Year:1993, Volume:71, Issue: N/A, Pages:171-78
Abstract: N/A

108. Effects of partial streamlining on aerodynamic response of bridge decks.
Authors: Bienkiewicz, B. ; Kobayashi, H.
Source: Journal of Structural Engineering
Month: N/A, Year:1993, Volume:119, Issue: N/A, Pages:342-8
Abstract: Available

109. Experimental study on aerodynamic characteristics of cables with surface roughness
Authors: Miyasaka, K. ; Yamada, Hitoshi ; Holmhansen, D.
Source: Bridge and Foundation Engineering
Month: N/A, Year:1993, Volume:27, Issue:9, Pages: N/A
Abstract: N/A

List of References Included in Database (cont.)

110. Modal identification of cable-stayed pedestrian bridge.
Authors: Gardner-Morse, ; Huston, Dryver R.
Source: Journal of Structural Engineering
Month: N/A, Year:1993, Volume:119, Issue: N/A, Pages:3384-404
Abstract: Available

111. The aerodynamic design of the Messina Straits Bridge
Authors: Drancaleoni, F. ; Diana, G.
Source: Journal of Wind Engineering and Industrial Aerodynamics
Month: N/A, Year:1993, Volume:48, Issue:2,3, Pages:395-409
Abstract: Available

112. An Experimental and Analytical Study of Autoparametric Resonance in a 3DOF Model of Cable-Stayed-Beam
Authors: Pacheco, Benito M.
Source: Nonlinear Dynamics
Month: N/A, Year:1993, Volume:4, Issue: N/A, Pages: N/A
Abstract: N/A

113. Keeping Cables Calm
Authors: Pacheco, Benito M.
Source: Civil Engineering ASCE
Month: Oct, Year:1993, Volume: N/A, Issue: N/A, Pages: N/A
Abstract: N/A

114. Effect of Non-Linear Structural Damping on Cable Lateral Vibrations
Authors: Huang, Y. P.
Source: Proceedngs of the Third International Offshore and Polar Engineering Conference
Month: Jun, Year:1993, Volume: N/A, Issue: N/A, Pages: N/A
Abstract: N/A

115. Dynamics of elastic cable under parametric and external resonances
Authors: Cai, Y. ; Chen, S. S.
Source: Journal of Engineering Mechanics
Month: N/A, Year:1994, Volume:120, Iss 8, Issue: N/A, Pages:1786-1802
Abstract: Available

116. Rain-wind excitation of cables on cable-stayed Higashi-Kobe bridge and cable vibration control
Authors: Saito, Toru ; Matsumoto, Masaru ; Kitazawa, Masahiko
Source: Proceedings of Conference on Cable-Stayed and Suspension Bridges
Month: N/A, Year:1994, Volume: N/A, Issue: N/A, Pages:507-514
Abstract: Available

117. An experimental-study on active control of inplane cable vibration by axial support motion
Authors: Fujino, Yozo ; Susumpow, T.
Source: Earthquake Engineering and Structural Dynamics
Month: N/A, Year:1994, Volume:23, Issue:12, Pages:1283-97
Abstract: Available

118. Experimental study on aerodynamic characteristics of cables with patterned surfaces
Authors: Miyata, Toshio ; Yamada, Hitoshi ; Hojo, Tetsuo
Source: Journal of Structural Engineering
Month: N/A, Year:1994, Volume:40A, Issue: N/A, Pages: N/A
Abstract: N/A

119. Vibration amplitudes caused by parametric excitation of cable stayed structures
Authors: Lilien, J. L.; Dacosta, A. P.
Source: Journal of Sound and Vibration
Month: N/A, Year:1994, Volume:174, Issue:1, Pages:69-90
Abstract: Available

120. Wind-induced nonlinear lateral-torsional buckling of cable-stayed bridges.
Authors: Boonyapinyo, Virote ; Yamada, Hitoshi ; Miyata, Toshio
Source: Journal of Structural Engineering
Month: N/A, Year:1994, Volume:120, Issue: N/A, Pages:486-506
Abstract: Available

121. Optimum Dancing of Vibrations of Stay Cables in Cable-Stayed Bridges
Authors: Premachandran, R. ; Wieland, Martin
Source: Australian Structural Engineering Conference
Month: Sep, Year:1994, Volume: N/A, Issue: N/A, Pages: N/A
Abstract: N/A

List of References Included in Database (cont.)

122. Active control of cable and cable structure system
Authors: Susumpow, T. ; Warnitchai, P.
Source: JSME International Journal Series C Dynamics Control Robotics Design and Manufacturing
Month: N/A, Year:1995, Volume:38, Issue:2, Pages:260-66
Abstract: N/A

123. Cable Aerodynamics and its stabilization
Authors: Matsumoto, Masaru
Source: Int. Symposium on Cable Dynamics, Proceedings, Liege (Belgium)
Month: N/A, Year:1995, Volume: N/A, Issue: N/A, Pages:289-96
Abstract: N/A

124. Control of cable vibrations with secondary cables
Authors: Yamaguchi, H.
Source: Int. Symposium on Cable Dynamics, Proceedings, Liege (Belgium)
Month: N/A, Year:1995, Volume: N/A, Issue: N/A, Pages:445-452
Abstract: N/A

125. Design of Cables for Cable-Stayed Bridges: the example of the Normandie Bridge
Authors: Virlogeux,
Source: Proceedings of the International Symposium on Cable Dynamics
Month: N/A, Year:1995, Volume: N/A, Issue: N/A, Pages: N/A
Abstract: N/A

126. Rain-wind-induced vibrations of steel bars
Authors: Ruscheweyh, H. P.; Verwiebe, C.
Source: Int. Symposium on Cable Dynamics, Proceedings, Liege (Belgium)
Month: N/A, Year:1995, Volume: N/A, Issue: N/A, Pages:469-472
Abstract: N/A

127. The Dynamics of Cables in Wind
Authors: Davenport, A. G.
Source: Proceedings of the International Symposium on Cable Dynamics
Month: N/A, Year:1995, Volume: N/A, Issue: N/A, Pages: N/A
Abstract: N/A

128. Wind tunnel tests on rain-induced vibration on the stay-cable
Authors: Honda, A. ; Yamanaka, T. ; Fujiwara, T. ; Saitoh, Tohru
Source: Int. Symposium on Cable Dynamics, Proceedings, Liege (Belgium)
Month: N/A, Year:1995, Volume: N/A, Issue: N/A, Pages:255-262
Abstract: N/A

129. Wind-induced vibrations of bridge stay-cables
Authors: Yoshimura, T. ; Tanaka,, H. ; Savage, M. S.; Nakatani, S. ; Hikami, Y.
Source: Int. Symposium on Cable Dynamics, Proceedings, Liege (Belgium)
Month: N/A, Year:1995, Volume: N/A, Issue: N/A, Pages:437-444
Abstract: N/A

130. Rain-wind induced vibration of cables
Authors: Flamand, Oliver A.
Source: Proceedings of the 1st IAWE European and African Regional Conference, Thomas Telford 1993
Month: N/A, Year:1995, Volume:57, Iss. 2-3, Issue: N/A, Pages:353-362
Abstract: Available

131. Response characteristics of rain-wind induced vibration of stay-cables of cable-stayed bridges
Authors: Matsumoto, Masaru ; Saitoh, Tohru ; Kitazawa, Masahiko ; Shirato, H. ; Nishizaki, T.
Source: Journal of Wind Engineering and Industrial Aerodynamics
Month: N/A, Year:1995, Volume:57, Issue: N/A, Pages:323-33
Abstract: N/A

132. Various mechanism of inclined cable aerodynamics
Authors: Matsumoto, Masaru ; Yamagishi, M. ; Aoki, J. ; Shiraishi, N.
Source: Proceedings of the 9th International Conference on Wind Engineering, New Delhi, India
Month: N/A, Year:1995, Volume: N/A, Issue: N/A, Pages:759-770
Abstract: Available

List of References Included in Database (cont.)

133. Vortex shedding and wake induced vibrations in single and bundle cables
Authors: Cigada, A. ; Diana, G. ; Falco, M. ; Fossati, F. ; Manenti, A.
Source: Proceedings of the 9th International Conference on Wind Engineering, New Delhi, India
Month: N/A, Year:1995, Volume: N/A, Issue: N/A, Pages:771-782
Abstract: Available

134. A nonlinear dynamic model for cables and its application to a cable structure system
Authors: Warnitchai, P. ; Fujino, Yozo ; Susumpow, T.
Source: Journal of Sound and Vibration
Month: N/A, Year:1995, Volume:107, Issue:4, Pages:675-710
Abstract: Available

135. Active control of multimodal cable vibrations by axial support motion
Authors: Susumpow, T. ; Fujino, Yozo
Source: Journal of Engineering Mechanics
Month: N/A, Year:1995, Volume:121, Issue:9, Pages:964-972
Abstract: Available

136. Aerodynamic stability analysis of cable-stayed bridges.
Authors: Pfeil, M. S.; Batista, R. C.
Source: Journal of Structural Engineering
Month: N/A, Year:1995, Volume:121, Issue: N/A, Pages:1784-8
Abstract: Available

137. Design considerations for delayed resonator vibration absorbers
Authors: Olgac, N. ; Holmhansen, D.
Source: Journal of Engineering Mechanics
Month: N/A, Year:1995, Volume:121, Issue:1, Pages:80-89
Abstract: Available

138. Full-scale dynamic testing of the Alamillo cable-stayed bridge in Sevilla (Spain).
Authors: Casas, Juan R.
Source: Journal of Structural Engineering
Month: N/A, Year:1995, Volume:24, Issue: N/A, Pages:35-51
Abstract: Available

139. Influence of cable vibration on seismic response of cable-stayed bridges
Authors: Tuladhar, R.; Dilger, W. H.; Elbadry, M. M.
Source: Canadian Journal of Civil Engineering
Month: N/A, Year:1995, Volume:22, Issue:5, Pages:1001-20
Abstract: Available

140. Nonlinear oscillations of a 4 degree of freedom model of a suspended cable under multiple internal resonance conditions
Authors: Denedettini, F. ; Rega, C. ; Alaggiao, R
Source: Journal of Sound and Vibration
Month: N/A, Year:1995, Volume:102, Issue:5, Pages:775-97
Abstract: Available

141. Prediction control of Sdof system
Authors: Hoshiya, M.
Source: Journal of Engineering Mechanics
Month: N/A, Year:1995, Volume:121, Issue:10, Pages:1049-55
Abstract: Available

142. Damping analysis of cable-stayed bridges
Authors: Loredo-Souza, A. M.; Davenport, A. G.
Source: Proc. of the International Conference on Urban Engr. in Asian Cities in the 21st Century, Bangkok
Month: N/A, Year:1996, Volume: N/A, Issue: N/A, Pages: N/A
Abstract: N/A

143. Oscillations of bridge stay cables induced by periodic motions of deck and/or towers
Authors: Pinto da Costa, A. ; Martins, J. A. C.; Branco, F.
Source: Journal of Engineering Mechanics
Month: N/A, Year:1996, Volume:122, Issue: N/A, Pages:613-22
Abstract: Available

144. Active Tendon Control of Cable-Stayed Bridges
Authors: Preumon, A. ; Achkire, Y.
Source: Earthquake Engineering and Structural Dynamics
Month: N/A, Year:1996, Volume:25, Issue: N/A, Pages:585-597
Abstract: N/A

List of References Included in Database (cont.)

145. Active Boundary Control of Elastic Cables: Theory and Experiment
Authors: Baicu, C. F.; Rahn, C. D.; Nibali, B. D.
Source: Journal of Sound and Vibration
Month: N/A, Year:1996, Volume:1, Issue:198, Pages: N/A
Abstract: N/A

146. Structural Damping of Tensioned Pipes with Reference to Cables
Authors: McConnell, Kenneth G.; Uhrig, A.
Source: Journal of Sound and Vibration
Month: N/A, Year:1996, Volume: N/A, Issue:193, Pages: N/A
Abstract: N/A

147. Structural Damping of Tensioned Pipes with Reference to Cables
Authors: Fang, J. ; Lyons, G. J.
Source: Journal of Sound and Vibration
Month: N/A, Year:1996, Volume:193, Issue:4, Pages: N/A
Abstract: N/A

148. Energy-based damping evaluation of cable-stayed bridges and application to Tsurumi Tsubasa Bridge
Authors: Yamaguchi, H. ; Takano, H. ; Ogasawara, M. ; Shimosato, T. ; Kato, M. ; Kato, H.
Source: Journal of Structural Engineering and Earthquake Engineering, JSCE (translated from Japanese)
Month: N/A, Year:1997, Volume:14, Issue:2, Pages:201s-213s
Abstract: N/A

149. Identification of dynamic characteristics of the Tsurumi Tsubasa Bridge by field vibration tests
Authors: Yamaguchi, H. ; Takano, H. ; Ogasawara, M. ; Shimosato, T. ; Kato, M. ; Okada, J.
Source: Journal of Structural Engineering and Earthquake Engineering, JSCE (translated from Japanese)
Month: N/A, Year:1997, Volume:14, Issue:2, Pages:215s-228s
Abstract: N/A

150. Measurement of stay-cable vibration
Authors: Jones, Nicholas P.; Porterfield, Michelle
Source: Proceedings of the Structures Congress, ASCE, Portland, 1997
Month: N/A, Year:1997, Volume: N/A, Issue: N/A, Pages:1290-1294
Abstract: Available

151. Modal analysis of tower-cable system of Tsing Ma long suspension bridge
Authors: Xu, Y. L.; Ko, J. M.; Yu, Z.
Source: Engineering Structures
Month: N/A, Year:1997, Volume:19, Issue: N/A, Pages:857-867
Abstract: Available

152. Modal Damping Estimation of Cable-Damper Systems
Authors: Xu, Y. L.; Ko, J. M.; Yu, Z.
Source: Proc. 2nd International symposioum on structures and foundations in civil engineering, Hong Kong
Month: N/A, Year:1997, Volume: N/A, Issue: N/A, Pages:96-102
Abstract: Available

153. Mode-dependence of structural damping in cable-stayed bridges
Authors: Yamaguchi, H. ; Ito, Manabu
Source: Journal of Wind Engineering and Industrial Aerodynamics
Month: N/A, Year:1997, Volume:72, Issue: N/A, Pages:289-300
Abstract: N/A

154. Recent research results concerning the exciting mechanisms of rain-wind-induced vibrations
Authors: Verwiebe, C. ; Ruscheweyh, H. P.
Source: Proc. 2nd European and African Conference on Wind Engineering, Geneva, Italy
Month: N/A, Year:1997, Volume: N/A, Issue: N/A, Pages:1783-1789
Abstract: Available

155. The cable stabilization at the wind and moving load effect
Authors: Kazakevitch, M. ; Zakora, A.
Source: Proc. 2nd European and African Conference on Wind Engineering, Geneva, Italy
Month: N/A, Year:1997, Volume: N/A, Issue: N/A, Pages:1775-1781
Abstract: Available

List of References Included in Database (cont.)

156. Vortex-induced oscillations in inclined cables
Authors: Hover, F. X.; Miller, S.N. ; Triantafyllou, M. S.
Source: Journal of Wind Engineering and Industrial Aerodynamics
Month: N/A, Year:1997, Volume:71, Issue: N/A, Pages:203-211
Abstract: Available

157. Wind-induced vibration of cables of cable-stayed bridges
Authors: Matsumoto, Masaru ; Dayto, Y. ; Kanamura, T. ; Shigemura, Y. ; Sakuma, S. ; Ishizaki, H.
Source: Proceedings of the 2 EACWE, Genova, Italy, 1997
Month: N/A, Year:1997, Volume: N/A, Issue: N/A, Pages:1791-1798
Abstract: Available

158. Parametric Excitation of Cable
Authors: Hsu., C. S.; Cheng, W. H.
Source: Seismic Engineering
Month: N/A, Year:1997, Volume: N/A, Issue: N/A, Pages: N/A
Abstract: N/A

159. Complex Analysis of Modal Damping in Inclined Sag Cables with Oil Dampers
Authors: Xu, Y. L.; Ko, J. M.
Source: Structures in the New Millenium
Month: N/A, Year:1997, Volume: N/A, Issue: N/A, Pages: N/A
Abstract: N/A

160. Analysis of Resonant Tangential Response in Submerged Cables Resulting from 1-to-1 Internal Resonance
Authors: Newberry, B. L.; Perkins, N. C.
Source: Proceedings of the Seventh International Offshore and Polar Engineering Conference
Month: May, Year:1997, Volume: N/A, Issue: N/A, Pages: N/A
Abstract: N/A

161. Vibration Damper for Cables of the Tsunami Tsubasa Bridge
Authors: Ito, Noboru
Source: Journal of Wind Engineering and Industrial Aerodynamics
Month: N/A, Year:1997, Volume: N/A, Issue: N/A, Pages: N/A
Abstract: N/A

162. Basic study on simultaneous identification of cable tension and flexural rigidity by extended Kalman filter
Authors: Zui, Hiroshi ; Nishikawa, Tohuru ; Higa, S. ; Yoshihiro, ; Shinki, ; Saito, Toru
Source: Structural Engineering/Earthquake Engineering, JSCE
Month: N/A, Year:1998, Volume:15, Issue:1, Pages:97-106
Abstract: Available

163. Bridge stay cable condition assessment using vibration measurement techniques
Authors: Takano, H. ; Mehrabi, A.B. ; Yen, W. P.
Source: SPIE
Month: N/A, Year:1998, Volume:3400, Issue: N/A, Pages:194-204
Abstract: Available

164. Dynamic response of cable-stayed bridge under moving loads
Authors: Yang, Fuheng ; Fonder, Ghislain A.
Source: Journal of Engineering Mechanics
Month: N/A, Year:1998, Volume:124, Issue:7, Pages:741-747
Abstract: Available

165. Exciiting mechanisms of rain-wind induced vibrations
Authors: Verwiebe, C.
Source: Journal of the International Association for Bridge and Structural Engineering (IABSE)
Month: N/A, Year:1998, Volume:8, Issue:2, Pages: N/A
Abstract: Available

166. Parametric identification of vortex-induced vibration of a circular cylinder from measured data
Authors: Christensen, C. F.; Roberts, U. B.
Source: Journal of Sound and Vibration
Month: N/A, Year:1998, Volume:211, Issue:4, Pages:617
Abstract: Available

167. Stayed cable dynamics and its vibration control
Authors: Yamaguchi, H. ; Fujino, Yozo
Source: Proc. of the International Symposium on Advances in Bridge Aerodynamics, Copenhagen, 1999
Month: N/A, Year:1998, Volume: N/A, Issue: N/A, Pages:235-253
Abstract: N/A

List of References Included in Database (cont.)

168. United Finite difference formulation for free vibration of cables
Authors: Mehrabi, A.B. ; Tabatabai, H.
Source: Journal of Structural Engineering
Month: N/A, Year:1998, Volume:124, Issue:11, Pages:1313-1322
Abstract: Available

169. Vibration control of cable-stayed bridges--Part 1: Modeling Issues
Authors: Schemmann, A. G.; Smith, H. Allison
Source: Earthquake Engineering and Structural Dynamics
Month: N/A, Year:1998, Volume:27, Issue:8, Pages:811-824
Abstract: Available

170. Vibration of Inclined Sag Cables with Oil Dampers in Cable-Stayed Bridges
Authors: Xu, Y. L.; Yu, Z.
Source: Journal of Bridge Engineering
Month: N/A, Year:1998, Volume:3, Issue:4, Pages:194-203
Abstract: Available

171. Discussion of Cable-stayed bridges--Parametric Study. T.P. Agrawal
Authors: Housner, G. W.; Singh, P. K.
Source: Journal of Bridge Engineering
Month: N/A, Year:1998, Volume:3, Issue:3, Pages:148
Abstract: N/A

172. Traveling wave dynamics in a translating string coupled to stationary constraints: energy transfer and mode localization
Authors: Lee., S. Y.; Mote, C. D.
Source: Journal of Sound and Vibration
Month: N/A, Year:1998, Volume:212, Issue:1, Pages:1
Abstract: Available

173. Vibration control of cable-stayed bridges--Part 2: Control Analyses
Authors: Schemmann, A. G.; Smith, H. Allison
Source: Earthquake Engineering and Structural Dynamics
Month: N/A, Year:1998, Volume:27, Issue:8, Pages:825-844
Abstract: Available

174. Forced Vibration Studies of Sagged Cables with Oil Damper Using a Hybrid Method
Authors: Xu, Y. L.; Ko, J. M.
Source: Engineering Structures
Month: N/A, Year:1998, Volume:20, Issue:8, Pages: N/A
Abstract: N/A

175. Forced Vibration Studies of Sagged Cables with Oil Damper Using a Hybrid Method
Authors: Xu, Y. L.; Ko, J. M.
Source: Engineering Structures
Month: N/A, Year:1998, Volume:20, Issue:8, Pages: N/A
Abstract: N/A

176. Mitigation of Three-Dimensional Vibration of Inclined Sag Cable Using Discrete Oil Dampers - I. Formulation
Authors: Xu, Y. L.
Source: Journal of Sound and Vibration
Month: N/A, Year:1998, Volume:4, Issue:214, Pages: N/A
Abstract: N/A

177. The Effects of Mechanical Dampers on Stay Cables with High Damping Rubber
Authors: Nakamura, A. ; Kasuga, A. ; Arai, H.
Source: Construction and Building Materials
Month: N/A, Year:1998, Volume:12, Issue:2-3, Pages: N/A
Abstract: N/A

178. A novel approach for aeroelastic wind tunnel modeling of cables
Authors: Loredo-Souza, A. M.; Davenport, A. G.
Source: Proceedings of the 10th International Conference on Wind Engineering, Copenhagen, 1999
Month: N/A, Year:1999, Volume:2, Issue: N/A, Pages:955-962
Abstract: Available

179. A study on wake-galloping for stay cables of extradosed bridges employing full aeroelastic cable model
Authors: Tokoro, S. ; Komatsu, H. ; Nakasu, M. ; Mizuguchi, K. ; Kasuga, A.
Source: Proceedings of the 10th International Conference on Wind Engineering, Copenhagen, 1999
Month: N/A, Year:1999, Volume:2, Issue: N/A, Pages:1055-1062
Abstract: Available

List of References Included in Database (cont.)

180. Dynamics of SDOF systems with nonlinear viscous damping
Authors: Terenzi, G.
Source: Journal of Engineering Mechanics
Month: N/A, Year:1999, Volume: N/A, Issue: N/A, Pages:956-963
Abstract: N/A

181. Energy balanced double oscillator model for vortex-induced vibrations
Authors: Krenk, S. ; Nielsen, S. R.K.
Source: Journal of Engineering Mechanics
Month: N/A, Year:1999, Volume:125, Issue:3, Pages:263-271
Abstract: Available

182. Estimation of the effects of rain-wind induced vibration in the desing stage of inclined stay cables
Authors: Geurts, C. P.W.; van Staalduinen, P. C.
Source: Proceedings of the 10th International Conference on Wind Engineering, Copenhagen, 1999
Month: N/A, Year:1999, Volume:2, Issue: N/A, Pages:885-892
Abstract: Available

183. Experimental study of vibration mitigation of bridge stay cables
Authors: Xu, Y. L.; Zhan, S. ; Ko, J. M.; Yu, Z.
Source: Journal of Structural Engineering
Month: N/A, Year:1999, Volume:125, Issue:9, Pages:977-986
Abstract: Available

184. Full-scale measurements of stay cable vibration
Authors: Main, Joseph A.; Jones, Nicholas P.
Source: Proceedings of the 10th International Conference on Wind Engineering, Copenhagen, 1999
Month: N/A, Year:1999, Volume:2, Issue: N/A, Pages:963-970
Abstract: Available

185. Full-scale measurements on the Erasmus bridge after rain/wind induced cable vibrations
Authors: Persoon, A. J.; Noorlander, K.
Source: Proceedings of the 10th International Conference on Wind Engineering, Copenhagen, 1999
Month: N/A, Year:1999, Volume:2, Issue: N/A, Pages:1019-1026
Abstract: Available

186. Mode localization in multispan cable systems
Authors: Poovarodom,, N. ; Yamaguchi, H.
Source: Engineering Structures
Month: N/A, Year:1999, Volume:21, Issue:1, Pages:45-54
Abstract: N/A

187. Modeling and semiactive damping of stay cables
Authors: Baker, G. A.; Johnson, E. A.; Spencer, BF,, B. F.; Fujino, Yozo
Source: Proceedings of the 13th ASCE Engineering Mechanics Division Specialty Conference, JHU, USA
Month: N/A, Year:1999, Volume: N/A, Issue: N/A, Pages: N/A
Abstract: N/A

188. Modeling of stay cables and its effect on free vibration analysis of cable-stayed bridges
Authors: Cheung, Y. K.; Au, F. T.K.; Cheng, Y. S.; Zheng, D. Y.
Source: Proceedings of the 13th ASCE Engineering Mechanics Division Specialty Conference, JHU, USA
Month: N/A, Year:1999, Volume: N/A, Issue: N/A, Pages: N/A
Abstract: Available

189. Nonlinear feedback control for the stabilization of cable oscillations: analytical and experimental model
Authors: Gattulli, V. ; Benedettini, F.
Source: Proceedings of the 13th ASCE Engineering Mechanics Division Specialty Conference, JHU, USA
Month: N/A, Year:1999, Volume: N/A, Issue: N/A, Pages: N/A
Abstract: Available

190. Seismic behaviour of cable-stayed bridges under multi-component random ground motion
Authors: Allam, S. M.; Datta, T. K.
Source: Engineering Structures
Month: N/A, Year:1999, Volume:21, Issue:1, Pages:62-74
Abstract: N/A

List of References Included in Database (cont.)

191. The mechanism of rain-wind induced vibration
Authors: Ruscheweyh, H. P.
Source: Proceedings of the 10th International Conference on Wind Engineering, Copenhagen, 1999
Month: N/A, Year:1999, Volume:2, Issue: N/A, Pages:1041-1048
Abstract: N/A

192. Vortex-induced vibration of inclined cables at high wind velocity
Authors: Matsumoto, Masaru ; Yagi, T. ; Shigemura, Y. ; Tsushima, D.
Source: Proceedings of the 10th International Conference on Wind Engineering, Copenhagen, 1999
Month: N/A, Year:1999, Volume:2, Issue: N/A, Pages:979-986
Abstract: Available

193. Semiactive Damping of Stay Cables: A Preliminary Study
Authors: Johnson, E. A.; Spencer, BF,, B. F.
Source: Proceedings of 17th International Modal Analysis Conference: February 8-11, 1999
Month: Feb, Year:1999, Volume: N/A, Issue:1, Pages: N/A
Abstract: N/A

194. Non-linear Vibration of Cable-Damper Systems Part I: Formulation
Authors: Xu, Y. L.
Source: Journal of Sound and Vibration
Month: N/A, Year:1999, Volume:225, Issue:3, Pages: N/A
Abstract: N/A

195. Non-linear Vibration of Cable-Damper Systems Part II: Application and Verification
Authors: Xu, Y. L.
Source: Journal of Sound and Vibration
Month: N/A, Year:1999, Volume:225, Issue:3, Pages: N/A
Abstract: N/A

196. Analysis and Implications of Low Damping for Seismic Response of Cable-Stayed Bridges
Authors: Wilson, John C.; Atkins, Jodie C.
Source: Earthquake Engineering and Structural Dynamics
Month: N/A, Year:2000, Volume: N/A, Issue: N/A, Pages: N/A
Abstract: N/A

197. Investigation of Dynamic Cable-Deck Interaction in a Physical Model of a Cable-Stayed Bridge. Part II: Seismic Response
Authors: Caetano, E. ; Cunha, A. ; Taylor, C. A.
Source: Earthquake Engineering and Structural Dynamics
Month: N/A, Year:2000, Volume: N/A, Issue:29, Pages: N/A
Abstract: N/A

198. Investigation of Dynamic Cable-Deck Interaction in a Physical Model of a Cable-Stayed Bridge. Part I: Modal Analysis
Authors: Caetano, E. ; Cunha, A. ; Taylor, C. A.
Source: Earthquake Engineering and Structural Dynamics
Month: N/A, Year:2000, Volume: N/A, Issue:29, Pages: N/A
Abstract: N/A

APPENDIX A2: INVENTORY OF U.S. CABLE-STAYED BRIDGES

An inventory of cable-stayed bridges in the United States was created to organize and share existing records with the Research Team. This database includes information on bridge geometry, cable properties, cable connections, aerodynamic detailing, site conditions, and observed responses to wind. The inventory is stored in Microsoft Access (Microsoft Office) database format, which allows for easy data entry and retrieval. Forms were designed to perform this task, complete with pull-down menus and control buttons, using the Visual Basic programming language. These forms for data entry include a "switchboard" form and three categories of bridge data forms: General bridge data, cable data and wind data.

Overall, 26 bridges have been added to the database, including several from outside the United States. Copies of contract drawings from which data was taken have been copied and filed for future reference. The following is the full list of bridges included in the inventory:

Table 8: Cable stayed bridge inventory.

Bridge	Location	Main Span (ft)
Annacis Bridge	British Columbia	1526
Greenville Bridge (US 82)	Mississippi	1378
Dames Point Bridge	Florida	1300
Fred Hartman Bridge	Texas	1250
Sidney Lanier Bridge	Georgia	1250
Luling Bridge	Louisiana	1222
Sunshine Skyway Bridge	Florida	1200
William Natcher Bridge	Kentucky	1200
Cape Girardeau Bridge	Missouri	1150
Talmadge Memorial Bridge	Georgia	1100
Maysville-Aberdeen Bridge	Kentucky	1050
Pasco - Kennewick Intercity Bridge	Washington	981
East Huntington Bridge	West Virginia	900
FA Route 63 over Mississippi River	Illinois	900
Weirton - Steubenville Bridge	West Virginia	820
Cochrane Bridge	Alabama	780
Clark Bridge	Illinois	756
Chesapeake and Delaware Canal Bridge	Delaware	750
Leonard P. Zakim Bunker Hill Bridge	Massachusetts	745
Sixth Street Bridge	West Virginia	740
Burlington Bridge	Iowa	660
Veterans Memorial Bridge	Texas	640
Varina Enon Bridge	Virginia	630
PR 148 over La Plata River	Puerto Rico	525
Sitka Harbor Bridge	Alaska	450
Foss Waterway Bridge	Washington	350

The inventory forms are described in detail in the following pages:

a) Switchboard

Overall control of data entry and referential integrity between categories is provided by a switchboard from which the user selects which type of data to enter or retrieve. An example of the switchboard is shown below. The user may select from the three categories to either add a new entry or edit an existing entry. The selection will open data entry forms for the category requested.

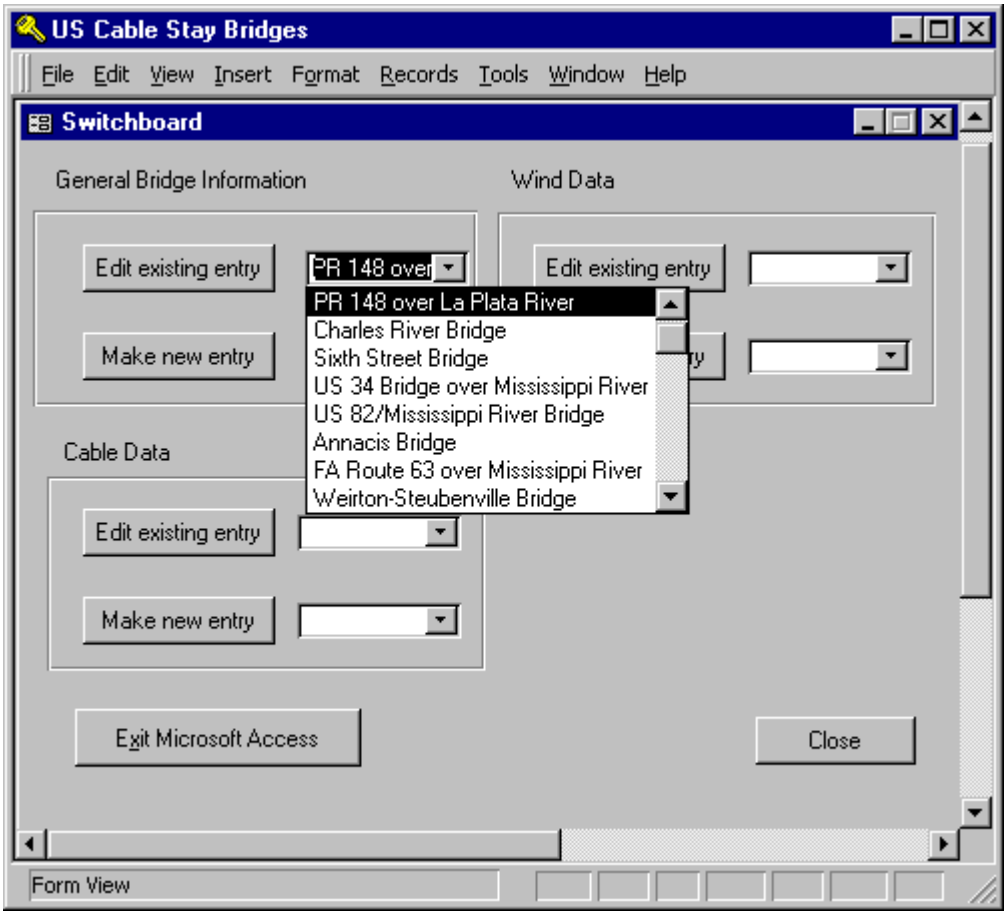

Figure 28: U.S. cable-stayed bridge database - Switchboard.

b) General Bridge Information

General bridge information is divided into two sections. General information includes bridge name, designers, suppliers and bridge location. Structural data includes information on the superstructure, tower, cable, anchorages, and cross-ties.

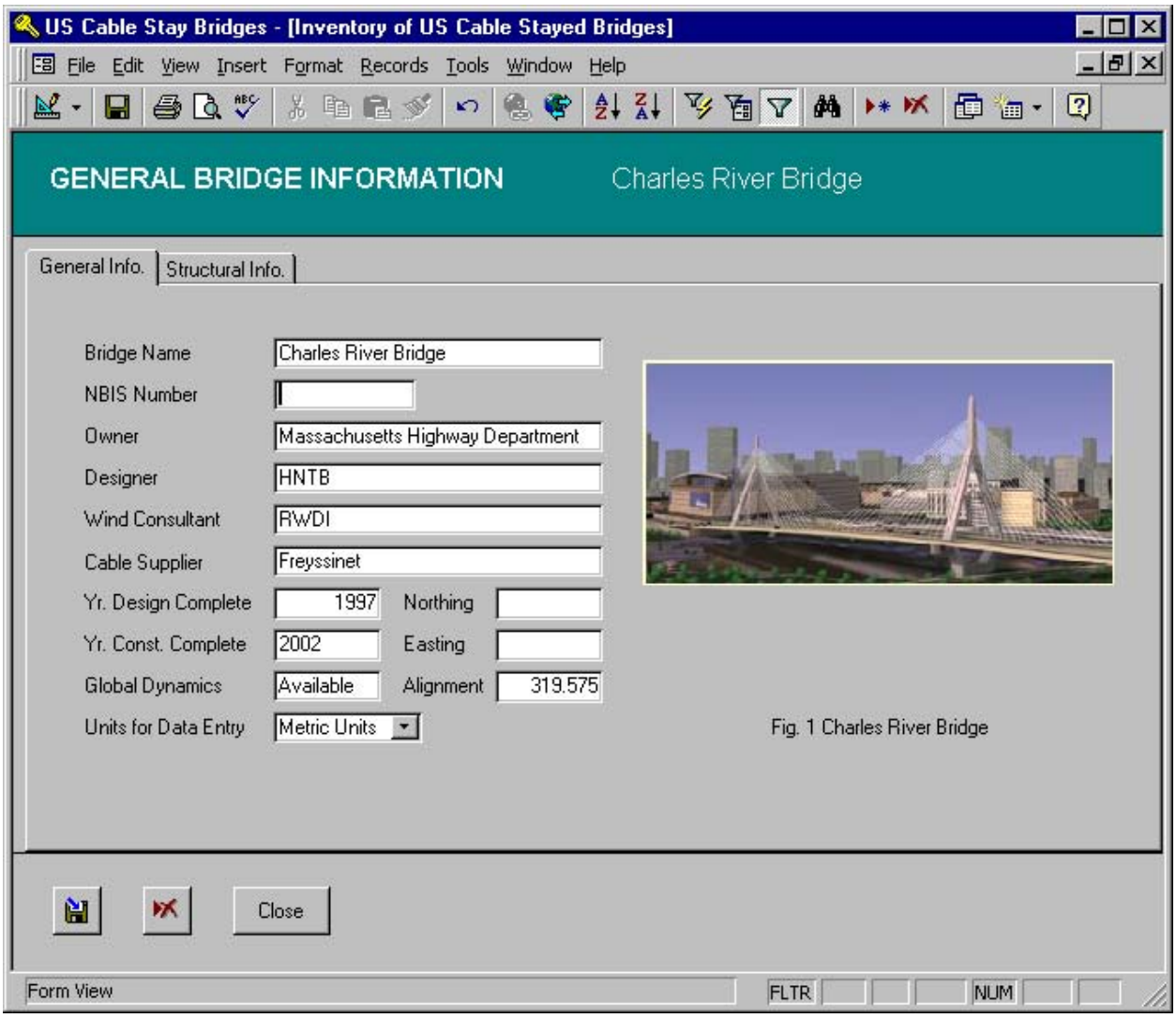

Figure 29: U.S. cable-stayed bridge database - General bridge information.

c) Cable Data

Cable Data is divided into four sections: cable geometry, cable properties, cable connections and aerodynamic details. Cable Geometry gives the end coordinates and calculates the cable length. Cable Properties includes strand type, size, dead load tension, and the protection system. Cable Connections describes upper and lower anchors and fatigue test information. Aerodynamic Details includes descriptions of dampers and sheathing surface treatment. Information for each cable of the bridge is given individually.

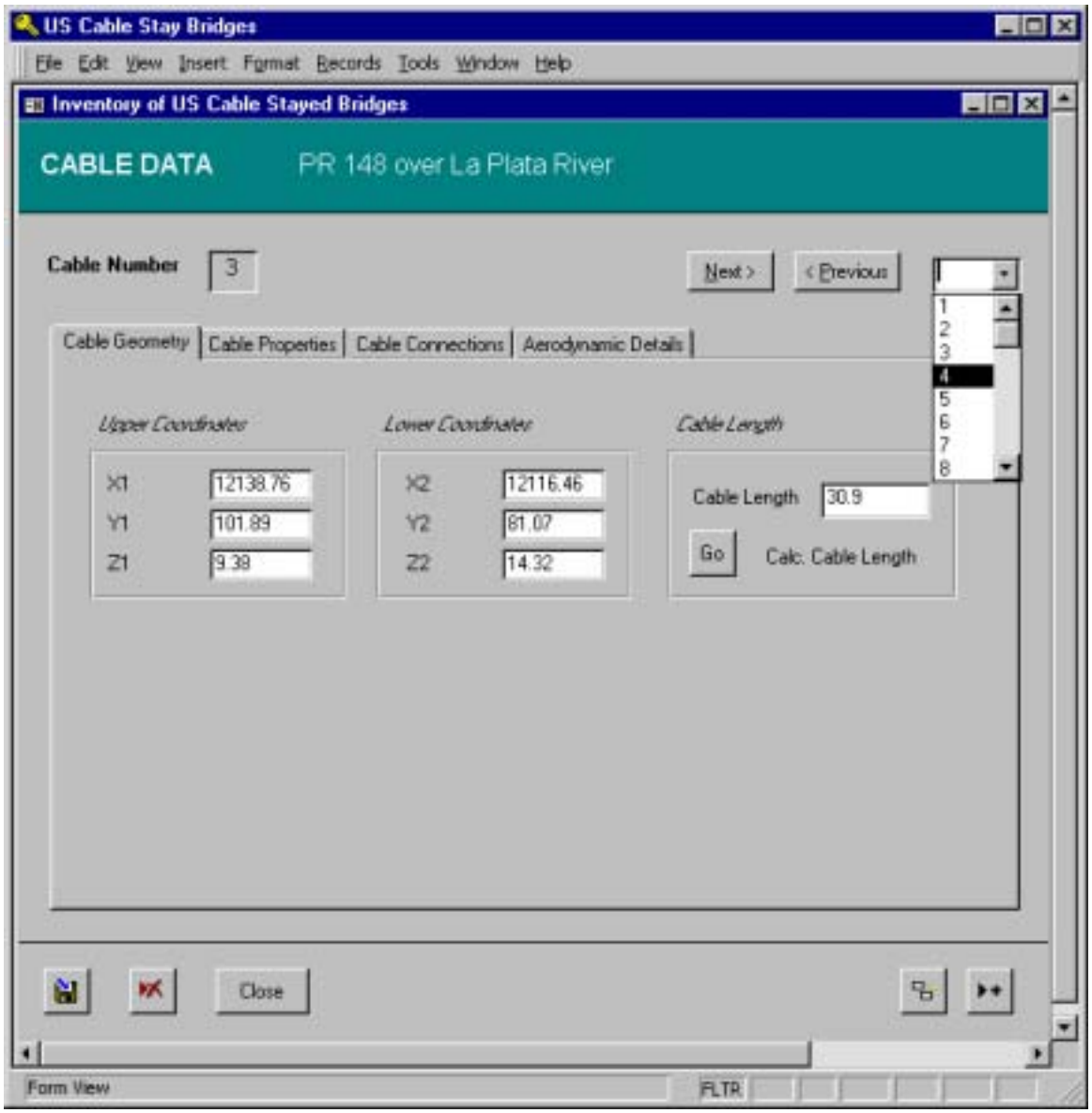

Figure 30: U.S. cable-stayed bridge database - Cable data.

d) Wind Data

Wind Data includes bridge dynamic modes, superstructure mass, design wind speeds, and vibration measurement information. Data has only been entered for the Cape Girardeau Bridge.

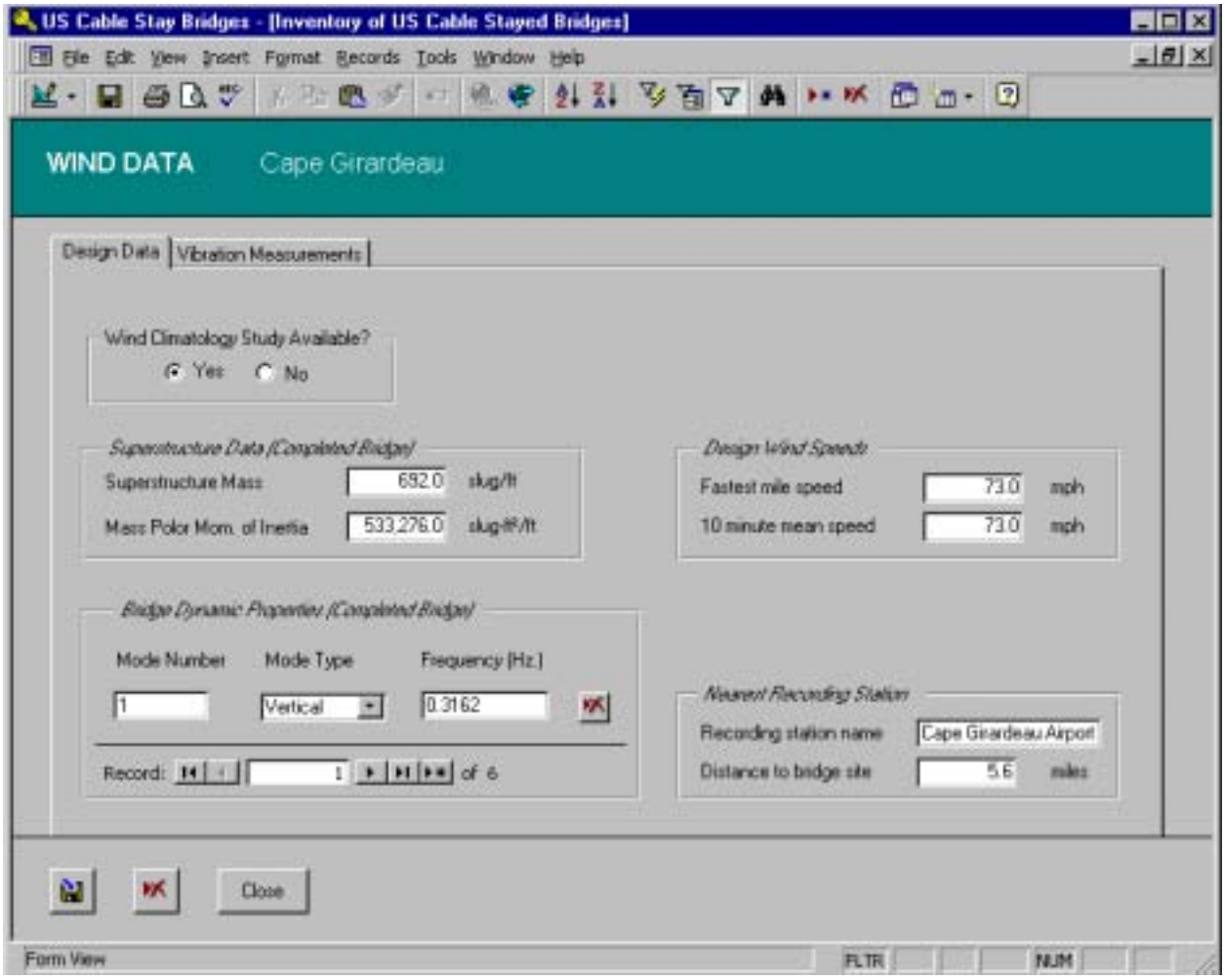

Figure 31: U.S. cable-stayed bridge database - Wind data.

APPENDIX B1: WIND INDUCED CABLE VIBRATIONS

B1.1 MECHANICS OF WIND-INDUCED VIBRATIONS

General Background

There are a number of possible types of wind-induced vibrations of cables.

1. Vortex excitation of an isolated cable
2. Vortex excitation of groups of cables
3. Wake galloping for groups of cables
4. Galloping of single cables inclined to the wind
5. Rain/wind induced vibrations of cables
6. Galloping of cables with ice accumulations
7. Galloping of cables in the wakes of other structural components (e.g. arches, towers, truss members etc.)
8. Aerodynamic excitation of overall bridge modes of vibration involving cable motion, e.g. vortex shedding off the deck may excite a vertical mode that involves relatively small deck motions but substantial cable motions
9. Motions due to buffeting by wind turbulence
10. Motion due to Fluctuating Cable Tensions

Some of these are more critical or probable than others, but they are all listed here for completeness. They are discussed in turn in the following sections.

Vortex Excitation of an Isolated Cable and Groups of Cables

Vortex excitation of a single isolated cable is caused by the alternate shedding of vortices from the two sides of the cable when the wind is approximately at right angles to the cable axis. The vortices are shed from one side of the cable at a frequency, n, that is proportional to the wind velocity U and inversely proportional to the cable diameter D. Thus

$$n = S(U/D) \tag{12}$$

where S is a non-dimensional parameter, the Strouhal number, that remains constant over extended ranges of wind velocity. For circular cross-section cables in the Reynolds number range 10^4 to about $3\text{x}10^5$, S is about 0.2.

Each time a vortex is shed it gives rise to a force at right angles to the wind direction. The alternate shedding thus causes an oscillating across-wind force. If the frequency of the oscillating force matches the frequency N_r of the rth natural mode of vibration of the cable, then oscillations of the cable in that mode will be excited. The wind velocity U_{VS} at which this matching of vortex shedding frequency n to natural frequency N_r occurs can be deduced from Equation 12 and is

$$U_{VS} = N_r D/S \tag{13}$$

Thus, as an example of a typical situation for a long stay cable, if the cable natural frequency N_r were 2 Hz and its diameter were D = 5.9 in (0.15 m) then, using a Strouhal number S = 0.2, it can be determined that the vortex shedding excitation of the rth mode will occur at a wind speed of U_{VS} = 3.4 mph (1.5 m/s). This is clearly a very low wind speed, showing that vortex shedding can begin in the lower modes at very modest speeds. For higher modes the wind speed will be higher.

The amplitude of the cable oscillations depends on the mass and damping of the cable. An approximate formula for the maximum amplitude y_0 as a fraction of the diameter is:

$$\frac{y_0}{D} \approx 0.008\left(\frac{C_L}{m\zeta/\rho D^2}\right) * \left(\frac{U_{VS}}{nD}\right)^2 \tag{14}$$

C_L = oscillating lift coefficient,
m = mass of cable per unit length,
ζ = damping ratio,
U_{VS} = wind velocity at peak of oscillations and
ρ = air density

The lift coefficient C_L has some dependence on oscillation amplitude as well as Reynolds number, but a rough value suitable for order of magnitude estimates is $C_L \approx 0.3$.

It can be seen from this relationship that increasing the mass and damping of the cables reduces oscillation amplitudes. The parameter ($m\zeta/\rho D^2$) is called the Scruton number. Higher values of Scruton number will tend to suppress vortex excitation and, as will be seen later, other types of wind-induced oscillation also tend to be mitigated by increasing the Scruton number.

It is difficult to give a precise estimate of the damping expected to occur in the cables of cable-stayed bridges, however, cable damping ratios can range anywhere from 0.0005 to 0.01 (0.05% to 1.0% of critical). The lower end of this range is typical of very long cable stays prior to cement grouting, while the upper end of this range is more typical of shorter cable-stays with grouting and some end damping.

For a bundled steel cable stay with a damping ratio of $\zeta = 0.005$, the Scruton number ($m\zeta/\rho D^2$) has a value in the range of about 7 to 12 depending on the sheathing material, on whether grouting is used, and if so, on how much of the cable system mass consists of grouting. The value of (U_{VS}/nD) ≈ 5, so the above expression leads to y_0/D ≈ 0.008 x 0.3 x (1/7) x 25 = 0.0084 for the lower end of the range of ($m\zeta/\rho D^2$). The lower end of the range of ($m\zeta/\rho D^2$) would correspond to a typical cable on a cable-stayed bridge prior to grouting. The predicted amplitude of oscillation is small, of order one percent of the cable diameter and it would drop to about y_0/D ≈ 0.0049 (i.e. about one half of a percent of the cable diameter) for the higher value of ($m\zeta/\rho D^2$) = 12 that corresponds to a grouted cable with 0.005 damping ratio.

If the damping ratio of the stay cables is extremely low, e.g. 0.001, as has been observed on some cable-stayed bridges prior to grouting being applied, then the amplitude could conceivably increase to about $y_0/D = 0.044$, i.e. about 4% of the cable diameter. Typically, 4% of the cable diameter would amount to not more than a few millimeters, i.e. still a small amplitude. Over many cycles at this amplitude it may be possible for fatigue problems to arise, but these larger oscillations are expected to be primarily a construction phase phenomenon when low values of ($m\zeta/\rho D^2$) occur on ungrouted and lightly damped cables. Therefore the time period involved is less likely to be long enough for fatigue problems to develop.

From the above discussion it is clear that the classical vortex type of excitation of a single isolated cylindrical shape is unlikely to lead to serious oscillations of typical bridge cables. The predicted amplitudes are small even for lightly damped stay cables prior to grouting.

When one cable is near to other cables, especially when it lies in their wakes, the interactions become very complex especially at close spacings, e.g. 2 - 6 diameters. The vortex shedding behavior is modified, occurring at slightly different wind speeds, and leading to amplitudes that can be several times larger than for the isolated cable. However, even with this further magnification of the vortex response due to interaction effects the amplitudes still do not reach magnitudes sufficient to explain the vibrations observed on some bridges.

Therefore a general conclusion is that vortex shedding from the cables themselves is unlikely to be the root cause of cable vibration problems on bridges. There are other more serious forms of wind-induced oscillations, as explained below, that are more likely candidates for causing fatigue problems. Almost any small amount of damping that is added to the cables will be sufficient to effectively suppress vortex excitation.

Wake Galloping for Groups of Cables

When a cable lies in the wake of another cable the wind forces on it depend on its position in the wake. When the cable is near the center of the wake the wind velocity is low and it can move upwind against a lower drag force. If it is in the outer part of the wake it experiences a stronger drag force and will tend to be blown downwind. Also, because of the shear flow in the wake of the upwind cable, the downwind cable will experience an across-wind force tending to pull it away from the wake center, the magnitude of this across wind force being a function of the distance from the wake center. These variations in drag and across wind forces can lead to the cable undergoing oscillations which involve both along wind and across wind components, i.e. the cable moves around an elliptical orbit. Over each complete orbit it can be shown that there is a net transfer of energy from the wind into the cable motion. For smaller spacings of the cables, say 2 - 6 diameters, the downwind cable moves around a roughly circular orbit. For larger spacings the orbit becomes more elongated into an ellipse with its major axis roughly aligned with the wind direction.

This type of instability is called wake galloping. The wind speeds involved are typically substantially higher than those for the onset of vortex excitation. It can cause oscillations much larger in amplitude than those seen in vortex excitation. For example oscillation amplitudes of order 20 cable diameters have been observed on bundled power conductors for cable spacings in the 10 - 20 diameter range. In some cases adjacent cables clashed with each other. This type of wake galloping could potentially occur on the cable arrays on cable stayed bridges or for grouped hangers. Less severe forms of galloping, but still problematic, can occur at smaller spacings in the 2 - 6 diameter range.

As for vortex excitation of the isolated cable, the Scruton number ($m\zeta/\rho D^2$) is an important guide as to the likelihood of there being a problem due to wake galloping effects. Cooper (1985) has proposed an approximate global stability criterion, based on earlier work by Connors (1970). This criterion gives the wind velocity U_{CRIT} above which instability can be expected due to wake galloping effects. It is given in terms of ($m\zeta/\rho D^2$) as follows:

$$U_{CRIT} = c\, N_r D \sqrt{\frac{m\zeta}{\rho D^2}} \qquad (15)$$

where c is a constant. For close cable spacings (e.g. 2 - 6 diameters) the value of the constant c appears to be about 25 but for spacings in the 10 to 20 diameter range it goes up to about 80. This relationship shows that increasing the Scruton number ($m\zeta/\rho D^2$) or natural frequency N_r will make the cable array stable up to a higher wind velocity.

Thus, if for example ($m\zeta/\rho D^2$) = 10, D = 6 inches, and N_r = 1 Hz then for the spacing in the range 2 - 6 diameters we find U_{CRIT} = 27 mph. This is quite low and is a common enough speed to have the potential to cause fatigue problems. However, N_r may be increased by installing cross-ties to the cables to shorten the effective length of cable for the vibration mode of concern. If cross-ties were used at two locations along this cable, dividing it into three equal

lengths, the frequency N_r would be tripled resulting in U_{CRIT} = 80 mph which is high enough to have a much smaller probability of occurring. Added to the stiffening effect of the spacers is the additional damping that they most likely cause. For a cable significant damping occurs at the points where it is clamped such as at its ends or at spacers placed along its length.

It should be noted that the values of *c* in Equation 15 quoted above were for wind normal to the axis of the cable. For cable-stayed bridges, wind normal to the axis of the cable typically is not possible, at least for wind directions where wake interference can occur. The angle is typically in the range 25° to 60° rather than 90°. Therefore, it is probable that for stay-cable arrays the values of *c* would be higher than those quoted above. Most cables on cable-stayed bridges are separated by more than six diameters. Therefore, it is probably conservative to assume a *c* value of 80 when estimating the critical velocity for wake galloping. More research is needed in this area to better define wake galloping stability boundaries for inclined cables.

The oscillations caused by wake galloping are known to have caused fatigue of the outer strands of bridge hangers at end clamps on suspension and arch bridges. Fatigue problems of this type have yet to be encountered on cable-stayed bridges, but could potentially occur on cross-cables. Therefore, it is good practice to avoid sharp corners where the cross-cables enter the clamps linking them to the main cables or the deck. Bushings of rubber or other visco-elastic materials at the clamps can help reduce fatigue and can be a source of extra damping.

Galloping of Dry Single Cables

Single cables of circular cross-section do not gallop when they are aligned normal to the wind. However, when the wind velocity has a component along the span it is no longer normal to the cable axis and for cables inclined to the wind an instability with the same characteristics as galloping has been observed. In Figure 32 the data of Saito et al. (1994) are shown plotted in the form of $U_{CRIT}/(f\,D)$ versus S_c. The data came from a series of wind tunnel experiments on a section of bridge cable mounted on a spring suspension system. Also plotted are curves calculated from Equation 15 for several values of c in the range 25 to 55. It can be seen that all the data points except one lie above the curve for c=40 and that this value could be used to predict the onset of single inclined cable galloping.

Another possible mechanism of single inclined cable galloping which has not received a lot of attention in the literature is the notion that the wind "sees" an elliptical cross-section of cable, for the typical wind directions where single cable galloping has been seen. Elliptical sections with ellipticity of about 2.5 or greater have a lift coefficient with a region of negative slope at angles of attack between 10° to 20°. An ellipticity of 2.5 would correspond to an angle of inclination of the cable of approximately 25°, which can occur in the outer-most cables of long-span bridges. (Ellipticity is defined as the maximum width divided by the minimum width - e.g., a circle has an ellipticity of 1.0.) The negative slope of the lift coefficient may result in galloping instability if the level of structural damping in the cables is very low. The ellipticity range and angle range where galloping occurs is likely to be sensitive to surface roughness and Reynolds number.

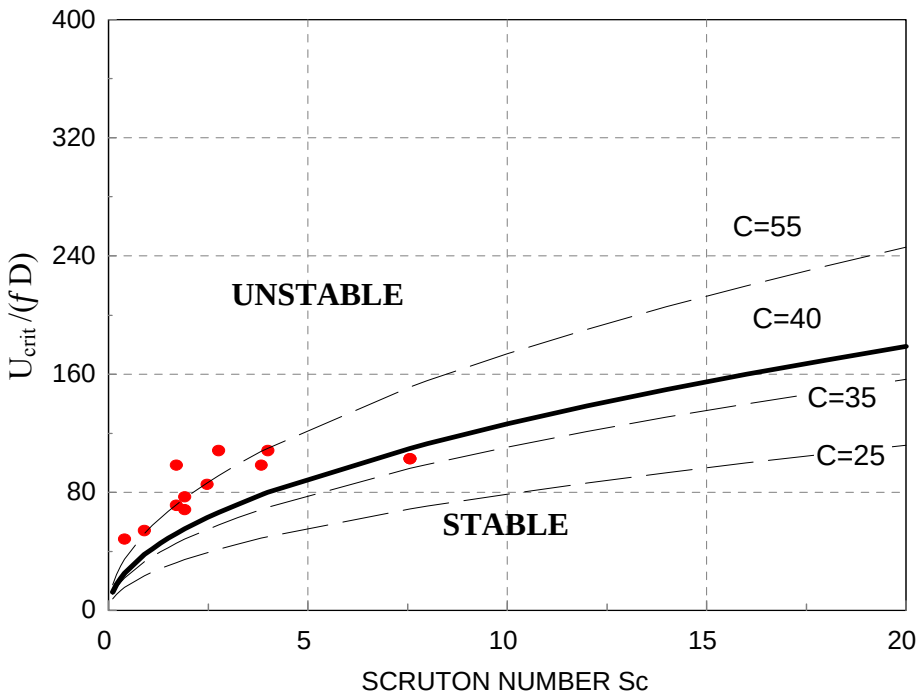

Figure 32: Galloping of inclined cables.

There is a need for further experimental studies to confirm the results of Saito et al. (1994) and to extend the range of conditions studied. Saito's results were nearly all at very low damping. There is a particular need to investigate if galloping of an inclined cable is indeed possible at damping ratios of 0.005 and higher.

The conclusion of recent testing (see Appendix B2) was that instability occurs at very low damping levels, however if enough damping is added these instabilities disappear. It is expected that if enough cable system damping is supplied to mitigate rain/wind vibrations, these vibrations should also be suppressed.

Rain/Wind Induced Vibrations

It has been observed on several bridges that the combination of rain and wind will cause cable vibrations. Hikami and Shiraishi (1987) described this phenomenon as it was observed on the Meikonishi cable stayed bridge on cables of about 5.5-in diameter. This well documented case is a good illustration of the phenomenon. Oscillation single amplitudes of more than 10-in developed. In other cases, amplitudes in excess of 3-ft have been observed. The cables, consisting of parallel wires inside a polyethylene pipe, had masses of 25 lb/ft and 35 lb/ft before and after cement grouting respectively. The damping ratio was reported to be in the range 0.0011 to 0.0046 depending on cable length, vibration mode and construction situation. It is probable that the lower values of damping corresponded to the ungrouted case. With this assumption the Scruton number for the ungrouted cables was as low as $(m\zeta/\rho D^2) = 1.7$. The cable lengths were in the range 210-ft to 650-ft.

The oscillations were seen in the wind speed range of 18 to 30 mph and the modes of vibration affected by oscillations all had frequencies in the 1 to 3 Hz range and were any one of the first four modes. Based on wind tunnel tests that reproduced the oscillations it was established that rivulets of water running down the upper and lower surfaces of the cable in rainy weather were the essential component of this aeroelastic instability. The water rivulets changed the effective shape of the cable. Furthermore they moved as the cable oscillated causing cyclical changes in the aerodynamic forces which led, in a not fully understood way, to the wind feeding energy into oscillations. The wind directions causing the excitation were at about 45 degrees to the plane of the cables with the affected cables being those sloping downwards in the direction of the wind. The particular range of wind velocities that caused the oscillations appears to be that which maintained the upper rivulet within a critical zone on the upper surface of the cable. A lower velocity simply allowed the water rivulet to drain down to the bottom surface and a higher velocity pushed it too far up onto the upper surface for it to be in the critical zone.

As with vortex excitation and galloping, any increase in the Scruton number ($m\zeta/\rho D^2$) is beneficial in reducing the cable's susceptibility to rain/wind vibrations. It is noteworthy that many of the rain/wind vibrations that have been observed on cable-stayed bridges have occurred during construction when both the damping and mass of the cable system are likely to have been lower than in the completed state, resulting in a low Scruton number. The grouting of the completed cables adds both mass and probably damping, and often sleeves of visco-elastic material are added to the cable end connections which further raises the damping. The available circumstantial evidence indicates that the rain/wind type of vibration primarily arises as a result of some cables with exceptionally low damping, down in the $\zeta = 0.001$ range.

Since many bridges have been built without experiencing problems from rain/wind vibration of cables it appears probable that in many cases the level of damping naturally present is sufficient to avoid the problem. The rig test data of Saito et al. (1994), obtained using realistic cable mass and damping values, are useful in helping to define the boundary of instability for rain/wind oscillations. Based on their results it appears that rain/wind oscillations can be avoided provided that the Scruton number is greater than 10,

$$m\zeta/\rho D^2 > 10 \tag{16}$$

This criterion can be used to assess how much damping a cable needs to avoid rain wind oscillation problems. Recent full-scale data have generally supported this criterion (Jones and Main, 2002).

Since the rain/wind oscillations are due to the formation of rivulets on the cable surface it is probable that the instability is sensitive to the surface roughness, or to small protrusions on the surface and to the type of sheathing material. One approach to solving the rain/wind problem is to have small protrusions running parallel to the cable axis or coiled around its surface. For example, Matsumoto et al. (1989) indicate that they found axially aligned protrusions of about 3/16-in height and 7/16-in width at 30 degree intervals around the perimeter of 6-in diameter cables were successful in suppressing oscillations. This method has been used on the Higashi-Kobe Bridge, and has proven effective. However, for longer main spans, the additional drag

force on the cables introduced by the protrusions can become a substantial part of the overall wind loads.

Flamand (1994) has used helical fillets 1/16-in high and 3/32-in wide with a pitch length of 2 ft on the cables of the Normandie Bridge. This technique has proven successful, with a minimal increase in drag coefficient. Work by Miyata and Yamada (1995) has shown that lumped surface roughness elements, typically of order 1% of cable diameter, can be used to introduce aerodynamic stability in rain/wind conditions with no appreciable increase in drag force.

Examples of these techniques are illustrated in Figure 33.

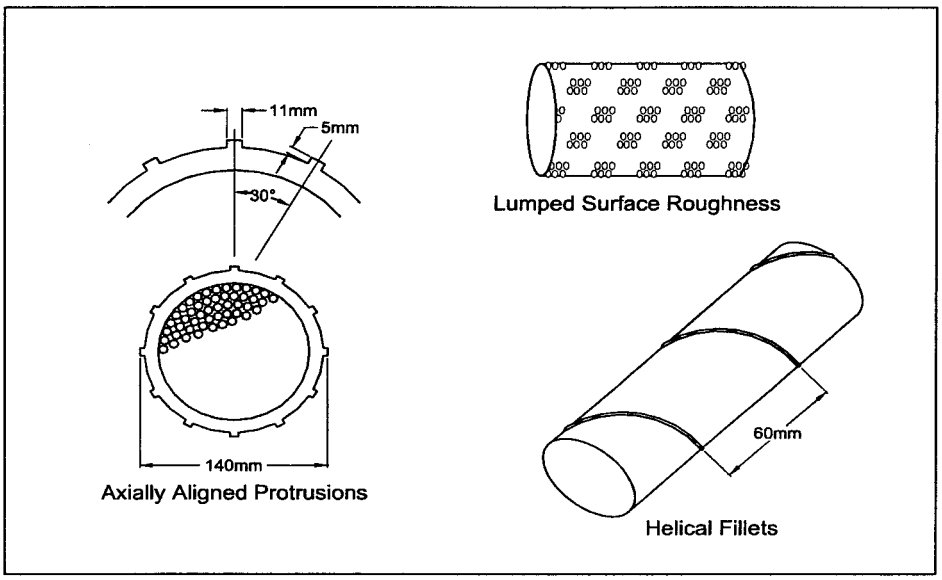

Figure 33: Aerodynamic devices.

Galloping of Cables with Ice Accumulations

The accumulation of ice on a cable in an ice or freezing rain storm can lead to an effective change in shape of the cable to one that is aerodynamically unstable. This has caused large amplitude oscillations of long power conductor cables and could potentially occur on bridge cables. However, we are not aware of this being a common problem on bridges. In the power industry special dampers such as the Stockbridge damper have been employed to mitigate this problem. For bridges the general measure of ensuring that cables do not have excessively low damping will probably be sufficient to avoid most problems from this source.

Galloping of Cables in the Wakes of Other Structural Components

The wakes of bridge components such as towers or arches have velocity gradients and turbulence in them, and if a cable becomes impacted by these disturbed flows they can in principle experience galloping oscillations. It might be difficult to distinguish oscillations caused by this

mechanism from those due to other causes such as buffeting, galloping in the wakes of other cables, or rain/wind oscillations. There do not appear to be any reports of cases where galloping in the wake of another structural component such as a bridge tower has been specifically identified. As with other types of instability, ensuring the cable has as high a damping as possible would be a good general preventive measure against this type of galloping.

Cable Oscillations due to Aerodynamic Excitation of Other Bridge Components

The natural modes of vibration of a long span bridge and its cables, treated as a single system, are numerous. Many of these modes involve substantial cable motions accompanying relatively small motions of other major components such as the deck. It is conceivable therefore that the deck could be excited, by vortex shedding for example, into very small oscillations which are of little significance for the deck but which involve concomitant motions of one or more of the cables at much larger amplitude. To the observer this type of response to wind could well appear like pure cable oscillations if the deck motions were too small to notice, and yet the source of the excitation would in this case be wind action on the deck.

Pinto da Costa et al. (1996) have shown analytically that small amplitudes of anchorage oscillation can lead to large cable responses if the exciting frequency is near the natural frequency of the lower modes of the cables. Anchorage displacement amplitudes as low as 1½-in are shown to cause steady-state cable displacements of over 6 ft for a 1450 ft stay cable with a critical damping ratio below 0.1%, typical of bridge stay cables during erection. Anchorage motions with frequencies equal to or double the first natural frequency of vibration of the cables are most likely to excite the cables. This type of excitation appears not to have been specifically identified in full scale observations of bridges. On the other hand it is a subtle effect that could easily be confused with other forms of cable excitation. It is a subject requiring further research.

Motions due to Buffeting by Wind Turbulence

Flexible structures such as long bridges and their cable systems undergo substantial motions in strong winds simply due to the random buffeting action of wind turbulence. Very long cables will have their lower modes of vibration excited by this effect but it is not an aeroelastic instability. Even very aerodynamically stable structures will be seen to move in strong winds if they are flexible. Buffeting motions are not typically a problem for bridge cables. However, they may be mistakenly identified as the beginnings of an aeroelastic instability. The buffeting motions increase gradually with wind speed, rather than in the sudden fashion associated with an instability.

Motion due to Fluctuating Cable Tensions

Fluctuating forces due to turbulence produces fluctuating tension in the stays, which induce fluctuating forces at the anchorage points (lifting on the deck and pulling on the tower). Davenport (1995) has noted that the fluctuating axial tension in cable stays produced by drag is an additional excitation mechanism for the cables. Denoting the change in drag per unit length of the cable by ΔF_D, the magnitude of the fluctuating tension as a fraction of the fluctuating lateral load on the stays is:

$$\frac{\Delta T}{\Delta F_D L} = \frac{k_e}{k_g} \bullet \frac{T/(mL)}{1 + (k_e/k_g) - (\omega/\omega_0)^2} \tag{17}$$

where:

L	= cable length
k_e	= elastic stiffness of the cables, AE/L,
k_g	= gravitational stiffness, $[m\pi^4/8][T/(mL)]^3$
ω_o	= natural frequency of the cable
ω	= exciting frequency

A strong multiplier effect is indicated in Equation 17 through the term $[T/(mL)]$, and the term $[1 + (k_e/k_g) - (\omega/\omega_o)^2]$ which has resonance characteristics at $\omega = \omega_o$.

It is important to note the relationship between anchorage displacements and cable tension. A combination of fluctuating tension in the stay cables and oscillation of the anchorage points will likely have the effect of feeding energy into the cables, amplifying the motion. Ensuring adequate damping levels for the stay cables will reduce cable motion considerably.

B1.2 MITIGATING MEASURES

From the above discussion it is clear that there are a number of causes of aerodynamic excitation of cables, so there are several possible approaches to developing mitigating measures. Some of these are not always practical for implementation but they are all listed below for completeness.

(i) **Modify Shape**: Increasing the surface roughness with lumped regions of roughness elements or helical fillets has the benefit of stabilizing the cables during rain/wind conditions without an increase in drag. Well-defined protrusions on the cable surface with a view to modifying the behavior of the water rivulets in rain/wind vibration (as discussed earlier, Figure 33) have been used in Japan. These methods are most effective for the rain/wind instability problem. It is unclear how effective these techniques are for solving the wake galloping problem. The use of helical fillets as cable surface treatment is becoming popular for new cable-stayed bridges, including Leonard P. Zakim Bunker Hill Bridge (MA), U.S. Grant Bridge (OH), Greenville Bridge (MS), Maysville-Aberdeen Bridge (KY), William Natcher Bridge (KY), and Cape Girardeau Bridge (MO).

(ii) **Modify Cable Arrangement**: The wake interaction effects of cables can be mitigated by moving the cables further apart. Clearly, the implications of this must be weighed against other design constraints such as aesthetics and structural design requirements.

(iii) **Raise Natural Frequencies**: By raising the natural frequencies of the cables the wind velocity at which aerodynamic instability starts is increased. The natural frequency depends on the cable mass, the tension and on the length. Often the tension and mass are not quantities that are readily adjusted without impacting other design constraints, but the effective cable length can be changed, at least in arrays of cables, by connecting the cables transversely with secondary cable cross-ties (Figure 34). The lowest natural frequency susceptible to aerodynamic excitation can be easily be raised several fold by this means. An example was given earlier in the section on wake galloping. Bridges where cross-ties are being provided include Dames Point Bridge (FL), Greenville Bridge (MS), Cape Girardeau Bridge (MO), Leonard P. Zakim Bunker Hill Bridge (MA), Maysville-Aberdeen Bridge (KY), and U.S. Grant Bridge (OH).

(iv) **Raise Mass Density**: By increasing the mass density of the cable one may increase the Scruton number and, as discussed in the earlier sections, this is universally beneficial in reducing susceptibility to aerodynamic instability. However, in practice the cable mass density can only be varied within a very limited range.

(v) **Raise Damping**: Increasing the damping is one of the most effective ways of suppressing aerodynamic instability, or postponing it to higher wind velocity and thus making it rare enough not to be of concern. Since the damping of long cables tends to be naturally very low, the addition of relatively small amounts of damping at or near the cable ends can provide dramatic improvements in stability. Several techniques have been successfully used on existing structures, including viscous (oil) dampers (Figure 35), neoprene bushings at the cable anchorages, petroleum wax in-fill in the guide-pipes, and visco-elastic dampers in the cable anchorage pipe (Figure 36). It should be noted that the

addition of cross-cables to the primary stay cables can also introduce additional damping to the system, on the order of 10 to 50 percent (Yamaguchi & Nagahawatta, 1995). Experimental studies (Saito et al. 1994) of the cables of the Higashi-Kobe Bridge in Japan have indicated that cable vibrations are not a problem at damping ratios above 0.3% of critical. Full-scale damping measurements on the long-lay cables of the Annacis Bridge in Vancouver, which include neoprene dampers at both ends of the cable, indicate damping ratios of 0.3% to 0.5% (Steimer & Taylor, 1988). This bridge has apparently had no reported difficulties with cable vibrations. Thus a damping ratio of about 0.5% appears to be a minimum threshold to meet to minimize potential cable instability problems.

A number of bridges that have reported cable vibration problems are listed in Table 9. Also listed in Table 9 are remedies used to solve the cable vibration problem. All of the remedies listed in the table use some of the measures discussed above, and have apparently been effective in mitigating the cable vibration problem. These methods are illustrated in Figures 33-36.

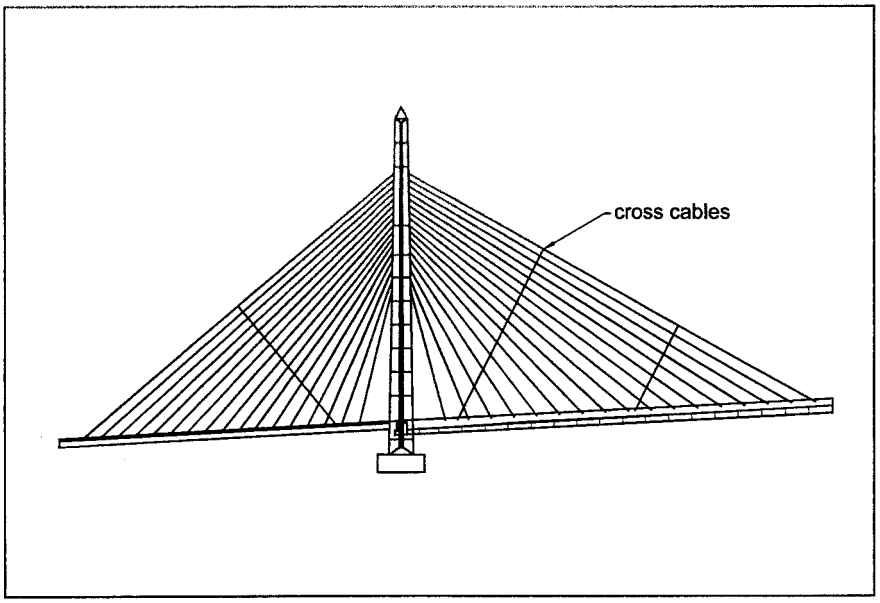

Figure 34: Cable cross-ties.

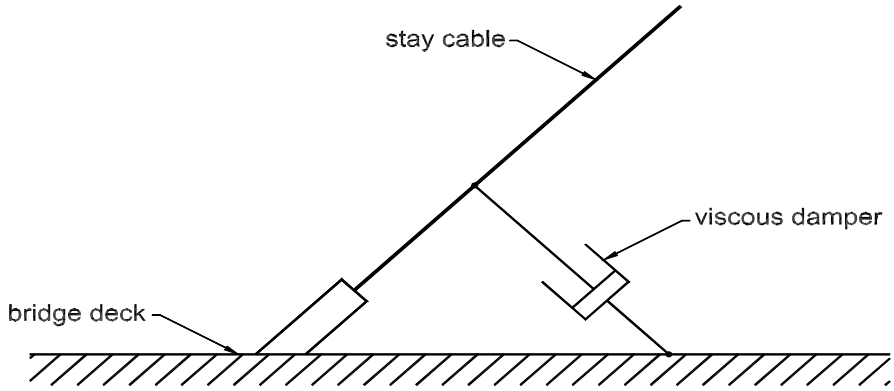

Figure 35: Viscous damping.

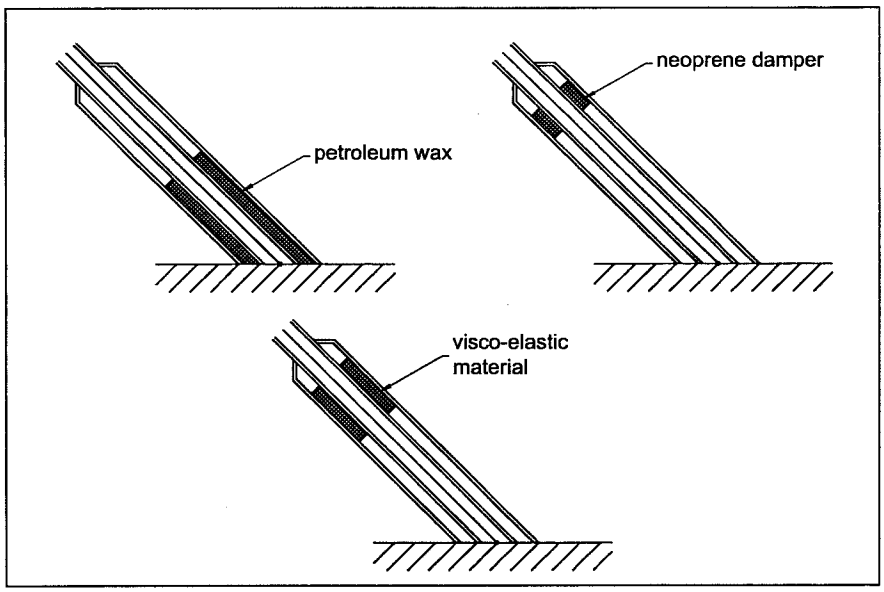

Figure 36: Material damping.

Table 9: Bridges reporting cable vibration and mitigating measures.

Name	Location	Length of main span (ft)	Observations	Double Amplitude of Vibration (ft)	Remedy*
Normandy	Le Havre, France	2800	cable vibrations during steady 1-2m/s winds	5	viscous dampers installed
Second Severn	Bristol, United Kingdom	1500	cable vibrations with and without rain	1.5-5	cross-cables installed
Helgeland	Sandnessjoen, Norway	1400	large cable vibrations; depending on deck motion	2	cross-cables installed
Meiko Nishi	Aichi, Japan	1325	vibration during light rain / low wind speeds	1.8	cross-cables installed
Tjorn Bridge	Gothenburg, Sweden	1180	vibration during light rain	-	viscous dampers installed
Tenpozan	Osaka, Japan	1150	vibration during rain and 10m/s winds-	6.5	-
Kohlbrandt	Hamburg, Germany	1070	-	3.3	viscous dampers installed
Brotonne	Rouen, France	1050	vibrating in 15m/s winds	2	viscous dampers installed
Weirton-Steubenville	W. Virginia, USA	820	vibrations noted when winds are parallel to deck	2	visco-elastic dampers to be installed in the guide pipe at deck level
Yobuko	Saga, Japan	820	vibration during light rain	0.5	manila ropes attached to cables
Aratsu	Kyushu Is., Japan	610	vibration during light rain	2	viscous dampers installed
Wandre	Wandre, Belgium	550	vibration during light rain and 10m/s winds	1.6	petroleum wax fill in the guide pipe
Ben-Ahin	Huy, Belgium	550	vibration noted during light drizzle and 10m/s winds	3.3	petroleum wax grout added in the guide pipe and cross-cables also added
Alzette	Luxembourg	425	vibration during drizzle and light winds	-	neoprene guides inside the guide pipe at deck and petroleum wax fill in the guide pipe

*see Figure 33-36 for illustrations of mitigating measures

APPENDIX B2: WIND-TUNNEL TESTING OF STAY CABLES

EXECUTIVE SUMMARY

In order to clarify the dry cable galloping phenomenon and verify the instability data by Saito et al. (1994), a series of wind tunnel tests of a 2D sectional model of an inclined cable was conducted. The wind tunnel tests were performed in the "Propulsion" wind tunnel at the Montreal Road campus of the Institute of Aerospace Research, National Research Council Canada (IAR/NRCC). The main findings of the current study can be summarized as follows:

1) Limited-amplitude high-speed vortex shedding excitations have been observed under a variety of conditions.
2) Motions that reached the limits of the test rig were observed at low damping for one case, i.e., 2C: it is possible that this was a divergent galloping instability.
3) The limited-amplitude vibration was observed only in the limited wind speed range at different wind speed levels corresponding to the critical Reynolds number. The maximum amplitude of the response depends on the orientation angle of the cable.
4) The limited-amplitude high-speed vortex excitation was easily suppressed by increasing structural damping.
5) If wind blows along the cable, for cables with a vertical inclination angle $\theta \leq 45°$, the increase of surface roughness makes the unstable range shift to lower wind speeds.
6) Since elastic bands were used to change the frequencies of the cable motion in the X-and Y-directions, which at the same time affects the system damping, no clear frequency ratio effect was identified from the test results. However, this parameter could be important for the aerodynamic behavior of the inclined dry cable, and thus is worthy of further investigation.
7) The instability data for inclined cable vibration defined by Saito et al. (1994) is found to be more conservative than the results obtained from the current study. The instability defined by the current findings has a much steeper slope than that given by Saito.
8) The Reynolds number effect, which results from the model surface condition and the orientation angle, needs to be further explored.

B2.1 INTRODUCTION

The focus of the test program was to examine the response of a dry cable (i.e. no rain-wind interaction) inclined at various angles to the wind. As discussed in the main text, various methods for suppressing rain-wind oscillations have been developed and appear to be effective, even though not all aspects of the excitation mechanism are fully understood. Therefore, tests on rain-wind excitation were concluded to be not at the top of the priority list. However, the question of oscillations of dry cables is still the subject of much debate. Some believe the only dry cable oscillations that occur are due to parametric excitation, in which the fluctuating aerodynamic forces acting on the deck and towers cause some oscillations of those components, which then feed energy into the cables causing them to develop much larger oscillations. Others believe wind action on the cables themselves, either involving Den Hartog type galloping or a high speed form of vortex excitation, is the source of oscillations. The aim of the test program was to investigate the direct action of wind on dry inclined cables with a view toward helping to resolve the debate. In particular, the tests would duplicate some of the conditions tested by Saito et al. (1994), and attempt to confirm or modify the criteria suggested in that paper for dry cable galloping.

Since the wind speeds where oscillations have been observed and the typical stay cable diameters result in the cables being in a critical range of Reynolds number (where the aerodynamic parameters such as drag coefficient and Strouhal number undergo rapid transformations), it was important to undertake the testing in the same Reynolds number range as experienced in the field. The "model" scale was therefore selected to be approximately 1:1. A segment of cable with overall diameter 6.3 in (160 mm) was selected (the outer PE sheath, without a spiral bead, being the same as used for the Maysville bridge). The test cable mass was selected to facilitate achieving realistic Scruton numbers. Also it was important to use a wind tunnel with a speed range similar to the range of wind speeds seen on bridges. The Propulsion wind tunnel at the National Research Council of Canada (NRCC) in Ottawa was selected for this purpose, having a speed range of 0 - 87 mph (0 - 39 m/s), and having working section dimensions of 20 ft in the vertical direction and 10 ft in the horizontal direction. The local assistance of Prof. Hiroshi Tanaka and his graduate student S.H. Cheng at the University of Ottawa was also obtained for the running of the tests, data analysis, and assistance in report preparation. The testing also benefited from the advice and experience of NRCC staff, including Dr. Guy Larose who had undertaken tests previously in Europe on cable vibration problems.

The dynamic test rig supporting the test cable was designed and constructed by Rowan Williams Davies & Irwin, Inc. (RWDI) and shipped to Ottawa after initial shake down tests in Guelph. RWDI staff also directed the test program. In designing the rig, use was made of the fact that, in the context of cable vibrations, wind does not know the difference between the vertical and horizontal directions. The only angle that matters as far as its interaction with a cable is concerned is the angle between the wind vector and the cable axis. This simplified the wind tunnel tests because it implied that the test cable could be maintained in a vertical plane aligned with the central axis of the wind tunnel. The only angle adjustment needed to cover the range of relative angles between wind and cable seen on a real bridge was the angle of the test cable to the horizontal. However, a cable on a bridge does have slightly different frequencies in the vertical plane and in lateral direction. Therefore, to the extent that this frequency ratio matters, it was felt that there should be the ability to alter the cable frequencies in two orthogonal directions on the model. This was made possible by having adjustable sets of orthogonal springs at each end of the test cable. The orientation of the test rig springs could be rotated to any angle about the test cable axis. This, combined with the adjustable angle between test cable and the horizontal axis of the wind tunnel, allowed various combinations of wind direction relative to the bridge axis and full scale cable angle relative to the horizontal to be simulated, covering most of the range of interest.

Other parameters of importance to cable vibrations, besides those already discussed, are the damping ratio, frequency ratio of vertical and horizontal cable frequencies and the surface roughness. Therefore the test program included an examination of the influence of these parameters.

B2.2 MODEL DESIGN

Cable Model

A 6.7 m long full-scale cable model is used for the purpose of the current project. It is supplied by RWDI. The cable, consisting of an inner steel pipe and outer smooth polyethylene (PE) tube, has an outside diameter of 160mm. A 3/8-16 machine screw was put on at one end only during the initial setup stage to prevent the inner steel pipe sliding out of the PE tube. The weight of the cable itself is 356.4kg (785 lb.), i.e. 53.2kg/m. The model is supported on a rig designed and manufactured by RWDI. When the cable vibrates, the effective cable mass should include that of the steel shaft at the pipe ends, and 1/3 of the spring mass on the supporting rig. Thus, the total active dynamic mass of the cable is 407.4kg, and the effective mass per cable length is 60.8 kg/m.

Angle relationships between the cable and mean wind direction

As shown in Figure 37, the orientation of the cable with respect to the mean wind direction can be represented by two angles. If the wind blows with a horizontal angle of β to the bridge axis, the projection of the cable on the horizontal plane makes a horizontal yaw angle β with the wind vector. Also, if the cable is assumed to be in a vertical plane parallel to the bridge axis, it has a vertical inclination angle θ.

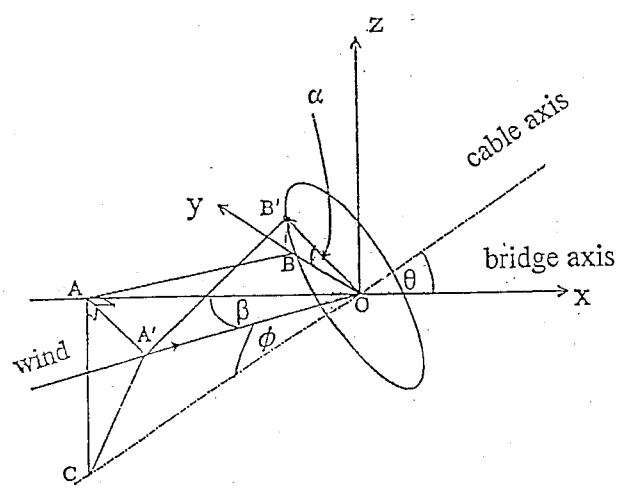

Figure 37: Angle relationships between stay cables and natural wind (after Irwin, P. A.).

The relative angle Φ between the wind direction and cable axis has the relationship with θ and β as follows

$$\cos \Phi = \cos \beta \cos \theta \qquad (18)$$

The direction of cable motion is normal to both the wind direction and the cable axis, and can be represented by the vector OB' given in Figure 37. OB' has an angle α with respect to its horizontal projection OB. This angle α also has a relationship with the orientation angles θ and β, given by

$$\tan \alpha = \tan \beta / \sin \theta \qquad (19)$$

Supporting Rig

The cable supporting rig was designed and built for the current project by RWDI. For the purpose of the test, there are a number of requirements for the design of the rig as follows:

a) To allow the vibration of a 6.7m long, 356.4kg full-scale cable model at the natural frequency of 1-2Hz;
b) To allow the convenient change of cable orientation angles for exploring more different setup cases;
c) This setup of the cable model allowed for approximately 6.0 m of the 6.7 m cable in the wind flow and maintained the upwind support out of the wind flow.
d) To keep the inherent structural damping of the whole system as low as possible, so that the level of damping for controlling dynamic behavior can be examined by supplying additional damping;
e) To be able to simulate a slight difference between the horizontal and vertical frequencies as it is expected of in the case of real stay cables.

The designed test rig meets all these requirements. It consists of the upper and bottom parts to support both ends of the cable model, as shown in Figure 38. There are two pairs of springs set in two perpendicular directions on each part of the rig. Both springs are in the plane perpendicular to the cable axis. The adjustment of the spring stiffness controls the change in cable frequencies in the spring direction. The total mass of the springs is 60 kg. The vertical spring constant is 4.99kN/m, and the horizontal one is 4.78kN/m, when one of them is placed horizontally.

TOP SPRING RIG BOTTOM SPRING RIG

Figure 38: Cable supporting rig.

Because of the size of the cable model and the limitation in the dimension of the wind tunnel facility, the simulation of real cable orientation angles, θ and β, for the range of interest is difficult to reproduce. Thus, the simulation of the corresponding wind-cable relative angle Φ and cable motion direction angle α are considered instead.

The cable model is set up in the wind tunnel with its upper wind end protruding through the tunnel ceiling and supported by the upper part of the rig. One panel of the wind tunnel ceiling was cut out to allow the cable to go through. The down wind end of the model is supported by the bottom part of the rig, which is supported on a horizontal H-shaped frame. Two sides of the frame are fixed on the wind tunnel wall. The distance from the tunnel floor to the plane of the frame can be adjusted by fixing the two sides of the frame at different heights on the tunnel wall. By doing so, different wind-cable relative angle Φ can be modeled. The cable model is in a similar orientation as the tests performed by Saito et al. (1994) by this setup.

In the present study, an aerodynamic instability is explored that is not a function of the gravitational force but of the inertial mass in the direction of motion. The two parts of the test rig can support the gravitational force of the cable model. Further, an axial cable is attached from the building frame to the upper end of the model to provide more support. The two pairs of springs at both ends can be rotated about the central axis of the cable model. Consequently, the horizontal and vertical vibration planes of the cable are rotated, and the ground plane is effectively being rotated. By rotating the ground plane, the direction of cable motion is changed, thus different cable motion direction angle α can be achieved. According to Equations 18 and 19, by choosing appropriate combinations of Φ and α, the desired orientation angles θ and β of stay cables in real cable-stayed bridges can be modeled in the wind tunnel tests.

For the initial setup, one pair of springs at each end was set along the horizontal direction, while another pair was set perpendicular to it (spring rotation angle $\Phi = 0°$). In this report, the direction coinciding with the initial horizontal spring is defined as X-direction, while that coinciding with the initial vertical spring is defined as Y-direction. The definition of X and Y directions is kept consistent in this report even in the cases where the spring rotation angle was other than 0°.

B2.3 WIND TUNNEL TESTS

Wind Tunnel Facilities

The Propulsion wind tunnel at the Montreal Road Campus of IAR/NRCC is used to carry out a series of tests for the project. It is an open circuit wind tunnel of the blowing type with fan at the entry. The flow enters the test section through a contraction cone, which accelerates the flow and improves the uniformity of the flow velocity. Figures 39 and 40 show the longitudinal section and cross-section of the tunnel respectively. There is a removable cap of 3.7m (12ft) long at the tunnel roof. An overhead travelling crane with a 15 ton capacity is available to lift the roof cap and install the model. The floor of the working section can be raised up to 0.46m to facilitate work on model installations, to simulate varying ground effects, or to modify floor boundary layer characteristics. The wind tunnel working section is 12m long, 3m wide and 6m high.

By using the electric drive in the tunnel, the maximum wind speed can reach 39 m/s. The non-uniformities of the working section velocity are generally less than 0.5% of mean wind velocity, and flow direction is within 1° of tunnel axis over most of the working section. Because the tunnel is of an open circuit type, the quality of the working section flow depends somewhat on the external wind conditions.

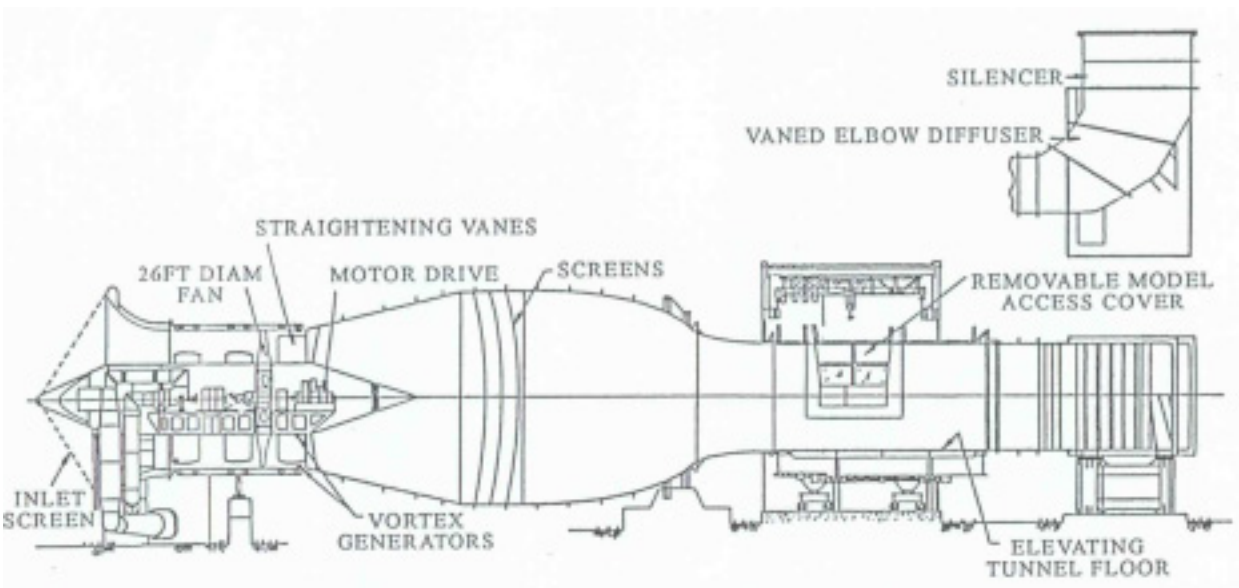

Figure 39: Longitudinal section of the "Propulsion" wind tunnel.

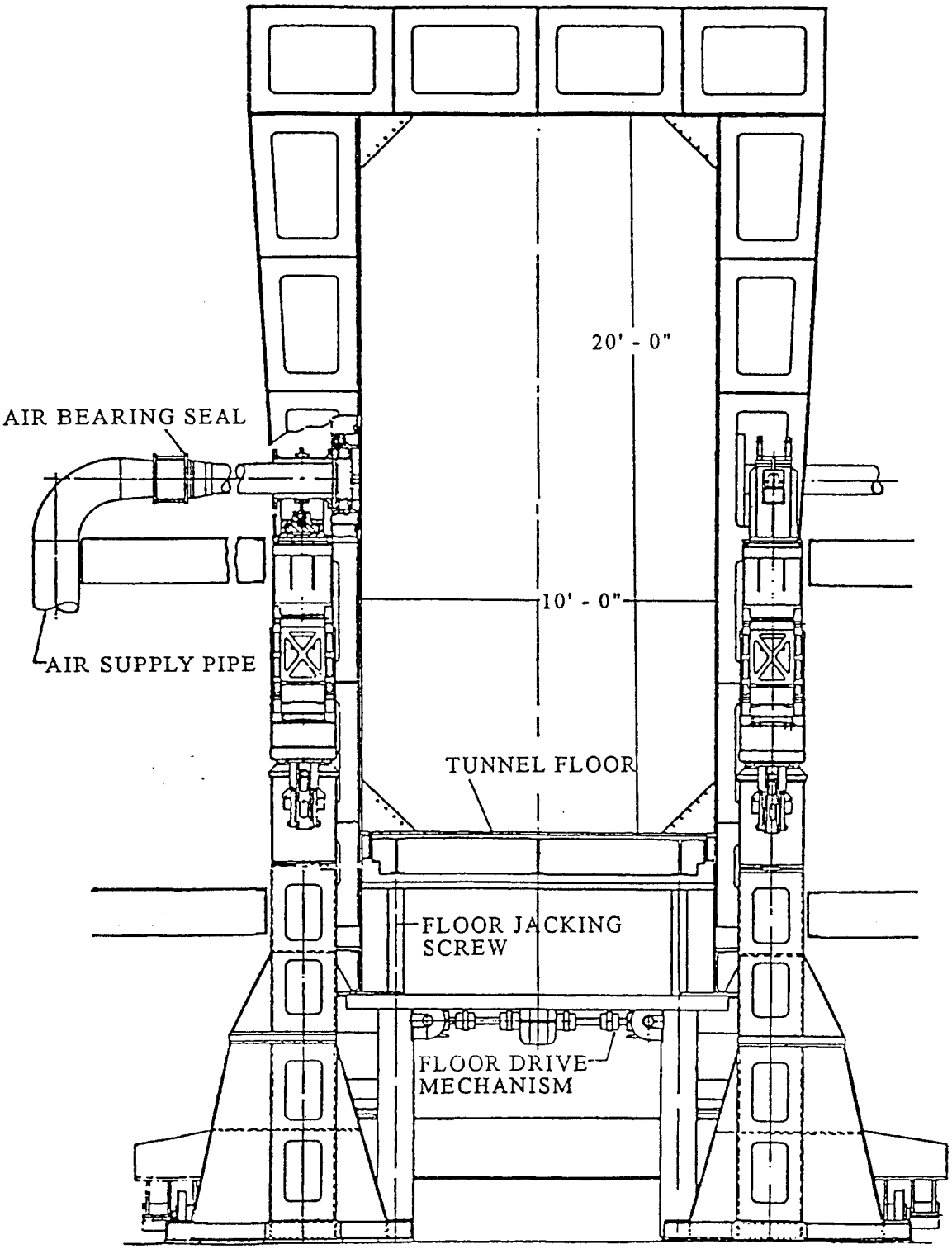

Figure 40: Cross-section of the working section of "Propulsion" wind tunnel.

Data acquisition system

The tests were conducted within the Labview environment. Seven channels were recorded simultaneously to collect the response data. The sampling frequency was 100Hz. The setup of the data acquisition system is shown in Figure 41.

Figure 41: Data acquisition system.

At each end of the model, two non-contact type laser displacement sensors (Model ANR 1226) and controllers (Model ANR 5141) were installed to measure the displacements along the X and Y directions. They were placed within the spring/damper housings and are protected from any influence of the flow. The range of the sensors is ±150mm with the linear error of less than 0.4%.

Two Pitot tubes were mounted separately on the two sides of the tunnel walls. They were placed upwind at the 2/3 points of the model to give a representative mean pressure over the full length of the cable, i.e. at 2.07m from the inlet and 3.61m above the tunnel floor. The pressure was read by a sensitive high differential pressure transducer Druck LPM 9381. The average pressure obtained from these two Pitot tubes was used for the calculation of wind tunnel speed.

The description of the input channels are given as follows:
Channel 1: Downwind end X direction displacement
Channel 2: Downwind end Y direction displacement
Channel 3: Upwind end X direction displacement
Channel 4: Upwind end Y direction displacement
Channel 5: Pitot tube #1
Channel 6: Pitot tube #2
Channel 7: Temperature

The real-time viewer of the collected response data contains three plots:
Plot 1: X-direction displacements vs. time at each end from laser sensors 1 and 3 (2 lines)
Plot 2: Y-direction displacements vs. time at each end from laser sensors 2 and 4 (2 lines)
Plot 3: Mean X- and Y-direction displacements vs. time, i.e. (Laser 1 + Laser 3)/2 and (Laser 2 + Laser 4)/2 (2 lines)

The measured real-time wind pressure in the tunnel given by Pitot tubes #1 and #2, the corresponding mean wind speed calculated based on the readings from these two Pitot tubes, and the instantaneous tunnel temperature were also displayed.

For each testing case, the collected data from those seven channels were saved in two files. The first file was a time history file. It contained the X- and Y-direction displacements at the two ends of the model recorded by the four laser sensors. The second file contained the summary statistics of the data collected from the seven channels, as well as the mean X-displacement ($(Laser1 + Laser3)/2$), mean Y-displacement ($(Laser2 + Laser4)/2$), mean angle ($Arc\tan\frac{Laser1 + Laser3}{Laser2 + Laser4}$) in terms of mean, RMS, maximum, and minimum, respectively.

The convention of the filenames allowed the identification of each individual testing case. It contains the following parameters:
Pipe finish (surface roughness): — "A": Smooth surface
— "B": Rough surface
Vertical inclination angle of the model: 2-digit descriptor in degrees
Spring rotation angle: 2-digit descriptor in degrees
Wind speed: 2-digit descriptor in m/s
Damping: 3-digits descriptor as fraction of critical
Excitation method: "h" for hard or manual excitation, "s" for soft excitation, i.e. without manual excitation
Multiple runs of the same case: 2-digit flag to identify the running sequence

As an example, for the testing case of a smooth pipe, with model inclination angle 45°, spring rotation angle 0°, wind speed 18m/s, structural damping 0.6% of critical, soft excitation, third trial of the same case, the file names would be
A_450018006_s03.tms for the time history file, and
A_450018006_s03.sta for the statistical summary file.

A monitor, which was linked to a video camera installed outside the window of the wind tunnel, was set up in the control room, the cable motion under different wind velocity levels during the tests could be monitored. Once the instability behavior of the cable motion was observed, it would be recorded on videotape.

Control of the damping level: airpot damper

The effect of damping level on the inclined dry cable vibration was examined. The airpot damper, as shown in Figure 42, was initially suggested to be used for supplying additional damping to the cable system at each end of the cable support; two airpot dampers installed along the directions of the two perpendicular springs. A cross-sectional view of the airpot damper is given in Figure 43.

Figure 42: Airpot damper.

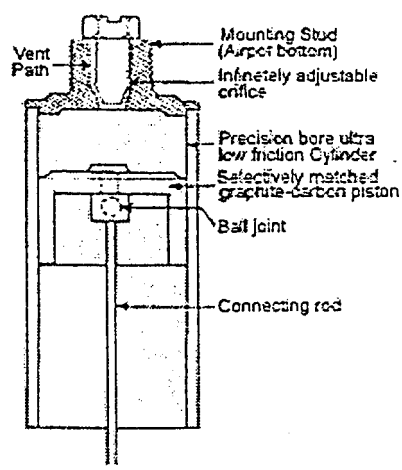

Figure 43: Cross-section of airpot damper.

The airpot damper uses the ambient air as the damping medium. The force to be damped is transmitted through the airpot piston rod, which moves the piston within the cylinder. The orifice setting and the diametric clearance between the piston and cylinder control the rate of air transfer. As the piston moves in response to the force exerted, there will be a change in volume and pressure in the airpot, causing ambient air to enter or leave the cylinder. The rate of airflow can be controlled to provide the exact degree of damping required by a simple adjustment of the orifice.

However, during the preparation of the tests, it was found that the frictional damping between the piston and the cylinder wall inside the airpot damper had a significant impact on the small-amplitude motion, which suppressed the hand-excited cable vibration in just a few cycles. Finally, the airpot damper was only used in the cases of very high level damping with the order of 1% of critical, while for the intermediate and high level damping cases, elastic bands were used along the spring coils to increase the system damping (Figure 44). By adjusting the number and locations of the elastic bands to be installed on the spring coils, the desired structural damping levels were achieved.

Figure 44: Elastic bands on the spring coils.

Surface Treatment

In order to explore the surface roughness effect on the cable oscillation, a kind of liquid glue was sprayed on the windward side of the model surface to simulate the accumulation of dirt and salt on the real cable.

Frequency Ratio

One distinguishing response characteristic of cable galloping is that the motion follows an elliptical trajectory. In the current model setup, the stiffness of the two pairs of perpendicular springs will affect the amplitude of motion in these two directions, and thus the resultant

oscillation path of the cable. By properly adjusting the spring stiffness of these two directions, the associated in-plane and out-of-plane vibration frequencies are changed. If the frequencies are close enough, the motions in these two directions would become resonant, which forms an elliptical shape of the motion path. Thus, the impact of the frequency ratio between the two perpendicular directions on the cable behavior of interest is worth studying.

Outline of Test Cases

The aerodynamic behavior of the inclined cable model has been investigated in this wind tunnel testing by different combinations of model setup, damping level and surface roughness as described in the following tables:

Table 10: Model setup.

Model Setup	Full scale cable angles (deg.)		Model cable angles (deg.)	
	θ	β	Φ	α
1B [#]	45	0	45	0
1C	30	35.3	45	54.7
2A	60	0	60	0
2C [*]	45	45	60	54.7
3A	35	0	35	0
3B	20	29.4	35	58.7

[#] Setup 1A ($\theta = 0°$, $\beta = 45°$) and 1B are identical in reality, except that the sway and vertical frequencies are switched.

[*] Setup 2C is the same case in which Miyata et al. (1994) have found the divergent motion of the inclined dry cable.

Table 11: Different damping levels of the model.

Damping Description	Dampers Used	Approximate Damping Range (% of critical) damping is amplitude dependent
Low damping	No damper added	0.03 to 0.09
Intermediate damping	16 elastic bands per sway spring	0.05 to 0.10
High damping	28 elastic bands per sway spring	0.15 to 0.25
Very high damping	Airpot damper with 1 ¼ dial turns	0.30 to 1.00

Table 12: Surface condition.

Smooth surface	Polyethylene (PE) Pipe with clean surface
Rough surface	Polyethylene (PE) Pipe with glue sprayed on the windward side of the cable

Figures 45-47 show the model set-ups of the investigated cases in the wind tunnel tests, and Figure 48 shows a picture of the inclined cable set up in the wind tunnel.

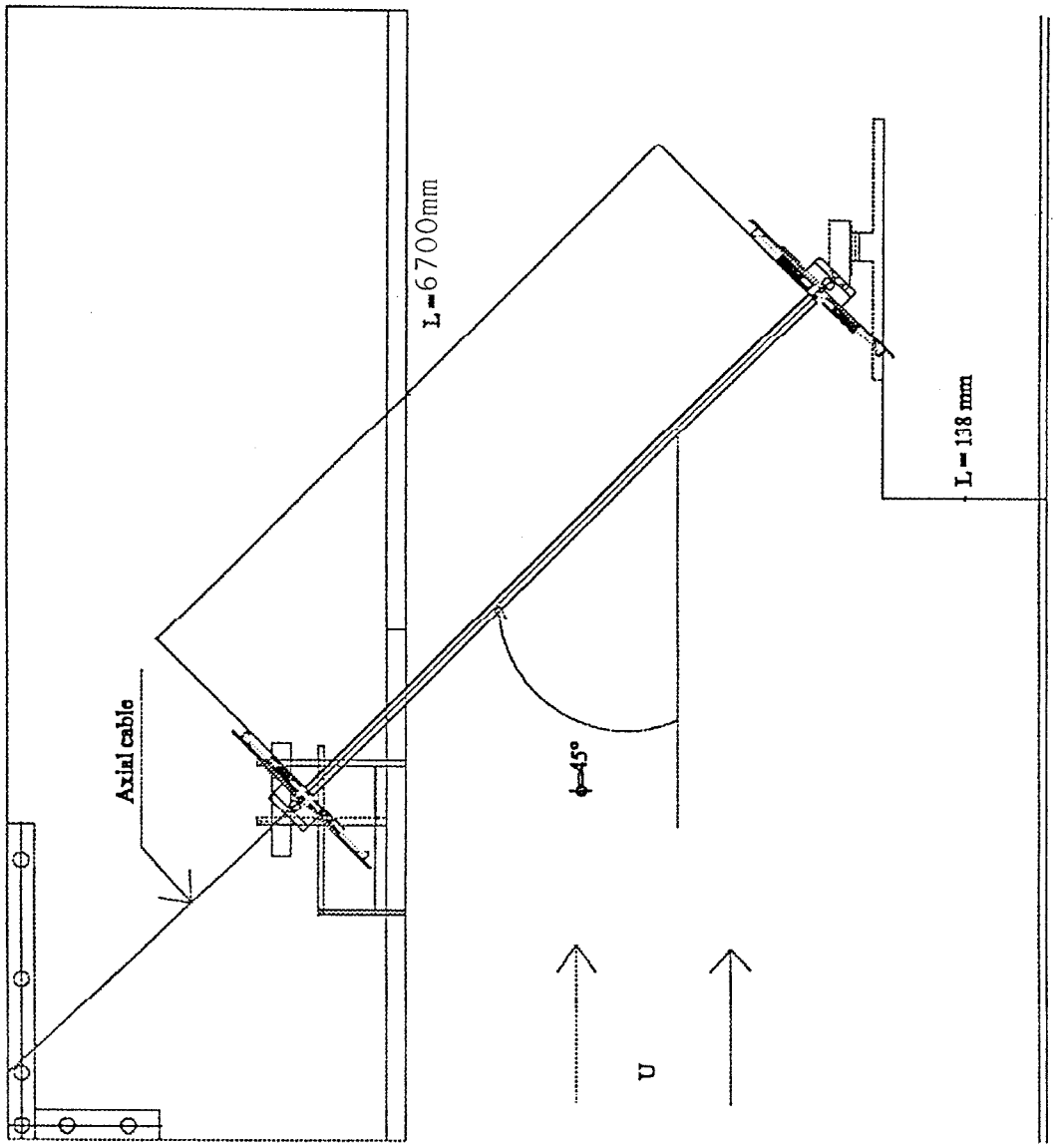

Figure 45: Side view of Setups 1B and 1C.

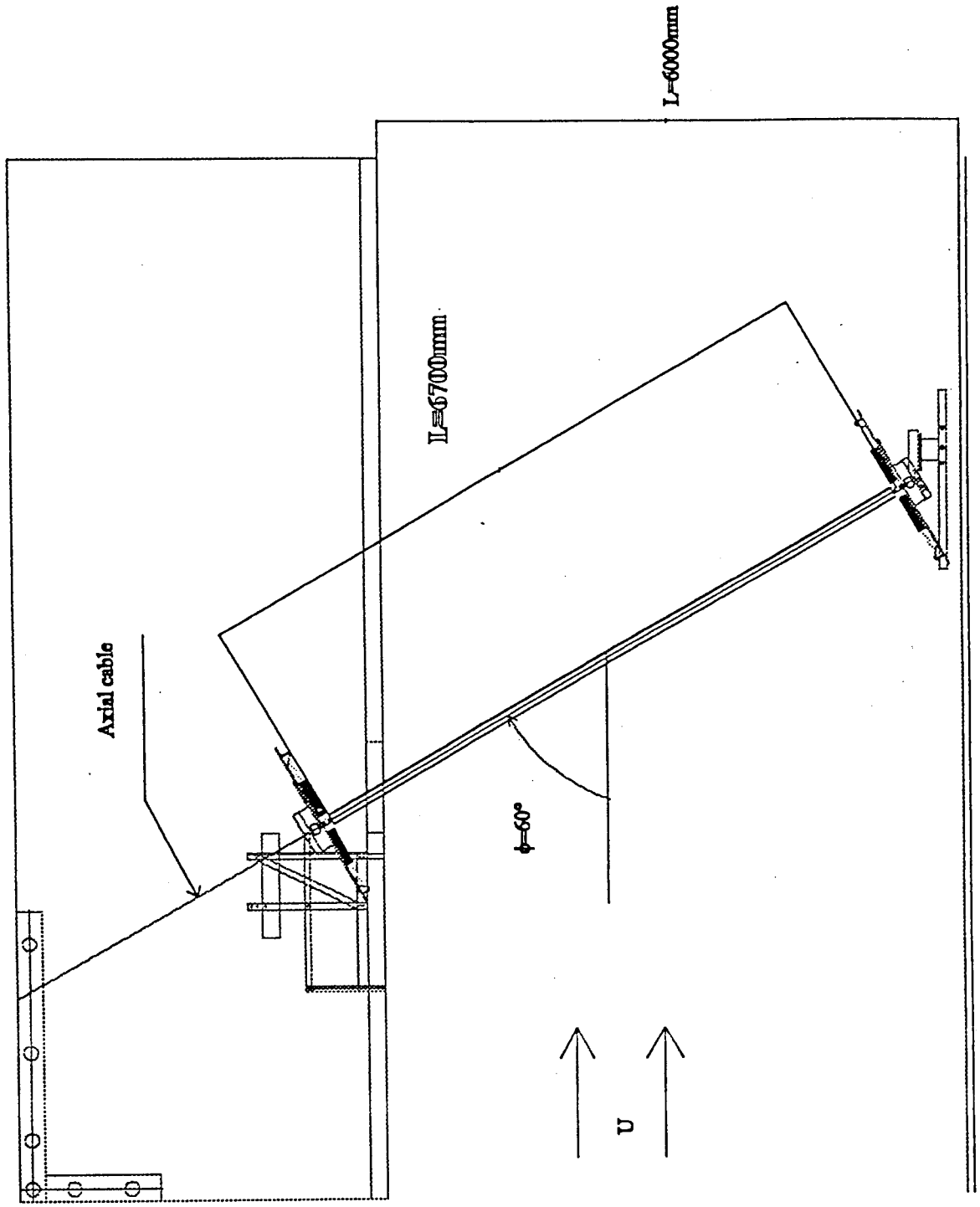

Figure 46: Side view of Setups 2A and 2C.

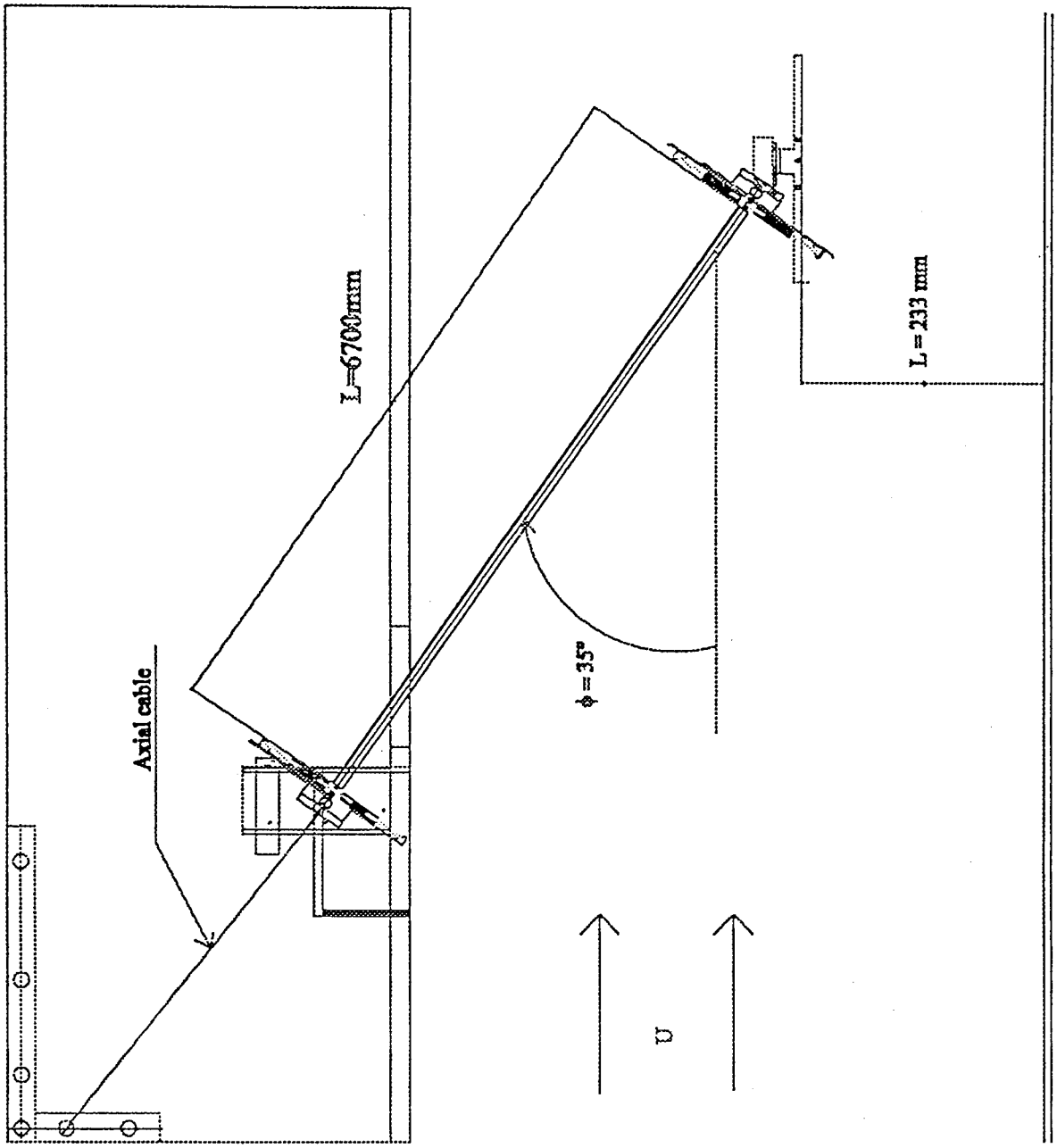

Figure 47: Side view of Setups 3A and 3C.

Figure 48: Cable set up in wind tunnel for testing.

B2.4 RESULTS AND DISCUSSION

General Procedures for a Given Test Setup

For a given case with its specific setup, the general procedures of the wind tunnel test are as follows:

i) In still air, take tare case of the model;

ii) Measure the system structural damping in X- and Y-directions by hand exciting the model along these two directions respectively. Once reached the desired amplitude level, stop the hand excitation and let the model undergo free vibration. The structural damping of the system and the vibration frequency can thus be identified;

iii) Start at the low wind speed (for the setup that is tested for the first time, take 7m/s, while for other cases, the starting value can be determined based on previous trials), increase in 2m/s increments. When the wind speed approaches the expected unstable range, increase the speed by 1m/s until unstable vibrations occur;

iv) In reality, some external effects such as wind turbulence and motions of the deck may help to initiate cable vibrations. Thus, during the tests, if no unstable vibration occurs within the expected wind speed range, hand excitation will be used to help initiate the unstable motion of the model and see if the motion decays or grows;

v) If the unstable behavior is observed, add additional damping to the system. Repeat the above procedure for different damping levels until the unstable motion is eliminated;

vi) For the low damping level (no additional damping added), change the surface roughness and repeat the same procedure.

Characteristics of Cable Motion

Both the divergent type of cable vibration and the limited-amplitude cable motion at a certain wind speed range have been observed in the current study.

Divergent type of motion

Motions of the cable that resembled divergence were observed only in Setup 2C. For this setup, the model has a vertical angle of $\Phi = 60°$, and the spring rotation angle of $\alpha = 54.7°$. This is equivalent to the full-scale cable orientation of the vertical inclination angle $\theta = 45°$ and horizontal yaw angle $\beta = 45°$.

The relationships between the system structural damping and response amplitude were obtained by hand exciting the model in X- and Y-directions, respectively. The maximum amplitude of the hand excitation was about 35mm. The free vibration immediately following the hand excitation was recorded for 15 minutes. The amplitude-dependent structural damping as a percentage of critical values in X- and Y-directions are given in Figure 49. The vibration frequency in X-direction is 1.400Hz, and that in Y-direction is 1.415Hz.

The wind-induced response of Setup 2C is given in Figure 50. The test started at a low wind speed of 10m/s. When wind speed reached 32m/s, the motion became more organized and the amplitude in the Y-direction was built up steadily from ± 20mm to ± 80mm within 3 minutes. As shown by Figures 51 and 52, which are the time histories in the X- and Y-motion at both ends of the model and the motion trajectory, the predominant motion occurs in the Y-direction. The motion had the tendency of growing further, but it had to be manually suppressed because of the clearance for the model setup at the wind tunnel ceiling. The recorded peak-to-peak amplitude was about 1D, where D is the cable diameter.

Limited-amplitude motion

The limited-amplitude unstable motion of the inclined cable model has been observed at certain wind speed levels under Setups 2A, 1B, 1C and 3A. The full-scale cable orientation angles, the model setup angles, and the unstable wind speed ranges corresponding to each individual case are given in Table 13.

Table 13: Limited-amplitude motion.

Model Setup	Full scale cable angles		Model cable angles		Unstable range			
	θ	β	Φ	α	U (m/s)	U_r *	Max. Amp. (mm)	$R_e = UD/\nu$
2A	60	0	60	0	18-19	79-84	67	$1.86 \sim 1.96 \times 10^5$
1B	45	0	45	0	24-26	106-114	31	$2.48 \sim 2.68 \times 10^5$
1C	30	35.3	45	54.7	34-38	150-167	25	$3.51 \sim 3.92 \times 10^5$
3A	35	0	35	0	22	96	20	2.27×10^5

* Ur = Reduced wind speed

Figures 53 ~ 62 show the time histories at both ends of the model as well as the trajectory of the motion for those four different setups when unstable behavior of the cable was observed.

Three sets of time histories are given in Figures 53 ~ 55 for Setup 2A. The first and second set describe the time history and trajectory of the cable motion at wind speed of 18m/s during the first and second 5 minutes, whereas the third set describes the time history and trajectory of the motion when wind speed increased to 19m/s. It can be clearly seen from these three sets that the vibration amplitude in the X-direction increases from about ± 20 mm to about ± 50 mm within the first 5 minutes of U = 18 m/s, then increases a little bit to ± 60 mm and stays steadily at that level during the second 5 minutes of U = 18 m/s. Once the wind speed increases to 19 m/s the vibration amplitude in the X-direction starts reducing slowly.

The relationship between the wind speed and response of these four setups are given in Figures 63 ~ 66. The unstable ranges are clearly indicated by the peaks in the response curves.

Based on observations, this limited-amplitude cable motion looks more like vortex shedding excitation rather than galloping. The characteristics of the motion are summarized as follows:

a) The amplitude of the motion is limited. As given in Table 13, the largest amplitude observed is in Setup 2A. When wind speed is 19m/s, the amplitude of the cable motion reaches 67mm;
b) The vibration was observed only in the limited wind speed range at different wind speed levels. The reduced wind velocities corresponding to these ranges are approximately the multiples of 20;
c) The maximum magnitude of the vibration depends on the orientation angle of the cable. It is larger with a greater vertical inclination angle, as given in Table 13. In Setup 3B, which represents the full-scale cable with a very shallow inclination angle of 20° and yaw angle of 29.4°, no unstable motion was observed within the wind speed range of 8m/s -34m/s. Figure 67 gives the response of the cable with respect to wind speed in Setup 3B. It can be seen that the amplitude of the motion stayed at less than 5mm.
d) At the wind speed range where the cable motion was observed, there are two types of response: one is an organized harmonic motion, another is with a regular beating, which is similar to what Matsumoto (1998) described as the case of 3D Karman vortex shedding excitation. He explains that this regular beating is caused by the aerodynamic interaction between the axial vortices along the inclined cable surface and the ordinary Karman vortices in the wake of the cable. The Karman vortex shedding is amplified intermittently by the axially produced vortices and induces the beating type motion of the inclined cable.
e) In some of the setups when the spring rotation angle is not 0°, which is equivalent to the wind horizontally oblique to the cable, an elliptical motion of the cable was observed, which correlates well with the field observation (Matsumoto et al., 1990)
f) The critical Reynolds number at which the sudden decrease in the drag coefficient occurs is influenced both by surface roughness and flow turbulence. The critical Reynolds number range for a smooth circular cylinder under uniform flow is $2 \sim 4 \times 10^5$, as shown in Figure 68 (Scruton, 1981). From the Reynolds numbers listed in Table 13, it is interesting to observe that for the current study, all of these instabilities occurred more or less at wind speeds corresponding to this critical Reynolds number range.

Damping Effect

Four different levels of damping, i.e. low, intermediate, high, and very high damping have been used in the tests to investigate the impact of structural damping on the aerodynamic behavior of the inclined cable.

A comprehensive set of damping tests was carried out with the model setup 1B, which represents the cable vertical inclination angle of 45° and horizontal yaw angle of 0° in full-scale bridge cables. No additional damper was applied for the low damping case. For the intermediate and high damping cases, the elastic bands were used to bind the spring coils together to increase the system damping, as shown previously in Figure 44. The achieved damping level depends on the

number and locations of the elastic bands. To obtain the intermediate level of damping, 16 elastic bands were used on each sway spring in the X-direction; while for the high damping level, 28 elastic bands were used on each spring in both X- and Y-directions. The very high damping level was achieved by installing the airpot dampers at both ends of the model with 1 ¼ dial turn.

The relationship between the critical damping ratio and the sway amplitude corresponding to these four levels of damping are given in Figure 69. Figure 70 gives the wind-induced response of the cable model with Setup 1B under those four levels of damping. As clearly shown in the figure, when the damping is increased, the response is significantly reduced, but the position of the unstable wind speed range does not change. This set of results indicates that this limited-amplitude unstable motion can be suppressed by increasing the damping of the cable.

Surface Roughness Effect

The cable model has been tested under both smooth and rough surface conditions. For the rough surface case, a kind of liquid glue was sprayed on the windward side of the model to simulate the accumulation of dirt and salt on the real cable.

Figures 71 ~ 73 describe the response of the model cable with Setups 3A, 1B and 2A under both smooth and rough surface conditions. These three cases are equivalent to wind blowing along the cable in full-scale situation. The vertical inclination angles θ are 35°, 45°, and 60°, respectively.

It can be seen from these three figures that for Setups 3A and 1B, of which the inclination angle $\theta \leq 45°$, the increase of cable surface roughness makes the unstable response range shift to lower wind speed. For Setup 2A, there are two peaks in the sway response curve of the smooth surface case: one is around 19m/s, and another is at about 34m/s. However, in the rough surface case, only one peak is identified, which is in the range of 31-32m/s. No clear peak shift phenomenon can be found for this setup. Since the inclination angles of these three setups are different, the difference in the responses given by those three figures not only include the surface roughness effect, but the influence of the orientation of the cable as well. Therefore, although the increase of cable surface roughness makes the unstable response range shift to lower wind speed for the cases of $\theta \leq 45°$, the conclusion regarding the surface roughness effect is still inconclusive from the present study alone.

The difference between the surface roughness would affect the flow separation point of the cable model, which changes the critical Reynolds number. This is likely to alter the lift and drag forces acting on the inclined cable, and thus changes its aerodynamic behavior. Further, recent study (Larose & Zan, 2001) shows that the change of orientation angle of the smooth cylinder will also affect the Reynolds number. In order to better understand the mechanism of the unstable motion of the inclined cable and develop methods to eliminate or mitigate the instability, it is very important to further explore this Reynolds number effect.

Frequency Ratio Effect

In real cable-stayed bridges, the horizontal and vertical frequencies of the stay cables are slightly different. The design of the cable model and supporting rig in the current project faithfully reproduced this characteristic. Results obtained from the tested cases show that for the vibration of the cable model, the predominant motion was always in the direction of higher frequency. In order to investigate the impact of frequency ratio on the aerodynamic behavior of inclined dry cable, efforts were made to change the frequency ratio between the horizontal and vertical motions. Tests were conducted for three different frequency ratios with Setup 2A:

i) f_s = 1.477 Hz, f_v = 1.452 Hz, f_s / f_v = 1.017;
ii) f_s = 1.460 Hz, f_v = 1.448 Hz, f_s / f_v = 1.008;
iii) f_s = 1.428 Hz, f_v = 1.432 Hz, f_s / f_v = 0.997;

where f_s is the sway frequency in the X-direction, and f_v is the vertical frequency in the Y-direction. All three cases were done with the smooth surface condition. For both case (i) and (ii), 28 elastics bands were applied on each spring. In case (i), the elastic bands were placed such that they not only bound the spring coils into several groups, but touched the steel rods inside the spring coils as well. In case (ii), only half number of the elastic bands touched the rods. In order to get higher frequency in the Y-direction in case (iii), the elastic bands on the sway springs were removed, and those kept on the vertical springs did not touch the steel rod.

Given in Figures 74 and 75 are the damping records and responses corresponding to these three cases. In Figure 74a, which is the damping of the motion in the X-direction, case (iii) has a much lower damping ratio within the same amplitude range as compared to case (i) and (ii). This is because in case (iii), the elastic bands on the sway springs were removed, which reduced the system damping in the X-direction. The larger sway response of case (iii) shown in Figure 75a correlates well with this fact.

From the response curves shown in Figure 75, no clear effect of the frequency ratio can be identified. This could be that the differences between the frequencies of those three cases are too small. Also, by using elastic bands to change the frequencies, the system damping was also affected. In order to further explore this frequency ratio effect, it will be a better approach to get different frequencies by adjusting the stiffness of the springs. Therefore, other effects, such as the change in the system damping, can be kept as small as possible.

Comparison with Other Studies

A limited number of experimental studies on inclined cables have been carried out particularly in Japan. Saito et al. (1994) defined an instability criterion for the inclined cable motion based on three different model setups. Two of them are exactly the same as Setup 1B and 2A in the current study. Miyata et al. (1994) investigated the inclined dry cable motion with one model setup, which corresponds to Setup 2C in the present series of tests. In order to make comparison, these two sets of results, as well as the results obtained from the current study are shown together in Figure 76. Among the results from current findings, only the one corresponding to Setup 2C exhibited signs of divergent galloping motion, whereas the others are all high speed vortex

shedding excitation. The Scruton number is defined as $Sc = m\zeta/\rho D^2$, where m is cable mass per unit length, ζ is the logarithmic decrement, ρ is the air density, and D is the cable diameter. As can be seen from the figure, the boundary for instability defined by Saito is much more conservative when compared with the results given by Miyata and the current study. In addition, the similar instability criterion that could be defined by current findings would have much steeper slope than that given by Saito, which implies that with the increase of the cable structural damping, the instability range of the inclined cable motion will be shifted to even higher wind speed level, or the motion would be effectively eliminated.

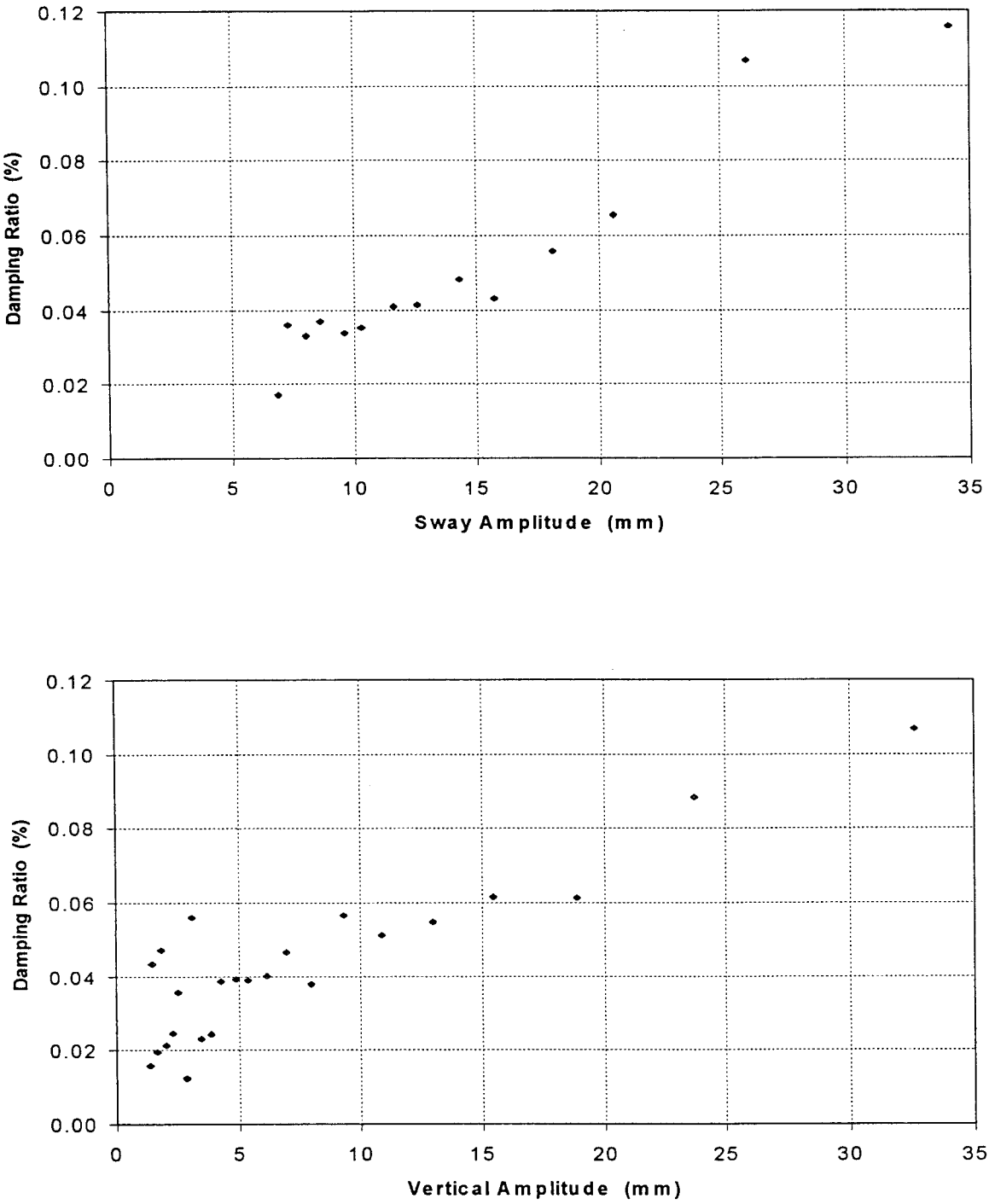

Figure 49: Amplitude-dependent damping with Setup 2C (smooth surface, low damping).

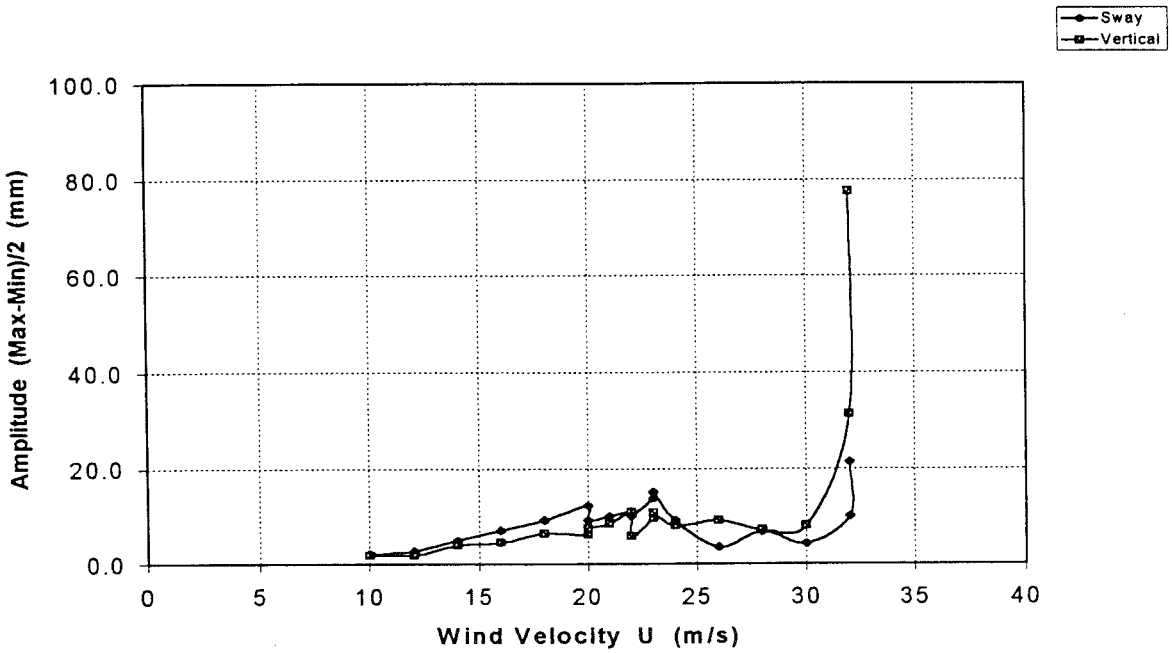

Figure 50: Divergent Response of Inclined Dry Cable (Setup 2C, smooth surface, low damping).

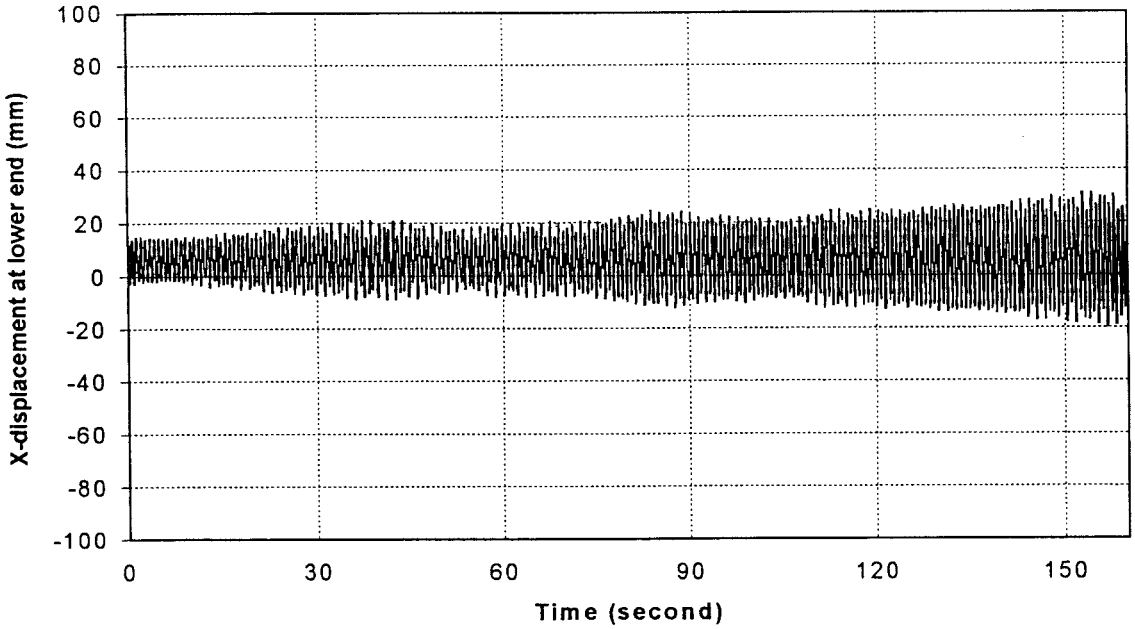

Figure 51a: Lower end X-motion, time history of Setup 2C at U=32 m/s.

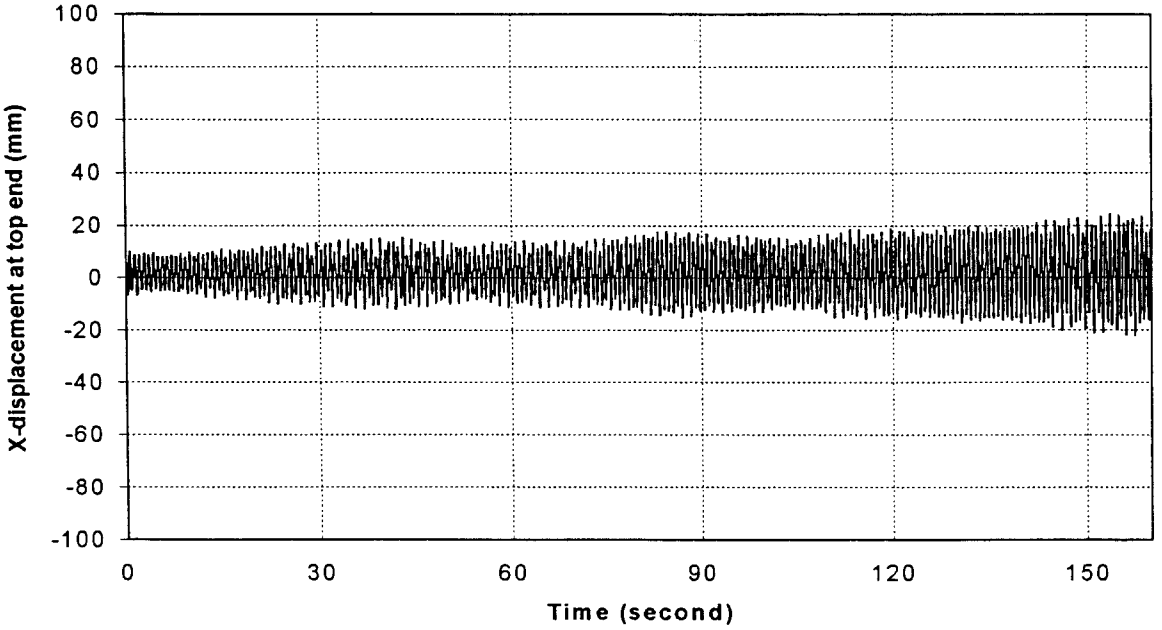

Figure 51b: Top end X-motion, time history of Setup 2C at U=32 m/s.

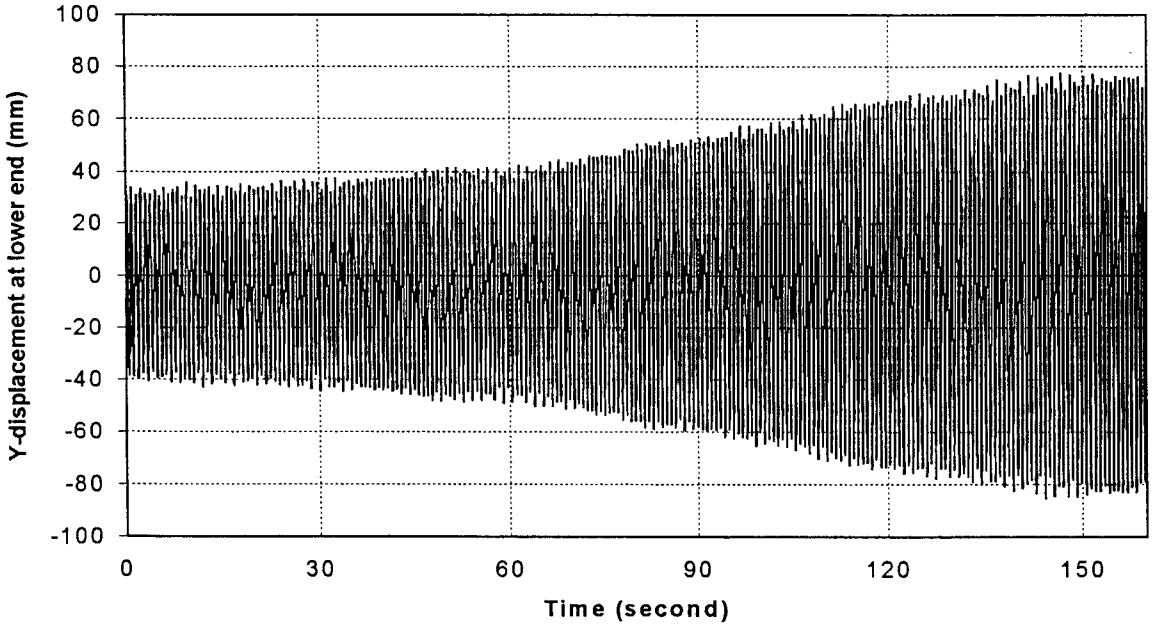

Figure 51c: Lower end Y-motion, time history of Setup 2C at U=32 m/s.

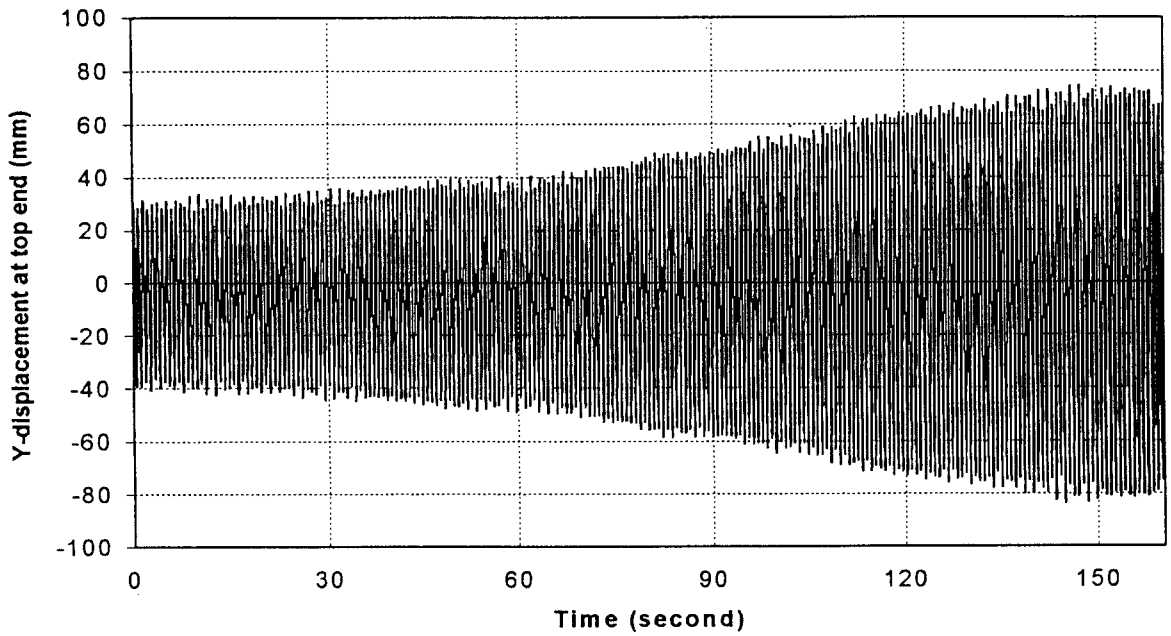

Figure 51d: Top end Y-motion, time history of Setup 2C at U=32 m/s.
(File: A_605532006_S02.tms, smooth surface, low damping)

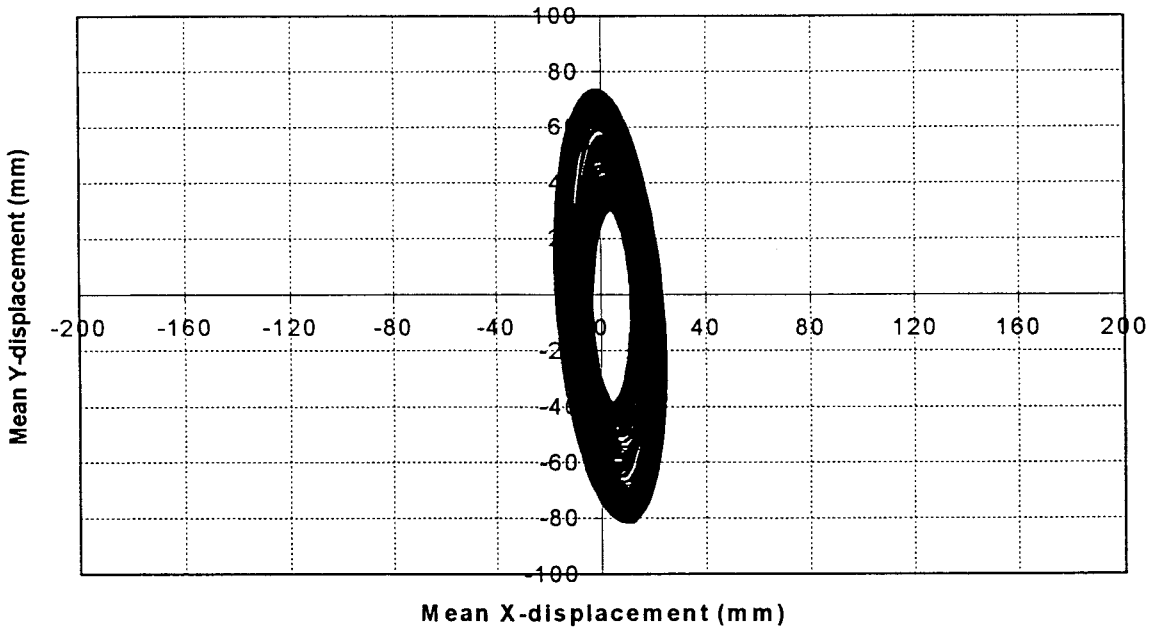

Figure 52: Trajectory of Setup 2C at U=32 m/s.
(File: A_605532006_S02.tms, smooth surface, low damping)

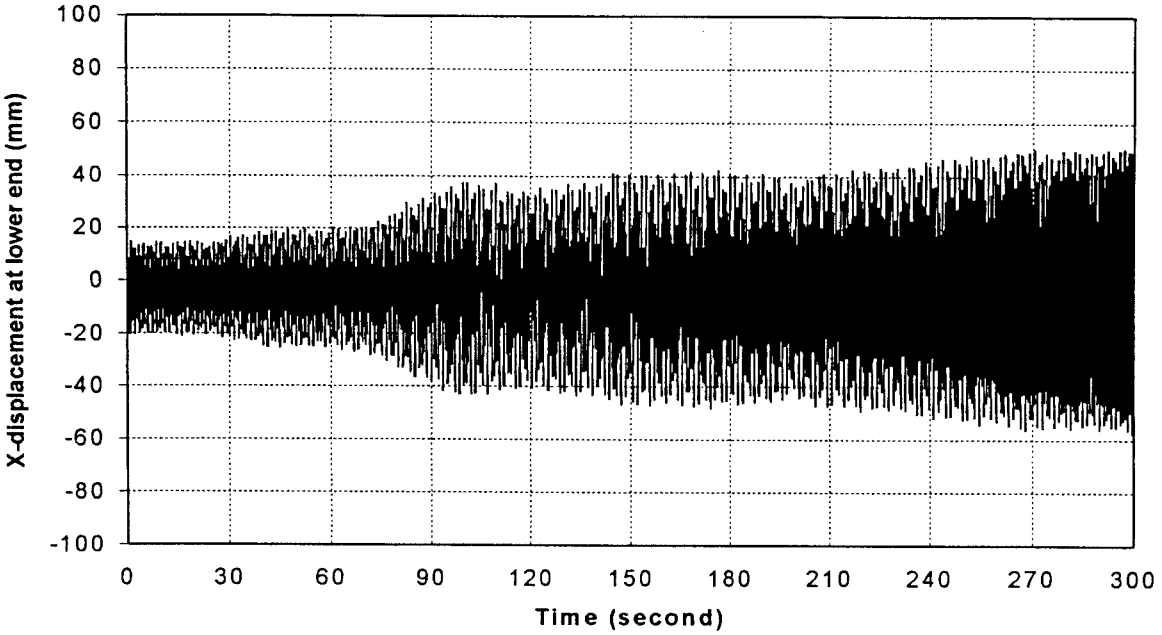

Figure 53a: Lower end X-motion, time history of Setup 2A at U=18 m/s in the first 5 minutes.

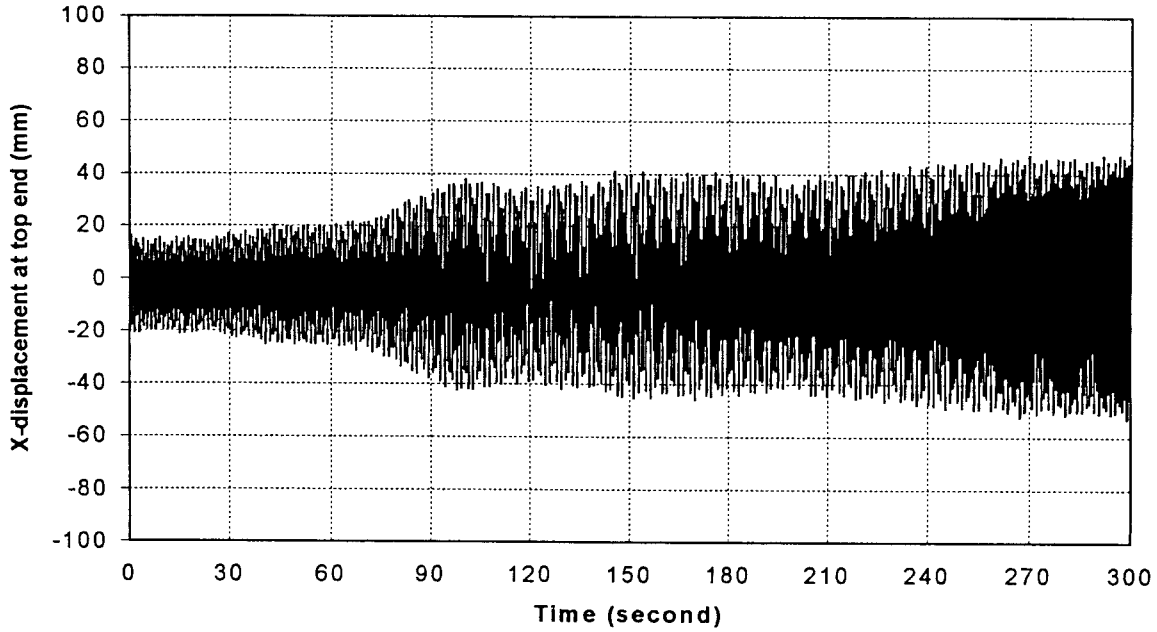

Figure 53b: Top end X-motion, time history of Setup 2A at U=18 m/s in the first 5 minutes.

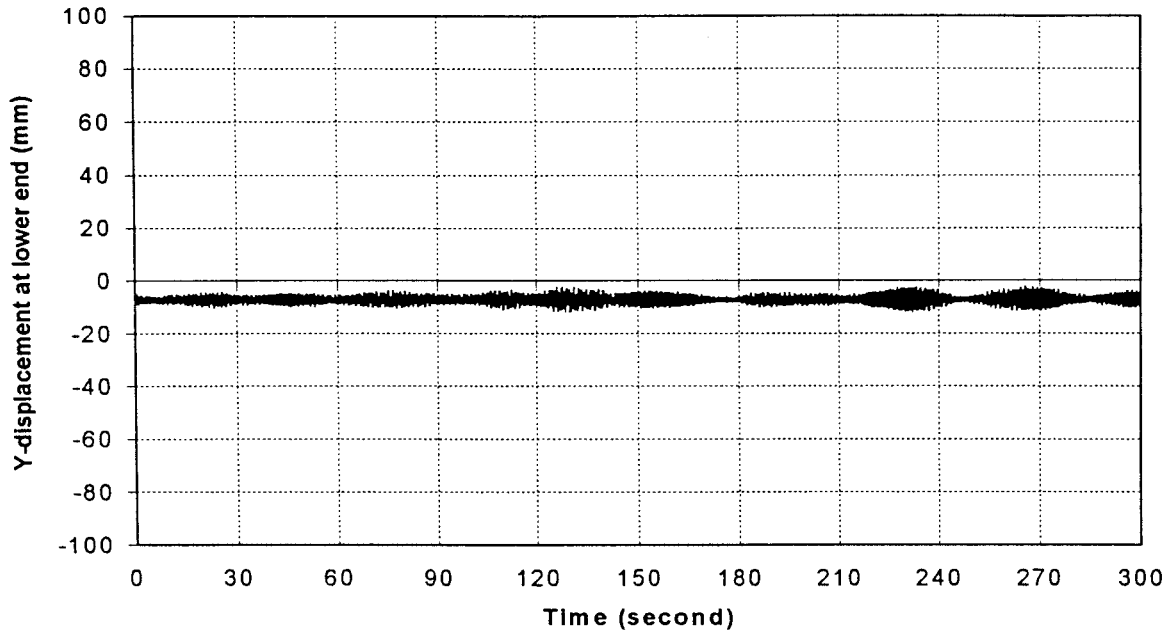

Figure 53c: Lower end Y-motion, time history of Setup 2A at U=18 m/s in the first 5 minutes.

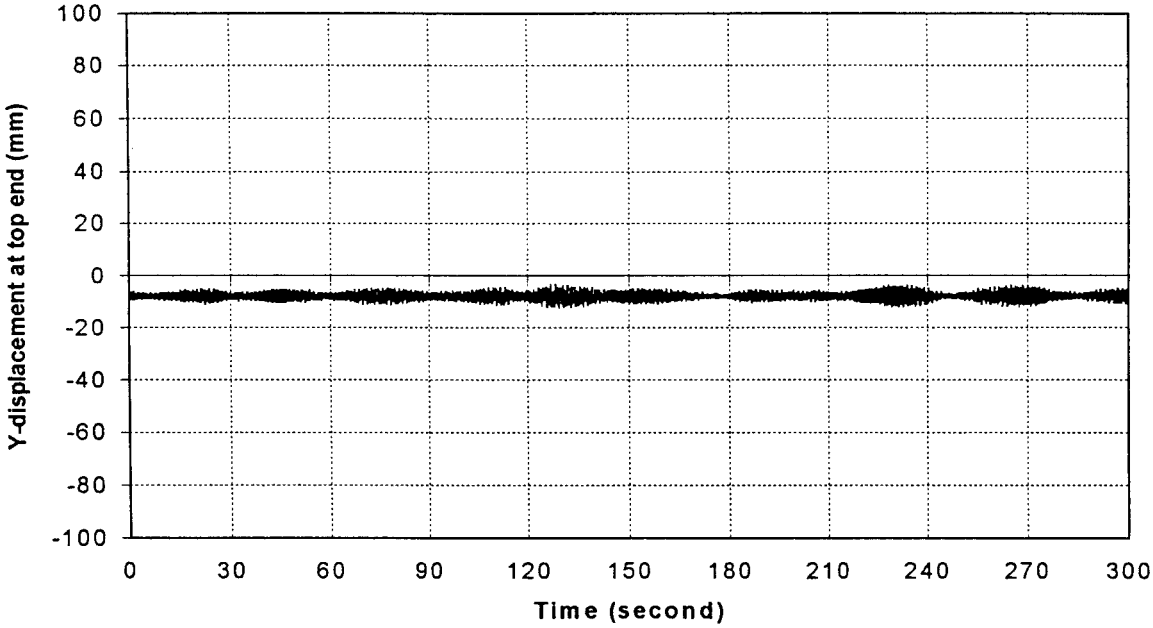

Figure 53d: Top end Y-motion, time history of Setup 2A at U=18 m/s in the first 5 minutes. (File: A_6000018006_S01.tms, smooth surface, low damping)

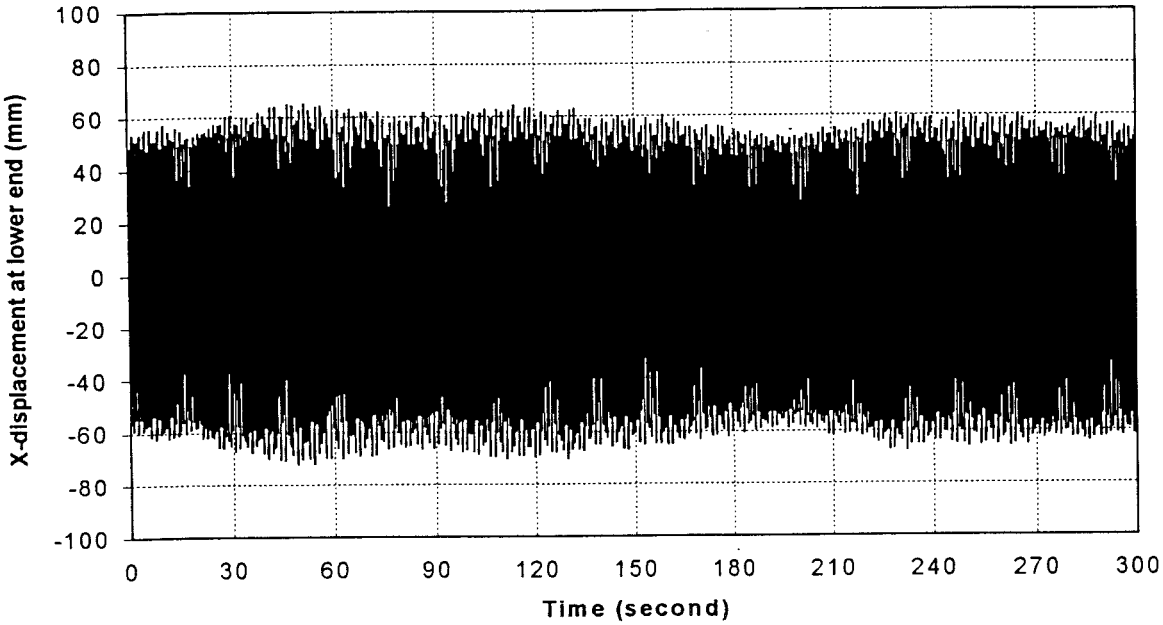

Figure 54a: Lower end X-motion, time history of Setup 2A at U=18 m/s in second 5 minutes.

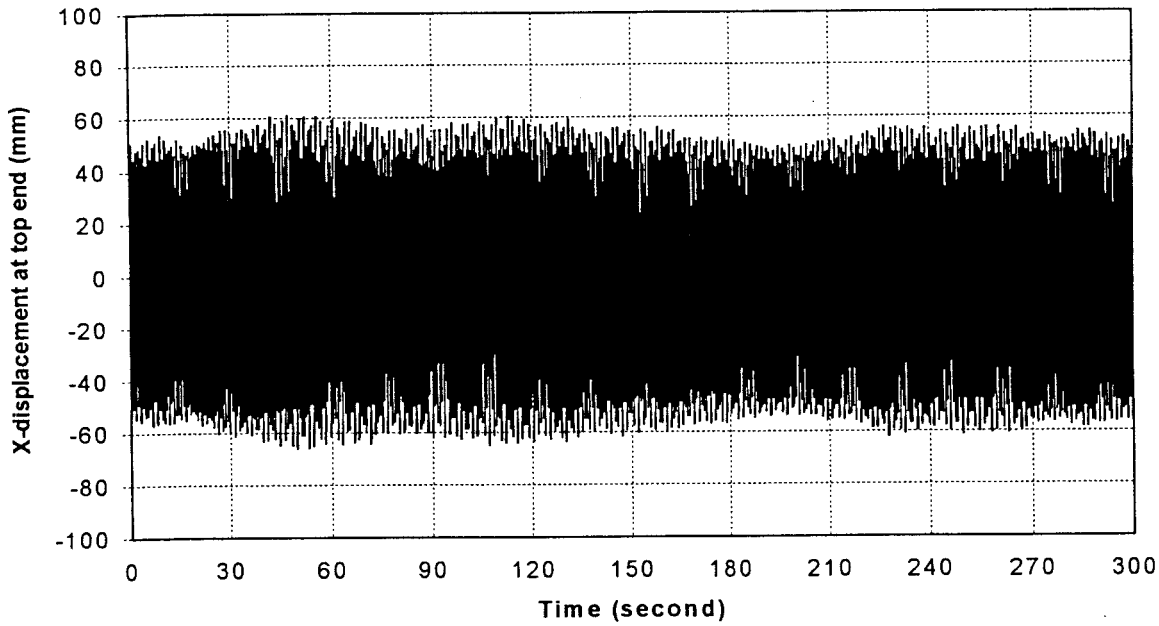

Figure 54b: Top end X-motion, time history of Setup 2A at U=18 m/s in second 5 minutes.

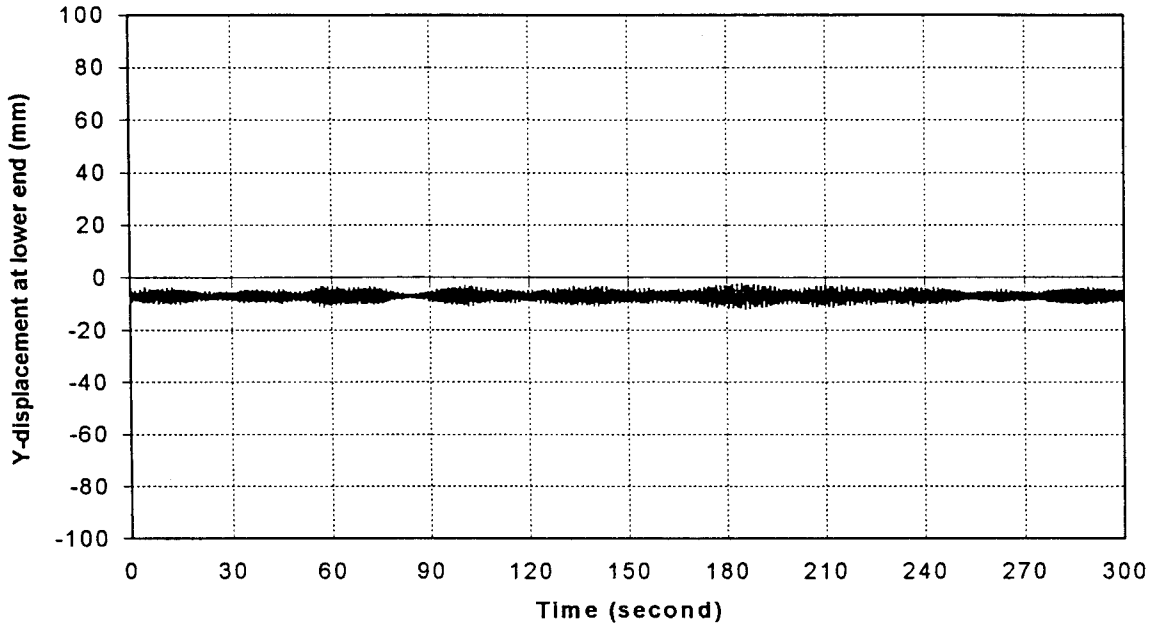

Figure 54c: Lower end Y-motion, time history of Setup 2A at U=18 m/s in second 5 minutes.

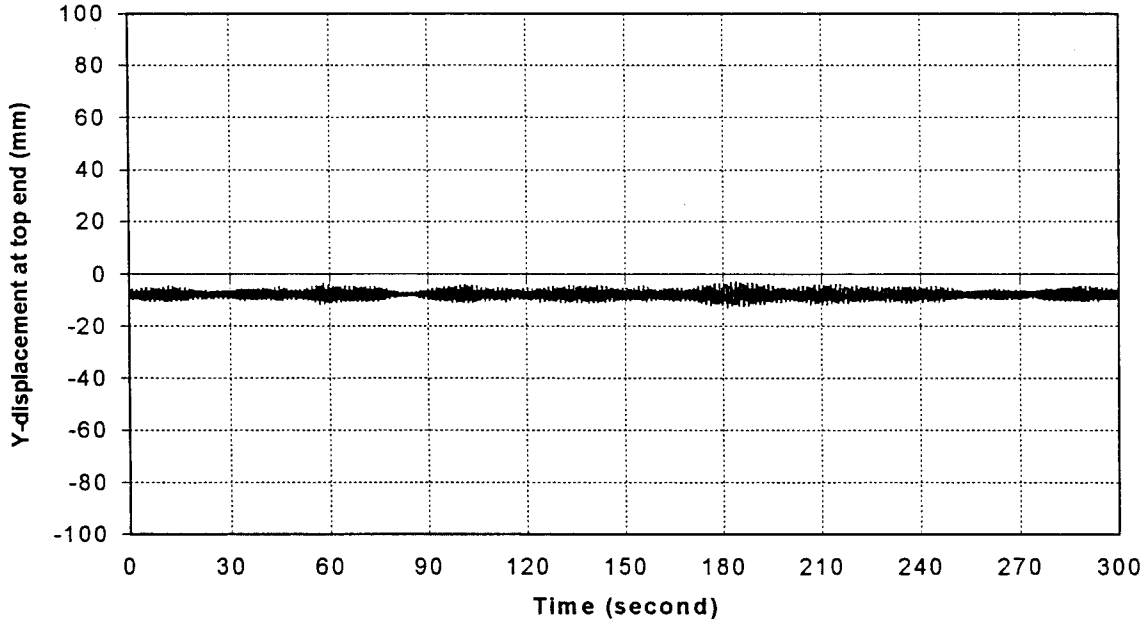

Figure 54d: Top end Y-motion, time history of Setup 2A at U=18 m/s in second 5 minutes. (File: A_6000018006_S02.tms, smooth surface, low damping)

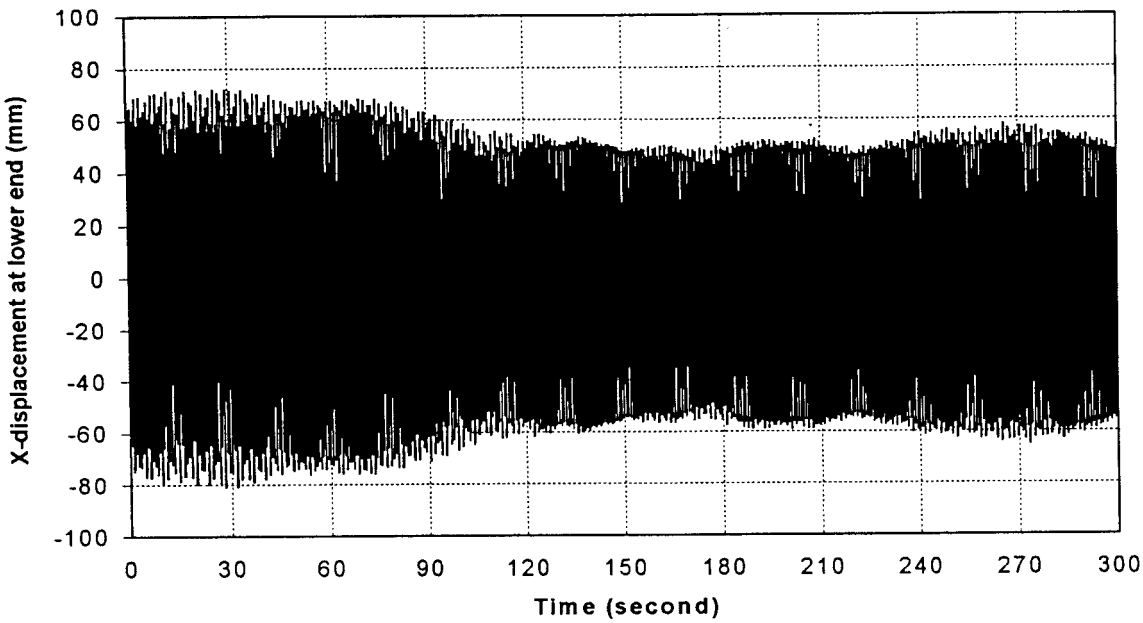

Figure 55a: Lower end X-motion, time history of Setup 2A at U=19 m/s.

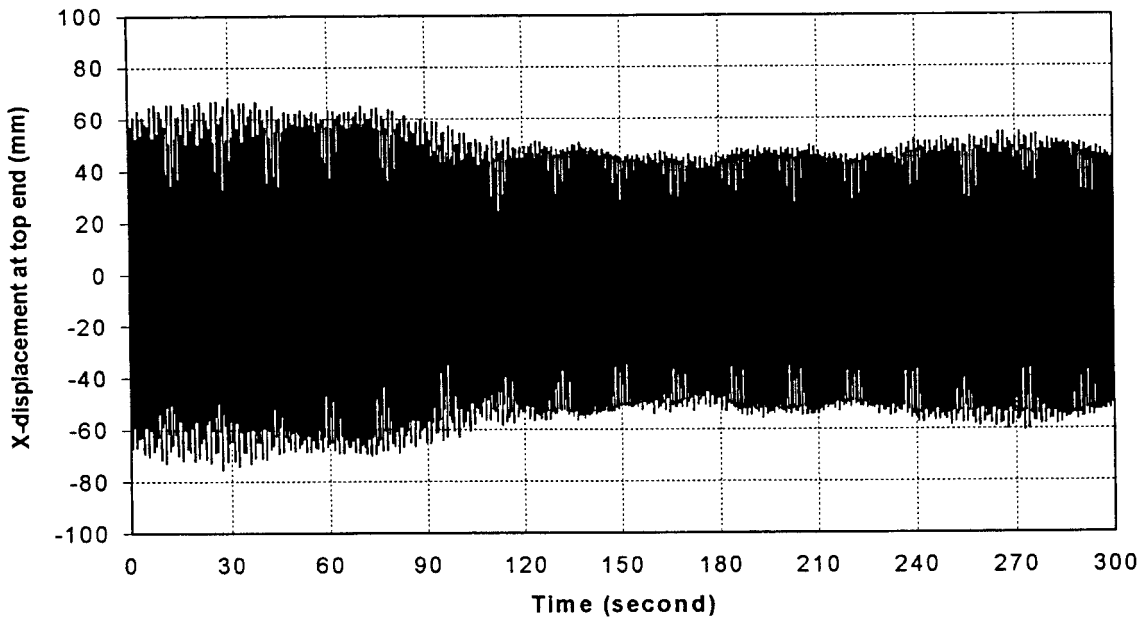

(b) Top end X-motion

Figure 55b: Top end X-motion, time history of Setup 2A at U=19 m/s.

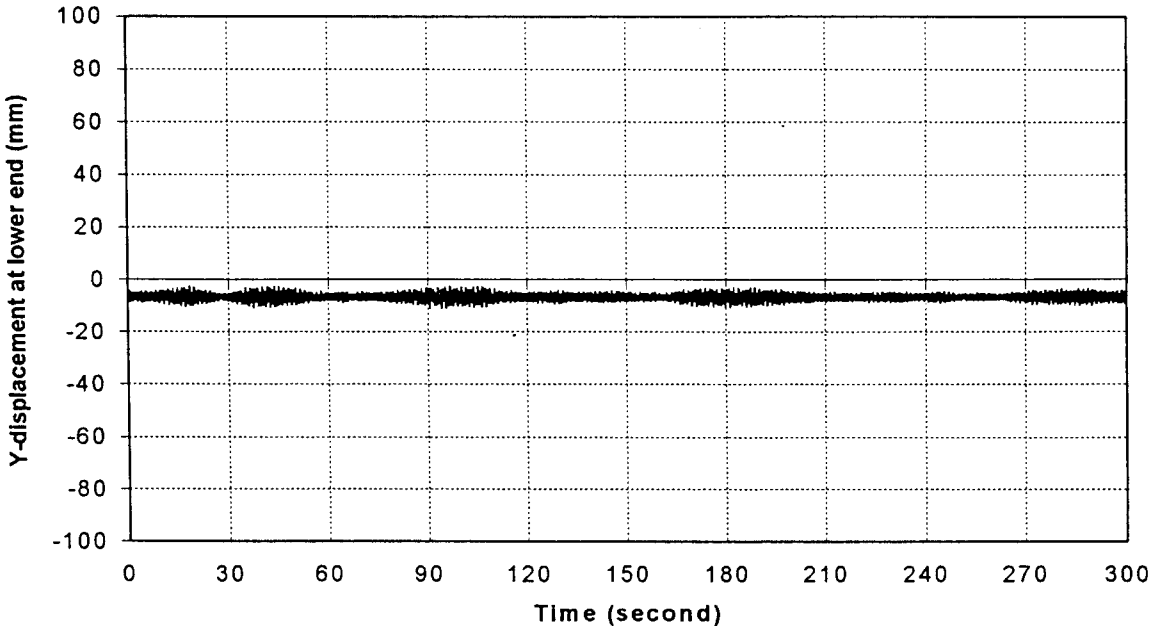

Figure 55c: Lower end Y-motion, time history of Setup 2A at U=19 m/s.

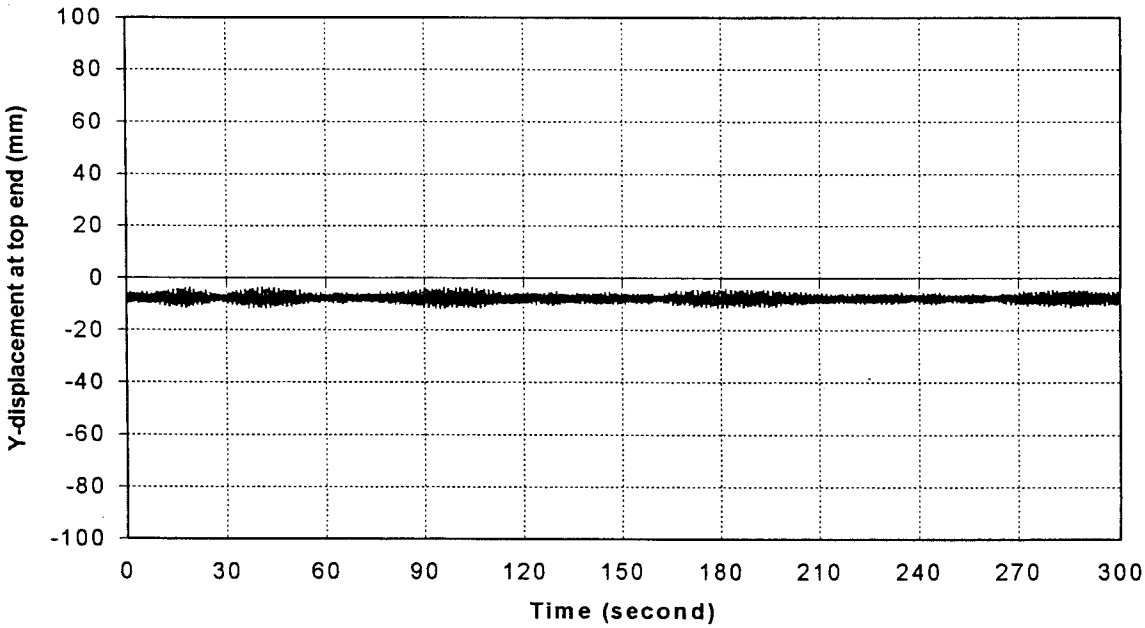

Figure 55d: Top end Y-motion, time history of Setup 2A at U=19 m/s.
(File: A_6000019006_S01.tms, smooth surface, low damping)

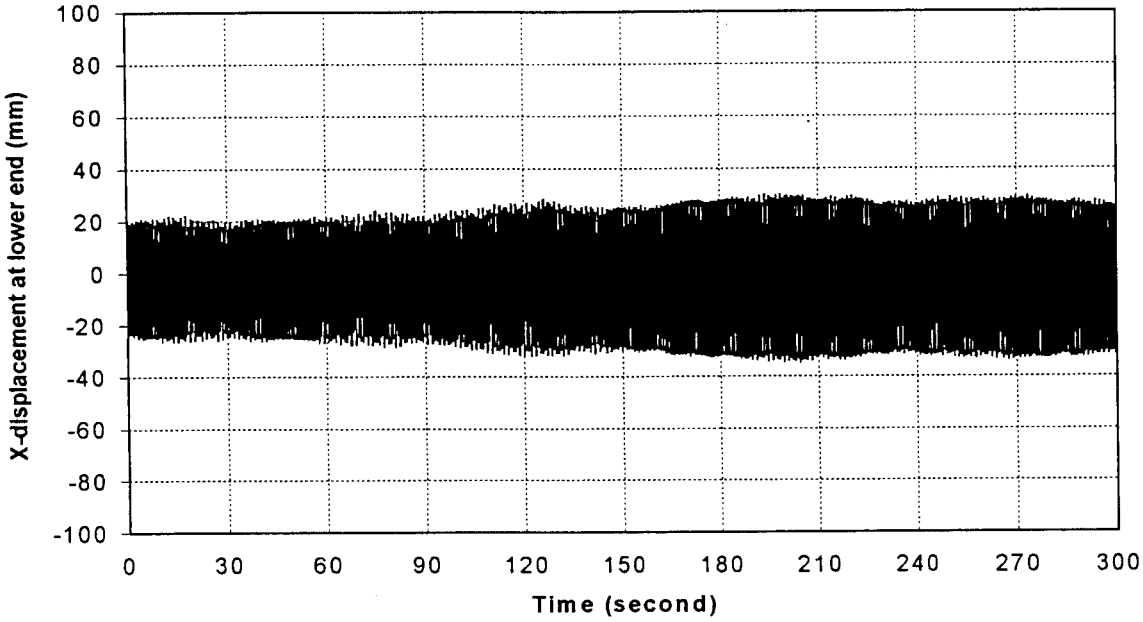

Figure 56a: Lower end X-motion, time history of Setup 1B at U=24 m/s.

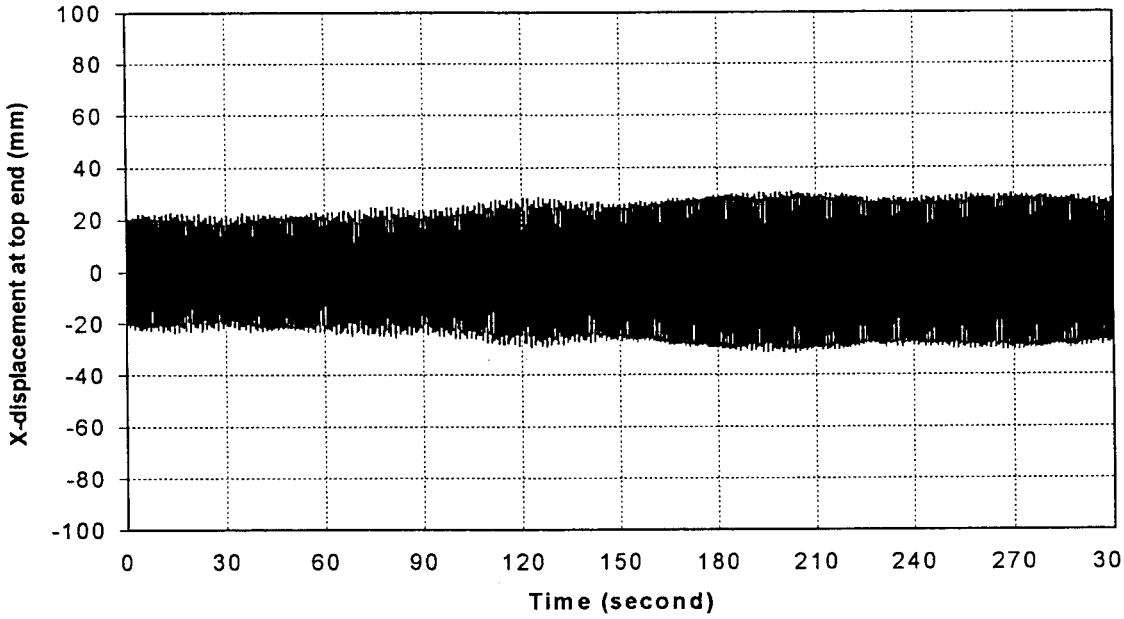

Figure 56b: Top end X-motion, time history of Setup 1B at U=24 m/s.

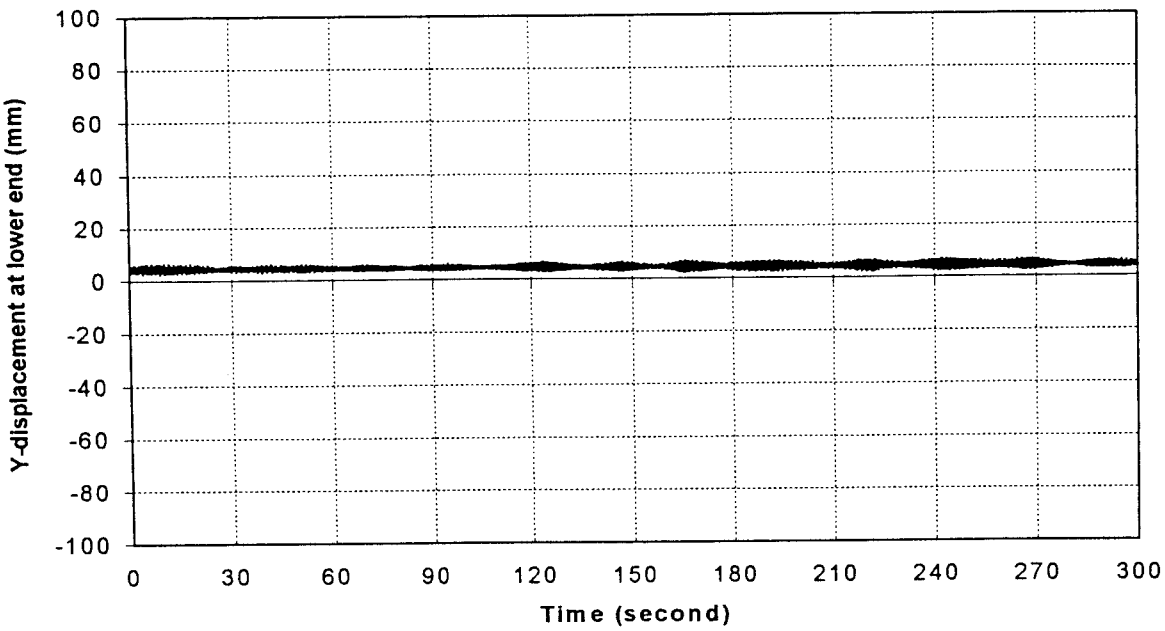

Figure 56c: Lower end Y-motion, time history of Setup 1B at U=24 m/s.

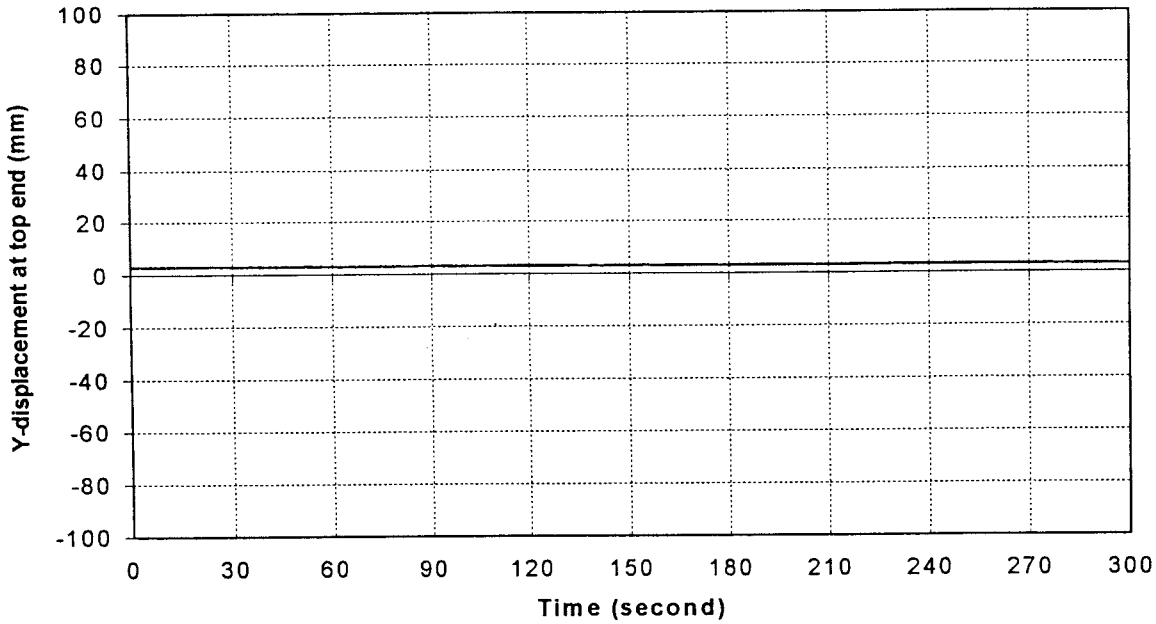

Figure 56d: Top end Y-motion, time history of Setup 1B at U=24 m/s.
(File: A_450024006_S05.tms, smooth surface, low damping)

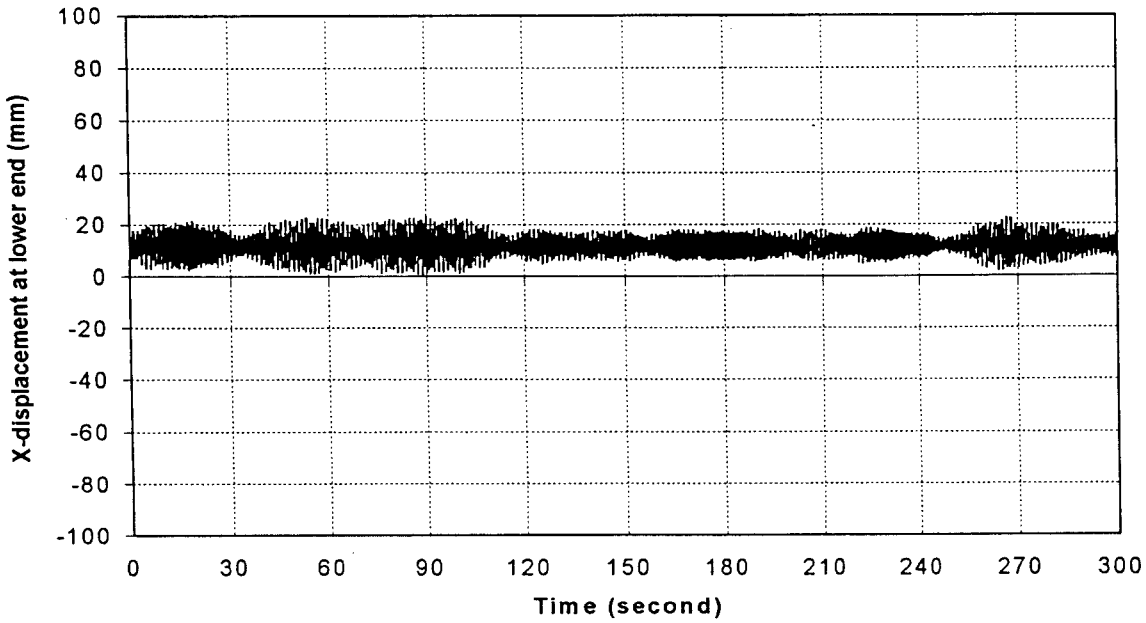

Figure 57a: Lower end X-motion, time history of Setup 1C at U=36 m/s.

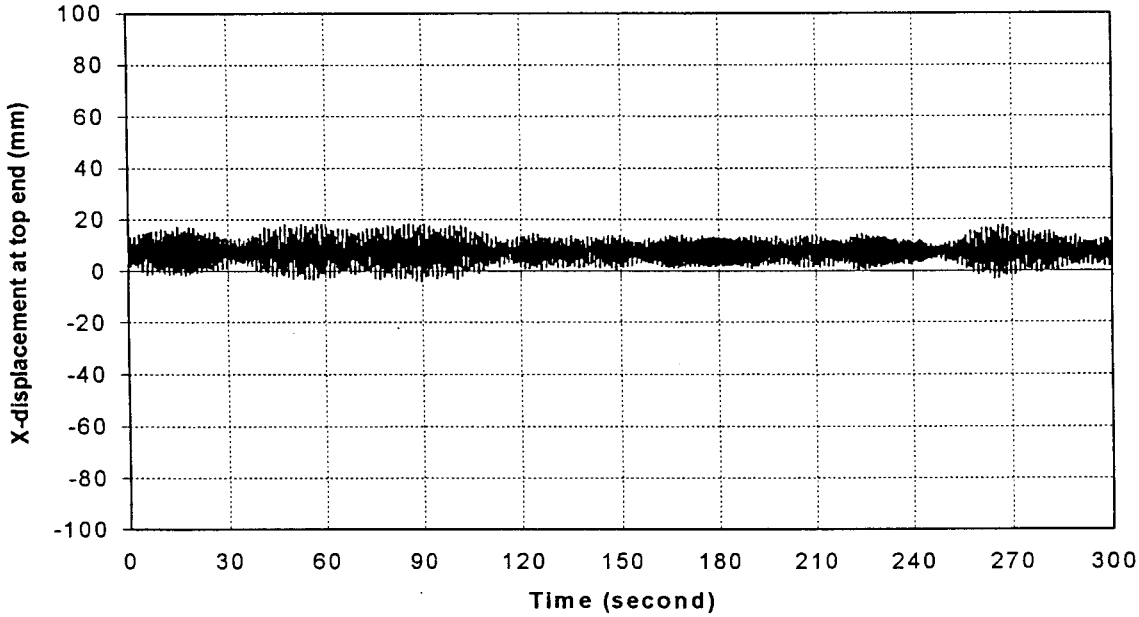

Figure 57b: Top end X-motion, time history of Setup 1C at U=36 m/s.

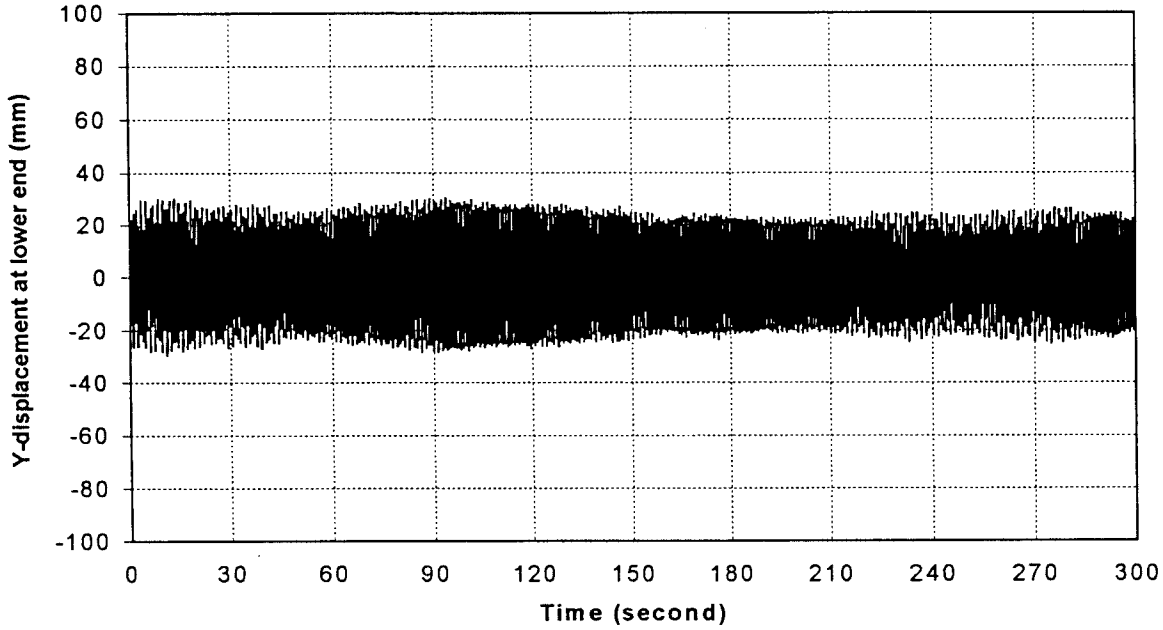

Figure 57c: Lower end Y-motion, time history of Setup 1C at U=36 m/s.

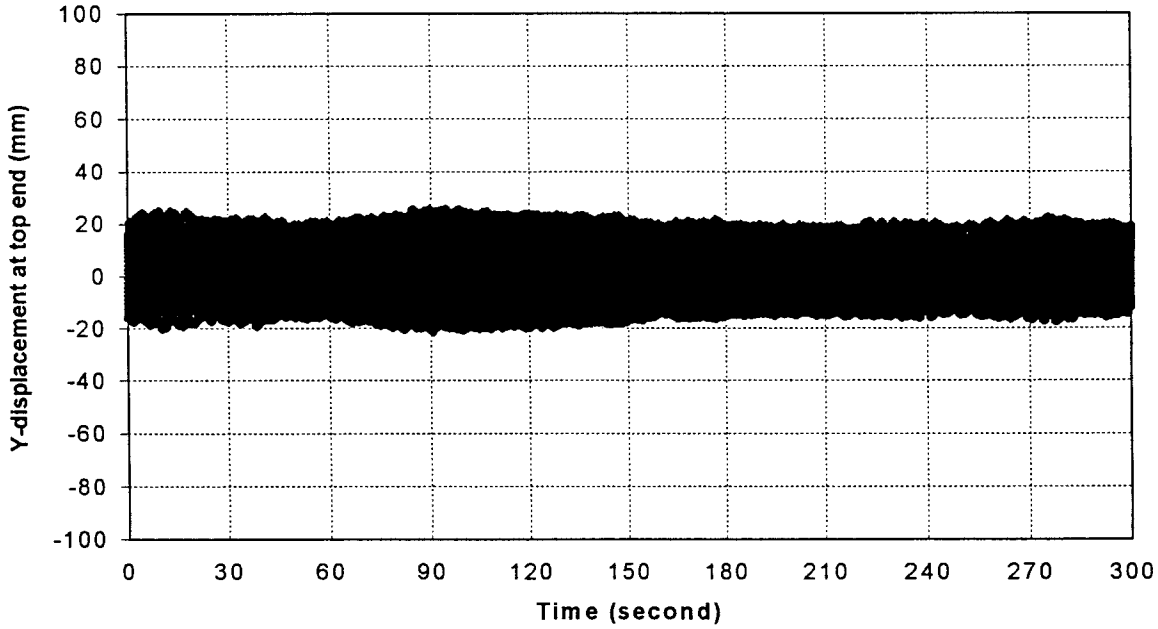

Figure 57d: Top end Y-motion, time history of Setup 1C at U=36 m/s.
(File: A_455536006_S02.tms, smooth surface, low damping)

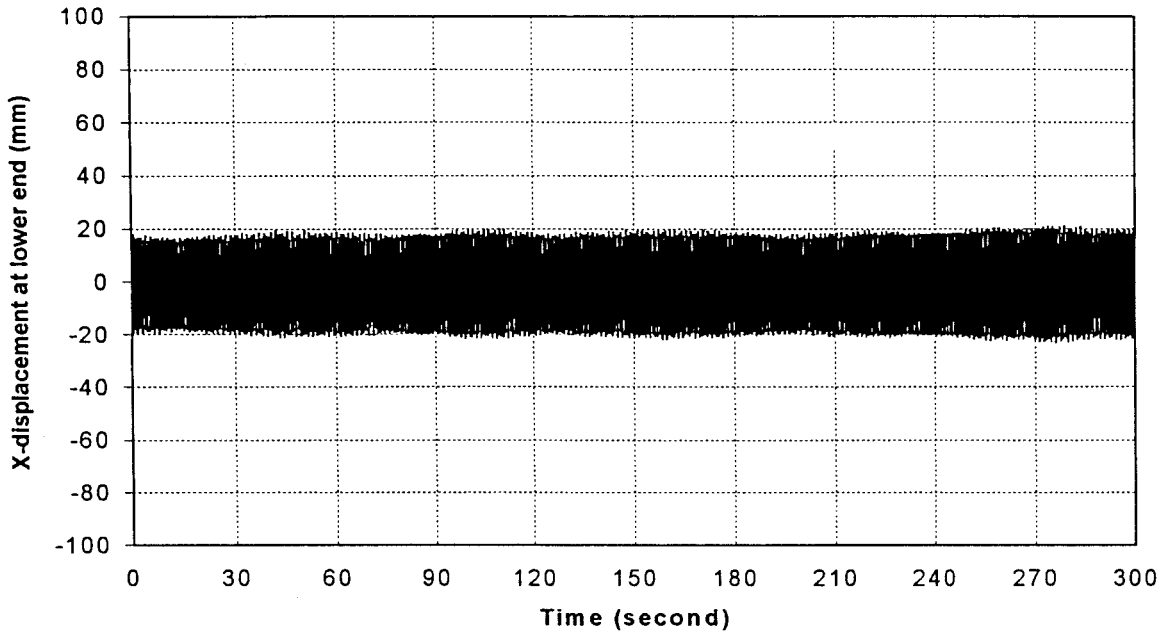

Figure 58a: Lower end X-motion, time history of Setup 3A at U=22 m/s.

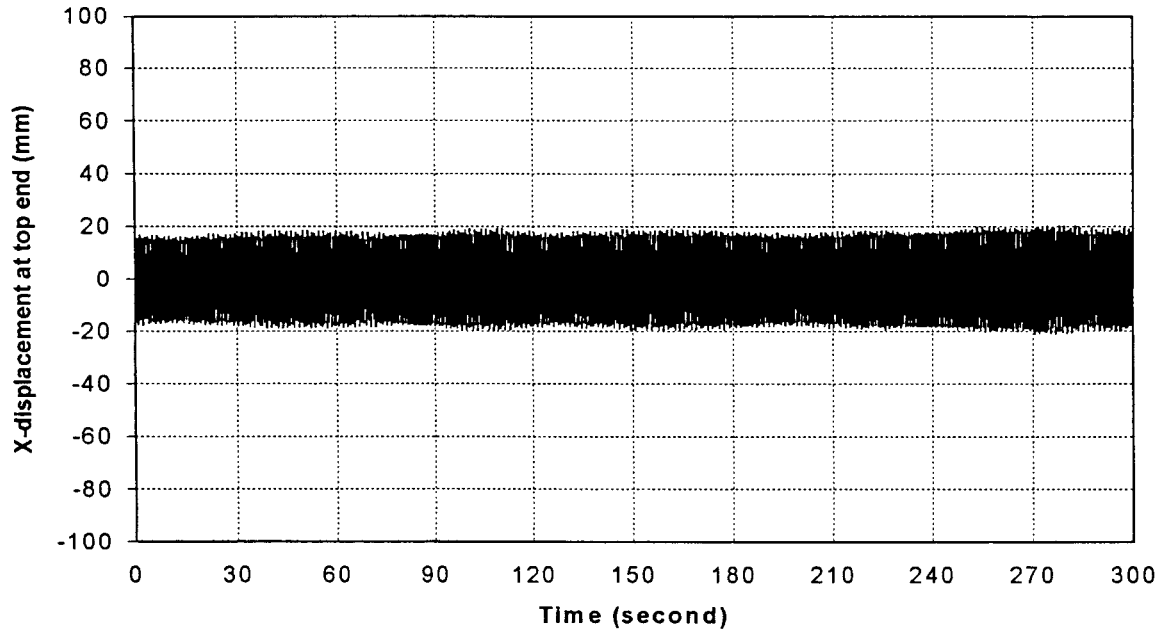

Figure 58b: Top end X-motion, time history of Setup 3A at U=22 m/s.

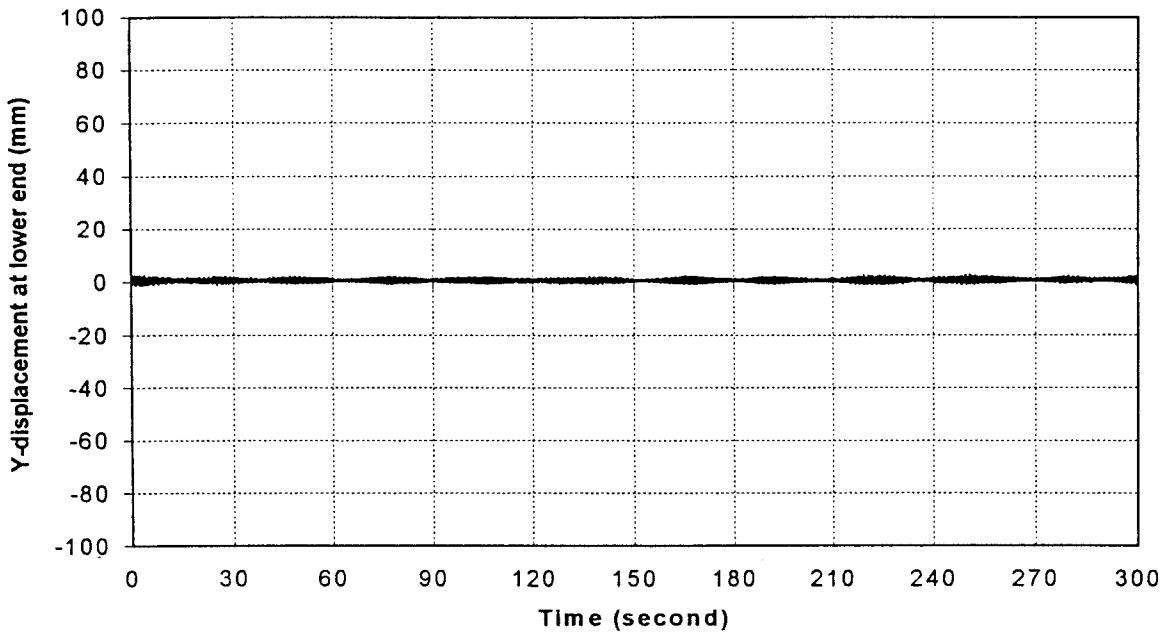

Figure 58c: Lower end Y-motion, time history of Setup 3A at U=22 m/s.

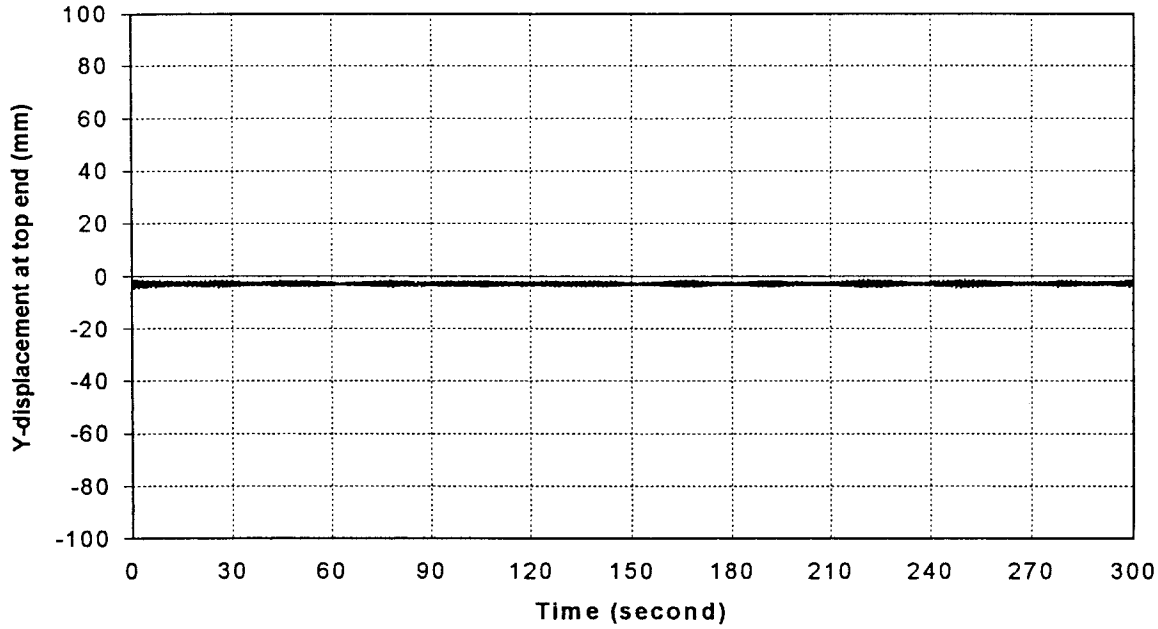

Figure 58d: Top end Y-motion, time history of Setup 3A at U=22 m/s.
(File: A_350022006_S03.tms, smooth surface, low damping)

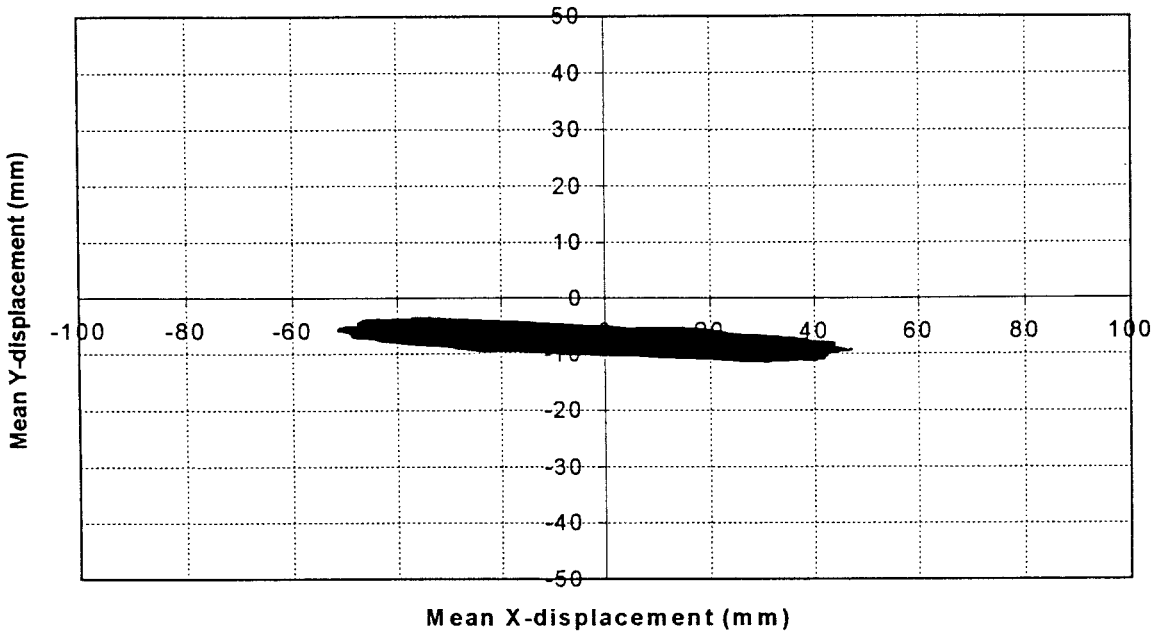

Figure 59a: Trajectory of Setup 2A at U=18 m/s, first 5 minutes.
(File: A_600018006_S01.tms)

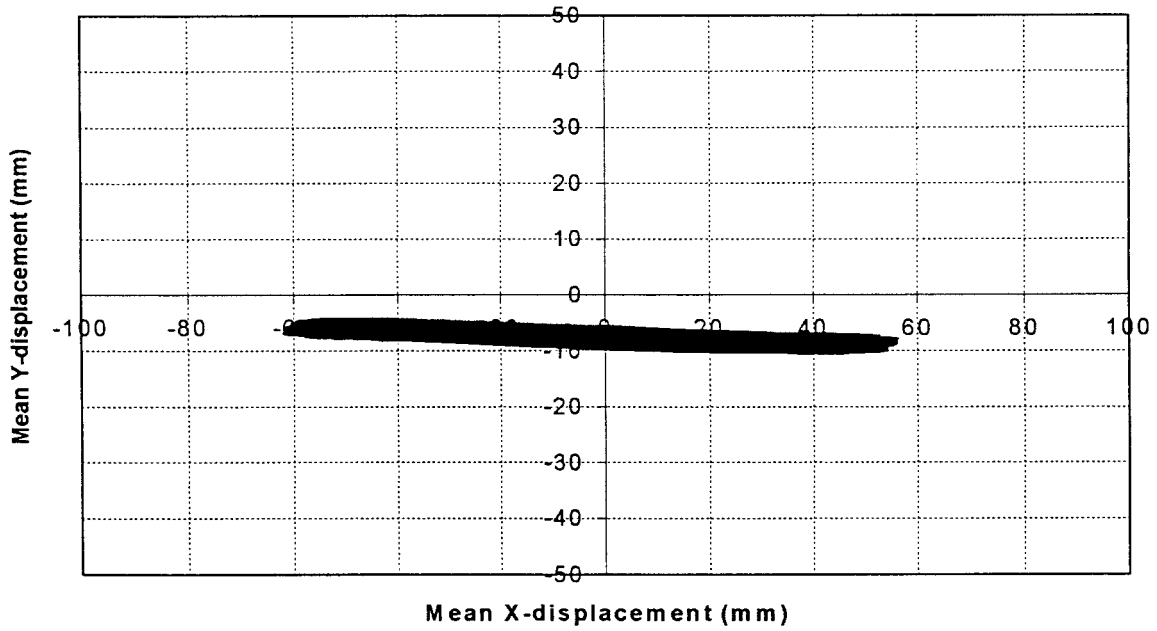

Figure 59b: Trajectory of Setup 2A at U=18 m/s, second 5 minutes.
(File: A_600018006_S02.tms)

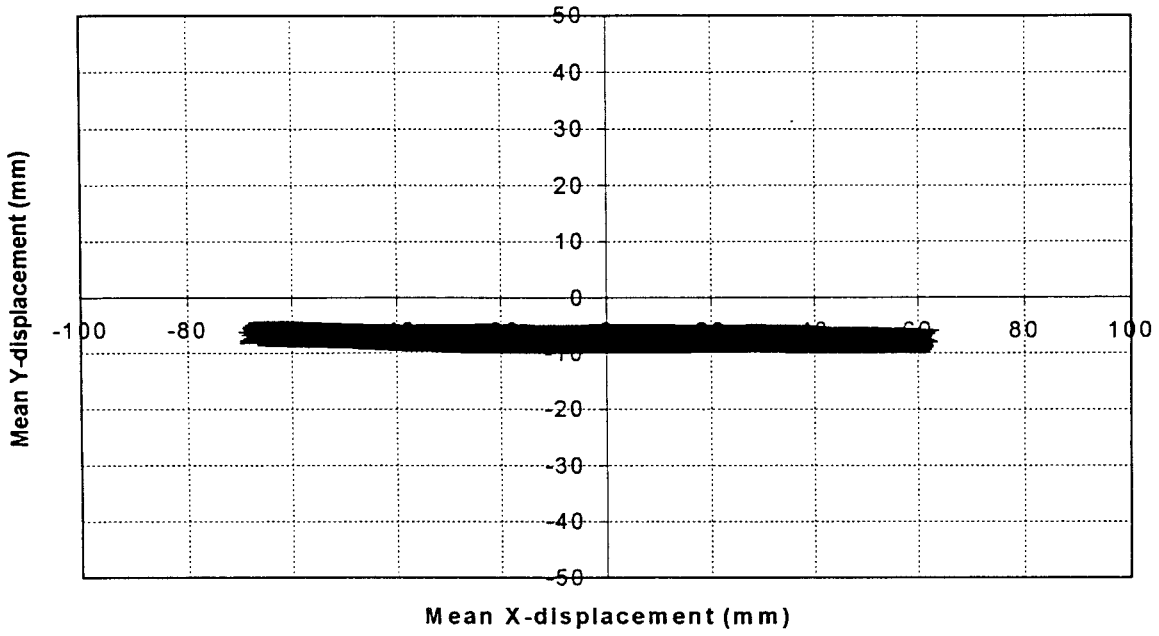

Figure 59c: Trajectory of Setup 2A at U=19 m/s.
(File: A_600019006_S01.tms, smooth surface, low damping)

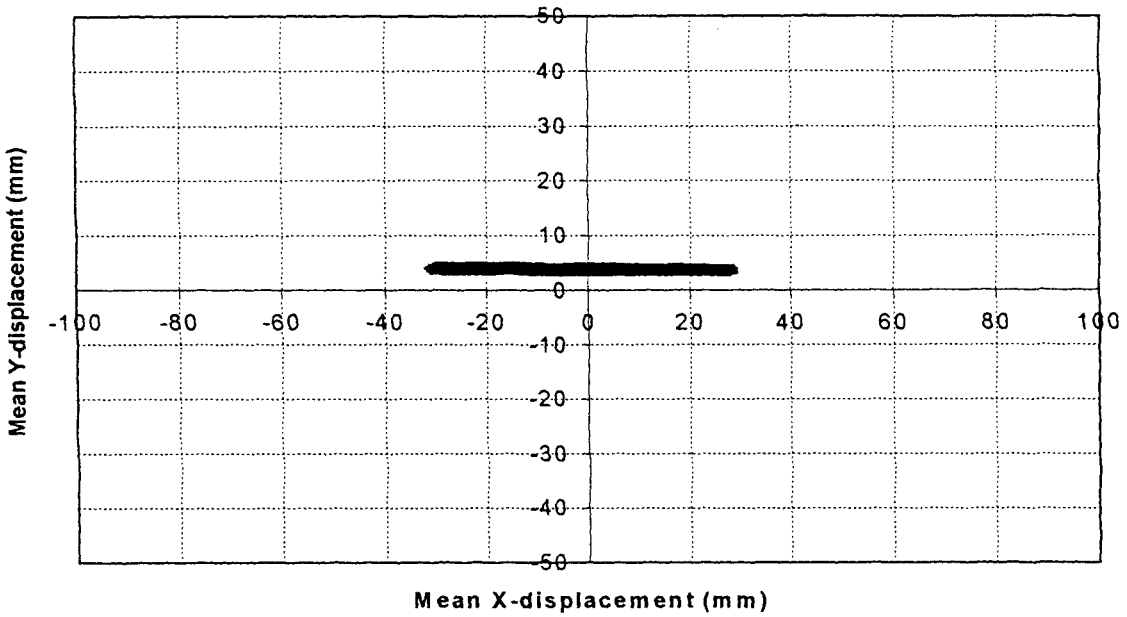

Figure 60: Trajectory of Setup 1B at U=24 m/s.
(File: A_450024006_S05.tms, smooth surface, low damping)

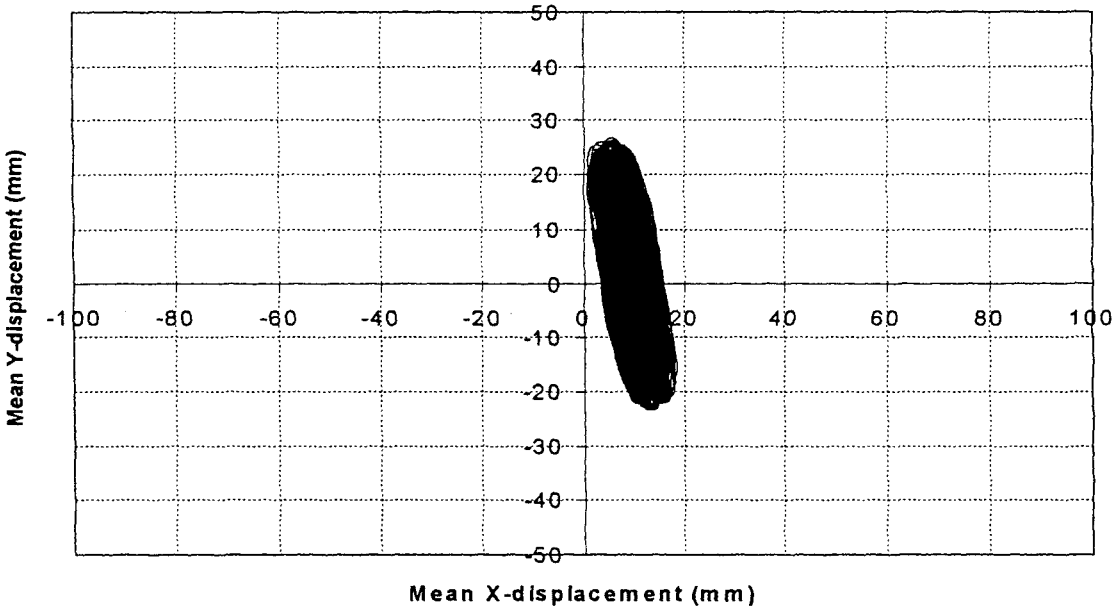

Figure 61: Trajectory of Setup 1C at U=36 m/s.
(File: A_455536006_S02.tms, smooth surface, low damping)

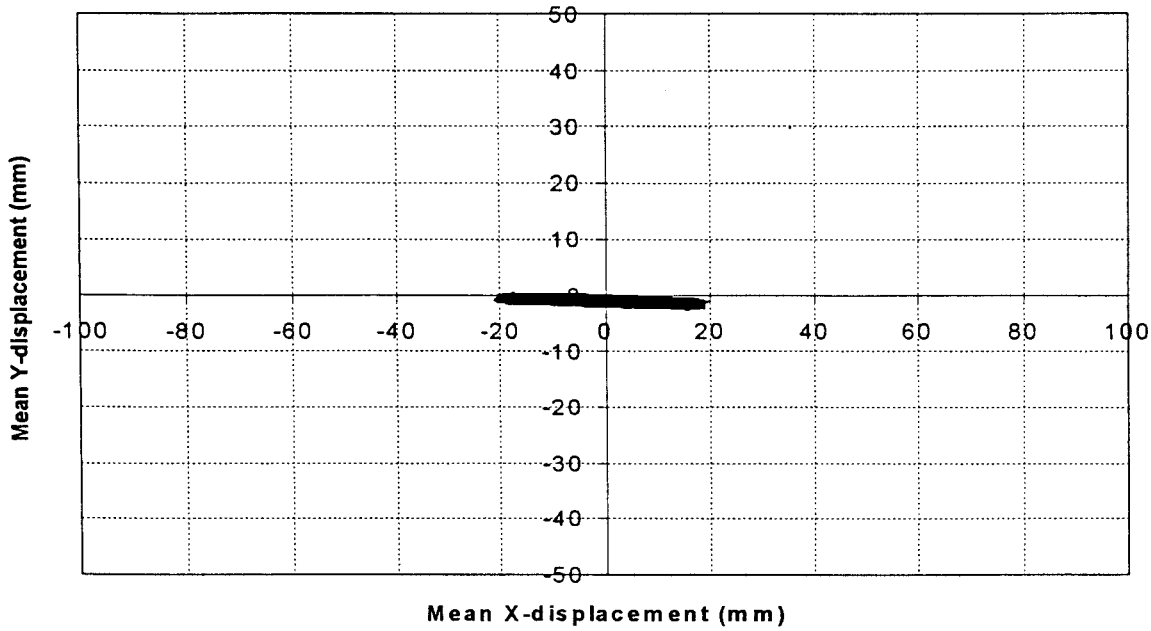

Figure 62: Trajectory of Setup 3A at U=22 m/s.
(File: A_350022006_S03.tms, smooth surface, low damping)

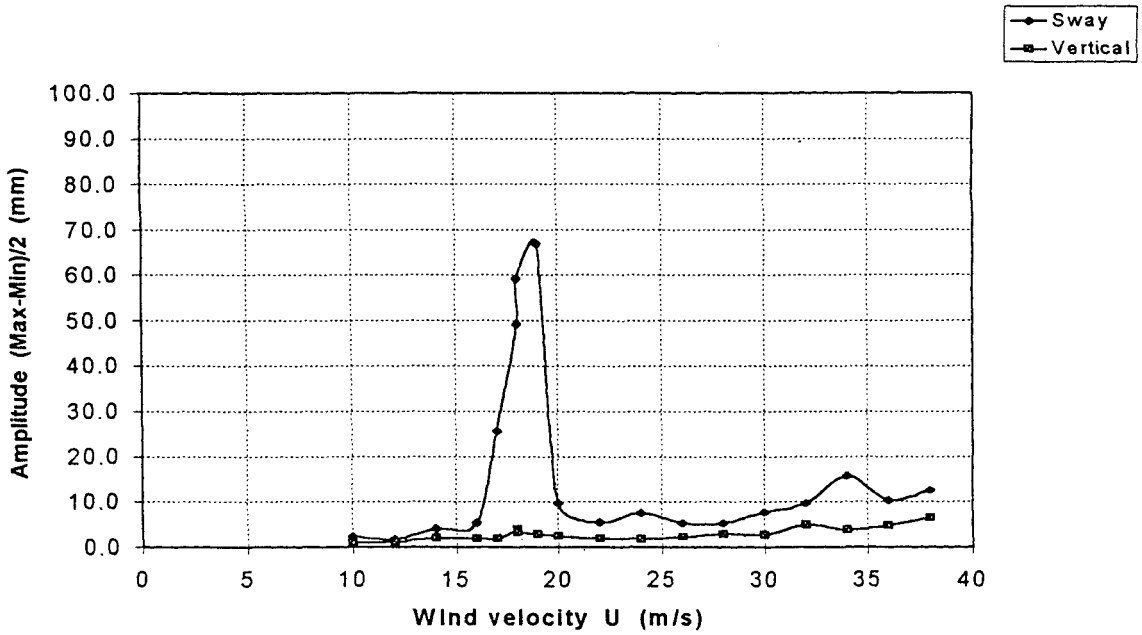

Figure 63: Wind-induced response of inclined dry cable.
(Set-up 2A, smooth surface, low damping)

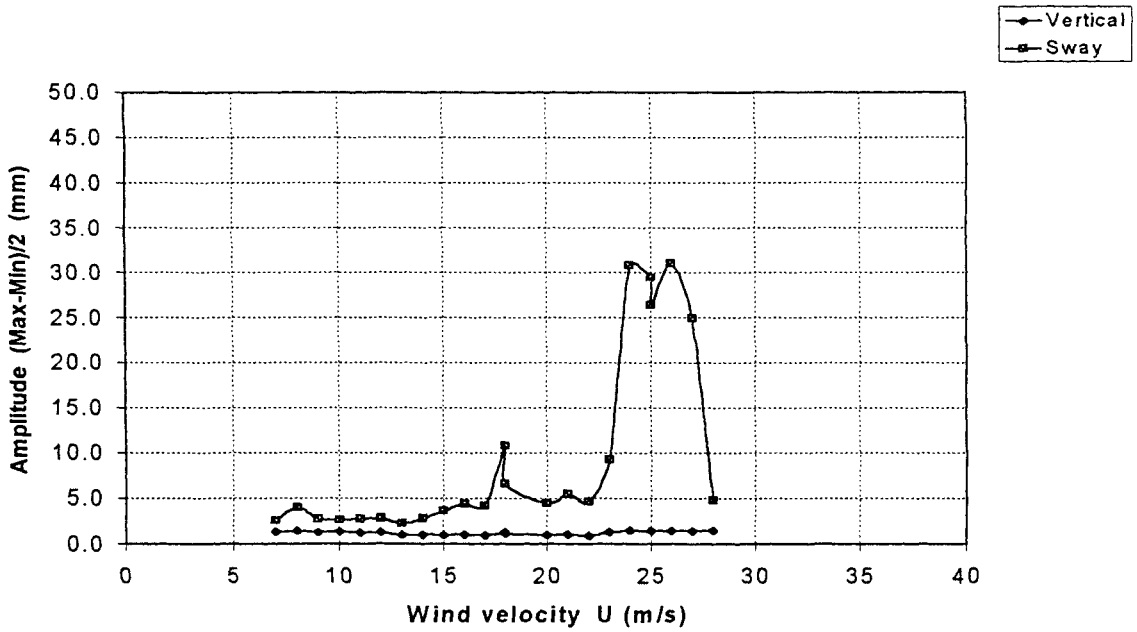

Figure 64: Wind-induced response of inclined dry cable.
(Set-up 1B, smooth surface, low damping)

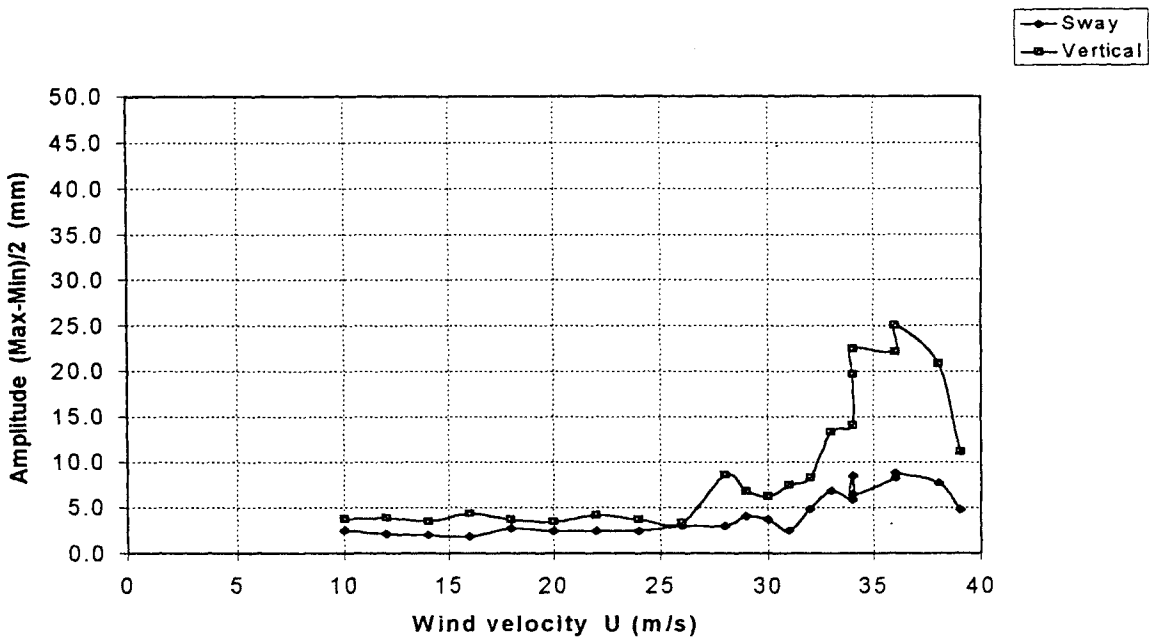

Figure 65: Wind-induced response of inclined dry cable.
(Set-up 1C, smooth surface, low damping)

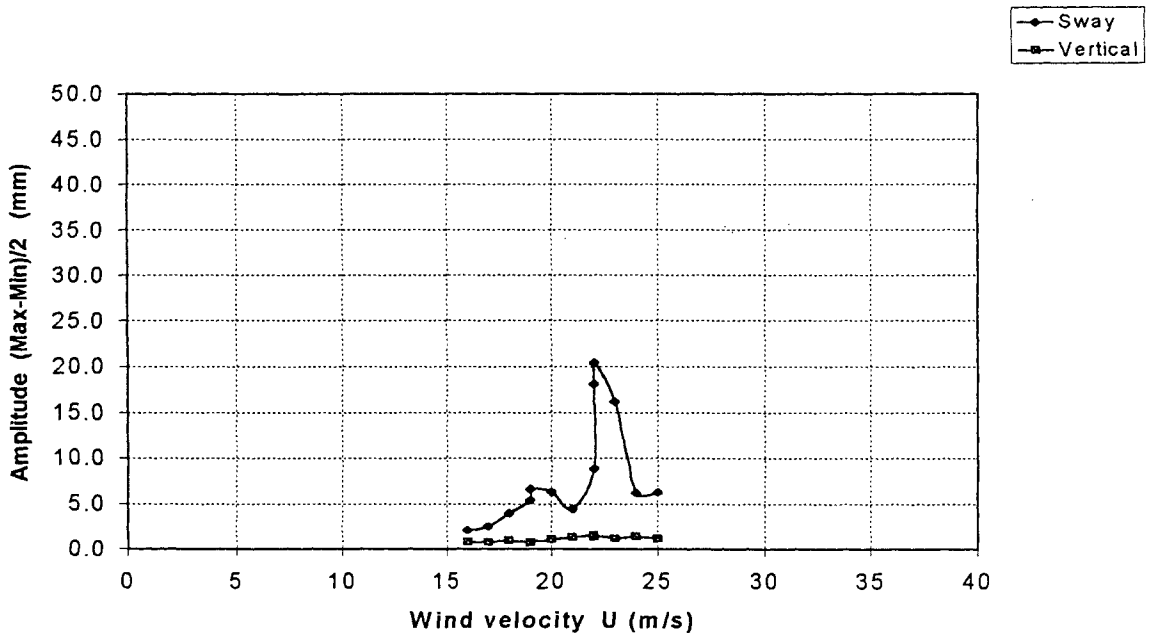

Figure 66: Wind-induced response of inclined dry cable.
(Set-up 3A, smooth surface, low damping)

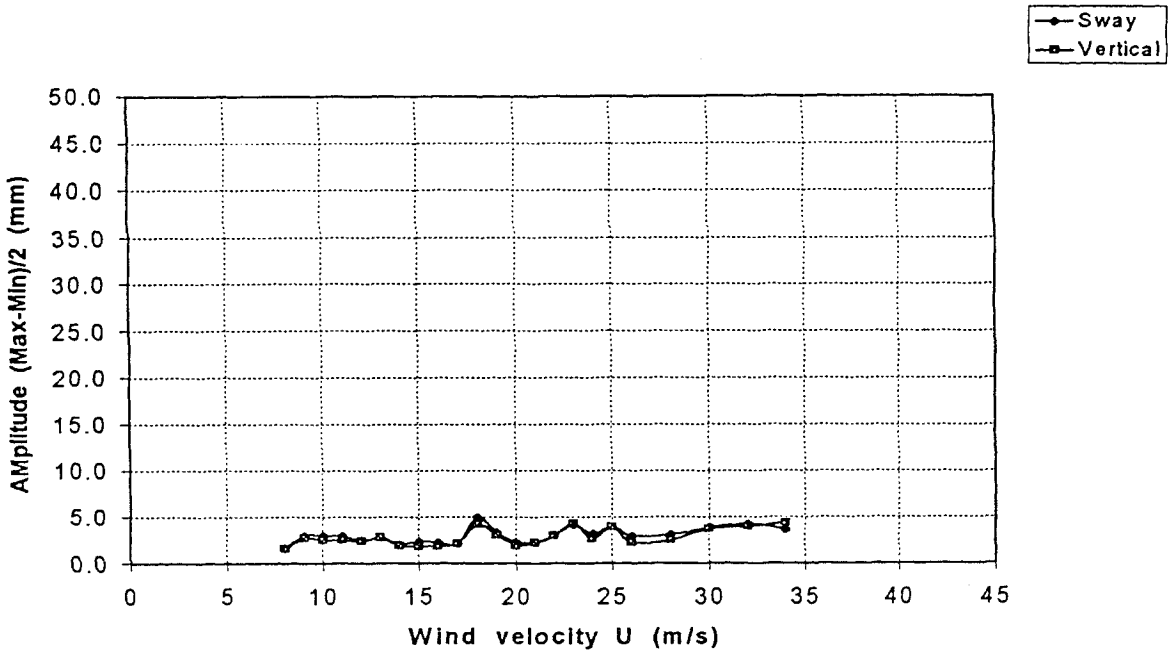

Figure 67: Wind-induced response of inclined dry cable.
(Set-up 3B, smooth surface, low damping)

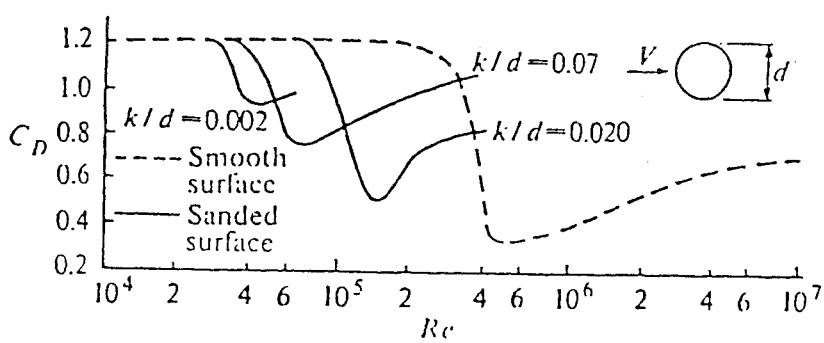

Figure 68: Critical Reynolds number of circular cylinder (from Scruton, 1981).

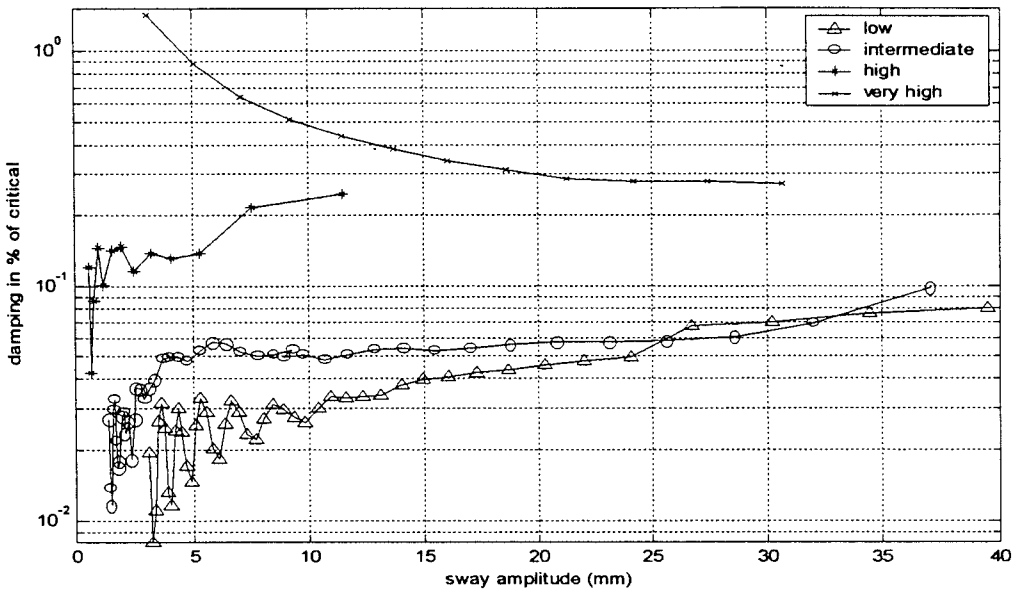

Figure 69: Damping trace of four different levels of damping.
(Set-up 1B, smooth surface)

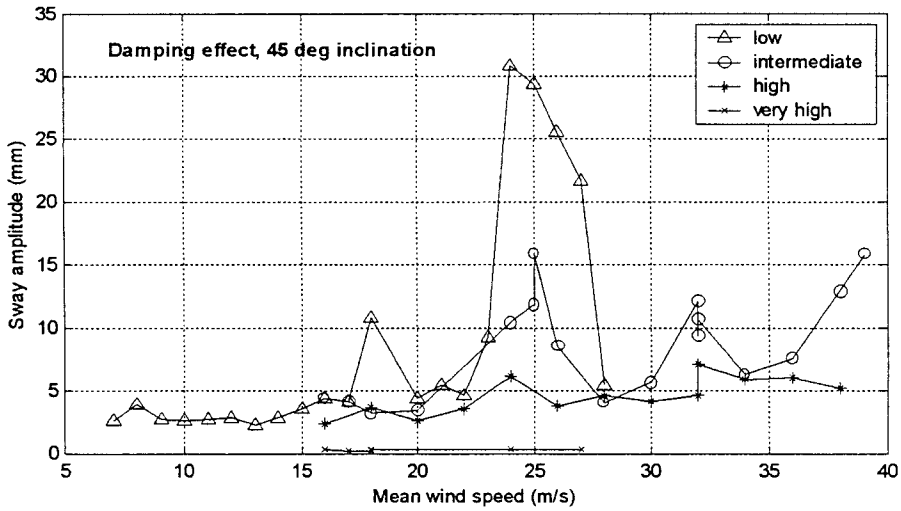

Figure 70: Effect of structural damping on the wind response of inclined cable.
(Set-up 1B, smooth surface)

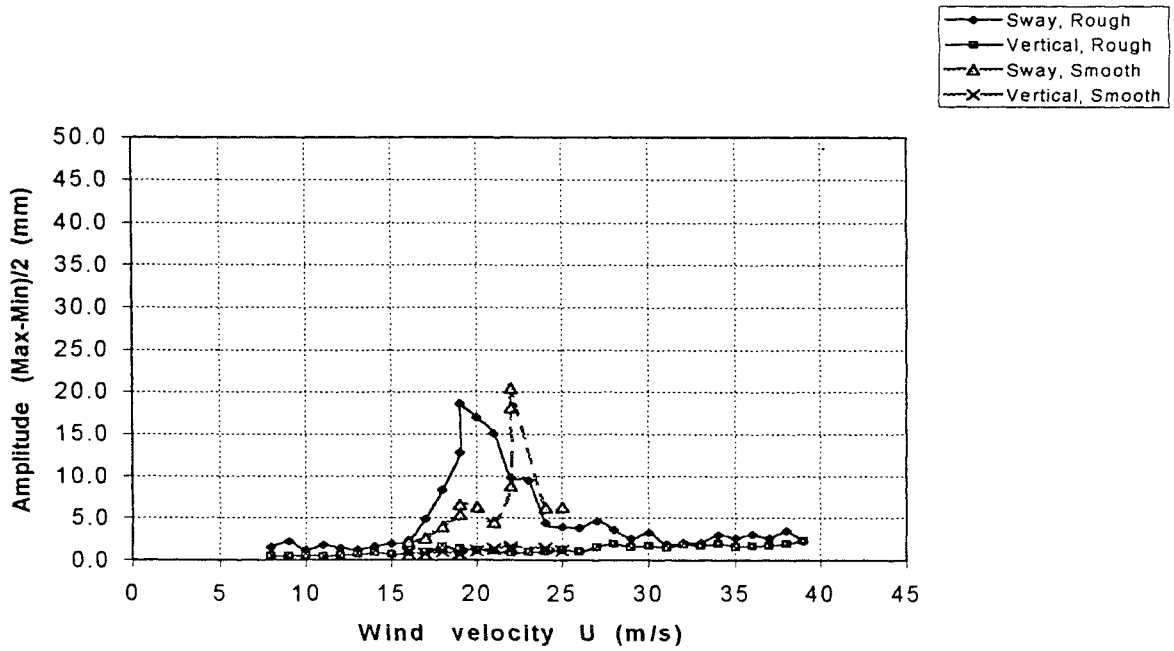

Figure 71: Surface roughness effect on wind-induced response of dry inclined cable. (Set-up 3A, low damping)

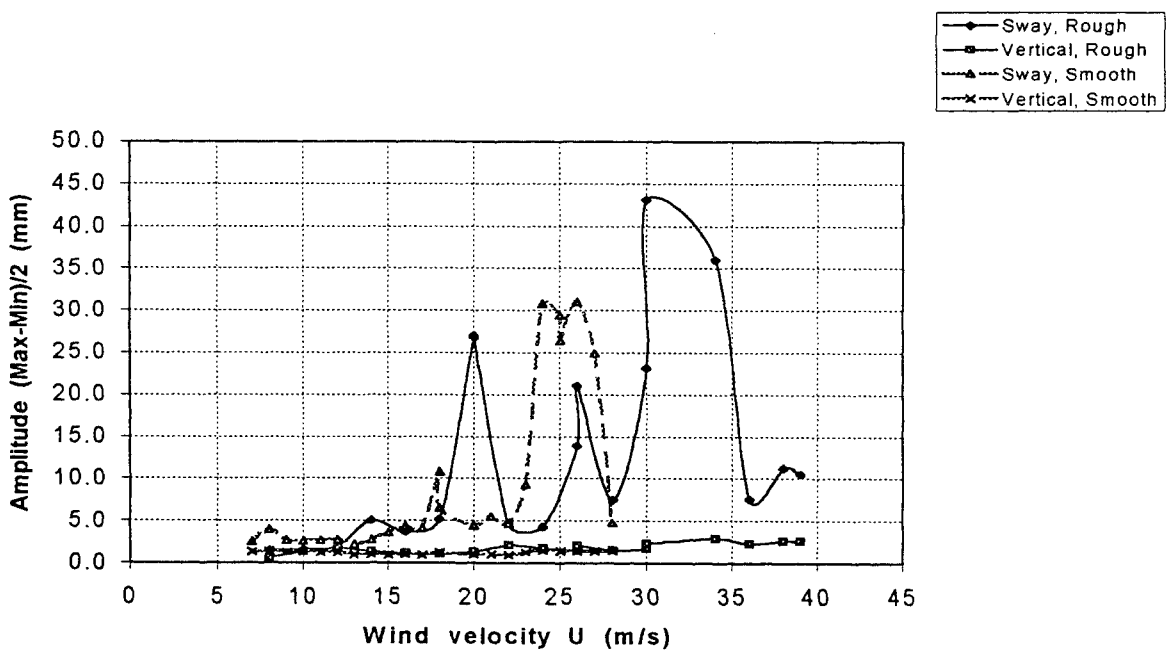

Figure 72: Surface roughness effect on wind-induced response of dry inclined cable. (Set-up 1B, low damping)

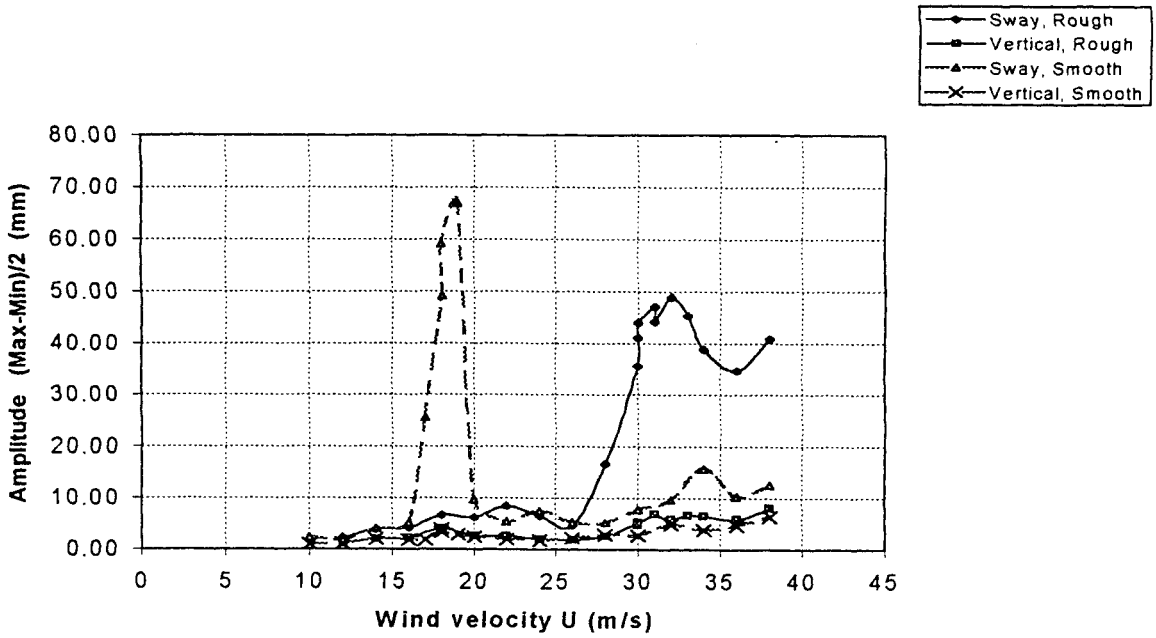

Figure 73: Surface roughness effect on wind-induced response of dry inclined cable. (Set-up 2A, low damping)

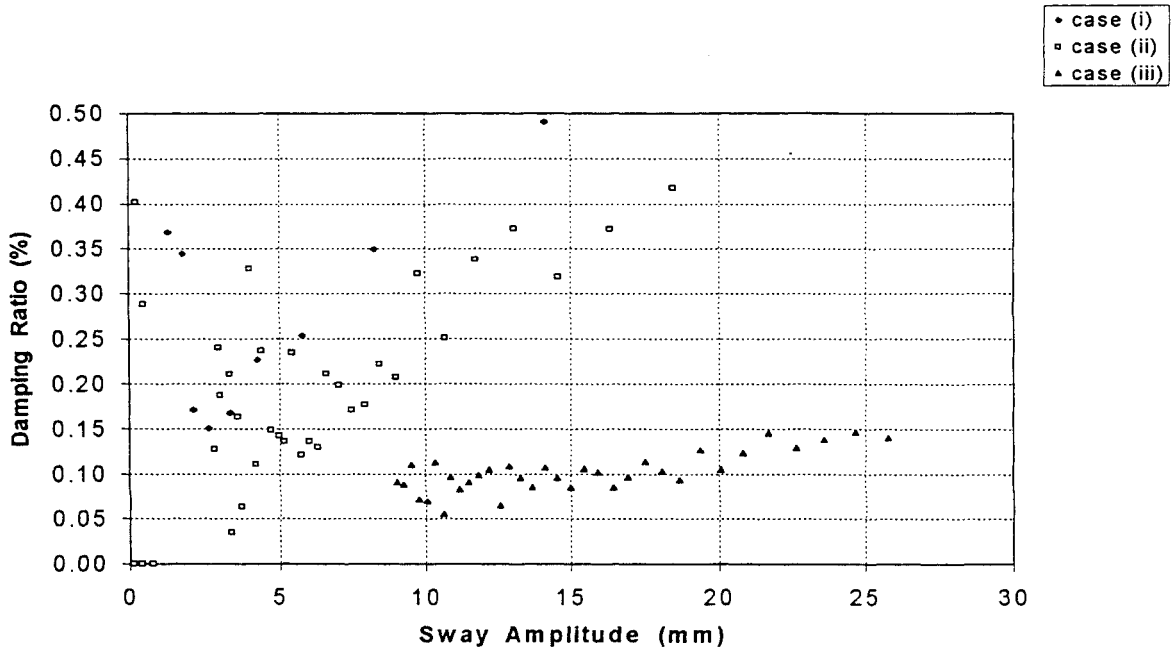

Figure 74a: Amplitude-dependent damping in the X-direction with Set-up 2A. (Frequency ratio effect)

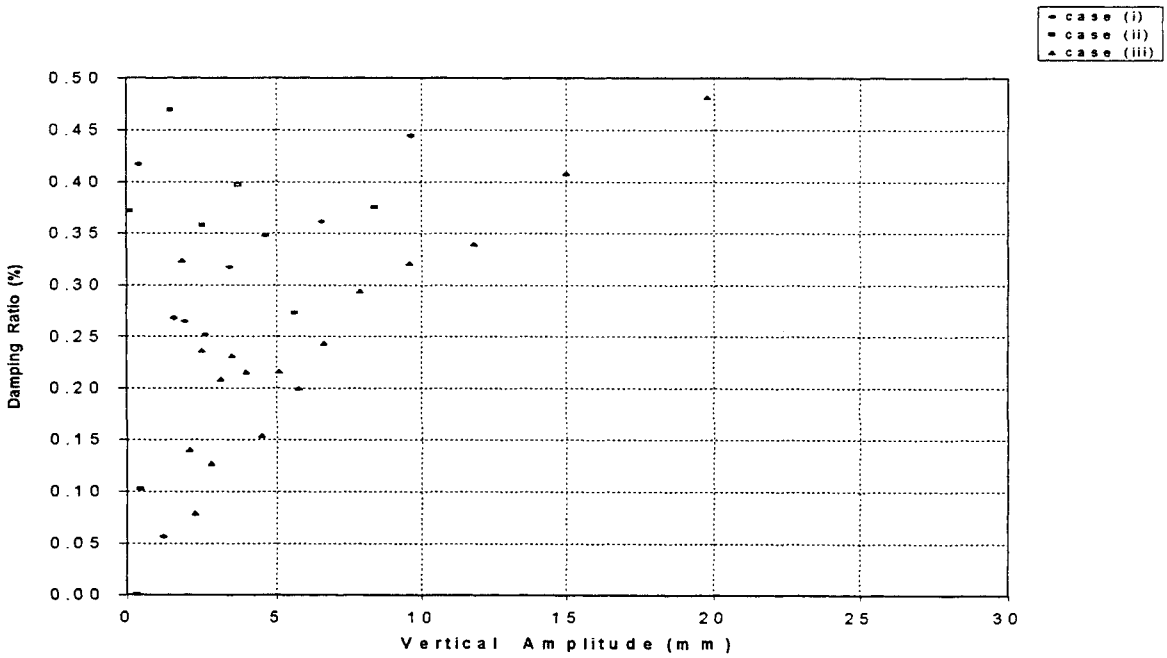

Figure 74b: Amplitude-dependent damping in the Y-direction with Set-up 2A. (Frequency ratio effect)

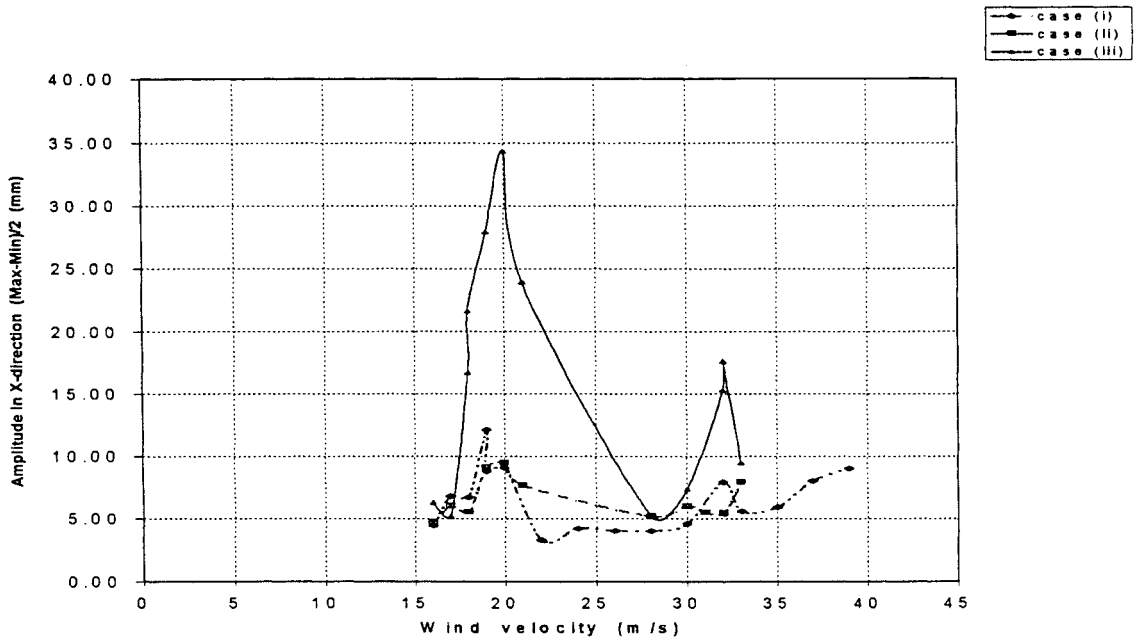

Figure 75a: Wind-induced response of inclined cable in the X-direction with Set-up 2A. (Frequency ratio effect)

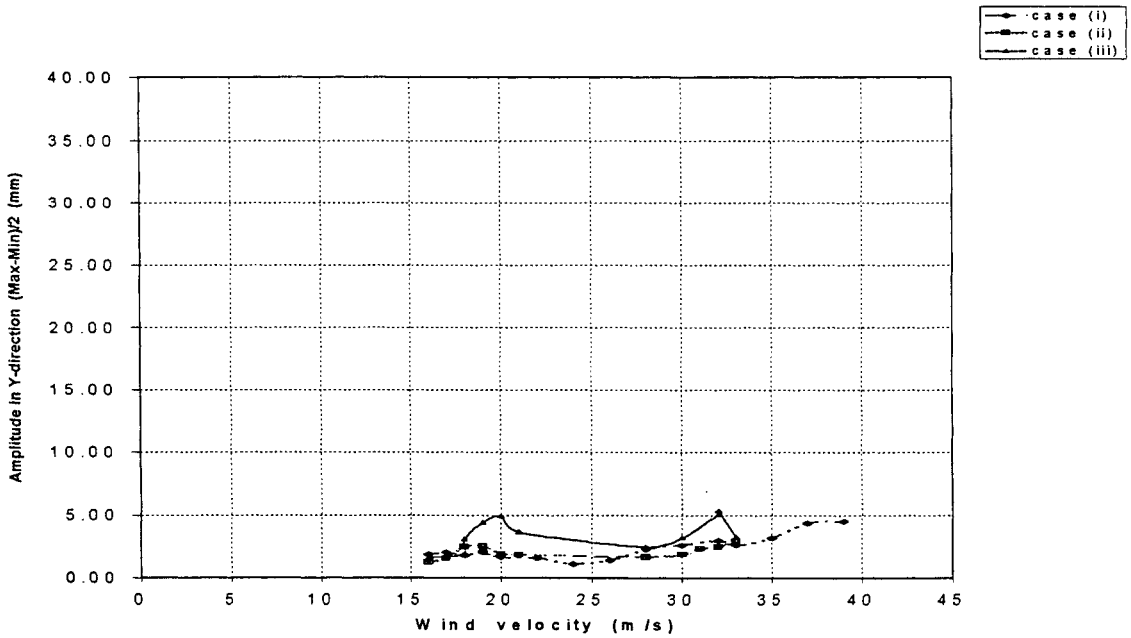

Figure 75b: Wind-induced response of inclined cable in the Y-direction with Set-up 2A. (Frequency ratio effect)

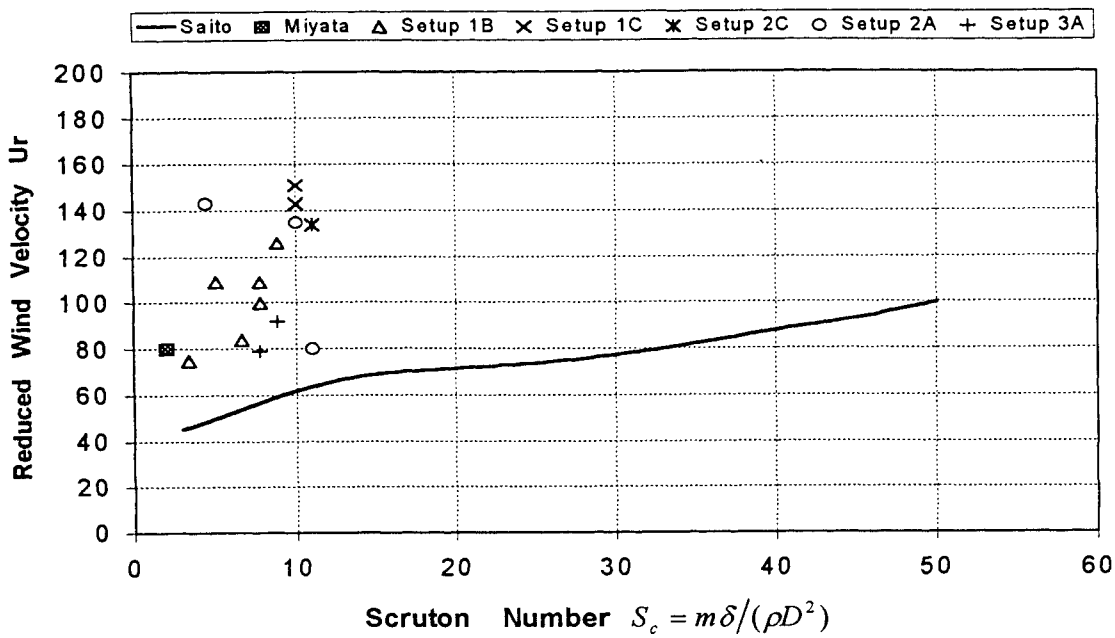

Figure 76: Comparison of wind velocity-damping relation of inclined dry cable.

APPENDIX C1 : LIST OF TECHNICAL PAPERS

The following technical papers were developed for this project as part of the investigation of mitigation methods. Most of these were transmitted to FHWA for review during the project as they were completed. The results of this research are summarized in Appendix C2 as extractions from these publications:

- Caracoglia, L. & Jones, N. P. (2002) "Analytical method for the dynamic analysis of complex cable structures." Proceedings, ASCE Engineering Mechanics Division Conference. Columbia University, NY.

- Caracoglia L., & Jones N. P. (2002) "In-plane dynamic behavior of cable networks I: formulation and basic solutions." *Journal of Sound and Vibration*. (In review)

- Caracoglia L., & Jones N. P. (2002) "In-plane dynamic behavior of cable networks II: Prototype prediction and validation." *Journal of Sound and Vibration*. (In review)

- Jones, N. P. & Zuo, D. (2002) "Measurement of Stay Damping - Sunshine Skyway Bridge, Tampa, FL" Report submitted to Lendis Corporation and FHWA.

- Jones, N. P. & Main, J. A. (2002) "Evaluation of Mitigation Strategies for Stay-Cable Vibration." Proceedings, Structures Congress. ASCE, Reston, VA.

- Main, J. A. & Jones, N. P. (2002) "Analytical Investigation of the Performance of a Damper with a Friction Threshold for Stay-Cable Vibration Suppression." Proceedings, ASCE Engineering Mechanics Division Conference. Columbia University, NY.

- Main, J. A. & Jones, N. P. (2001) "Analysis and design of linear and nonlinear dampers for stay cables." Proceedings Fourth International Symposium on Cable Dynamics, Montreal, Canada, AIM.

- Main, J. A., & Jones N. P. (2002) "Free Vibrations of a Taut Cable with Attached Damper. I: Linear Viscous Damper." Journal of Engineering Mechanics, ASCE, 128(10), 1062-1071.

- Main, J. A., & Jones N. P. (2002) "Free Vibrations of a Taut Cable with Attached Damper. II: Nonlinear Damper." Journal of Engineering Mechanics, ASCE, 128(10), 1072-1081.

- Main, J. A., & Jones, N. P. (2001) "Measurement and mitigation of stay-cable vibration." Proceedings Asia-Pacific Conference of Wind Engineering. Kyoto University, October.

- Main, J. A., & Jones, N. P. (2001) "Stay-cable vibration in cable-stayed bridges: Characterization from full-scale measurements and mitigating strategies." Journal of Bridge Engineering. ASCE, 6(6), 375-387.

- Main, J. A., Jones, N. P. & Yamaguchi, H. (2001) "Characterization of rain/wind induced stay-cable vibrations from full-scale measurements." Proceedings Fourth International Symposium on Cable Dynamics. Montreal, Canada, AIM.

- Ozkan, E. & Jones, N. P. (2001) "Investigation of cable-deck interaction using full-scale measurements on a cable-stayed bridge." Proceedings 1st Americas Conference of Wind Engineering. Clemson University, June.

- Ozkan, E., Main, J. A. & Jones, N. P. (2001) "Full-scale measurements on the Fred Hartman Bridge." Proceedings Asia-Pacific Conference of Wind Engineering. Kyoto University, October.

- Ozkan, E., Main, J. A. & Jones, N. P. (2001) "Long-term measurements on a cable-stayed bridge." Proceedings IMAC-XIX. Society for Experimental Mechanics.

APPENDIX C2 : ANALYTICAL AND FIELD INVESTIGATIONS

C2.1 OUTLINE OF RESEARCH AREAS

Development of recommended design approaches for mitigation measures has focused on the following:

A. Addition of linear and nonlinear dampers
   1) Response of a taut cable with an attached linear damper
   2) Response of a taut cable with an attached linear damper with a friction threshold
   3) Response of a taut cable with an attached nonlinear damper (exponent other than one as in the case of a linear damper)

B. Cross tying of stay cables
   1) Response assessment of cross-tied stays with rigid and spring connectors
   2) Dampers in combination with cross-ties

C. Field assessment of damper and cross-tie performance, focusing on the systems installed on the Fred Hartman Bridge
   1) Performance of linear dampers
   2) Performance of cross ties.
   3) Detailed study of damper performance

C2.2 ADDITION OF LINEAR AND NONLINEAR DAMPERS

Stay cables have very low levels of inherent mechanical damping, rendering them susceptible to multiple types of excitation (Yamaguchi & Fujino, 1998). To suppress the problematic vibrations, dampers are often attached to the stays near the anchorages. Although the mechanisms that induce the observed vibrations are still not fully understood, the effectiveness of attached dampers has been demonstrated. The potential for widespread application of dampers for cable vibration suppression necessitates a thorough understanding of the resulting dynamic system.

Response of a Taut Cable with an Attached Linear Damper

Background:

Carne (1981) and Kovacs (1982) were among the first to investigate the vibrations of a taut cable with an attached damper, both focusing on determination of first-mode damping ratios for damper locations near the end of the cable; Carne developed an approximate analytical solution, obtaining a transcendental equation for the complex eigenvalues and an accurate approximation for the first-mode damping ratio as a function of the damper coefficient and location, while Kovacs developed approximations for the maximum attainable damping ratio (in agreement with Carne) and the corresponding optimal damper coefficient (about 60% in excess of Carne's

accurate result). Subsequent investigators formulated the free-vibration problem using Galerkin's method, with the sinusoidal mode shapes of an undamped cable as basis functions, and several hundred terms were required for adequate convergence in the solution, creating a computational burden (Pacheco et al., 1993). Several investigators have worked to develop modal damping estimation curves of general applicability (Yoneda & Maeda 1989; Pacheco et al., 1993), and Pacheco et al. (1993) introduced nondimensional parameters to develop a "universal estimation curve" of normalized modal damping ratio versus normalized damper coefficient, which is useful and applicable in many practical design situations. To consider the influence of cable sag and inclination on attainable damping ratios, Xu et al. (1997) developed an efficient and accurate transfer matrix formulation using complex eigenfunctions. Recently, Krenk (2000) developed an exact analytical solution of the free-vibration problem for a taut cable and obtained an asymptotic approximation for the damping ratios in the first few modes for damper locations near the end of the cable. Krenk also developed an efficient iterative method for accurate determination of modal damping ratios outside the range of applicability of the asymptotic approximation.

Previous investigations have focused on vibrations in the first few modes for damper locations near the end of the cable, and while practical constraints usually limit the damper attachment location, it is important to understand both the range of applicability of previous observations and the behavior that may be expected outside of this range. Damper performance in the higher modes is of particular interest, as full-scale measurements indicate that vibrations of moderate amplitude can occur over a wide range of cable modes. The approach herein uses an analytical formulation of the free-vibration problem to investigate the dynamics of the cable-damper system in higher modes and without restriction on the damper location. The basic problem formulation in this paper follows quite closely the approach used by Krenk (2000), although it was developed independently as an extension of the transfer matrix technique developed by Sergev and Iwan (1981) and Iwan and Jones (1984) to calculate the natural frequencies and mode shapes of a taut cable with attached springs and masses. A similar approach was used by Rayleigh (1877) to consider the vibrations of a taut string with an attached mass. Using this formulation, the important role of damper-induced frequency shifts in characterizing the system is observed and emphasized. Consideration of the nature of these frequency shifts affords additional insight into the dynamics of the system, and when the shifts are large, complicated new regimes of behavior are observed.

The influences of sag and bending stiffness are neglected in this section, because the linear taut-string approximation is considered applicable to many real stay cables, and the simplifications introduced by these approximations allow for a more efficient formulation of the problem and a more detailed investigation of the dynamics of the system. It has been shown that moderate amounts of sag can significantly reduce the first-mode damping ratio, while the damping ratios in the higher modes are virtually unaffected (Pacheco et al., 1993; Xu et al., 1997). However, using a database of stay cable properties from real bridges, Tabatabai and Mehrabi (2000) found that for most stays the influence of sag is insignificant even in the first mode, while the influence of bending stiffness could be significant for many stays, especially for damper locations near the end of the cable. This is investigated more fully in the following.

Theory:

Only the basic aspects of the theory are summarized here. The reader is referred to the full publication (Main & Jones, 2002a) for more details.

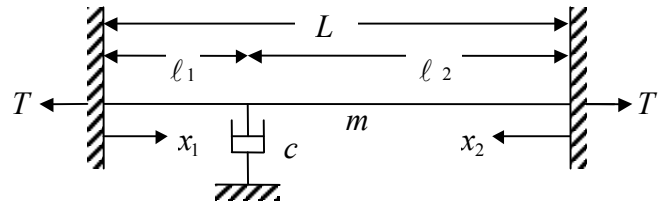

Figure 77: Taut cable with a linear damper.

In designing a damper for cable vibration suppression, it is necessary to determine the levels of supplemental damping provided in the first several modes of vibration for different values of the damper coefficient and different damper locations. Due in part to the multiple excitation mechanisms causing stay-cable oscillation, it is also important to consider the damping performance in higher modes. In the case of taut cable with a linear viscous damper (Figure 77), the supplemental damping ratios can be determined from a complex eigenvalue analysis of the damped cable in free vibration. The solution of the governing partial differential equation over the two cable segments on each side of the damper using separation of variables leads to the following expressions for the cable displacement:

$$y_1(x_1,\tau)=\gamma\frac{\sinh(\pi\lambda\frac{x_1}{L})}{\sinh(\pi\lambda\frac{\ell_1}{L})}e^{\lambda\tau}; \qquad y_2(x_2,\tau)=\gamma\frac{\sinh(\pi\lambda\frac{x_2}{L})}{\sinh(\pi\lambda\frac{\ell_2}{L})}e^{\lambda\tau} \tag{20a, b}$$

where τ is a nondimensional time, $\tau=\omega_{o1}t$, ω_{o1} is the undamped fundamental natural frequency of the cable, $\omega_{o1}=(\pi/L)\sqrt{T/m}$, and λ is the nondimensional eigenvalue, which is complex in general, and for small damping is "mostly" imaginary. Equilibrium of forces at the damper location can be written as

$$T\left[-\frac{\partial y_2}{\partial x_2}\bigg|_{x_2=\ell_2}-\frac{\partial y_1}{\partial x_1}\bigg|_{x_1=\ell_1}\right]=c\frac{\partial y_1}{\partial t}\bigg|_{x_1=\ell_1} \tag{21}$$

Substituting the solution form (Equation 20) into the equilibrium Equation 21 leads to the following transcendental equation for the nondimensional eigenvalue λ:

$$\sinh(\pi\lambda)+\pi\frac{c}{mL\omega_{o1}}\sinh(\pi\lambda\frac{\ell_1}{L})\sinh(\pi\lambda\frac{\ell_2}{L})=0 \tag{22}$$

Equation 22 can be solved numerically for the complex eigenvalues to obtain the modal damping ratios in as many modes as desired to an arbitrary degree of accuracy. The damping ratio in the ith mode can be readily obtained from the following expression:

$$\zeta_i = \left(\frac{\varphi_i^{\,2}}{\sigma_i^{\,2}} + 1 \right)^{-\frac{1}{2}} \tag{23}$$

where $\sigma_i = \mathrm{Re}(\lambda_i)$ and $\varphi_i = \mathrm{Im}(\lambda_i)$. It is noted that φ_i is the nondimensional frequency of damped oscillation in mode *i*. Previous numerical investigations revealed nondimensional groupings of parameters allowing the results of the eigenvalue analysis to be presented as a very useful "universal estimation curve" of normalized modal damping ratio versus normalized damper coefficient, which is applicable in the first few modes for dampers located near the end of the cable (Pacheco et al., 1993) and allows easy determination of optimal design values. Krenk (2000) demonstrated that an explicit analytical equation for this universal curve could be obtained from the transcendental eigenvalue equation using asymptotic approximations. The resulting approximate expression is a generalization to higher modes of the approximation previously obtained by Carne (1981) for the damping ratio in the fundamental mode.

For damper locations resulting in small frequency shifts (e.g., dampers near the end of the stay), the expression can be written as:

$$\frac{\zeta_i}{(\ell_1 / L)} \cong \frac{\pi^2 \kappa}{(\pi^2 \kappa)^2 + 1} \tag{24}$$

where κ is a nondimensional parameter grouping defined as

$$\kappa \equiv \frac{\mathrm{c}}{\mathrm{mL}\omega_{\mathrm{o1}}} \mathrm{i} \frac{\ell_1}{\mathrm{L}} = \frac{1}{\pi} \frac{\mathrm{c}}{\sqrt{\mathrm{Tm}}} \mathrm{i} \frac{\ell_1}{\mathrm{L}} \tag{25}$$

Equation 24 gives the damping attainable in a particular mode of vibration *i* as a function of the damper coefficient *c*, mass per unit length *m*, cable length *L* and fundamental circular frequency ω_{o1} as well as normalized damper location ℓ_1/L.

Results:

In Figure 78, the normalized damping ratio $\zeta/(\ell_1/\mathrm{L})$ has been plotted against the nondimensional damping parameter, κ, for the first five modes for a damper location of ℓ_1/L=0.02, and it is evident that the five curves collapse very nearly onto a single curve in good agreement with the approximation of Equation 24. It is important to note that because the mode number is incorporated in the nondimensional damping parameter κ, the optimal damping ratio can be achieved in only one mode of vibration in the case of a linear damper. This is a potential limitation, because it is currently unclear how to specify, a priori, the mode in which optimal performance should be achieved for effective suppression of stay-cable vibration, and designing a damper for optimal performance in a particular mode may potentially leave the cable susceptible to vibrations in other modes.

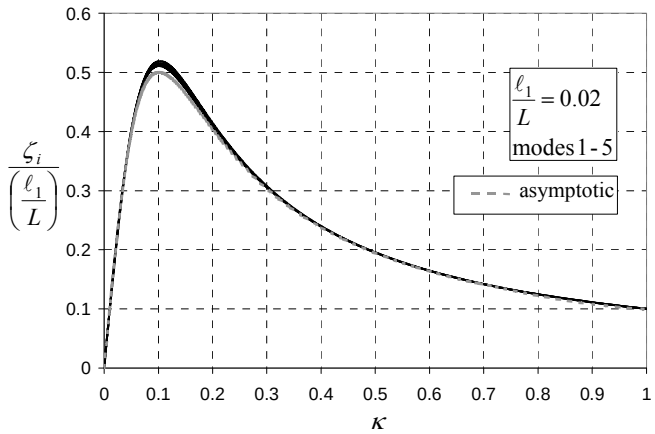

Figure 78: Normalized Damping Ratio versus Normalized Damper Coefficient.

Summary:

Free vibrations of a taut cable with an attached linear viscous damper were investigated in detail. An analytical formulation of the complex eigenvalue problem was used to derive an equation for the eigenvalues that is independent of the damper coefficient. This "phase equation" reveals the attainable modal damping ratios ζ_i and corresponding oscillation frequencies for a given damper location ℓ_1/L, affording an improved understanding of the solution characteristics and revealing the important role of damper-induced frequency shifts in characterizing the response of the system.

When the damper-induced frequency shifts are small, an asymptotic approximate solution has been developed, relating the damping ratio ζ_i in each mode to the nondimensional damper coefficient, κ.

When the damper is far from the end of the stay, different regimes of behavior can be observed, potentially significantly altering the performance of the damper. For such situations, the reader is referred to the publication Main and Jones (2002a).

Response of a Taut Cable with an Attached Linear Damper with a Friction Threshold

This section presents an analytical investigation of the influence of a friction threshold on damper performance for stay-cable vibration suppression. An asymptotic solution for the modal damping ratios is presented for a taut cable with a linear viscous damper, based on previous investigations, and an "equivalent viscous damper" formulation is used to extend these results to a viscous damper with a friction threshold. The relevant nondimensional parameter groupings are identified: a viscous damper parameter κ and a friction parameter μ. The approximate solution is appropriate only for relatively small values of the friction parameter μ, for which the assumption of nearly sinusoidal motion is valid. It is observed that the influence of friction is to reduce the optimal value of the viscous damper parameter κ, and for sufficiently large values of μ, to reduce the attainable damping ratios as well.

Ongoing measurements of damper forces, both in the field and in the laboratory, seem to indicate that the dampers possess a friction threshold that is quite large relative to the force levels engaged by wind-induced oscillations of the stays. When the forces in a damper are below this friction threshold, the damper simply locks the cable at the attachment point, shifting the oscillation frequencies without providing any supplemental damping.

Motivated by the potentially large magnitude of the damper friction threshold and the apparent significance of its effect in the measured data, this section presents an analytical investigation of the influence of a friction threshold on damper performance. Carne (1981) and Kovacs et al. (1999) previously developed approximate solutions for the damping ratios in the case of a purely frictional damper using equivalent viscous solutions, and a similar approach is taken herein. Asymptotic approximate solutions for the damping ratios in the case of a taut cable with a linear viscous damper are summarized from the results of investigations reported above. An equivalent viscous damping formulation is then developed to extend the results for a linear viscous damper to a viscous damper with a friction threshold. The relevant nondimensional parameter groupings are identified, and the solution characteristics are explored.

Problem formulation:

The problem under consideration is the vibration of a taut cable with an attached viscous damper having a friction threshold, depicted in Figure 79a. The nonlinear force-velocity relationship for the damper with a friction threshold is modeled by the following equation:

$$F_d(v) = F_o \,\mathrm{sign}(v) + c^* v \tag{26}$$

where v is the velocity of the cable at the damper attachment point. The resulting force-velocity curve is depicted in Figure 79b.

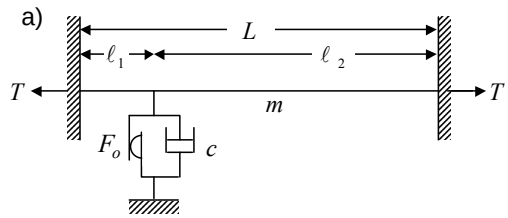

Figure 79a: Cable with Attached Friction/Viscous Damper

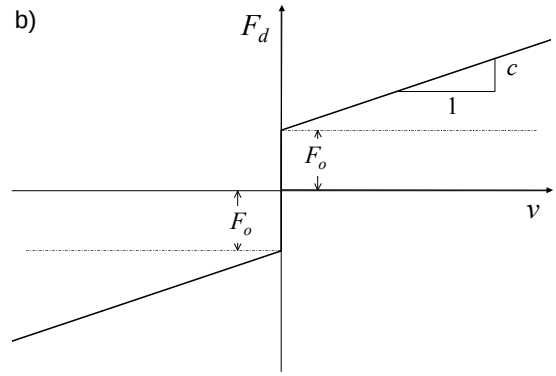

Figure 79b: Force-Velocity Curve for Friction/Viscous Damper

In the case of a purely viscous damper ($F_o = 0$), an exact solution to the free-vibration problem has been obtained (Krenk, 2000; Main and Jones, 2002a) which yields a transcendental equation for the complex eigenvalues and an explicit asymptotic solution for the modal damping ratios in the first few modes for damper locations near the end of the cable ($\ell_1 << \ell_2$). This solution has also been extended to develop an approximate solution for the effective damping ratios for a nonlinear power-law damper (Main and Jones, 2002b). The asymptotic solution for the linear viscous damper is extended here to the friction/viscous damper by computing an equivalent viscous damper coefficient, c_{eq}, using an equivalent energy dissipation criterion. This equivalent viscous solution is less appropriate when the forces in the damper are below the friction threshold for a significant portion of the oscillation cycle; in such cases, the damper is locked for much of the cycle, so that the motion at the damper is far from sinusoidal, and the spatial form of the solution also differs significantly from the solution for the linear viscous damper. Further work is necessary to better model this frictional "sticking" in order to develop more accurate solutions in cases for which this effect is significant.

Asymptotic Solution for Taut Cable with Linear Viscous Damper:

In the case of a taut cable with a linear viscous damper, when the damper-induced frequency shifts are small, as is the case for vibrations in the first few modes when $\ell_1 << \ell_2$, an asymptotic approximation can be obtained relating the damping ratio in the ith mode to the "clamping ratio", a normalized measure of the damper-induced frequency shift in that mode (Main and Jones, 2002a):

$$\frac{\zeta_i}{(\ell_1 / L)} \cong \sqrt{\Theta_{ci}(1-\Theta_{ci})} \tag{27}$$

The "clamping ratio" Θ_{ci} is defined as

$$\Theta_{ci} = \frac{\varphi_i - i}{\Delta\varphi_i}; \quad 0 \le \Theta_{ci} < 1 \tag{28}$$

where γi φ_i is the nondimensional frequency of oscillation in the ith mode [the dimensional frequency is given by $\omega_{o1}\varphi_i$, where ω_{o1} is the undamped fundamental frequency of the cable: $\omega_{o1} = (\pi/L)\sqrt{T/m}$]. The term $\Delta\varphi_i = i\left(\ell_1/\ell_2\right)$, in the denominator of Equation 28, is the difference between the "clamped" frequency $\varphi_{ci} = i\left(L/\ell_2\right)$, associated with a rigid damper ($c \to \infty$), and the undamped frequency $\varphi_{oi} = i$, associated with $c \to 0$. Consequently, $\Theta_{ci} \to 0$ as $c \to \infty$, and $\Theta_{ci} \to 1$ as $c \to \infty$. Equation 27 is independent of the mode number, indicating a maximum damping ratio of $\zeta_i = (1/2)(\ell_1/L)$ in each mode, corresponding to an optimal clamping ratio of $\Theta_{ci} = 1/2$. Physically, this means that the optimal damping performance in a given mode is achieved when the damper has shifted the frequency of oscillation in that mode to a value halfway between the undamped frequency and the clamped frequency. Equation 27 also indicates that the damping ratio in a given mode approaches zero as the clamping ratio approaches unity and the damper effectively locks the cable at the damper location.

Figure 80a shows a plot of Equation 27 along with curves corresponding to the exact solution in each of the first five modes for a damper location of ℓ_1/L = 0.02, and for this damper location the exact solutions agree quite well with the approximation of Equation 27. An additional asymptotic approximation can be obtained relating the clamping ratio to the viscous damper coefficient:

$$\kappa \cong \frac{1}{\pi^2}\sqrt{\frac{\Theta_{ci}}{1-\Theta_{ci}}} \tag{29}$$

where κ is a normalized viscous damper coefficient previously defined in Equation 25 as

$$\kappa \equiv \frac{c}{mL\omega_{o1}} i\frac{\ell_1}{L} = \frac{1}{\pi}\frac{c}{\sqrt{Tm}} i\frac{\ell_1}{L}$$

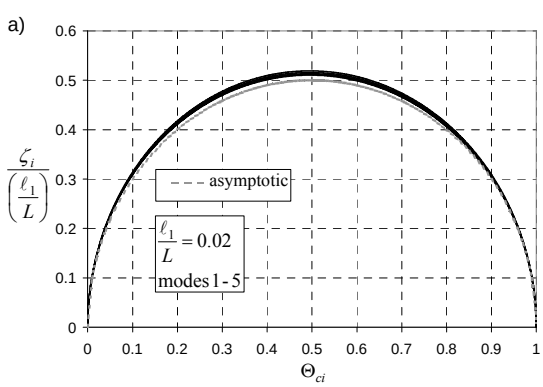

Figure 80a: Normalized Damping Ratio vs. "Clamping Ratio".

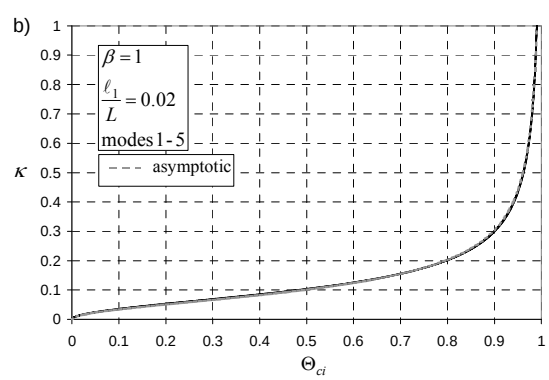

Figure 80b: Normalized Viscous Damper Coefficient vs. "Clamping Ratio".

Figure 80b shows a plot of Equation 29 along with curves corresponding to the exact solution in each of the first five modes for a damper location of $\ell_1/L = 0.02$, and for this damper location the exact solutions agree quite well with the approximation of Equation 29. An asymptotic approximation can also be obtained relating the amplitude at the damper attachment point γ to the peak modal amplitude A:

$$|\gamma / A| \cong \pi i(\ell_1 / L)\sqrt{1-\Theta_{ci}} \tag{30}$$

Equations 27, 29, and 30 will prove useful in extending the solution for a taut cable with a viscous damper to develop an approximate solution for the friction/viscous damper.

Equivalent Viscous Damper Formulation:

At a given amplitude and frequency of oscillation, a nonlinear damper can be approximated by an equivalent linear viscous damper which dissipates the same amount of energy in one cycle of oscillation. If the cable can be assumed to be oscillating nearly sinusoidally at a frequency ω with an amplitude γ at the damper attachment point, the velocity of the cable at the damper attachment point can be expressed as

$$v(t) = \gamma\omega \sin \omega t \tag{31}$$

The work done by the damper in one cycle of oscillation can then be expressed as

$$\Delta W_d = \int_0^{2\pi/\omega} F_d \cdot v \, dt \tag{32}$$

Substituting $F_d = c_{eq} \cdot v$ into Equation 32, substituting Equation 31 for v, and performing the integration yields the following expression for the work done by the equivalent viscous damper in one cycle of oscillation:

$$\Delta W_d^{(eq)} = \pi c_{eq} \gamma^2 \omega \tag{33}$$

The value of the equivalent viscous damper coefficient c_{eq} for a nonlinear damper can then be obtained by equating the work done by the nonlinear damper in one cycle of oscillation to the expression in Equation 33 and solving for c_{eq}, which yields the following expression:

$$c_{eq} = \frac{\Delta W_d}{\pi \gamma^2 \omega} \tag{34}$$

where ΔW_d, computed from Equation 32, is the work done by the nonlinear damper in one cycle of oscillation at a given amplitude and frequency. Substituting the force-velocity relation for the friction/viscous damper in Equation 26 and the velocity in Equation 31 into Equation 32 yields the following expression for the work done in one cycle for the friction/viscous damper:

$$\Delta W_d = 4F_o\gamma + \pi c\gamma^2\omega \tag{35}$$

Substituting this value into Equation 34 yields the following expression for the equivalent linear damper coefficient:

$$c_{eq} = \frac{4F_o}{\pi\omega\gamma} + c \tag{36}$$

When the damper-induced frequency shifts are small, the frequency of oscillation in a given mode i is close to the undamped frequency: $\omega \cong i\omega_{o1} = i(\pi / L)\sqrt{T/m}$. Substituting this approximation into Equation 36 along with the previously developed approximation for the amplitude at the damper (Equation 31) and normalizing by $\sqrt{Tm}$ yields the following nondimensional expression for the equivalent viscous damper coefficient:

$$\frac{c_{eq}}{\sqrt{Tm}} = \frac{4}{\pi^3 i^2 (\ell_1 / L)\sqrt{1-\Theta_{ci}}}\frac{F_o}{T}\frac{L}{A} + \frac{c}{\sqrt{Tm}} \tag{37}$$

The asymptotic relation between the damper coefficient and the clamping ratio for a linear damper (Equation 29) can be generalized to a nonlinear damper by substituting c_{eq} for c in the definition of κ in Equation 25 to yield the following equation:

$$\frac{1}{\pi}\frac{c_{eq}}{\sqrt{Tm}} i \frac{\ell_1}{L} \cong \frac{1}{\pi^2}\sqrt{\frac{\Theta_{ci}}{1-\Theta_{ci}}} \tag{38}$$

Substituting the expression for the equivalent damper coefficient (Equation 38) into Equation 38 then yields, after some simplification, the following relation between the clamping ratio Θ_{ci} and two nondimensional parameters:

$$\mu \cong (\pi^2 / 4)[\sqrt{\Theta_{ci}} - \pi^2\kappa\sqrt{1-\Theta_{ci}}] \tag{39}$$

where μ is a nondimensional friction parameter

$$\mu \equiv \left(\frac{F_o}{T}\right)\left(\frac{Ai}{L}\right)^{-1} \tag{40}$$

and κ is the normalized viscous damping parameter as defined previously in Equation 25.

Solution characteristics:

For a given value of the clamping ratio Θ_{ci}, Equation 39 indicates a linear relationship between μ and κ. Figure 81 shows a plot of μ versus κ for several different values of Θ_{ci}.

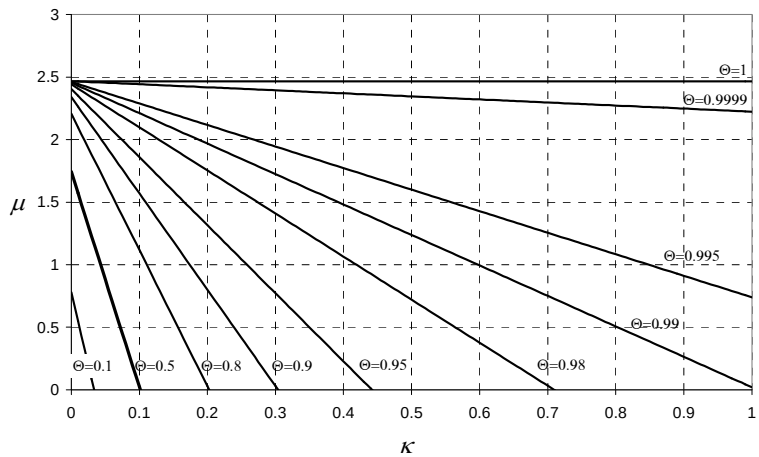

Figure 81: Relationship between Nondimensional Parameters μ and κ with Different Values of the Clamping Ratio Θ_{ci} for a Friction/Viscous Damper.

When $\Theta_{ci} = 1$, corresponding to the "clamped" limit in which the cable is completely restrained at the damper location, Equation 39 reduces to

$$\mu_c = (\pi^2 / 4) \cong 2.47 \tag{41}$$

When $\mu \geq \mu_c$, corresponding to a relatively large friction force and/or small amplitude, the damper is completely locked and provides no energy dissipation. The condition at which the damper is completely locked by friction can also be computed directly by considering equilibrium of forces at the damper location, and this approach gives a value of $\mu_c = \pi$, which differs significantly from the value obtained in Equation 41 from the equivalent viscous damper formulation. This discrepancy arises because, as discussed previously, when the damper approaches the limit of being completely locked by friction, the damper is "stuck" for a significant portion of the oscillation cycle, causing the motion at the damper to be far from sinusoidal, and the equivalent viscous damper approximation developed herein is inappropriate. Consequently, the solution developed herein should only be considered accurate for relatively small values of the friction parameter μ, corresponding to low values of the friction threshold or large amplitudes. Preliminary efforts to model the frictional "sticking" indicate that the equivalent viscous solution gives fairly accurate results for $\mu < 0.5$, while the discrepancies can be significant for larger values of μ.

When $\Theta_{ci} = 0.5$, corresponding to optimal damping, Equation 39 reduces to

$$\mu_{opt} \cong (\pi^2 \sqrt{2} / 8)(1 - \pi^2 \kappa_{opt}) \tag{42}$$

Equation 42 is the equation of the line in Figure 81 labeled "$\Theta_{ci} = 0.5$", and it specifies the combinations of μ and κ for which optimal damping is obtained. Equation 27 can be used in conjunction with Equation 39 to generate curves of normalized modal damping ratio versus κ for different values of μ, as depicted in Figure 82.

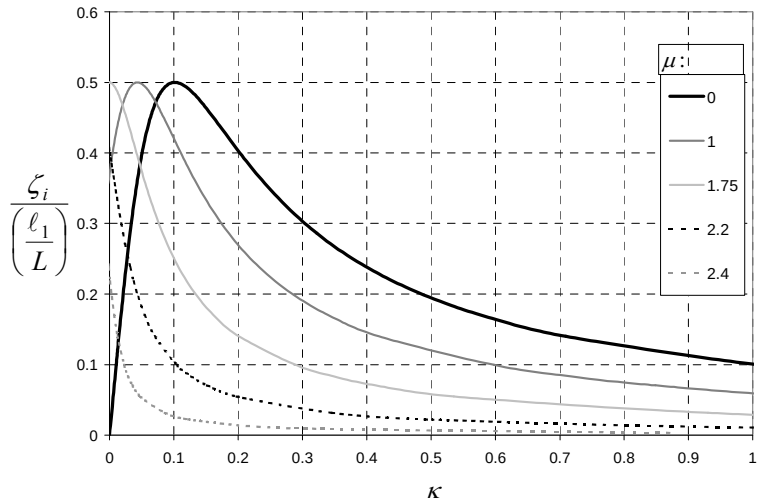

Figure 82: Normalized Damping Ratio vs. κ with varying μ.

The curve labeled "$\mu = 0$" corresponds to the asymptotic solution for the linear viscous damper, for which the optimal value $\kappa_{opt} = 1/\pi^2 \cong 0.101$ can be obtained from Equation 42 by setting $\mu = 0$. The effect of increasing friction is to shift the optimal portion of the curve to the left. When μ exceeds a critical value, optimal damping can no longer be achieved. This critical value can be obtained from Equation 42 by setting $\kappa = 0$, and is given by $\mu = \pi^2\sqrt{2}/8 \cong 1.75$.

Summary:

An asymptotic solution for the damping ratios in the case of a taut cable with a linear viscous damper was extended to the nonlinear case of a viscous damper with a friction threshold using an "equivalent viscous damper" formulation. Relevant nondimensional parameter groupings were identified, and the solution characteristics were explored. It is observed that this formulation does a poor job of estimating the amplitude at which the damper is completely locked due to friction, and the results of this analysis should only be considered accurate for relatively small values of the friction parameter μ, for which the assumption of nearly sinusoidal oscillation is appropriate. The observed effect of the friction threshold is to reduce the optimal value of the viscous damping parameter κ and ultimately to reduce the attainable damping ratios from the values for a purely viscous damper.

Response of a Taut Cable with an Attached Nonlinear Damper (exponent other than one).

Recent investigations indicated that a nonlinear damper may potentially overcome the limitation in performance of a linear damper whereby optimal damping performance can only be achieved in one mode of vibration. Kovacs et al. (1999) recently reported on the implementation of a friction damper on the Sunningesund Bridge. The exact formulation of the free-vibration problem for a taut cable with a linear damper can be extended to develop an approximate analytical solution for the amplitude-dependent effective damping ratios in the case of a nonlinear damper, for which the damper provides a dissipative force proportional to the cable velocity at the damper attachment point raised to an arbitrary positive exponent, β. The formulation is extended by assuming a single-mode response, assuming the solution has the same form as in the linear case (Equation 42a,b), and minimizing the error in the equilibrium equation over a half-cycle of oscillation. Asymptotic approximations then yield the following expressions:

$$\kappa \cong \frac{1}{\pi^{\beta+1}} \frac{f(\beta)}{g(\beta)} \sqrt{\frac{\Theta_{ci}}{(1-\Theta_{ci})^{\beta}}} \; ; \text{ where } \quad \kappa \equiv \frac{c\left(\frac{A_\tau}{L}\right)^{\beta-1}}{m(L\omega_{o1})^{2-\beta}} i^{(2\beta-1)} \left(\frac{\ell_1}{L}\right)^{\beta} \qquad \text{(43a, b)}$$

where A_τ is approximately the peak modal amplitude of oscillation, is the clamping ratio (Equation 28), and $f(\beta)$ and $g(\beta)$ are given by:

$$f(\beta) = \frac{2}{\pi} \int_0^{\pi} \sin^{(\beta+1)}(\theta) d\theta = \frac{2}{\sqrt{\pi}} \frac{\Gamma\left(1+\frac{\beta}{2}\right)}{\Gamma\left(\frac{3}{2}+\frac{\beta}{2}\right)} \; ; \; g(\beta) = \frac{2}{\pi} \int_0^{\pi} \sin^{2\beta}(\theta) d\theta = \frac{2}{\sqrt{\pi}} \frac{\Gamma\left(\frac{1}{2}+\beta\right)}{\Gamma(1+\beta)} \qquad \text{(44a, b)}$$

The new definition of the nondimensional damping parameter, κ, in Equation 43b reduces to Equation 25 in the case of a linear damper (β=1). Equation 25 can then be written, eliminating the clamping ratio, to obtain an implicit asymptotic approximate expression relating the normalized damping ratio to the nondimensional damping parameter κ, which may be regarded as a generalization of the universal estimation curve of Pacheco et al. (1993) to the case of a nonlinear damper. The shape of the curve is slightly different for each value of damping exponent, β, but for a given damping exponent the curve is nearly invariant with damper location and mode number over the same range of parameters as the universal estimation curve for the linear case. Figure 83 shows a plot of normalized damping ratio versus κ in the first five modes for a square-root damper.

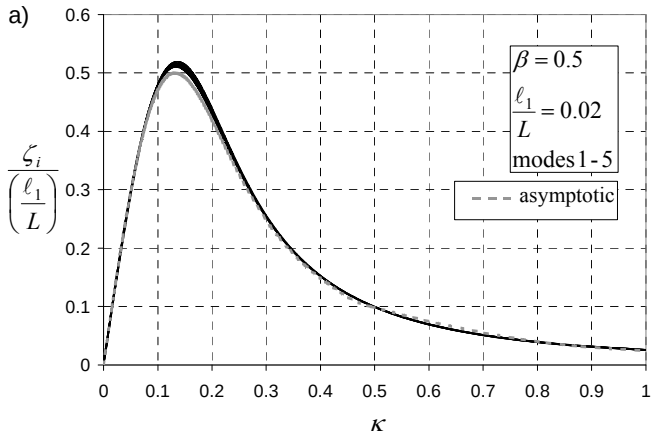

Figure 83: Normalized Damping Ratio versus Normalized Damper Coefficient: β=0.5.

Because the nondimensional damping parameter κ depends on both the amplitude and mode number of oscillation, the optimal damping performance will be achieved, in general, at different amplitudes of vibration in each mode. An "optimal" value for the damper coefficient can be determined by specifying a design amplitude of oscillation in a given mode at which the optimal performance is desired. This amplitude at which the maximum effective damping ratio is to be achieved will be denoted A_{opt}, and the corresponding mode number will be denoted i_{opt}. The notion of specifying a design-level oscillation amplitude is familiar to designers, as even in the case of a linear damper an amplitude of oscillation must be specified to determine the stroke and energy dissipation requirements for a linear damper. The value of the damper coefficient necessary to achieve the specified performance is then given by:

$$c_{opt} = m(L\omega_{o1})^{2-\beta}\left(\frac{\ell_1}{L}\right)^{-\beta}\left(\frac{A_{opt}}{L}\right)^{1-\beta}\left(i_{opt}\right)^{1-2\beta}\frac{\left(\sqrt{2}\right)^{\beta-1}}{\pi^{\beta+1}}\frac{f(\beta)}{g(\beta)} \tag{45}$$

With the damper coefficient designed according to Equation 45, the following asymptotic expression can be obtained relating the amplitude and mode number of oscillation to the clamping ratio:

$$\left(\frac{A_\tau}{A_{opt}}\right)^{\beta-1}\left(\frac{i}{i_{opt}}\right)^{2\beta-1} \cong \left(\sqrt{2}\right)^{1-\beta}\sqrt{\frac{\Theta_{ci}}{(1-\Theta_{ci})^{\beta}}} \tag{46}$$

Equation 46 may then be used to characterize the amplitude-dependence and mode-dependence of damper performance. In the case of a linear damper (β=1), the amplitude-dependence in Equation 46 vanishes, as expected, and the normalized damping ratio can be plotted directly against the mode number ratio i/i_{opt}, as shown in Figure 84a. Interestingly, in the case of a square-root damper (β=1/2), the mode dependence in Equation 46 disappears, and the damping performance depends only on the amplitude of vibration. Figure 84b shows the effective damping ratio plotted against amplitude ratio, A_τ/A_{opt}, for the square-root damper. Because this

curve is independent of mode number, in designing a square-root damper it is sufficient to specify only the amplitude, A_{opt}, and the optimal damping performance is achieved at the same amplitude in each mode. This special mode independence of the square root damper suggests that it may offer some advantages over a linear damper. When β=0, (a friction damper), the amplitude and the mode number in Equation 46 are raised to the same power, and the effective damping ratio is a function of the product ($A_\tau i$). Consequently, the optimal amplitude is inversely proportional to the mode number, and the optimal performance is achieved at lower amplitudes in higher modes. In designing a friction damper, it is sufficient to specify the value of the product, $(A_\tau i)|_{\text{opt}}$, at which optimal damping performance is desired, rather than specifying A_{opt} and i_{opt} independently. Figure 84c shows the effective damping ratio versus $(A_\tau i)/(A_\tau i)|_{\text{opt}}$ for the friction damper. It is evident that there is a critical amplitude for the friction damper, below which no energy is dissipated by the damper. Comparing Figures 84b and 84c, the performance of the square-root damper can be argued to be more "robust" with amplitude than that of the friction damper, because the damping performance degrades more quickly away from the optimal amplitude in the case of the friction damper.

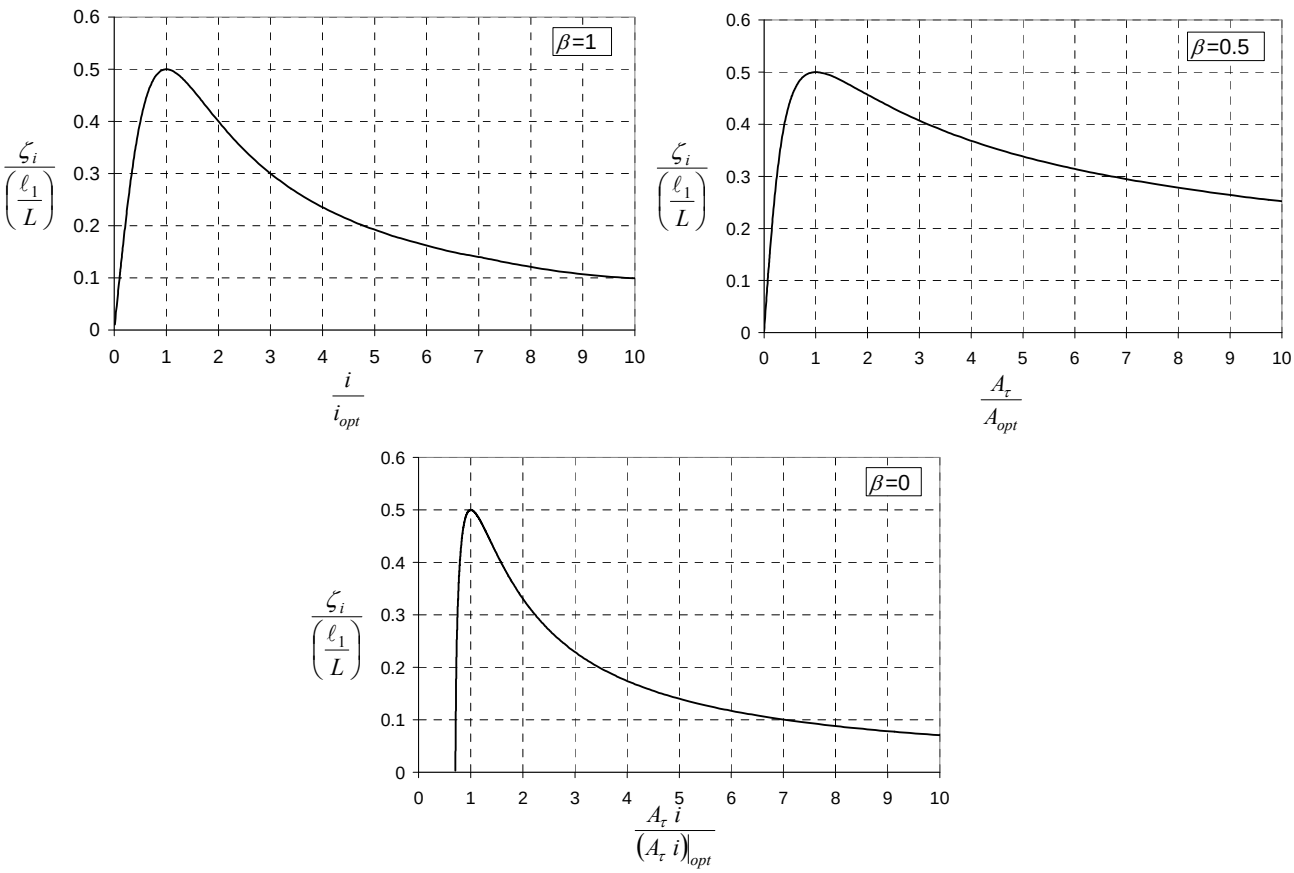

Figure 84a: Normalized Damping Ratio versus Mode Ratio (β=1).
Figure 84b: Normalized Damping Ratio versus Amplitude Ratio (β=0.5).
Figure 84c: Normalized Damping Ratio versus Mode-Amplitude Ratio (β=0).

Summary:

The dynamic behavior of a taut cable with a passive, nonlinear, power-law damper attached at an intermediate point was investigated. The exact formulation of the complex eigenvalue problem for a taut cable with a linear damper was extended to develop a single-mode approximation for the amplitude-dependent effective damping ratios for the power-law damper by minimizing the mean-square of the error in the force equilibrium equation at the damper over one half-cycle of oscillation. This formulation yielded the same "phase equation" that held in the case of a linear damper, giving the range of attainable damping ratios and corresponding oscillation frequencies in every mode. An asymptotic approximate solution revealed a nondimensional grouping of parameters that was used to extend the universal estimation curve for the linear damper to the case of a nonlinear damper. The shape of the resulting curve was slightly different for each value of damping exponent, β, but for a given damping exponent the curve was nearly invariant with damper location and mode number over the same range of parameters as the universal estimation curve for the linear case. The dependence of nonlinear damper performance on the amplitude and mode number of oscillation was investigated, and it was observed that a nonlinear damper could potentially allow optimal damping performance to be achieved over a wider range of modes than in the linear case. In the special case of β=0.5 (a square-root damper), it was observed that the damping performance is independent of mode number, so that the optimal damping ratio can be achieved in each mode at the same amplitude of oscillation. These features suggest that nonlinear dampers may offer some advantages over linear dampers for cable vibration suppression, while retaining the advantages of economy and reliability offered by a passive mitigation strategy.

C2.3 CROSS-TYING OF STAY CABLES

One of the methods that is sometimes adopted to counteract the undesired oscillations is to increase the in-plane stiffness of stays by connecting them together by means of a set of transverse cables, defined as cross-ties (or "aiguilles"). According to Gimsing (1983) these cables are also used to reduce the cable sag variations among the stays of different length, ensuring a more uniform axial stiffness on the consecutive stays. From the dynamic perspective, the properties of the single cable, considered as a separate element, are modified by the presence of the lateral constraints that influence its oscillation characteristics. Similarly, a connection of simple suspended elements is transformed into a more complex cable network; a closed-form solution to the dynamic problem is more elusive.

The literature contains examples of performance improvement for a vibrating cable; for example, the widely studied case of adding a transverse damper. However it is evident that detailed studies of cross-ties and interconnected cable systems are not well reported and most of the recommendations that are currently followed seem to be linked to practice or previous experience. A fundamental study to support these problems seemed therefore necessary. It is worth mentioning that a cable network can be a very complex system and finite element analysis has been preferred in the past. An example was given by Ehsan and Scanlan (1990), who used component-mode synthesis and finite element approaches for the solution of a three-dimensional cable problem. Reviews of cable vibration that address the most commonly used techniques for reducing motion amplitudes also identified this problem as one that still needs to be investigated (Hirsch, 1991).

Experience gained in the field of transverse restrainers was analyzed by Virlogeux (1998) who pointed out recent failures or unexpected behavior of the cross-ties (Pont de Normandie, Foro Bridge in Denmark). He addressed the issues of transverse cable stiffness, tension and internal damping. He also suggested that simplified approaches (equivalent static analyses) can be sometimes efficient in terms of design recommendations.

Yamaguchi and Jayawardena (1992) and Yamaguchi and Nagahawatta (1995) analyzed the problem through a set of experiments, conducted on a model of two interconnected cables, and a subsequent finite element simulation of the configuration. An energy approach for the determination of the damping contribution linked to the complex network was used. Among their comments, it is interesting to emphasize that the contribution to damping, due to cross-ties, can be negative or positive, depending on the chosen system and cable characteristics and that not only the overall stiffer configuration must be considered but also the possibility of exploiting the energy dissipation potential of the restrainers.

Several examples of vibration analysis of cable nets were found in the literature, even though most of them are related to high-tension systems, in which the excitation force is mainly orthogonal to the net configuration (i.e., membrane behavior – for example, Zingoni, 1996). In most cases a finite element analysis was performed. An interesting approach for the out-of-plane vibration analysis of a non-linear cable system was applied by Mesarovic and Gasparini (1990) to the study of a complex truss.

The novel contribution herein is the development of an analytical method and efficient numerical procedure that models the behavior of a set of interconnected cables. Observations of the behavior of these cross-tied systems were investigated through the detailed study of specific examples. This approach offers a number of advantages over the finite element method and provides a tool that is useful in the design and optimization of such systems for practical application.

Response Assessment of Cross-tied Stays with Rigid and Spring Connectors.

Basic Theory:

The initial problem formulation is depicted in Figure 85. The example shows a simplified network, defined by a set of two taut cables, connected by means of a vertical rigid rod (to be relaxed later). The generic *j-th* cable is divided into *m* segments, each of which is labeled as *p* (the generic element is denoted by *j,p*). The *j*-th cable is restrained at both ends; it is characterized by a length L_j, with $L_1>L_2$ in this case, tension H_j and mass per unit length μ_j. The horizontal offset between the two cables has been denoted by l_1 and the position of the vertical connection, with respect to the right-hand side of cable "2" has been assumed equal to l_2 (segment 2,1). The quantity $l^* = l_1 + l_2$ represents the same dimension in the coordinate system of the upper cable. The x_{jp} along-axis coordinate of the *p*-th segment of the *j*-th cable has been taken in accordance with Figure 85. Vertical displacements are considered positive downwards. The position of the vertical connector relative to the cable is general, and the only additional physical constraints are expressed by $L_2 \le L_1$; $l_2 \le L_2$; $l_1 + L_2 \le L_1$.

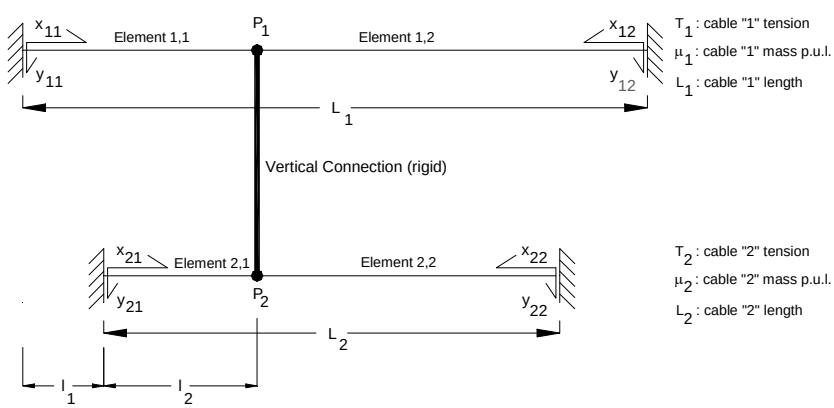

Figure 85: General problem formulation.

The free-vibration problem for this case is concerned with the solution of a system of four partial differential equations, corresponding to the four cable branches $y_{jp}(x_{jp},t)$, with j=1,2 and p=1,2, where t denotes the time variable:

$$H_j \frac{\partial^2 y_{jp}}{\partial x_{jp}^2} = \mu_j \frac{\partial^2 y_{jp}}{\partial t^2}, \tag{47}$$

where $j=1...n$ number of cables and $p=1...m$ number of segments, for each cable.

This system requires eight boundary, compatibility and equilibrium conditions, which can be expressed in terms of: *a)* displacements at cable ends; *b)* displacement continuity at point *P1* between branches "*1,1*" and "*1,2*", and at *P2* for segments "*2,1*" and "*2,2*"; *c)* equality of displacement at each time instant at *P1* and *P2* between the two cables; *d)* force equilibrium at the vertical rod. These can be written as follows:

$$y_{jp}(x_{jp}=0,t) = 0 \quad (\text{for } j=1,2 \text{ and } p=1,2); \tag{48a}$$

$$y_{11}(x_{11}=l^*,t) = y_{12}(x_{12}=L_1-l^*,t); \quad y_{21}(x_{21}=l_2,t) = y_{22}(x_{22}=L_2-l_2,t); \tag{48b}$$

$$y_{11}(x_1=l^*,t) = y_{21}(x_3=l_2,t); \tag{48c}$$

$$H_1\left(\left.\frac{\partial y_{11}}{\partial x_{11}}\right|_{x_1=l^*} + \left.\frac{\partial y_{12}}{\partial x_{12}}\right|_{x_2=L_1-l^*}\right) + H_2\left(\left.\frac{\partial y_{21}}{\partial x_{21}}\right|_{x_3=l_2} + \left.\frac{\partial y_{22}}{\partial x_{22}}\right|_{x_4=L_2-l_2}\right) = 0\,. \tag{48d}$$

A purely oscillatory motion of each cable element can be developed using the classical solution in which time-dependent and spatial-coordinate effects can be separated as $y_{jp}(x_{jp},t) = Y_{jp}(x_{jp})e^{i\omega t}$, where ω is the natural circular frequency of vibration of the coupled network (unknown). Equations 47 can be therefore reduced to a system of ordinary equations, as follows:

$$H_j \frac{d^2 Y_{jp}}{dx_{jp}^2} + \mu_j \omega^2 Y_{jp} = 0\,; \quad (j=1,2\ p=1,2). \tag{49}$$

From Equation 49 and the conditions in Equation 48a the solution can be proposed of the form:

$$Y_{11,12}(x_{11,12}) = A_{11,12}\sin\left(\frac{\alpha\pi}{L_1}x_{11,12}\right), \quad Y_{21,22}(x_{21,22}) = A_{21,22}\sin\left(\frac{\alpha f\pi}{L_1}x_{21,22}\right). \tag{50a, b}$$

In Equations 50 the upper cable is considered as reference element; α represents the reduced frequency of the system, and f is a parameter that takes into account geometrical and stiffness differences of cable "2" with respect to "1", defined as scaled frequency ratio. From Equation 49 such quantities can be redefined according to:

$$\begin{aligned} \omega &= \alpha\frac{\pi}{L_1}\left(\frac{H_1}{\mu_1}\right)^{1/2} = \alpha\omega_{01}, \\ f &= \left(\frac{H_1}{H_2}\right)^{1/2}\left(\frac{\mu_2}{\mu_1}\right)^{1/2} = \frac{\omega_{01}}{\omega_{02}}\frac{L_1}{L_2}. \end{aligned} \tag{51}$$

In these equations ω_{01} and ω_{02} are the fundamental circular frequencies of the unconnected cables. Equations 50a and 50b generally satisfy the requirements of the system given by Equation 49. The unknown parameters A_{jp}, representing the four modal amplitudes of each *p-th* segment, must be solved from the four boundary conditions (48b-48d). In this way the solution to the free-oscillation problem, and the determination of the natural frequencies in terms of α, can be transformed into a system of four algebraic equations, linked to (48b-48d), in a matrix form:

$$\mathbf{SA} = \mathbf{0}\,, \tag{52a}$$

$$\mathbf{A} = \begin{bmatrix} A_{11} & A_{12} & A_{21} & A_{22} \end{bmatrix}^T, \tag{52b}$$

$$\mathbf{S} = \begin{Bmatrix} \sin(\alpha\pi\xi_1) & -\sin[\alpha\pi(1-\xi_1)] & 0 & 0 \\ 0 & 0 & \sin(\alpha\pi\Delta\xi) & -\sin\left[\alpha f\pi\left(\dfrac{L_2}{L_1} - \Delta\xi\right)\right] \\ \sin(\alpha\pi\xi_1) & 0 & -\sin(\alpha f\pi\Delta\xi) & 0 \\ \cos(\alpha\pi\xi_1) & \cos[\alpha\pi(1-\xi_1)] & \dfrac{f}{h}\cos(\alpha f\pi\Delta\xi) & \dfrac{f}{h}\cos\left[\alpha f\pi\left(\dfrac{L_2}{L_1} - \Delta\xi\right)\right] \end{Bmatrix}, \tag{52c}$$

where all quantities have been reduced into the following dimensionless parameters: $h = H_1/H_2$; $\xi_1 = l^*/L_1$; $\xi_2 = l_1/L_1$; $\Delta\xi = l_2/L_1 = (\xi_1 - \xi_2)$. The infinite set of nontrivial solutions ($\mathbf{A} \neq \mathbf{0}$) to the homogeneous system (6a) can be identified through the condition $\det[\mathbf{S}] = 0$. This condition is given by the roots of the following polynomial *p(α)*:

$$\begin{aligned} p(\alpha) = \sin(\alpha\pi)\left\{\cos\left[\alpha f\pi\left(2\Delta\xi - \frac{L_2}{L_1}\right)\right] - \cos\left(\alpha f\pi\frac{L_2}{L_1}\right)\right\} + \\ + \frac{h}{f}\sin\left(\alpha f\pi\frac{L_2}{L_1}\right)\{\cos(2\alpha\pi\xi_1 - \alpha\pi) - \cos(\alpha\pi)\}. \end{aligned} \tag{53}$$

Equation 53 represents the frequency-equation that relates the general solution to a specific value of the system reduced frequency *α*, for which the modal amplitudes of the *r*-th segment can be obtained through the linearly independent equations of Equation 52. The roots of Equation 53 cannot be found analytically in closed form for the general case, since little further simplification is possible; a numerical technique can be adopted in this general case.

Generalization:

The above approach can be generalized to a system of multiple cables and cross ties. Readers are referred to the complete paper for details of this development, which will not be repeated here for brevity. This more general approach of necessity must be implemented and solved numerically.

Results:

The free-vibration analysis method, presented above was applied to the study of a cable network that was modeled after the Fred Hartman Bridge, a twin-deck cable-stayed bridge over the Houston Ship channel, with central span of 380m and side spans of 147m. The deck is composed of precast concrete slabs on steel girders with four lanes of traffic, carried by a total of 192 cables in four inclined planes, connected at 15m intervals.

The investigated system corresponds to the south-tower central-span portion, a set of twelve stays with a three-dimensional arrangement (Figure 86); the geometric and structural characteristics are summarized in Table 14. Stay "24S" is assumed as reference element; all other stay quantities are normalized with respect to this element.

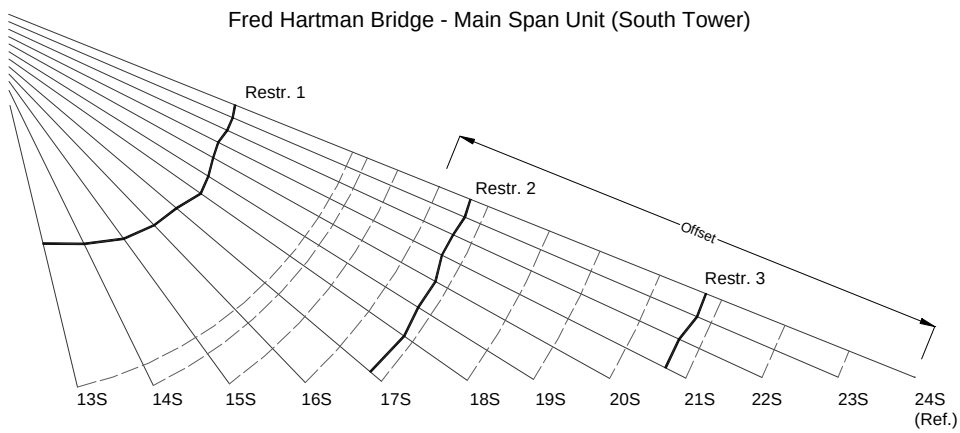

Figure 86: General problem formulation (original configuration).

Table 14: Geometrical and structural characteristics of the Fred Hartman system.

Stay-cables

Stay	mass (lb/ft)	mass (kg/m)	T (kips)	T (N)	L (m)	Lred (-)	ω (rad/s)	freq (1/s)	f_j (-)	ν_j (-)
13S	21.84	32.50	371	1.65E+06	59.523	0.3009	11.895	1.893	0.3258	0.3947
14S	32.21	47.93	359	1.60E+06	67.345	0.3404	8.516	1.355	0.4551	0.4715
15S	32.21	47.93	427	1.90E+06	76.549	0.3869	8.171	1.300	0.4744	0.5142
16S	32.21	47.93	485	2.16E+06	87.333	0.4414	7.633	1.215	0.5078	0.5481
17S	35.53	52.87	538	2.39E+06	99.377	0.5023	6.727	1.071	0.5762	0.6062
18S	35.53	52.87	614	2.73E+06	112.280	0.5675	6.360	1.012	0.6094	0.6476
19S	43.81	65.20	720	3.20E+06	125.779	0.6357	5.537	0.881	0.7000	0.7788
20S	47.12	70.12	753	3.35E+06	139.701	0.7061	4.916	0.782	0.7885	0.8260
21S	47.12	70.12	861	3.83E+06	154.076	0.7788	4.766	0.759	0.8132	0.8832
22S	47.12	70.12	797	3.55E+06	168.403	0.8512	4.195	0.668	0.9238	0.8497
23S	51.09	76.03	963	4.29E+06	183.056	0.9252	4.074	0.648	0.9513	0.9726
24S	51.09	76.03	1018	4.53E+06	197.847	1.0000	3.876	0.617	1.0000	1.0000

The transverse connectors, an "eight-loop" steel wire rope system, are located in accordance with the existing system (Figure 86). The characteristics of these elements are provided in Table 14. The three-dimensional cable network was reduced to an equivalent two-dimensional problem. As a result of this transformation to equivalent 2D problem, the overall pattern of the model is slightly irregular, since the lengths of each cable segment were selected at symmetric locations with respect to each stay but not to the global network.

The definitions of the modal frequencies and mode shapes of the network (free-vibration analysis) was performed through the study of the roots of the determinant of the system matrix as a function of the reduced frequency of the structure α, $\det[\mathbf{S}(\alpha)]$ and $\frac{d}{d\alpha}\{\det[\mathbf{S}(\alpha)]\}$; in this case f_{01} = 0.617 Hz.

A careful study of the solution patterns showed two categories of roots. The first are associated with "global modes", in which the whole set of cables is involved in the oscillation and with a substantial increment in the generalized mass of the mode, with respect to the individual cable modes. The second category is one of "localized modes", in which the response of network is not global but the maximum amplitudes are located in the intermediate segments of specific cables only. Moreover the overall characteristics of these modal forms (both symmetric or antisymmetric) can be different from the solution for individual cables, and influenced by the presence and the location of the transverse connectors. The solutions are antisymmetric or pseudo-symmetric. The wavelength of these modes is essentially governed by the distance between two consecutive connectors (being almost coincident with the nodes of the modal shape). The high density of solutions is related to the fact that these modes are the components of high-order modes of the individual cables with different magnitude, for which the location of the connector on each cable represents a node of the individual mode shape.

Figure 87 depicts the eigenfunctions of the fundamental modes of the two-dimensional model corresponding to the Hartman Bridge, normalized so that the resulting modal mass of the network is unitary. In this way the presence of a localized mode is emphasized (modes 4-8) by solutions for three comparative cases (NET_3C, original configuration; NET_3RC perfectly rigid transverse links; NET_3CG modified non-rigid configuration with ground restrainers) is presented in Figure 88, in which the natural frequencies (Hz) are plotted as a function of the mode number and compared to the individual cable behavior. A similar representation was introduced by Abdel-Ghaffar and Khalifa (1991) for the numerical study of vibration problems of cable-stayed bridges, in which global (deck, towers) and local modes were identified. From this figure, the structural behavior can be efficiently and graphically characterized: the sequence of fundamental global modes is followed by a high-density solution pattern, corresponding to the localized modes that can be related to the symmetric components of the individual cable segments.

A typical plateau can be identified for all the sets; the upper and lower frequency limits, as indicated in Figure 88, are influenced by those frequencies of the individual cable solutions, the modal shape of which is characterized by wavelength close to the distance between restrainers. The modes included in this region are defined as local, governed by the geometry of internal elements of the system, the distance between consecutive nodes of the grid ($P_{j,p}$) but largely uninfluenced by the structural properties of the connectors. An upper and lower limit frequency can be detected, in this case 1.9 and 2.7 Hz, respectively.

Both limits are connected by the frequency of antisymmetric second modes in the individual stays; the upper α is directly related to the frequency of shorter cables while the lower value is influenced by a combination of the stays in the central part of the structure (presence of pseudo-symmetric components). The high density of frequencies, reflected in the behavior of the determinant, $\det[\mathbf{S}(\alpha)]$, suggests a potential sensitivity to forced oscillations, exciting the network within this range of α, in which the dynamics can be influenced by a combination of these modal forms. Beyond this upper limit the situation reverts to a set of higher network modes and thereafter, a second plateau appears in the frequency range coincident with high-order antisymmetric individual segment modes; this pattern of consecutive "steps" defines a typical pattern for the behavior.

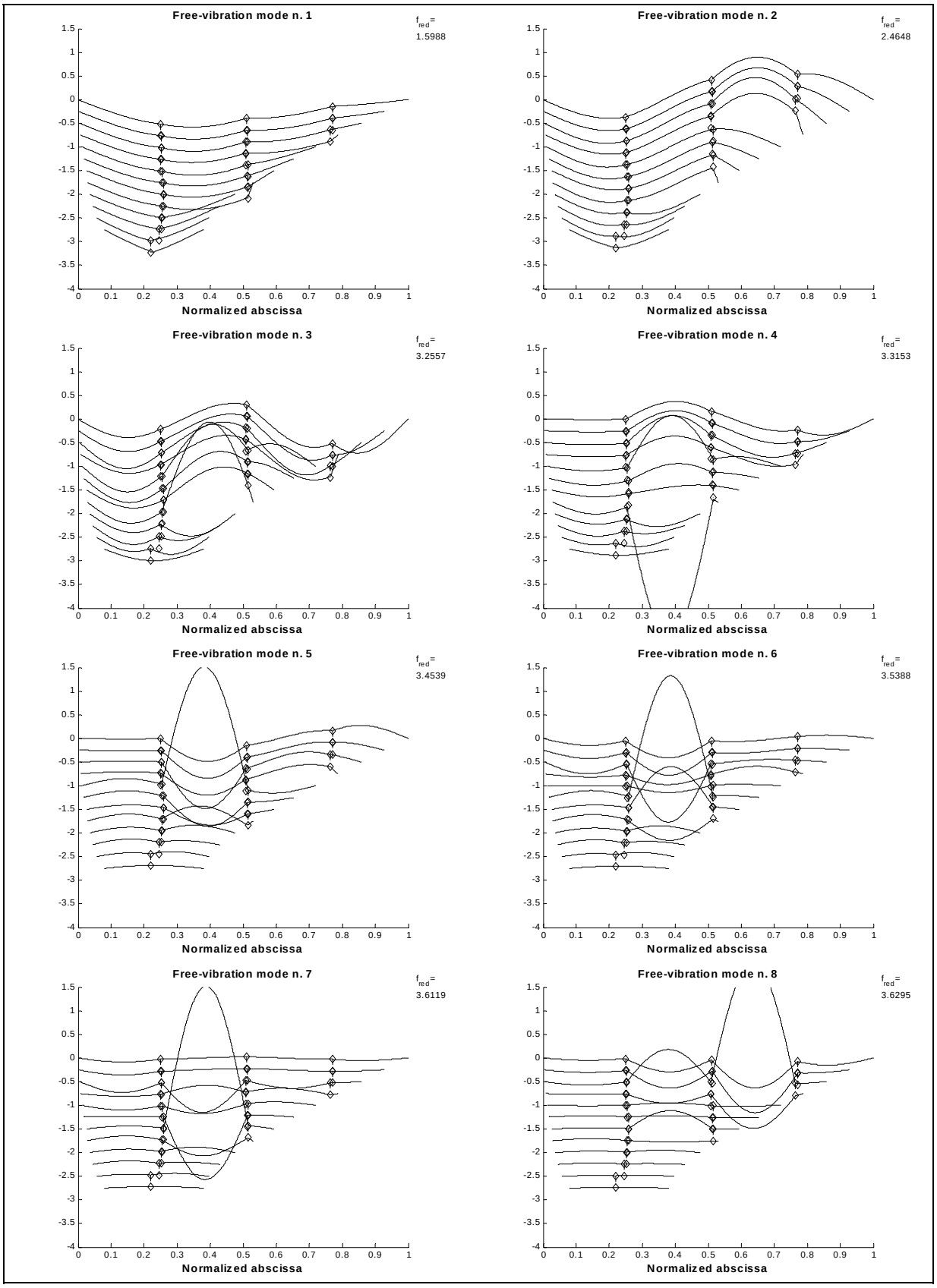

Figure 87: Eigenfunctions of the network equivalent to Fred Hartman Bridge; 1st – 8th modes.

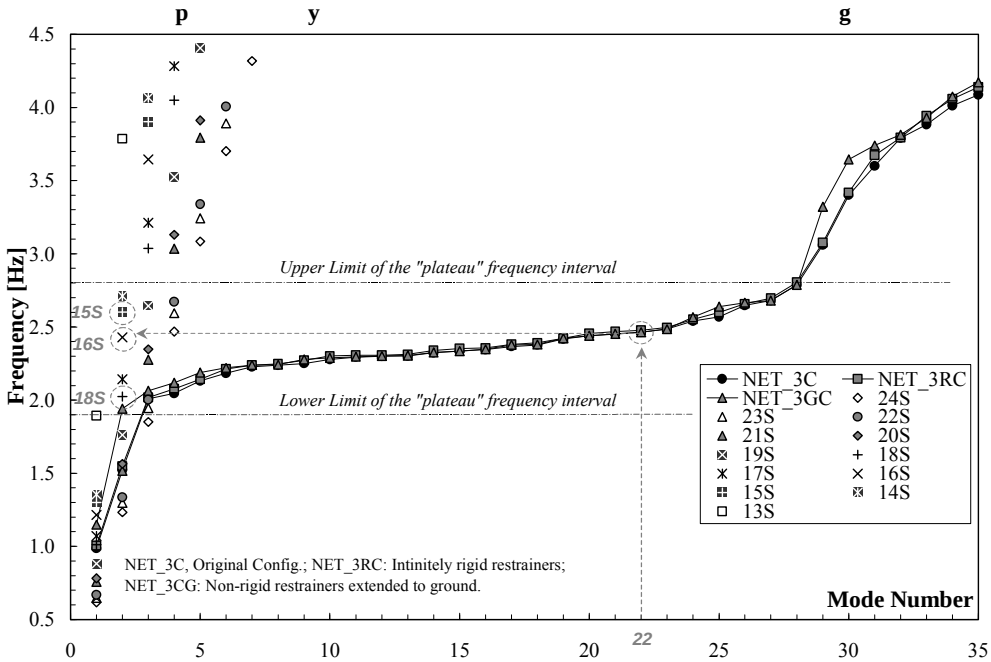

Figure 88: Comparative analysis of network vibration characteristics and individual-cable behavior; Fred Hartman Bridge; NET_3C, original configuration; NET_3RC, infinitely rigid restrainers; NET_3CG, spring connectors extended to ground (Restr. 2,3).

For practical purposes, the connectors in the original configuration can be considered as effectively rigid, since the two graphics (NET_3C, NET_3RC) essentially overlap (the increase in the frequency of the fundamental frequency is only about 3% only).

The action of progressively increasing the stiffness of the restrainers produces modifications and increments in the frequency of the first global modes (and, to a lesser extent, of the higher global solutions). The presence of the ground connectors (Restrainers 2,3) is able to modify only global modes (1-3, beyond 27), influencing the response at low frequencies (first modes) and, subsequently, only for much higher solutions, in a frequency range of lower importance for design purposes. Modal amplitudes are clearly reduced in the portion of the stays connected to the deck for purely symmetric modes almost becoming zero. The same behavior is also recorded for antisymmetric global modes in which the oscillations are mostly confined to a restricted region of the network (two or three columns of elements on the left side).

No variations for the intermediate modes (local modes) on the plateau can be seen; solutions are localized and internal portions of the cables or components of higher modes of the individual cables are involved. Frequencies in this range are also strongly influenced by a diminution of the modal mass, associated with a reduction in the size of the contributing components.

Figure 88 also suggests a methodology for evaluating or comparing the efficiency of a system. The rate of change of this function might represent a measure of the system behavior for the first and non-localized modes, higher values of the slope being related to a significant increment in the associated frequency. Alternatively the extension of the plateau on the mode number axis can be seen as an equivalent way of identification; broad almost-horizontal regions should be

avoided since they correspond to a large number of local modes, which may be difficult to control (for example through dampers). The height of the plateau with respect to the frequency axis can also be considered as a means of assessing the performance of the system, this being a metric of the separation between the fundamental modes and the local ones.

Summary:

Limited study of in-plane vibrations of complex cable networks has usually been performed by means of finite element methods due to the number of cable elements that are involved and the variability of the global characteristics of the system, also connected to local variations in the cross-tied configuration. An alternative methodology for the analytical derivation of the equation of motion (free-vibration problem) of a network, based on the taut-cable theory has been extended and applied to the study of a real case. The central and side span configurations of the Fred Hartman Bridge were considered; a sensitivity analysis of the modal characteristics and frequencies, based on a set of modifications to the original design, contributed to the formulation of some preliminary general criteria to be considered for the optimization of this type of systems. Advantages and limitations with respect to finite-element simulations are evident.

This approach showed some clear advantages with respect to the finite element simulations, not only because a direct link with the mechanics of the phenomenon can be always referred to the characteristics of the basic solutions, but also because the behavior of a very complex system can be represented through a simple but efficient characterization, very useful in design or subsequent mitigation analyses. The identification of global and local network modes was also possible, suggesting that the control of this category of structures can become very challenging at higher frequencies due to the nature of the modes that are involved. The general frequency increment in the fundamental modes that is usually attained by the introduction of transverse connectors must be balanced with the potential undesirable behavior of the local modes. This aspect might potentially reduce the overall benefit of enhancing the performance of individual stay behavior by a network.

Design Considerations:

From the analysis of the previous cases a set of considerations for the improvement of the response of a cable network can be proposed.

The sequence of global modes and intermediate localized modes is responsible for typical behavior with consecutive steps or plateau. A first suggestion is to keep the location of the first plateau as high as possible, distant from the fundamental modes, in order that the antisymmetric individual-cable modes (2nd mode) that mostly contribute to the network modal shape are those of the shorter cables. Symmetric configurations of the restrainers with respect to intermediate-length cables is preferred to increase the frequency interval (lower limit in particular) corresponding to local modes, since they minimize the longest segment length.

Relative stiffness of the transverse restrainers does not seem to play a significant role in the definition of the modal characteristics; on the contrary the frequency ratio among different stays f_j, related to the reference cable frequency, seems to be responsible for the network mode sequence. A good compromise between small f_j (shorter stays) and high values (longer stays) is preferred for the optimization of the system. Unfortunately this aspect is not connected to the cross-tied configuration but to the existing setup of the bridge.

A cable network cannot be designed to withstand all possible excitations; the best thing that can be done is to select some sources of vibrations and "tune" the network not to respond to them, since the behavior becomes complex due to the presence of the plateau; localized modes are practically unmanageable since they mainly concern internal elements of the system, although in these cases the vibration is confined to a selected portion of the structure and the potential implications for long-term structural sensitivity (fatigue damage) are less relevant.

A network combined with additional mechanical dampers, connected to the deck at specific locations, might be seen as an efficient way of vibration reduction. The presence of pseudo-symmetric behavior should be carefully assessed: it generates "non-dampable" modes (half of the structure is at rest). This behavior is enhanced by the presence of ground connectors. It might be possible to use a ground-restrainer in the proximity of the shortest cable, close to the tower in combination with dampers on the segments on the right side of the longest cables closest to the deck. In fact the first pseudo-symmetric modes, in this model, are those related to the unconstrained regions of the network and the presence of a damper in this position might become efficient. This opportunity must be balanced with the fact that, when the addition of these devices is necessary, the high inclination of the short cables might make them difficult to install.

Finally the optimal design of a network should be based not only on structural performance considerations but also on cost previsions (installation, maintenance). In this way the preferred solution should be suggested perhaps through a more extended optimization technique.

C2.4 DAMPERS IN COMBINATION WITH CROSS-TIES

The method outlined above can also be extended to a cable network in which the secondary restrainers, originally simulated through linear spring elements, can be combined with discrete dampers placed in the system as an additional measure for the reduction of the oscillations. The procedure is also based on results on the problem of performance improvement for a vibrating cable by adding a transverse damper (Main and Jones, 2002a). The combination of cross ties with dampers is not usually considered in the literature and only marginally addressed in the design for this type of structure, even though the opportunity of a larger overall benefit linked to a "coupled" behavior might be present with few modifications to the undamped configuration.

Problem Formulation

Elements of the more general problem formulation are depicted in Figure 89. The example shows a cable network configuration, simulated by a set of parallel cables, interconnected by means of appropriate restrainers, on occasion extended to ground.

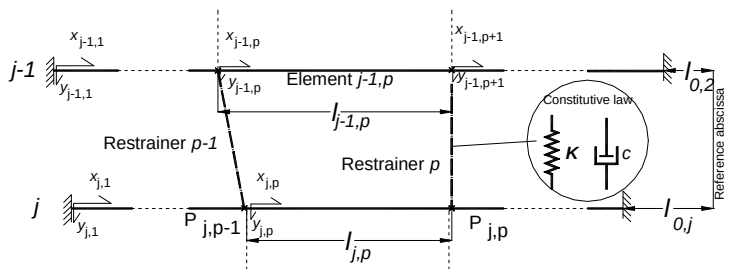

Figure 89: Generalized cable network configuration.

The constitutive law for these connectors can be simulated by linear springs or a viscous damping model. The generic j-th cable (j=1,…,n) is divided into m_j segments (with j variable for each cable) due to the presence of the transverse cross-ties. The j-th cable is restrained at both ends. The geometric and physical characteristics of the j-th cable are indicated as: length L_j, tension H_j and mass per unit length μ_j. The free-vibration problem can be solved through a system of partial differential equations, corresponding to each cable segment,

$$H_j \frac{\partial^2 y_{jp}}{\partial x_{jp}^2} = \mu_j \frac{\partial^2 y_{jp}}{\partial t^2}. \tag{54}$$

The x_{jp} along-axis coordinate of the p-th segment of the j-th cable (with j=1,…,n; p=1,…,m_j) has been taken in accordance with Figure 89; transverse displacements, $y_{jp}(x_{jp},t)$, where t denotes the time variable, are considered positive downwards. The motion of each element can be postulated as $y_{jp}(x_{jp},t) = \mathrm{Re}[Y_{jp}(x_{jp})e^{i\omega t}]$, where ω is the complex frequency of vibration of the coupled network to allow for the presence of localized damping in the structure. Equation 54 can be therefore reduced to a system of ordinary differential equations,

$$H_j \frac{d^2 Y_{jp}}{dx_{jp}^2} + \mu_j \omega^2 Y_{jp} = 0 \cdot \tag{55}$$

A solution of the form

$$Y_{j,p}(x_{j,p}) = A_{j,p}\sin\left(\frac{\gamma\pi}{L_j} f_j x_{j,p}\right) + B_{j,p}\cos\left(\frac{\gamma\pi}{L_j} f_j x_{j,p}\right) \tag{56}$$

can be proposed, which can be expressed for each segment, in terms of complex trigonometric functions and by selecting a reference cable (upper; $j=1$) with natural frequency (real) $\omega_{01} = \frac{\pi}{L_1}\sqrt{H_1/\mu_1}$ and a normalized complex frequency $\gamma = \alpha + i\beta$, with $i = \sqrt{-1}$, such that $\omega = \gamma\omega_{01}$.

The term $f_j = \omega_{01}/\omega_{0j}$ corresponds to the generic j-th cable frequency ratio and $\nu_j = \sqrt{(\mu_j/\mu_1)(H_j/H_1)}$ to a mass-tension reduction factor. The length of the p-th segment of the j-th cable, the limits of which are defined by the nodes $P_{j;p-1}$ and $P_{j;p}$, is denoted as $l_{j,p}$; accordingly, a dimensionless length with respect to the total extension of the j-th stay can be taken as $\xi_{j,p} = l_{j,p}/L_j$. Equation 56 can be solved in terms of the unknown amplitudes A_{jp}, B_{jp}, by means of a set of compatibility, continuity and equilibrium equations that are related to the constitutive law that is assigned to the restrainer (linear spring or viscously damped element), leading to a homogeneous system of $2r = 2\sum m_j$ equations (Caracoglia and Jones, 2002a). This set can be rewritten in a more compact matrix form as $S\Phi = 0$ (algebraic system of nonlinear equations), where the vector Φ contains the unknown A_{jp}, B_{jp}. The infinite set of nontrivial solutions ($\Phi \neq 0$), associated with the condition det[S] = 0, can be solved for the normalized frequency γ, as an equivalent eigenvalue/eigenvector problem (in general complex); a numerical technique is required for all but simple systems. Details are omitted for brevity in this study.

Basic Solutions:

The investigation of basic solutions that are concerned with a reduced number of cables is very useful in the understanding of the mechanics of the problem. As part of this analysis a collection of relevant examples can be constructed, both to identify the physical behavior and to reveal any interesting characteristics that can be also identified not only in a simple structure but in a more generalized $2r \times 2r$ system. The study of these simple examples therefore represents a useful support to the analysis of multi-stayed networks.

In particular in this section this method is applied to the study of a symmetric twin cable arrangement, in which the natural frequencies of the two isolated cables, are coincident ($\omega_{01} = \omega_{02}$), and H, L, μ are constant. The additional independent variable is represented by the normalized connector location $\xi = 1/L$, where $0 \leq \xi \leq 1$ (Figure 90).

In these cases the characteristic polynomial can be analytically derived and, subsequently, the mode. Two examples were analyzed: in the first one (a) the restrainer was simulated by means of a linear spring of stiffness K; in the second one (b) this type of connection was replaced by a dash-pot, characterized by a perfectly viscous behavior with damper coefficient c. In both cases the solution can be expressed as a function of the non-dimensional location ξ and the physical

properties of the transverse element. The solution is associated in both cases with a transcendental equation that needs to be numerically solved.

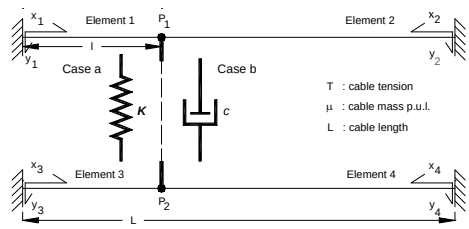

Figure 90: Twin cable with variable position connector.

For the linear spring model the frequency is real ($\gamma = \alpha$) and the modal eigen-functions turn out to be strictly trigonometric. This quantity can be related to a normalized stiffness parameter, $d_K = H/(KL)$. The limit $d_K \to \infty$ represents the case in which the stiffness of the connection is zero, i.e., a completely disconnected system, while $d_K = 0$ is related to the case of a perfectly rigid bar. In Figure 91a the typical behavior of the real solution for the modal frequency is depicted for the first "pseudo-symmetric" mode, as a function of ξ and d_K. The connector is in fact responsible for the presence of such modes with localized form, along with the symmetric and anti-symmetric solutions of the individual case, in which no frequency variation is recorded ($\alpha = 1,2,...N$). Similar contour plots can be also generated for the higher modes. Moreover it can be seen that, as d_K tends to 0, approaching the rigid case, the frequency follows a typical hyperbolic law $\gamma \equiv \alpha = 1/(1-\xi)$, corresponding to a modal form in which nodes P_1, P_2 and elements 1,3 (Figure 90) are at rest while segments 2 and 4 are vibrating out of phase with wavelength $L - l$ (Figure 91c).

For the dash-pot model the polynomial, the roots of which are associated with the frequency $\gamma = \alpha + i\beta$, is complex. The numerical technique develops this polynomial into a system of two equations corresponding to real and imaginary part, which need to simultaneously vanish. This example presents clear similarities with the concepts of single-degree-of-freedom damped oscillator, as equivalently derived by Main and Jones (2002a) for the single cable with dash-pot to ground. The generic γ_k can be expressed as a combination of an oscillatory decaying solution with frequency $\omega_k = \omega_{0k}\sqrt{1-\eta_k^2} = |\gamma_k|\omega_{01}$ and damping ratio η_k. A critical value of damping can be defined in terms of the dimensionless damping parameter $\rho = c/\sqrt{H\mu}$. In Figure 91b the typical solution curves in α, β (or ω_k, η_k) for the analyzed example are depicted: a restricted set of values for the α, β pair can be found, as ρ varies from 0 to infinity, corresponding to the two perfectly oscillatory cases with no damping in the absence of the connector ($\rho \to 0$, $\gamma \equiv \alpha = 1,2,k,...,N$) and the perfectly rigid restrainer of Figure 91c ($\rho \to \infty$; diamond symbol in Figure 91b) with pseudo-symmetric modes with $\gamma \equiv \alpha = k/(1-\xi), k/\xi$. The evolution of the solutions between these limits can also be seen for modes 1 to 5.

Differences can be seen (Figure 91b) between mode 2, which reflects this aspect, and mode 1 as ($\eta \to 1$).

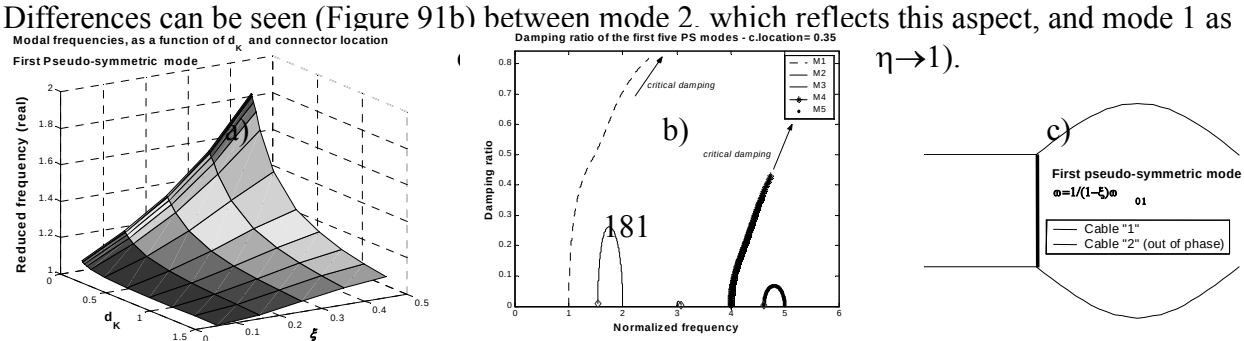

Figure 91a: Twin cable system, with connector location ξ = 0.35, example of frequency solution for linear spring model.
Figure 91b: Typical solution curves of the complex frequency for the dash-pot.
Figure 91c: Intermediate segments of specific cables only.

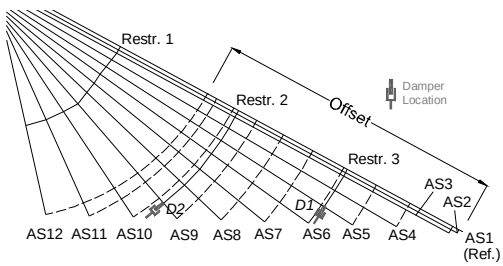

Figure 92a: Fred Hartman Bridge ("A-line") 3D network.

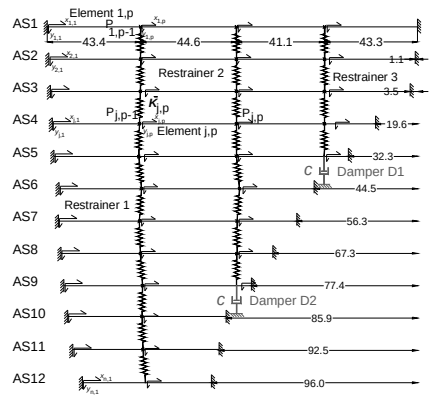

Figure 92b: Equivalent model.

The collection of behavioral observations from these (and other not reported here) simplified examples will be applied and compared in the next section to the study of a real example of cable network.

Cable Network Analysis In The Presence Of Discrete Dampers:

In this section, a modification to the "A-line" original system described earlier considers the addition of dampers in specific locations of the structure, as depicted in Figure 92. Dampers *D1* and *D2*, directly connected to the deck, are introduced at the location of restrainers 3 and 2, respectively. The first results of this investigation are presented in Figure 93a, which shows the behavior of the fundamental global mode (1) in terms of the evolution of (ω_k, η_k) as a function of the dimensionless damping parameter ρ.

In the first example (thin line of Figure 93a) the influence of only damper *D1* was investigated. A behavior very similar to the basic solutions can be observed. The solution emanates from the real frequency coincident with the solution with zero damping, denoted by "M1[uu]" in the figure, reaches a maximum value of optimal damping ("M1[uo]") and then decreases, tending to the purely oscillatory case of a fixed connection to ground ("M1[ru]").

In the second case, the addition of damper *D2* was considered as a function of a the damping parameter ρ_{D2}; moreover it was assumed that *D1* was optimally designed for the first mode per the previous example, with $\rho_{D1}^{opt} = 6.25$, corresponding to a damper coefficient c_{D1} approximately equal to 131 kN-s/m (about 9000 lbf-s/ft).

The thick line of Figure 93a shows the solution evolution for this new configuration. The ω,η pair originates from the point corresponding to the case with only damper *D1* active (optimized system "M1[uo]" – circle symbol), and subsequently increases (as ρ_{D2} progressively grows) towards a new maximum value related to the introduction of this second device. The solution partially deviates from the basic behavior, despite the presence of a similar trend, since it does not converge to a perfectly oscillatory solution as $\rho_{D2} \to \infty$ ("M1[rr]"), due to the presence of *D1*, although the difference is not evident in the figure. In addition, the location of *D2* (mid-span) is clearly more efficient, at least for the fundamental network mode; in fact the recorded peak value of the damping ratio is considerably larger than the previous case, and the device that seems necessary requires a relatively low c_{D2} (about 11800 lbf-s/ft, or 172 kN-s/m).

Figure 93b shows, as an example, the complex eigen-function associated with the first mode of the optimized system "M1[uo]" ($\rho_{D1}^{opt} = 6.25$); real and imaginary parts are separately plotted to highlight the presence of in-phase and out-of-phase components. It is worth observing that the effective mode shape of the system corresponds to a combination of these two functions.

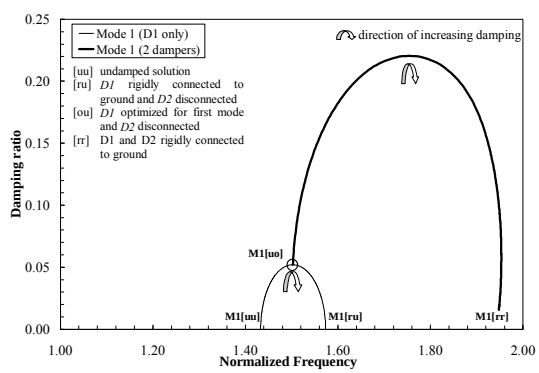

Figure 93a: Frequency solutions (1st mode) for the damped cable network ("A"-line).

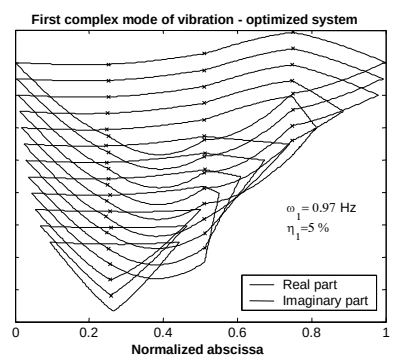

Figure 93b: Complex modal form (1st mode) for the optimized system "M1[uo]".

Comments:

The introduction of dampers at specific locations of the network was analyzed. Results suggest a potentially wide range of practical applications, related to design and post-erection mitigation analyses. In particular, the combined role of dampers and cross-ties seems promising. Future enhancements will include the study of the role of dampers in cable networks for higher and localized modes and the effect of cross-tie mass on the system.

C2.5 FIELD ASSESSMENT OF DAMPER AND CROSS-TIE PERFORMANCE

To suppress problematic vibrations in stay cables, dampers are often attached to stay cables near the anchorages to supplement the low levels of inherent damping. Dampers can potentially be attached unobtrusively near the stay anchorage at the deck or tower, and thus detract minimally from the aesthetics of the structure. While multiple types of excitation are likely to be encountered in the field, and although the mechanisms that induce the observed vibrations are still not fully understood, attached dampers render stay cables less susceptible to many types of excitation by increasing the low levels of inherent mechanical damping. For these reasons, dampers have had relatively widespread use, and their effectiveness in mitigating stay-cable vibrations is now fairly widely accepted. However, criteria for damper design are not well established. Current recommendations for required damping levels to suppress rain-wind vibrations were developed using simplified wind-tunnel models (Irwin, 1997), and it is not clear whether these guidelines are adequate or appropriate for vibration suppression in the field. In addition, it is important to note that vibrations can occur in more than one mode of the cable, and little has been done to address the question of how much damping should be provided in each mode.

In order to evaluate damper effectiveness and facilitate the design of even more effective and economical systems, it is important to perform a quantitative assessment of damper performance under various types of excitation. Toward this end, this investigation seeks to evaluate the effectiveness of passive linear dampers installed on two stays on a cable-stayed bridge in the United States by comparing response statistics before and after the damper installation and by investigating in detail the damper performance in a few selected records corresponding to different types of excitation. To provide background for this evaluation, a summary is presented of measured vibration characteristics before the damper installation. Recent developments are discussed in the modeling of a taut cable with attached damper and the determination of modal damping ratios and damping-induced frequency shifts, and some limitations in the performance of linear dampers are discussed. Other types of damping devices, including semiactive dampers (Johnson et al., 1999) and friction dampers (Kovacs et al., 1999), have been previously investigated in attempts to achieve improved damping performance over the linear damper.

Performance of Linear Dampers

Viscous dampers have been installed for evaluation on two stays on the Fred Hartman Bridge, and at the time of writing, data have been collected for almost three years after the damper installation to evaluate the damper performance. Properties of the two stays on which evaluation dampers have been installed are given in detail in Main and Jones (2001).

The dampers under investigation were designed for optimal performance in the fundamental mode of vibration which – according to the Scruton criterion mentioned above – should provide adequate damping in the first several modes to suppress wind-rain vibration (i.e., approximately more than 0.5%). Figure 94 shows the damping ratios for both stays in each of the first 10 modes of vibration, computed from numerical solution of the eigenvalue equation. Curves corresponding to the damping ratios predicted by the asymptotic expression for the universal

curve are also plotted with these values. As discussed in (Main & Jones 2002a), the error in the predictions of the universal curve are most significant near the optimal portion of the curve, and it is evident here that the asymptotic approximate value differs most significantly from the exact value in mode 1, for which the damper is nearly optimal. This error near the optimal portion of the curve becomes more significant in the higher modes, but because the damper is far from optimal in the higher modes in these cases, the universal curve gives quite good predictions of the damping ratios in these modes.

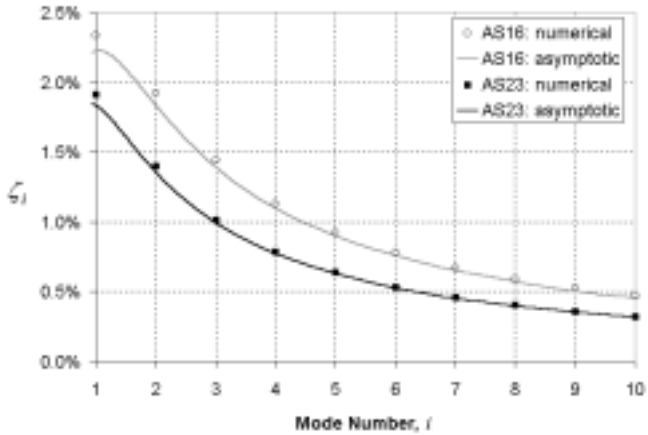

Figure 94: Damping vs. mode number for Hartman stays A16 and A23

In the figures included herein, wind speed reported is at deck level and is computed according to the following priority scheme. Data from the tower-top are given priority, because the tower-top anemometer is not influenced by interference from the bridge deck. The deck-level anemometers were found to be well correlated with the tower-top anemometer except for winds from the west, where interference from the bridge deck reduces the measured velocities at deck-level. Consequently, data from the deck-level anemometers are used only when data from the tower top are unavailable, and then only in the range of wind direction where the correlation with the tower-top anemometer is good. In every case, deck-level wind speeds are presented, and in cases where data from the tower-top anemometer are used, these values are scaled down to deck-level using a scale factor generated from a linear regression analysis of the deck-level and tower-top data (approximately 0.66). Wind direction is measured in degrees clockwise from the bridge axis, with zero degrees corresponding to wind approximately from the north, directly along the bridge axis.

Acceleration data are reported from transducers installed on the stays usually about 6 m vertically above deck level. In some analyses, these data are reported in terms of peak modal amplitude, with adjustment for location included. For the purposes of this investigation and for the data reported herein, the accelerations are reported at the transducer location.

Global Damper Performance:

The global performance of the dampers installed on stays A16 and A23 is summarized in Figures 95 and 96, respectively, which illustrate the following

- Characterization of oscillations (in-plane) occurring before installation of the damper as a function of wind speed and direction.
- Characterization of oscillations (in-plane) occurring after the installation of the damper as a function of wind speed and direction.
- Measurement of damper force as a function of wind speed and direction.

Before the damper is installed, both stays show similar characteristics, and patterns that are consistent with other field and wind tunnel observations that are described earlier. A high density of points is seen near the abscissa, which generally corresponds to vortex-induced vibration in a variety of modes and low-level buffeting response of the stay to random excitations. Both figures clearly indicate the characteristic signature of wind-rain oscillation as the multiple points over a wide range of wind speeds that are of high amplitude i.e., root-mean-square (RMS) accelerations greater than 0.5g. One-minute mean wind speeds at deck level reached 15 m/s before the dampers were installed, and almost 18 m/s in the period after installation. This latter value corresponds to a one-minute average wind speed of 27 m/s (60 mph) at the top of the tower, recorded during a thunderstorm. The dependence on wind direction is also clear, with A16 showing its peak responses between 90 deg and 160 deg, and A23 over a narrower range between 90 deg and 135 deg. The primary goal of a mitigation system is to reduce significantly or eliminate these large-amplitude events, while respecting the fact that the stays and bridge form dynamic systems and will always exhibit some level of dynamic response.

The corresponding figures after the installation of the dampers are also presented. These figures suggest the following:

- Amplitudes are significantly reduced across all recorded wind speeds (up to 18 m/s at deck level) with maximum RMS acceleration amplitudes of around 0.5g.
- The dependence on wind direction has been altered significantly, with the previously preferred range now largely unapparent, and the largest of the responses now nearer to a 90 deg angle of incidence. The characteristics of selected records corresponding to these locations will be discussed in more detail later.
- The third pair of figures shows the RMS damper force measured in kN for the two installed devices as a function again of wind speed and direction. Clearly, the dampers are functioning and providing dissipative force to the stays as intended.

For stay A16, the pattern of forces resembles closely the pre-damper acceleration figures (both in terms of wind speed and direction), suggesting that the dampers are being engaged by the stays to suppress proclivity towards wind-rain vibration. Indeed, relatively high-magnitude forces are seen in the complementary range of 225 deg to 270 deg, which represent wind directions also corresponding to the declining direction of the stay (but now from the southwest rather than southeast.)

For stay A23, the behavior is similar, though perhaps not as clear as in the previous case. Much of the high force data for this stay is now clustered around and incident angle of 90

deg, although some up to 110 deg are evident. An interesting and unusual cluster of points labeled as "Record C" is discussed in Main and Jones (2001). Note that in all the records, the highest amplitude RMS force recorded is approximately 5.6kN (1125lb) – a relatively modest level of load.

More detailed comparisons and discussion can be found in Section 2.6 and Main and Jones (2001).

Recent and ongoing analyses suggest the evaluation of the damper performance is indeed more complex than the simple assessment outlined above. The presence of a significant static frictional component in the dampers, coupled with their design for mode 1 results in very stiff systems. While the dampers are still clearly effective, interpretation of why they are effective is more complicated than originally thought.

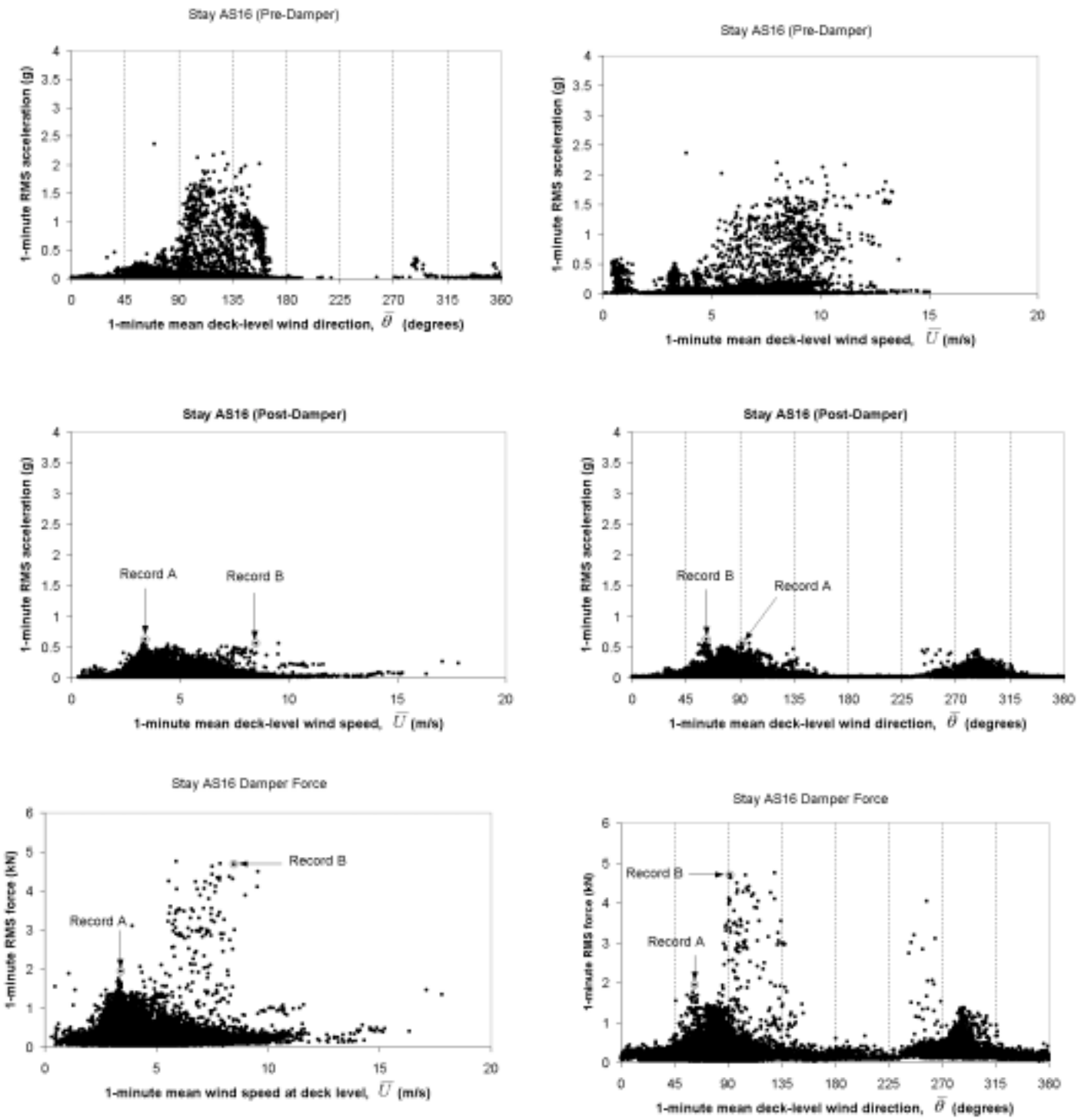

Figure 95: Stay vibration and damper force characteristics; Stay A16.

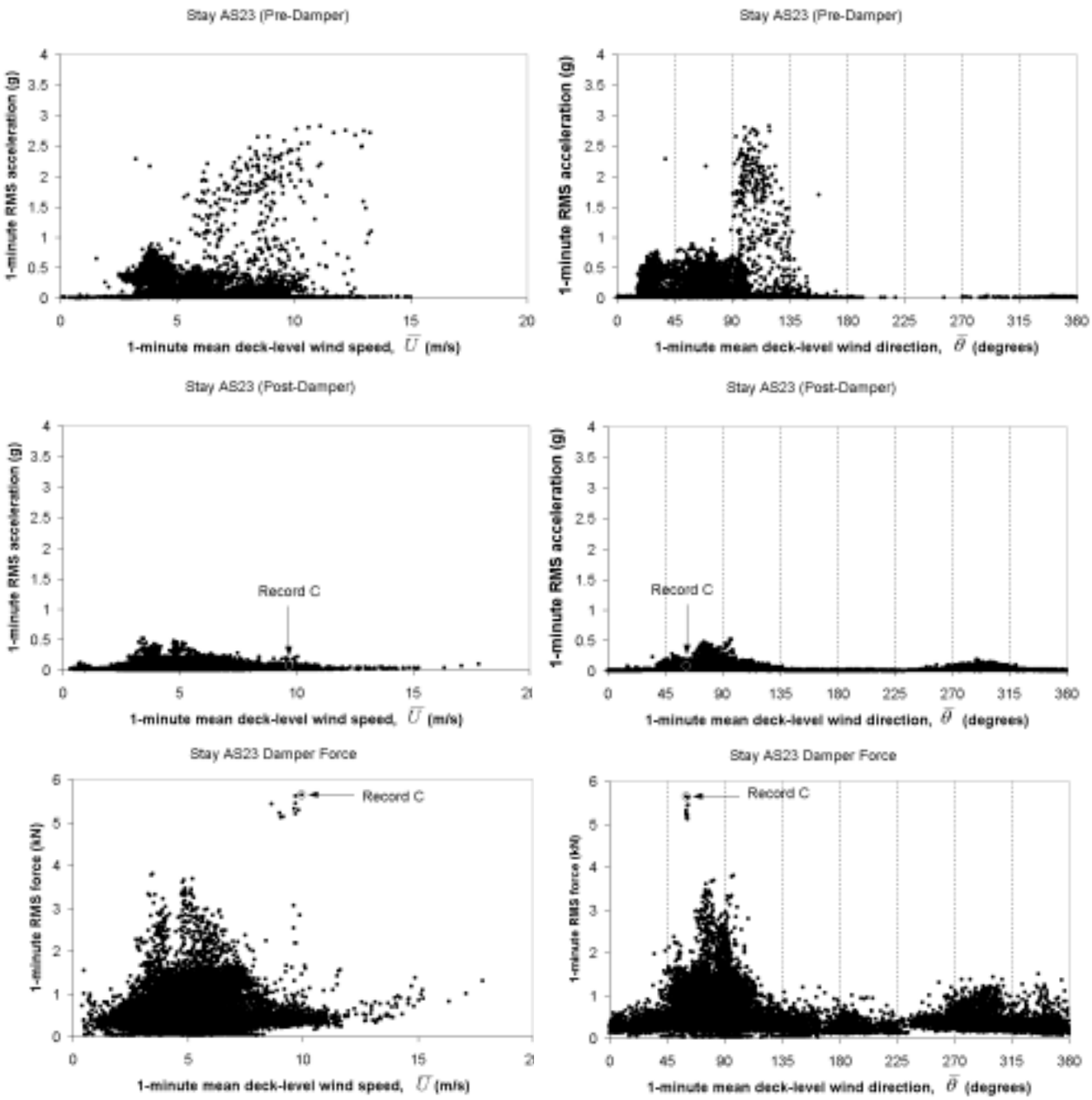

Figure 96: Stay vibration and damper force characteristics; Stay A23.

Performance of Cross-ties

The validation of the analysis approach for cross-tied systems was performed by the comparison of a specific study example with a set of experimental data. A long-term ambient vibration survey is currently in progress on the Harman Bridge to monitor stay-cable vibration and to better understand the overall performance of the structure and its modal characteristics. More than ten thousand trigger files have been recorded during a period of three years.

The methodology was applied to the study of the side-span unit of the south tower of the bridge. The cable network is configured by means of three transverse restrainers, similar to those presented earlier. The data set was extracted from the records of four in-plane and out-of-plane accelerometers, placed along stays AS1, AS3, AS5 and AS9 at a height of approximately 7m from the deck level. The correspondence between the predicted modal characteristics and the real behavior was carried out by simultaneous spectral analysis of the in-plane acceleration record database of the four locations. The analysis was founded on the simultaneous identification of the same dominant in-plane frequency on all the four investigated cables. More than 2000 trigger files from the years 2000 and 2001 have been considered (after the installation of the restrainers). An algorithm was designed for the automatic processing of the records.

The investigation considered the presence of cable network behavior along with individual cable and, eventually, global (deck) structure modes. The fundamental frequencies of each stay were identified in a previous experimental campaign and were adopted as input data in the numerical procedure to allow for a consistent comparison of the results with the real situation.

The numerical analysis was performed by using as reference the measured frequency values of Table 15, after comparison with the current data set available on the four stays, such as the acceleration time histories associated with the out-of-plane unrestrained vibration of the cables. Other physical characteristics that are required by the procedure were indirectly deduced. The results of the simulation are summarized in Table 16, in which the modal frequencies of the modes between 0 and 4 Hz are indicated. In addition the subdivision into global and local network modes is indicated along with information about the general characteristics of the modal shape.

The fundamental frequency (NM1) is 0.93 Hz, slightly lower than that deduced for the central span arrangement; a different network configuration of the cables and connectors in the latter case is probably the cause of these differences. An interesting observation is that the computed frequency of NM1 is close to the 10th bending mode of the bridge (0.924 Hz), which suggests, in theory, a potential susceptibility to interaction of the deck-stay system in this range. Low-density values of frequency can be seen up to 2.4 Hz (NM5) and beyond 3 Hz (NM30). The plateau behavior was detected between 2.4 and 3.0 Hz, associated the local behavior and a high density of solutions (NM5-NM29).

Table 15: Individual cable frequencies (0-4 Hz) of the A-line side span stays of the Fred Hartman Bridge (direct measurement).

Stay	Mode n. 1 (*)	2	3	4	5	6
AS1	0.646	1.2920	1.9380	2.5840	3.2300	3.876
AS2	0.687	1.374	2.061	2.748	3.435	4.122
AS3	0.655	1.310	1.965	2.620	3.275	3.930
AS4	0.720	1.440	2.160	2.880	3.600	4.320
AS5	0.810	1.620	2.430	3.240	4.050	4.860
AS6	0.864	1.728	2.592	3.456	4.320	5.184
AS7	1.032	2.064	3.096	4.128	5.160	6.192
AS8	1.104	2.208	3.312	4.416	5.520	6.624
AS9	1.255	2.510	3.765	5.020	6.275	7.530
AS10	1.355	2.710	4.065	5.420	6.775	8.130
AS11	1.794	3.588	5.382	7.176	8.970	10.764
AS12	1.700	3.400	5.100	6.800	8.500	10.200

(*) Derived from previous direct measurement

= Monitored stays in this study

Table 16: Cable network modes (0-4 Hz) predicted by the model (A-line system).

Mode N.	NM1	NM2	NM3	NM4	NM5	NM6	NM7	NM8	NM9	NM10	NM11	NM12	NM13	NM14	NM15	NM16	NM17	NM18
Frequency [Hz]	0.926	1.458	2.043	2.332	2.368	2.406	2.430	2.448	2.467	2.472	2.500	2.556	2.582	2.600	2.631	2.644	2.662	2.677
Mode type	G-S	G-AS	G-S	L	L	L	L	L	L	L	L	L	L	L	L	L	L	L

Mode N.	NM19	NM20	NM21	NM22	NM23	NM24	NM25	NM26	NM27	NM28	NM29	NM30	NM31	NM32	NM33	NM34	NM35	NM36
Frequency [Hz]	2.689	2.697	2.720	2.747	2.765	2.797	2.819	2.862	2.956	2.994	3.018	3.217	3.347	3.417	3.456	3.689	3.948	4.077
Mode type	L	L	L	L	L	L	L	L	L	L	L	G-S	G-S	G-S	L	G-AS	L	L

G = Global Network mode; L= Local Network mode; S = symmetric; AS = antisymmetic

The experimental identification of network modes of Table 16 in the records of AS1, AS3, AS5 and AS9 was restricted to a subset of "visible" components in accordance with the location of the accelerometers, since predicted local modes that are concentrated in the central and upper portion of the system could not be physically detected. The power spectral densities of the four in-plane accelerations of AS1, AS3, AS5 and AS9 have been compared to the predicted values of the network.

The results of the data analysis showed consistent similarities with the predictions, also indicating the potential presence of some of the "new" modal forms in frequency ranges in which modal characteristics from other sources (individual stays, global structure, etc.) were often excluded.

NM1, as network mode, was clearly identified in one occasion only for a continuous time interval of about fifteen minutes, corresponding to an extremely rare occurrence in terms of ambient-induced vibration. This event was mainly driven by the high-amplitude motion of the deck due to vortex shedding and related to a strong wind with direction almost perpendicular to the bridge axis.

Simultaneous peak amplitudes in the acceleration spectra from the stays were found in a significant number of realizations that corresponded to the simulated frequencies of the second global antisymmetric mode (NM2, 1.46 Hz) and higher global symmetric modes (NM30-31, 3.2 Hz). Clear indication of the potential development of local network modes rather than individual stay oscillation was also detected in frequency intervals predicted by the model.

More figures and details of the comparison are included in Caracoglia and Jones (2002b).

It is noted that recent investigation of recorded data suggests instances of relative large-amplitude oscillation for the stays when the wind is parallel to the deck. The cross ties were ineffective at damping these oscillations, whereas the dampers seemed to be quite successful. It is anticipated that these large amplitude oscillations are due to a form of wake galloping. The analysis of these records is in progress and will be reported as soon as it is complete. The implication of this discovery for cross tie systems is important, however.

C2.6 DETAILED STUDY OF DAMPER PERFORMANCE

Despite the demonstrated effectiveness, the design of passive dampers still remains semi-empirical. An efficient and reliable way to estimate the inherent damping in the cables is still not available. The traditional logarithmic decrement method has so far been the most widely adopted for this task. But the effectiveness of this method is limited, because the highly vibration-amplitude dependent nature and some other existing but not clearly understood nonlinearities of the inherent damping in cables cannot be readily handled by this approach. In addition, vibrations can occur in more than one mode of the cables, and understanding of modal inherent damping is essential for damper design. But it is difficult to force the cables to vibrate at desired amplitude in the modes with relatively high (say, >2 Hz) or low (say, <0.5 Hz) frequencies. This fact also limits the number of modes the logarithmic decrement method can handle. Application of other traditional methods such as the "half-power-bandwidth-method" and the more recent "random decrement method" are also likely to have limited success because of their respective limitations.

Analytical work by Yamaguchi and Jayawardena (1992) suggested that modal damping ratios in stay cables are proportional to the dynamic strain energy in the cables. A theoretical model based on this relation was also established for model damping estimation, but the validity and robustness of this model still needs further investigation and verification. On the other hand, criteria that address how much supplemental damping is needed to suppress the vibrations or how much damping the dampers can provide are still not well established. Current recommendations for required damping levels were developed using simplified wind-tunnel models discussed herein (Irwin, 1997), but despite the advances made in this project and elsewhere in recent years, it is not completely clear weather these guidelines are adequate or appropriate for field implementation. In addition, little has been done to address the problem of how much damping is needed in each mode to mitigate the vibration and for which mode the damper should be optimized.

Although substantial progress has been made in assessing the damping in cables of cable-stayed bridges, understanding from the aforementioned efforts have been focused on theoretical formulation or simplified wind tunnel tests and are yet to be subjected to evaluation. Additional insights from actual cable vibrations in the field are still needed. The primary objective of this sub-effort has been to extract damping information for stay cables, both with and without dampers, using the measured vibration data. Damping ratios identified are analyzed together with the characteristics of cable vibration to evaluate the dependence of inherent damping upon the vibration amplitudes. Results for the cables before and after damper installation have been compared to assess the performance of the dampers under various conditions. Particular attention has also be paid to the important role of rain on the damping of stay cables in attempt to shed some light upon the problem of negative damping.

Additional Characteristics of Vibration

Discussions earlier have been focused on vibrations in the in-plane direction of the cables. But as noted highly two-dimensional vibrations have actually been frequently observed. In some cases, vibrations in the lateral direction have been the more dominant. This fact is evident in Figure 97 which plots the one-minute RMS displacement amplitude in the in-plane direction against that in the lateral direction for stays AS16 and AS23. The records represented were chosen from those collected before the dampers were installed, with RMS displacement amplitude of the in-plane vibration or the lateral vibration greater than 0.5 cm. Points in Figure 97 for cable AS16 formed three distinct clusters, as illustrated, around three lines. Analysis of the modal RMS displacements of the records show that points in cluster A represent in-plane vibrations strongly dominated by the first mode, points in cluster B represent in-plane vibrations strongly dominated by the second mode and points in cluster C represent in-plane vibrations dominated by more than one single mode. No clear clustering of points has been observed for stay AS23 in Figure 97, although the vibrations still appear to be highly two-dimensional.

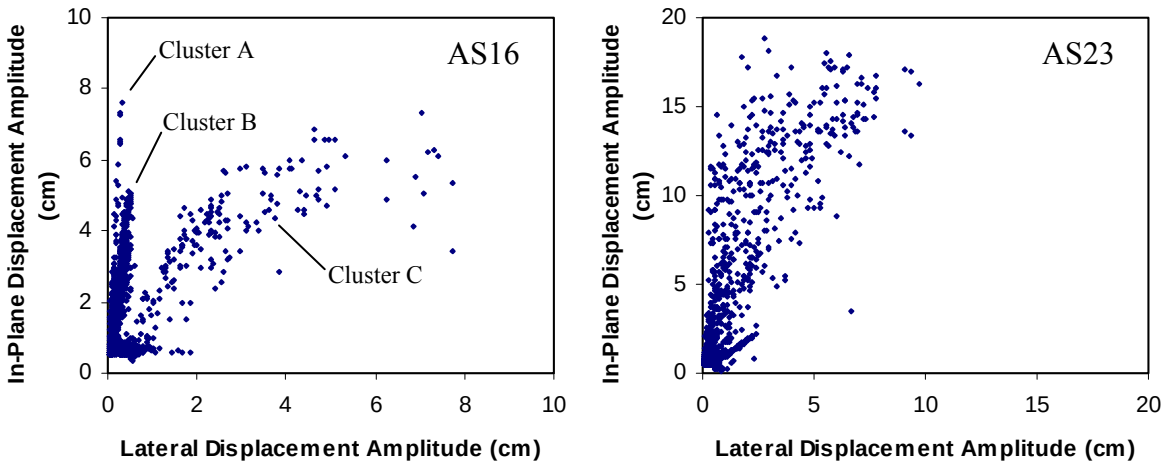

Figure 97: In-plane vs. lateral RMS displacement for AS16 and AS23.

Figure 98 shows sample Lissajous plots (in-plane displacement against lateral displacement) for two different records (1 and 2) from stay AS16. Record 1 is chosen from cluster A in Figure 97 and record 2 is from cluster C. Although the in-plane displacement amplitudes for both records are comparable, the lateral displacement amplitude for record 2 is significantly larger than record 1. Power spectral densities of these two records (Figure 99) show that both in-plane and lateral vibrations of record 1 are dominated by the first mode, but vibrations of record 2 in both directions have significant contribution from all the first three modes. Records in cluster B are found to have similar dimensional and modal contributory properties as records in cluster A.

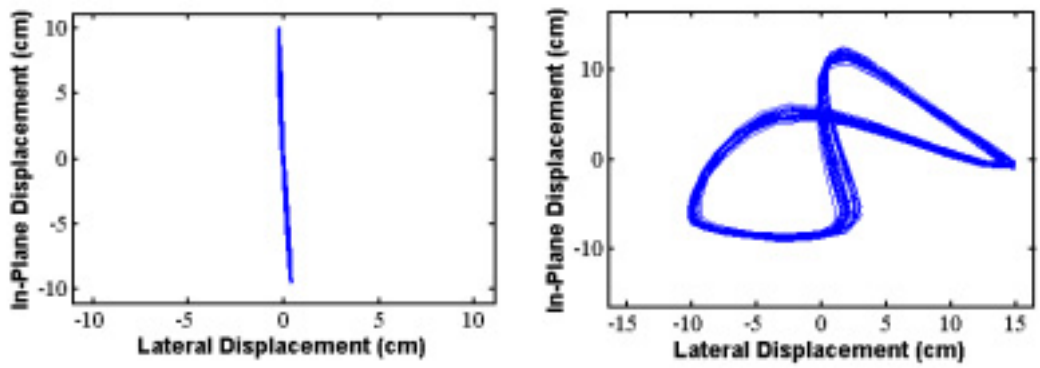

Record 1 from AS16 Record 2 from AS16

Figure 98: Sample Lissajous plots of displacement for two records from AS16.

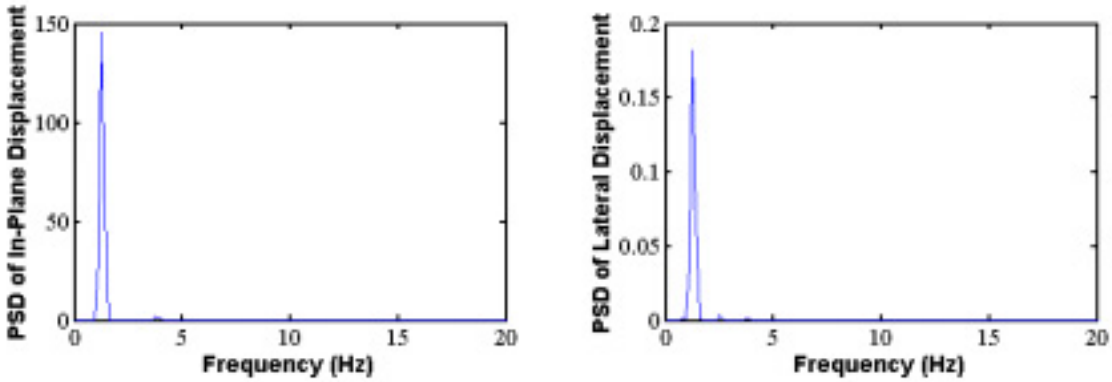

Record 1 from AS16

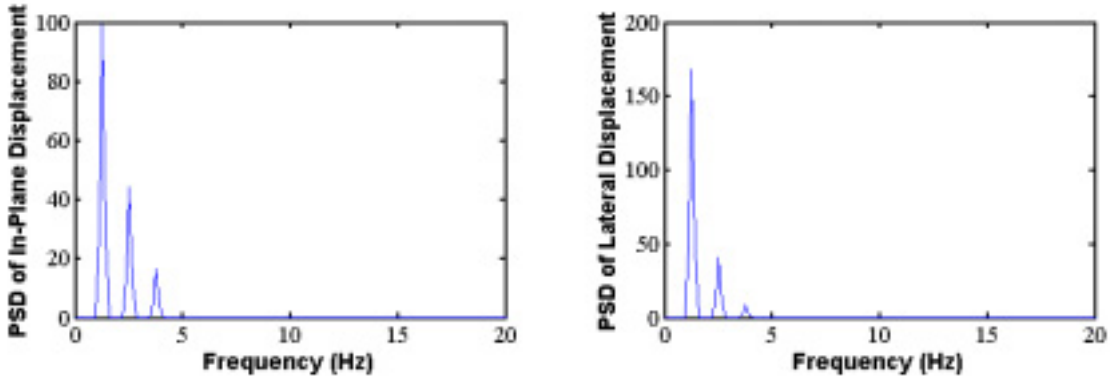

Record 2 from AS16

Figure 99: Power spectral density of displacement of two records from AS16

Similar Lissajous (Figure 100) and power spectral density (Figure 101) plots have been made for two records (1 and 2) from stay AS23. Record 1 has vibration primarily in the in-plane direction, while vibration of record 2 is rather two-dimensional. Figure 101 shows that, unlike in the case of record 2 for AS16, even though the vibration of record 2 for stay AS23 is highly two-dimensional, vibrations in both directions are still both dominated by a single mode (mode 3). While most highly two-dimensional vibrations for stay AS16 have been found to be dominated

by a single mode, most highly two-dimensional vibrations for stay AS23, however, are dominated by multiple modes. This difference in both dimensionality and modal participation of vibrations for the two cables suggests strong dependence of cable vibration on its physical characteristics.

In future analysis, more attention will be directed to detailed investigation of dimensionality, as well as its dependence on modal participation, of stay cable vibrations, in conjunction with collected wind and rain data. This may give further insight into the mechanism of stay cable vibrations and help identify different categories of vibration.

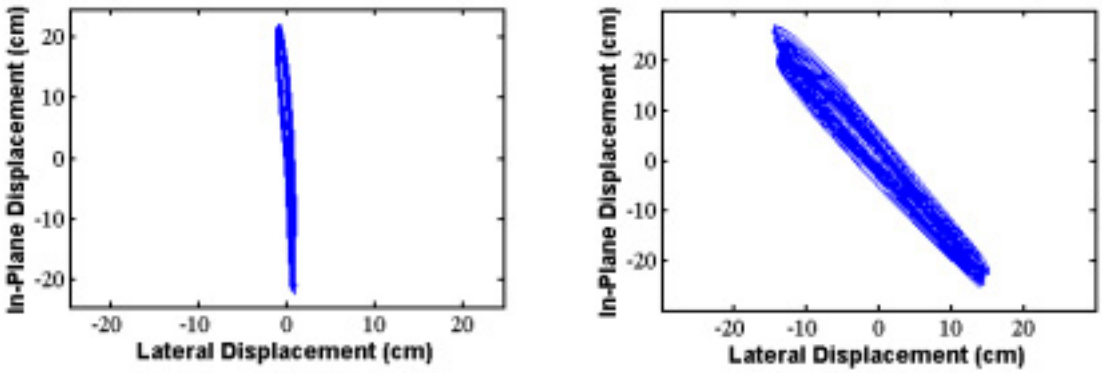

Record 1 from AS23 Record 2 from AS23

Figure 100: Sample Lissajous plots of displacement for two records from AS23.

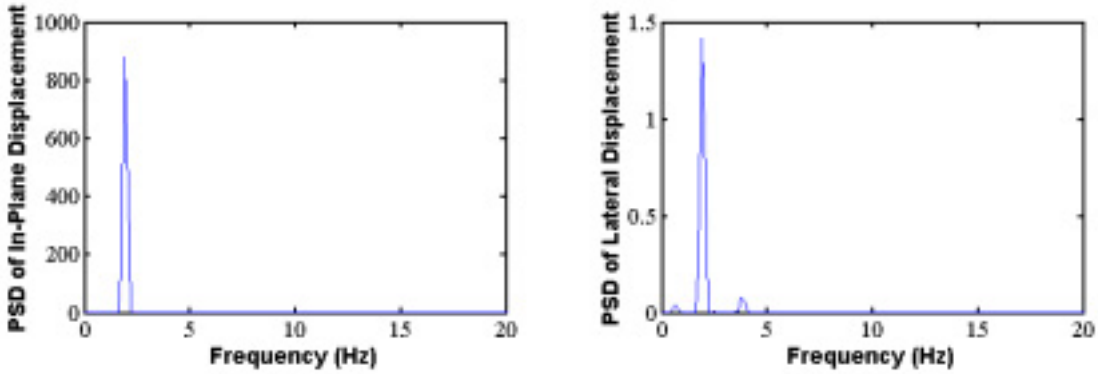

Record 1 from AS23

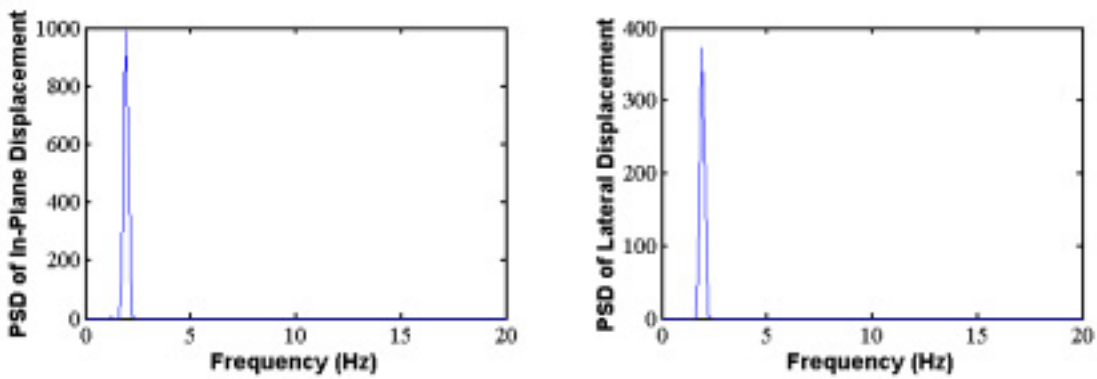

Record 2 from AS23

Figure 101: Power spectral density of displacement of two records from AS23.

Damper Effects on Vibration

Discussion so far has been focused on vibrations of the two cables before dampers were installed. Collected records demonstrate that, except in a very few cases, the dampers on both cables have been effective in mitigating excessive vibrations, despite the difference in the properties and vibration characteristics of the two cables and the fact that the dampers were designed semi-empirically. Figure 102 shows again the one-minute RMS displacement in the in-plane direction against that in the lateral direction for stays AS16 and AS23 collected after the dampers were installed. All records also have RMS displacement amplitude greater than 0.5 cm in either the in-plane direction or the lateral direction. By comparing Figure 102 and Figure 97, it is evident that very few records with RMS displacement amplitude greater than 0.5 cm has been recorded after damper installation and that the amplitude has been mostly kept below 2 cm, except in very rare individual cases. This confirms that the damper has been generally effective in suppressing large-amplitude vibrations.

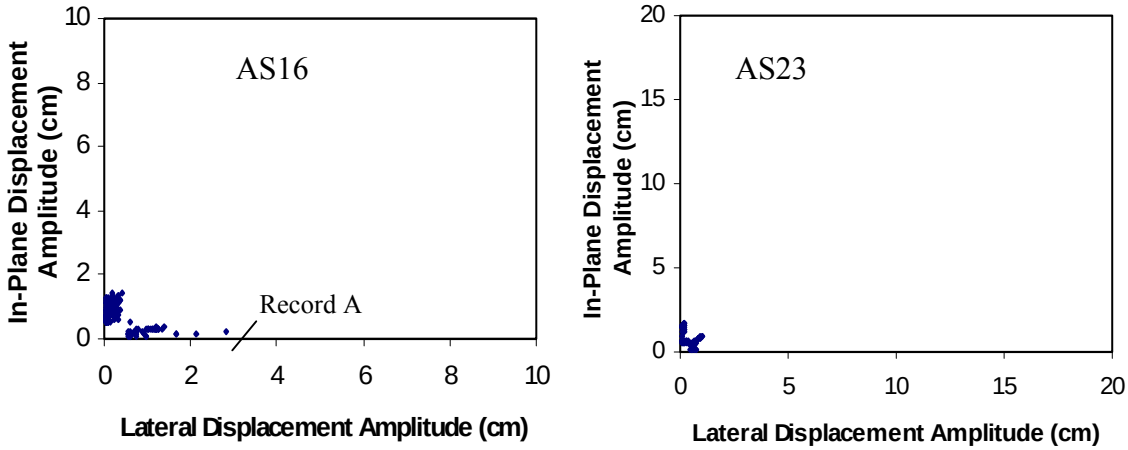

Figure 102: In-plane vs. lateral RMS displacement for AS16 and AS23 after damper installation.

Special attention has been focused on record A and adjacent ones in Figure 102 because, for these records, the RMS displacement amplitude in the lateral direction is quite large but the RMS displacement amplitude in the in-plane direction is rather small. This may indicate that the damper on stay AS16, which is oriented in the in-plane direction, has not been able to suppress vibration in the lateral direction in these special cases. Figure 103 shows the Lissajous and power spectral density plots for record A. It is evident in the figures that, even though the vibration is basically one-dimensional, unlike in the case when the vibration is primarily in the in-plane direction, the lateral displacement of record A has significant contribution from all the first three modes, rather than being dominated by a single mode. This fact suggests that when large vibration is primarily in the lateral direction, its cause and mechanism may be different from the case when the cable vibrates primarily in the in-plane direction. Collected wind data revealed that when vibration in record A occurred, the wind speed is about 12 m/s, which is in the range of wind speed for large-amplitude vibration for stay AS16, but the wind direction is around 350°, which is far away from either 120° or 260° shown in Figure 100 (for Record 2) to be the preferred wind direction for large-amplitude in-plane vibration. In fact, the wind direction in this case is almost parallel to both the bridge axis and the axis of the stay cables. Further analysis revealed that the cables adjacent to AS16 had the same pattern of vibration too, except

stay AS24, which is the first cable to "meet the wind" and had large-amplitude vibration in both directions. Another observation was that the cables on the south side of the same tower, which have opposite inclination direction to AS16, did not have the same pattern of large-amplitude vibration as AS16. Heavy rainfall has been found to accompany the cable vibration. Whether or not it is the rainfall that triggered the vibration of stay AS24, which consequently caused the lateral vibrations on the other cables, still needs further investigation. The vibration occurred on stay AS16 still cannot be positively concluded to be wake galloping. What can be stated here is that this type of vibration may reach quite large amplitude and dampers may not be effective in suppressing it. The same type of vibration has also been found on cables on the south side of the same tower when wind is coming from about 180°, which is also parallel to the bridge axis and in the inclination direction of these cables. The important fact observed is that the cross-ties installed on these cables were also ineffective in mitigating this type of vibration.

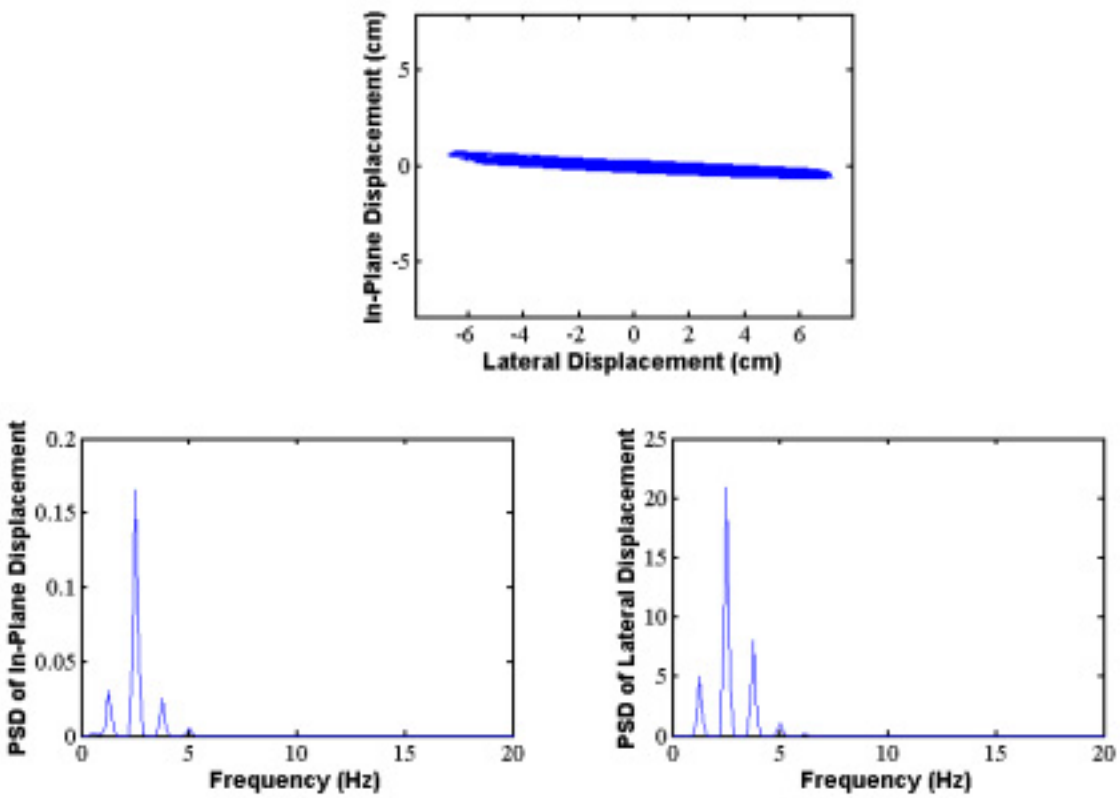

Figure 103: Lissajous and power spectral density plots of displacement for record A.

Frequency Estimation

The modal frequencies of a cable are decided by its length, mass, stiffness and damping ratio in each mode. Among these properties, the stiffness and the damping ratio may be dependent on the vibration amplitude, and thus renders the frequencies variable too. Figure 104 shows the averages of estimated modal frequencies for the first several modes of stay AS16 and AS23. In these figures, frequencies of the cables with and without damper attached are presented separately to show the effects of the dampers. The estimated natural frequencies are found to be in very good agreement with the values obtained by searching for the peaks of power spectral densities of the response. Frequency shifts introduced by addition of dampers, which were suggested by Main and Jones' (2000) analytical work, are also evident in the figures.

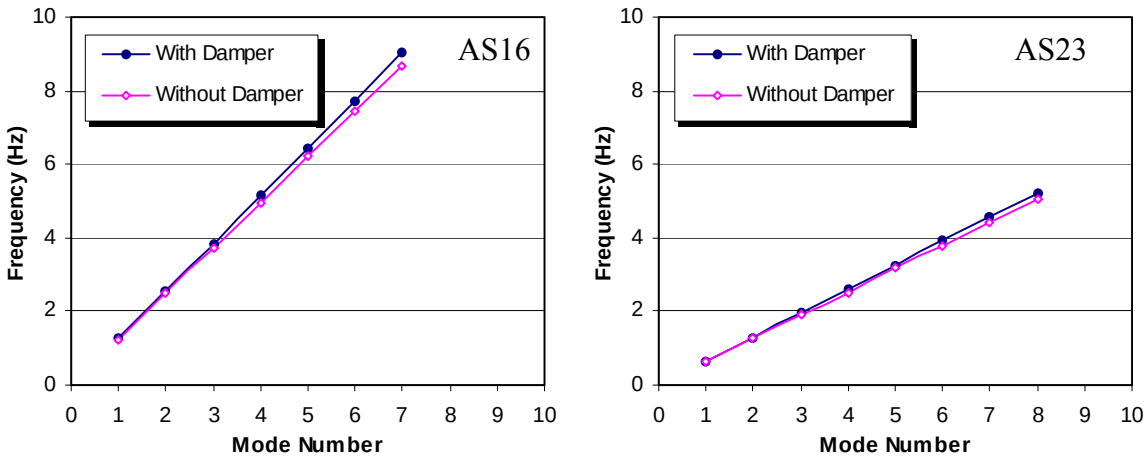

Figure 104: Modal frequencies of stay AS16 and AS23.

In Figure 105, the estimated second-mode frequency of stay AS16 without damper attached is plotted against the RMS displacement at the accelerometer location. Very small variance is found in the estimates from record to record, but a trend is evident that the modal frequency increases with displacement when the RMS displacement is greater than about 2 cm. Similar trends have been observed for the other modes too but will not be presented here. At this point it is suggested that this trend is caused by the change of the effective support condition of the cable with vibration amplitude. On the Fred Hartman Bridge, stay AS16 goes through a guide pipe before it reaches the anchorage and there is a neoprene ring between the cable and the pipe. When the amplitude of the vibration is large enough, the gap between the cable and the pipe will be gradually closed, which results in realistically a shorter cable with higher modal frequencies. Figure 105 shows the same relation for stay AS16 after the damper was installed. The variance of the estimates is again very small but no increase of the frequency with displacement amplitude is evident. This may partly be due to the fact that, with the presence of the damper, the vibration did not reach sufficient amplitude as to close the gap between the cable and the pipe. It may also be partly due to the fact that the damper itself may have been acting as a "pseudo-anchorage" of the cable when vibration amplitude is low.

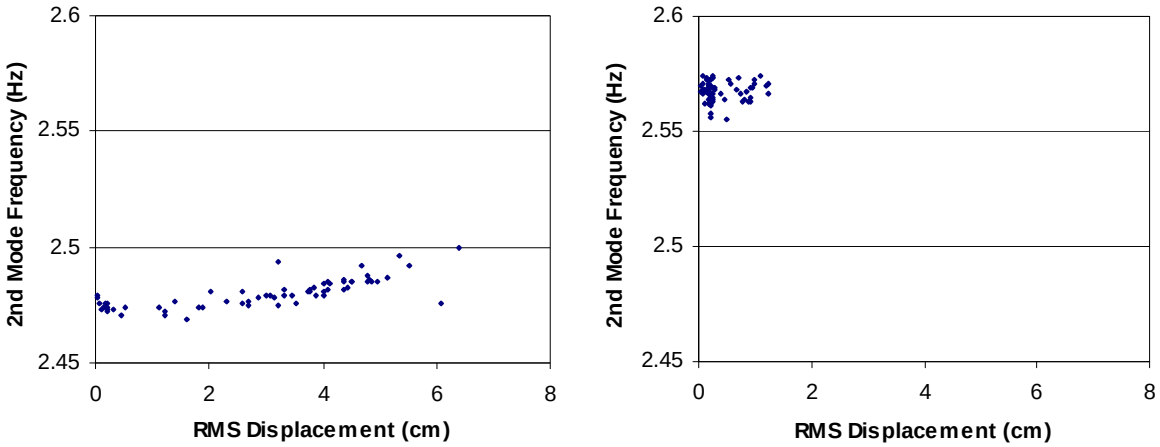

Figure 105: Second-mode frequency vs. RMS displacement for stay AS16.

Damping Estimation

Compared to frequency, damping is a much more complicated property and its source and mechanism are still not well understood. In the case of wind or rain-wind induced stay-cable vibration, the problem is further complicated by the introduction of the so-called "negative damping", which, unlike conventional damping, adds energy into the system instead of dissipating it. Preliminary estimation results have been analyzed with some attention directing to details in a case-by-case manner. Special attention has been paid to the effects of damper on the effective damping of the cable vibration system. The effect of rainfall has also been preliminarily analyzed because it has been proved to be an important contributory factor to stay-cable vibration.

Figure 106 shows the effect of the attached damper on the damping ratios of stay AS16. Averages of estimated modal damping ratios are used in the figures and will continue to be used in the subsequent figures for discussion of damping estimation. As shown, the inherent damping (cable damping without contribution from rainfall and damper) in each mode of the cable, according to the estimation, is very low and decays very rapidly in the first several modes. It is unexpected, however, that the addition of the damper to the system did not appear to result in significant increase of the modal damping ratios. The largest increase by about 0.15% of critical damping comes in the first mode of vibration when the cable vibrates without rainfall. With rainfall, the largest increase comes in the second mode, which is frequently the most dominant mode for rain-wind induced vibration. But this increase is very small too, by just 0.06% of critical damping. This estimation result is not only against intuition that external dampers will bring large supplemental damping into the system, but also against the observed fact that the damper on stay AS16 has been successful in suppressing excessive vibrations. These observations are still under detailed investigation, along with analysis and comparison of records with and without rainfall. Similar patterns have been observed in the damping estimation results for stay AS23.

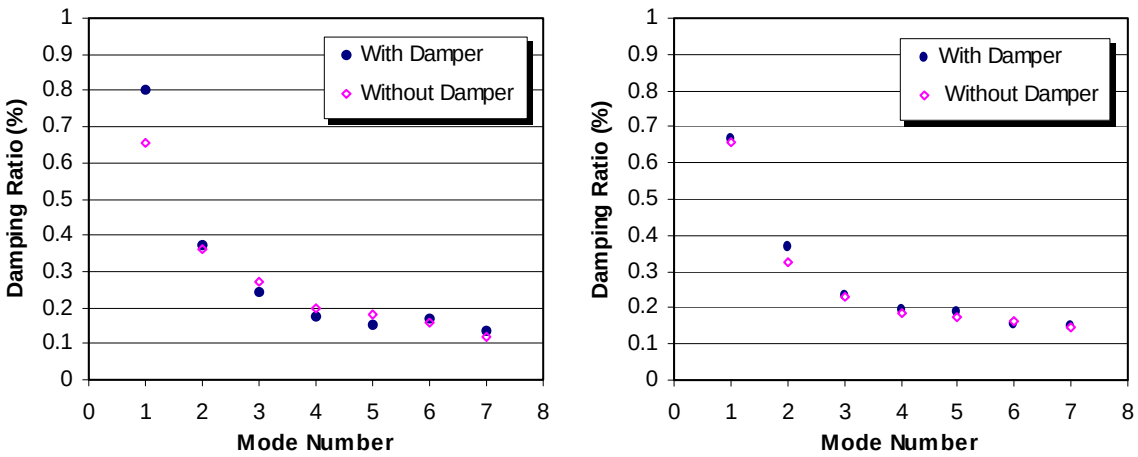

Without Rain With Rain

Figure 106: Estimated modal damping of Stay AS16 showing effect of damper.

Figure 107 shows the histograms of the damping estimation results for mode two of stay AS16 and mode three of stay AS23 from records without rainfall, before dampers were installed. It is evident in these two figures that the distributions of these results are rather broad. A similar pattern of distribution has been found for estimation results for the other modes of the cables. This means that the average values used above for discussion may not be very appropriate for comparison purposes. Better categorization and interpretation of the estimation results is thus desired and will be a major focus of future research. Additional analysis investigating dependence of damping on wind speed and vibration amplitude have been conducted. Results as of time of writing are not fully conclusive, and are not reported here.

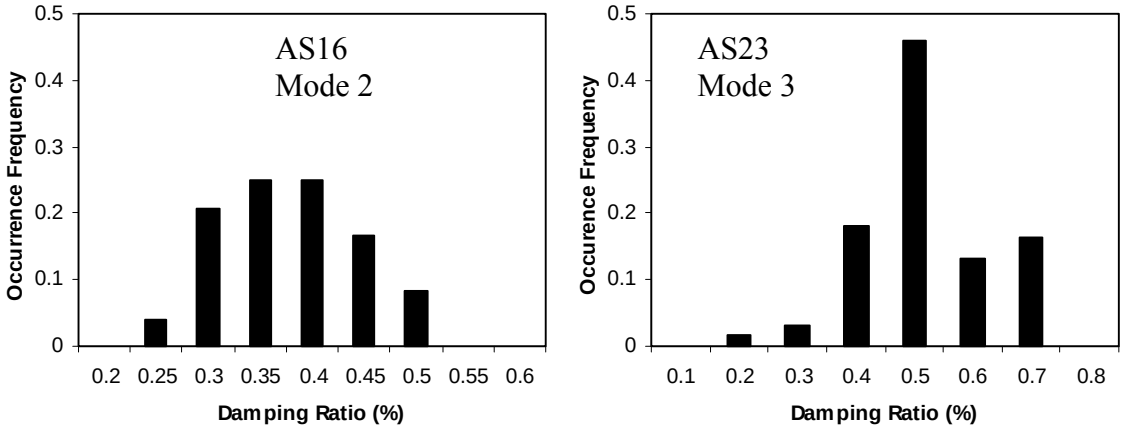

Figure 107: Histogram of estimated damping for mode 2 of AS16 and mode 3 of AS23.

Figure 108 shows the relation between the estimated damping in the second mode of stay AS16 with corresponding five-minute RMS damper force. The points are scattered, but a noticeable though not clear trend is present that the modal damping ratio decreases when the damper is "more engaged." More investigation into this trend is needed but, if it is true, it potentially suggests that, in some cases, although supplemental damping is supplied by the damper, the effective damping level in the system may still remain low.

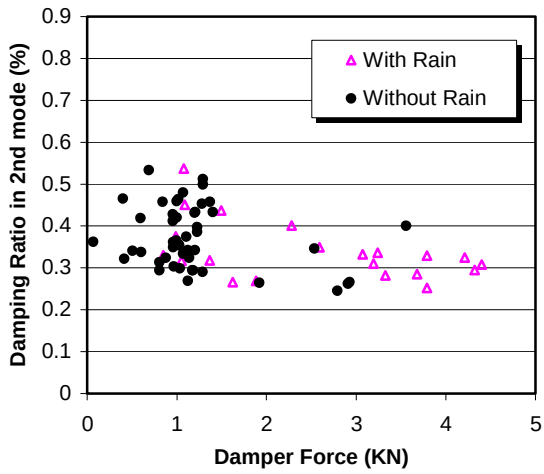

Figure 108: Dependence of modal damping on damper force.

It has to be emphasized again that the observations above were made through preliminary analysis of a limited number of records. Much more work still remains to be done before general conclusions can be reached. Nonetheless, at least one controversial problem is apparent in the current findings: according to the estimation results, the addition of dampers to the two cables did not result in a large enough increase of damping into the systems, especially with the occurrence of rain, while also according to the measurements, excessive rain-wind vibrations have been effectively suppressed by the dampers. According to Irwin (1997), rain-wind induced vibration could be avoided if the Scruton number is greater than 10. The Scruton number is defined as:

$$(Sc)_n = \frac{m\,|\,\zeta_n\,|}{\rho D^2} \tag{57}$$

where m is cable mass per length, ζ_n is the modal damping ratio, ρ is the air density, and D is the cable diameter. Analysis of the modal damping ratio needed according to the Scruton number criterion to suppress rain-wind induced vibration, together with the averages of estimated modal damping in stays AS16 and AS23 with damper attached, suggest that if the estimation and the Scruton number criterion were both valid, the damper could not have suppressed the rain-wind induced vibration in the second mode of stay AS16 and the third mode of stay AS23. This is obviously contradictory to the observations from measurement. In addition, the estimated damping results are also inconsistent with the results from damping prediction methods.

These inconsistencies in damping estimation are important. Detailed investigation of these discrepancies is needed and will be a focus of future research. A tentative explanation is proposed in the following section.

Possible Explanation for Discrepancies in Damping Estimation

It has been revealed that the dampers on stay AS16 and AS23 may not have frequently been effectively engaged, instead, they may have been working more like a supporting point for the cables when the vibration amplitude was low. Figure 109 shows the one-minute RMS damper force against the one-minute RMS in-plane displacement at the accelerometer location and the one-minute RMS in-plane displacement at the damper-cable connection point, respectively, for stay AS16. All the records shown in the figures were chosen to have one-minute RMS damper force greater than 0.5 KN. Figure 109 for AS16 reveals a very clear relationship between the RMS damper force and the RMS displacement at the accelerometer location. The four clusters (A, B, C and D) of points in the figure are found to represent in-plane vibrations in the second, fourth, fifth and seventh modes of the cable, respectively. However, for cable AS23 no similar relationship is evident between the RMS damper force and the RMS displacement at the damper-cable connection. These and other observations suggest that the damper may haven been frequently locked-up and produced no or little energy dissipation to the system, which may partially explain why the "average" supplemental damping estimated was very low.

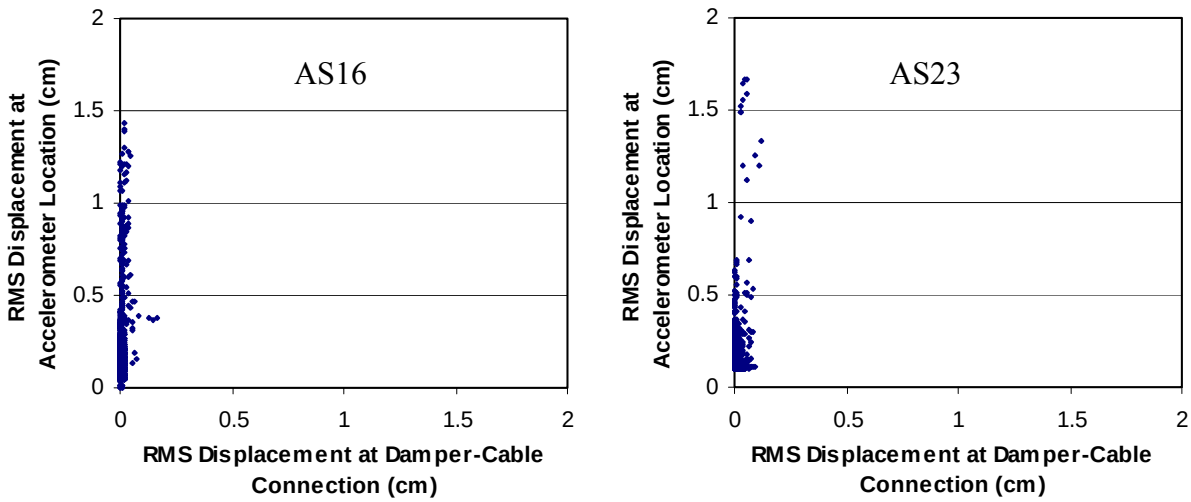

Figure 109: RMS damper force vs. RMS displacements for AS16 and AS23.

Figure 110 plots the measured damper force against the displacements and velocities at two locations of stay AS16 for a segment of a sample record. The "integrated displacement" and "integrated velocity" in the figure were integrated from the acceleration time history measured by the accelerometer, but were scaled down by a constant factor to have approximately the same amplitudes as those of the displacement and velocity at the damper-cable connection. The phase difference between these two locations has also been approximately corrected using the method proposed by Krenk (2000) and Main and Jones (2000). The "differentiated velocity" was directly differentiated from the displacement measured at the damper-cable connection. The abrupt changes of the curvatures in the force-displacement plots and the slopes of the lines in the force-velocity plots suggest that the damper did not behave viscously, as it was assumed to be. Instead, it had been effectively locked-up until the damper force passed a certain level. This record is not a special case. In fact, this pattern of damper behavior has been found to be very common in records in which the dampers are believed to be suppressing excessive cable

vibration. It was later confirmed by the manufacture of the dampers that this force is the residual static friction in the dampers. Because of the friction, the dampers would remain locked-up and act as new supporting points for the cables until the vibration amplitude becomes large enough and the friction threshold is overcome. It has also been noticed but not presented in detail here that the friction threshold for each damper varies from record to record in a certain range, according to characteristics in mode participation and dimensionality of the vibration. It is hypothesized here that the existence of the friction threshold reduces the supplemental damping the dampers can effectively add to the system, which partly explains the estimation result that the amount of damping added by the dampers is very small. The validity of this hypothesis is to be subjected to future research and the approach to verify it will be proposed in the next section. It has to be noted, however, that even when the dampers were locked-up, they will still introduce frequency shifts into the cable systems because the cables in this case just vibrates in a shorter length. This is similar to but not the same as the case Main and Jones (2000) discovered that, if the damper is designed to be too stiff, it essentially results in the length of the cable being effectively shorter.

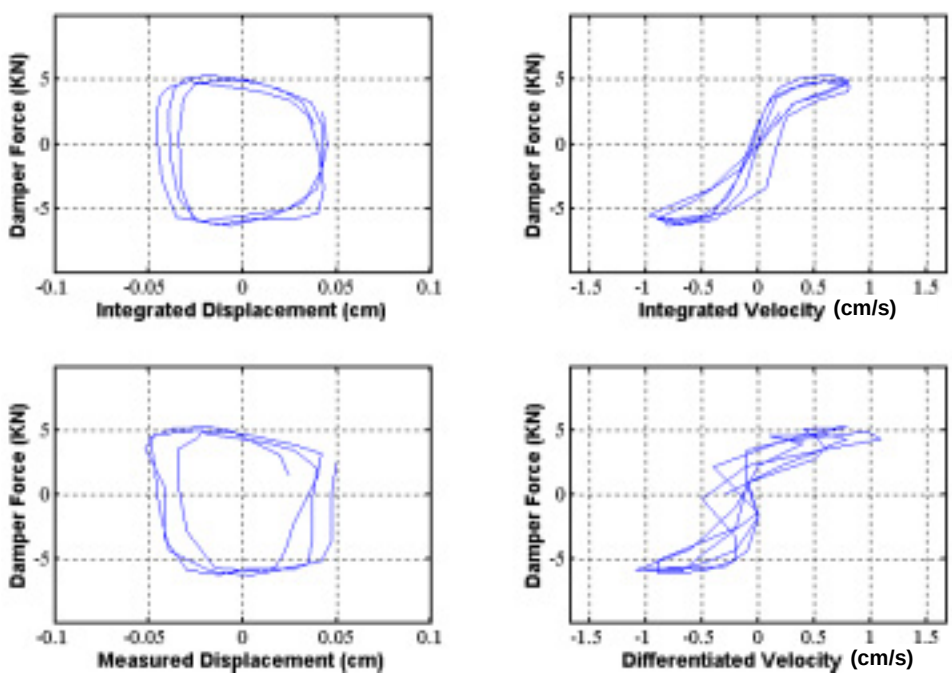

Figure 110: Damper force vs. displacement and velocity for a segment of a sample record.

Although the discussion so far tentatively explains why the supplemental damping provided by the dampers appears low, it did not explain why the dampers have been successfully suppressing excessive vibrations. Figure 111 shows the time histories of displacement and damper force for a sample five-minute record for stay AS16. It is clear in the figure how the vibration of the cable built up at the beginning and was subsequently suppressed by the damper. But the means by which the damper suppressed the vibration is of interest. The correlated periodic increasing and decreasing of amplitudes in both time histories suggests that the damper might not have been engaged all through the record. Rather, it appears that the damper had been working periodically, only when the displacement amplitude was large enough. It can also be noticed in

the time histories that the amplitudes of the peaks are almost at the same level, suggesting that the damper seemed to be keeping the vibration below a certain level. This pattern of damper performance, again, is not just a special case. It has been observed often in the records when the damper is believed to be suppressing excessive cable vibration.

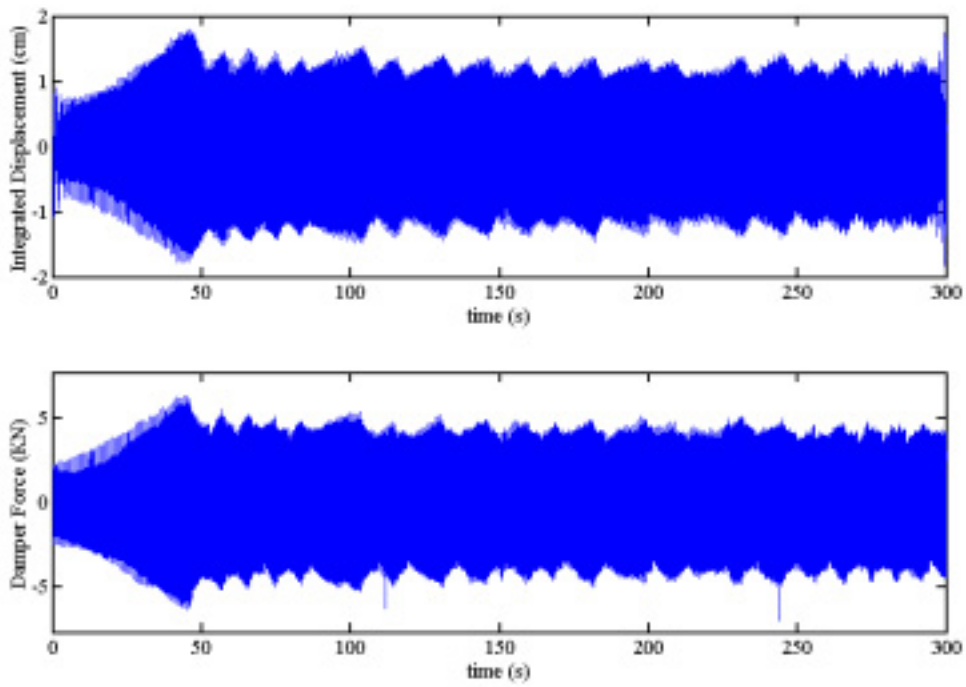

Figure 111: Displacement and damper force time histories of a sample record.

The reason why the damper behaves this way has to be investigated in association with the unique nature of wind- or wind-rain- induced stay cable vibration. Unlike other forced vibration of other structures, wind- and rain-wind-induced cable vibration is self-excited, which means that the wind, or the combination of wind and rain, and the vibration itself both have to meet a certain criterion for the vibration amplitude to increase. The role of the damper in the stay cable vibration system, then, is to bring the vibration from unstable back to stable by dissipating energy. But it is hypothesized here that the amount of the energy the damper has to dissipate does not necessarily have to be large. If this amount of energy is indeed small, it will be another reason why the estimated amount of damping the dampers added to the cable vibration system is small. To verify this hypothesis, at least two questions have to be answered: one is how the vibration builds up; the other is how much energy is actually dissipated by the damper.

APPENDIX D1 : INTRODUCTION TO MECHANICS OF INCLINED CABLES

D1.1 STAY CABLE STATIC PROPERTIES

This section provides mathematical descriptions of the various properties of a typical stay cable. Exact mathematical functions are given and then power series approximations (for relatively "tight" cables) are provided for ease of computation and to allow checking of exact equations.

A typical stay cable is shown in Figure 112:

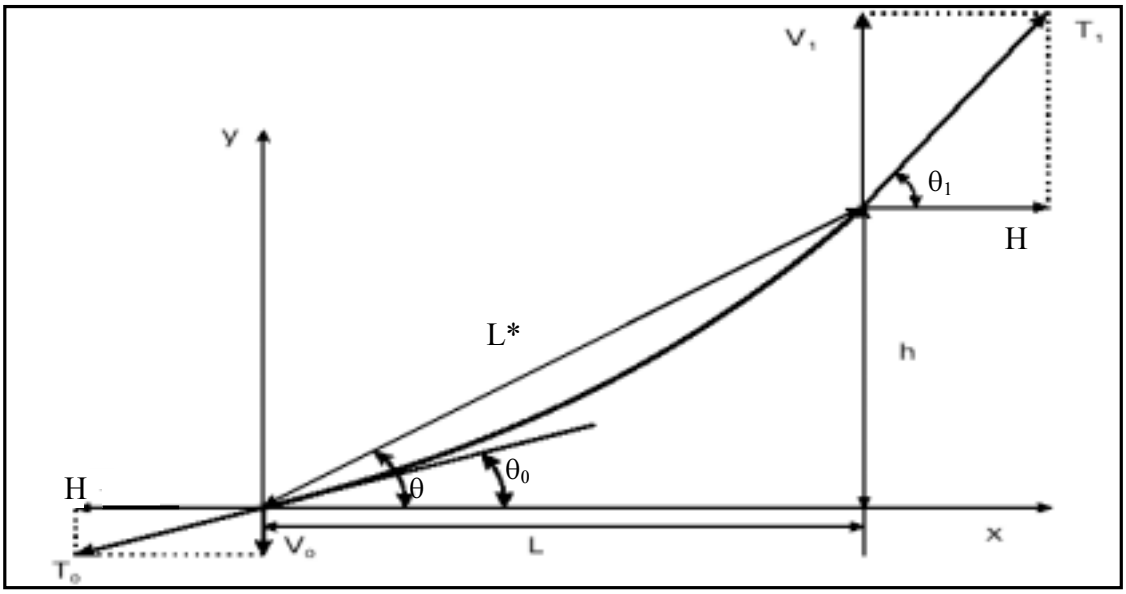

Figure 112: Incline stay cable properties.

The following basic cable properties are required:

T_0, T_1 = Lower and upper cable tensions, respectively (kN , kips)

H = Horizontal component of the cable tension (kN , kips)

m = Cable mass per unit length (kg/m , kips/ft)

A = Total cross-sectional area of cable strands (mm^2 , in^2)

E = Cable modulus of elasticity (MPa , ksi)

σ_{UTS} = Cable yield stress -- Ultimate Tensile Stress (MPa , ksi)

h = Cable rise (m , ft)

L = Cable run (m , ft)

s = Cable sag (m , ft)

The following properties can then be calculated:

$w = m \times g$ cable weight per unit length (kN/m , kips/ft)
(g = acceleration due to gravity)

$L^* = \sqrt{h^2 + L^2}$ cable chord length (m , ft)

$\theta = \operatorname{atan}\left(\frac{h}{L}\right)$ angle of chord to horizontal

Catenary Equations (Exact Solutions)

Coordinates of cable nodes are defined using the parameters described above and the catenary equations for this cable (Dean, 1962).

From the free body diagram for any point on the cable, the slope is:

$$y' = \frac{dy}{dx} = \sinh\left(\frac{w}{H}x + K_1\right)$$

Integrating this expression yields the equation for the cable coordinates:

$$y = \frac{H}{w}\cosh\left(\frac{w}{H}x + K_1\right) + K_2$$

The constants K1 and K2 can be obtained from evaluating the boundary conditions:

x = 0 , y = 0
x = L , y = h

Thus:

$$K_1 = \operatorname{asinh}\left(\frac{wh}{2H\sinh\frac{wL}{2H}}\right) - \frac{wL}{2H} \quad ; \quad K_2 = -\frac{H}{w}\cosh(K_1)$$

The length of the cable, C (m, ft), is then:

$$C = \frac{H}{w}\left(\sinh\left(\frac{wL}{H} + K_1\right) - \sinh(K_1)\right)$$

The slopes at the ends of the cables are then:

$$\theta_0 = \operatorname{atan}(\sinh(K_1)) \qquad = \text{lower slope (rad)}$$

$$\theta_1 = \operatorname{atan}\left(\sinh\left(\frac{wL}{H} + K_1\right)\right) \qquad = \text{upper slope (rad)}$$

Following from these angles, the cable end vertical reactions are:

$$V_0 = H(\tan(\theta_0)) \qquad = \text{lower end reaction (kN , kips)}$$

$$V_1 = H(\tan(\theta_1)) \qquad = \text{upper end reaction (kN , kips)}$$

By way of verification, it may be checked that the difference in the cable end vertical reactions should equal the mass of the cable. That is:

$$V_1 - V_0 = w \times C$$

The cable end tensions are:

$$T_0 = H(\sec(\theta_0)) \qquad = \text{Lower Tension (kN , kips)}$$

$$T_1 = H(\sec(\theta_1)) \qquad = \text{Upper Tension (kN , kips)}$$

The maximum cable axial stress (MPa , ksi) is:

$$\sigma_{Axial} = \frac{T_1}{A}$$

And the maximum ratio of the Ultimate Tensile Stress utilized is then:

$$\text{Ratio}_{UTS} = \frac{\sigma_{Axial}}{\sigma_{UTS}}$$

The elastic elongation of the cable is (m , ft):

$$\Delta = \frac{HL}{AE}\left[\frac{wh^2}{2HL}\coth\left(\frac{wL}{2H} + \frac{1}{2} + \frac{H}{2wL}\sinh\left(\frac{wL}{H}\right)\right)\right]$$

Finally, the unstressed length of the cable (m , ft) is defined as:

$$USL_0 = C - \Delta$$

Power Series Approximations to Exact Solutions

It may be more convenient to express the exact hyperbolic relationships in terms of power series expansions of the hyperbolic functions. This is particularly effective for "tight" cables, defined as those for which:

$$r = \frac{wL}{2H} \leq 0.5$$

The relationships below are used and terms up to and including r^4 are retained:

$$\sinh(x) = x + \frac{x^3}{6} + \frac{x^5}{120} + \ldots$$

$$\cosh(x) = 1 + \frac{x^2}{2} + \frac{x^4}{24} + \frac{x^6}{720} + \ldots$$

$$\operatorname{acoth}(x) = \frac{1}{x} + \frac{x}{3} - \frac{x^3}{45} + \frac{2x^5}{945} - \ldots$$

Then, the cable length C is defined as:

$$C = (L^*)\left[1 + \frac{\cos(\theta)^2}{6} r^2 + \left(\frac{\cos(\theta)^2}{45} - \frac{\cos(\theta)^4}{72}\right) r^4 + \ldots\right]$$

The lower end slope is defined as:

$$\theta_0 = \operatorname{atan}\left[\frac{h}{L} - r\frac{s}{L} + \frac{hr^2}{3L} - \frac{s\cos(\theta)^2}{6L} r^3 - \frac{hr^4}{45L} \ldots\right]$$

The upper end slope is defined as:

$$\theta_1 = \operatorname{atan}\left[\frac{h}{L} + r\frac{s}{L} + \frac{hr^2}{3L} + \frac{s\cos(\theta)^2}{6L} r^3 - \frac{hr^4}{45L} \ldots\right]$$

The cable elongation is defined as:

$$\Delta = \frac{HL\sec(\theta)^2}{AE}\left[1 + \frac{r^3}{3} - \frac{r^4}{45}\left(1 - 4\frac{L^2}{(L^*)^2}\right) \ldots\right]$$

D1.2 STAY CABLE DYNAMIC PROPERTIES

Dynamic properties of stay cables may be examined in two ways:

- The "taut string" simplified approximation (Figure 113A)
- The theoretically correct dynamic properties for an inclined cable (Figure 113B)

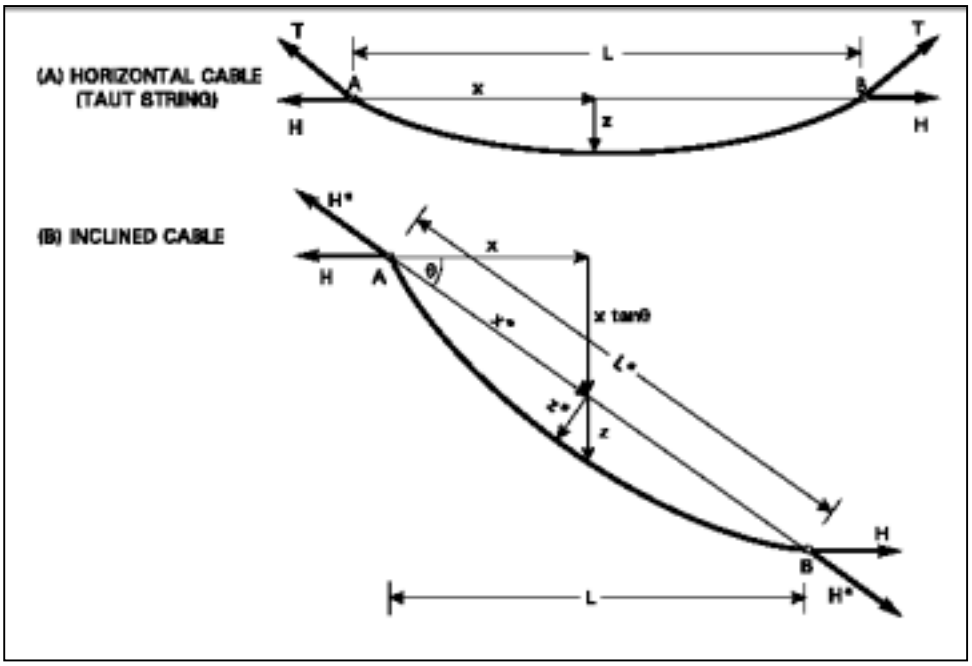

Figure 113: Definition diagram for a horizontal cable (taut string), compared to the definition diagram for an inclined cable.

Taut String

For the taut string, it is assumed the sag of the cable is small compared to its length , the cable is perfectly elastic, and the cable is inextensible. The accuracy of the taut string approximation is usually adequate for practical purposes.

The natural frequencies, ω_i, of stay cables can be approximated (often accurately enough) using the expressions for a taut string (Figure 113A) as (Gimsing, 1997):

$\omega_i = \frac{i\pi}{L}\sqrt{\frac{T}{m}}$, which yields the natural circular frequencies in radians/sec.

The more practical form:

$f_i = \frac{i}{2L}\sqrt{\frac{T}{m}}$ yields natural frequencies in Hz.

Inclined Cable

In the case of an inclined cable (Figure 113B), it is convenient to deal with transformed coordinates x* measured along the cable chord from point A) and z* (perpendicular distance from the chord to the profile), rather than with coordinates x and z. After performing the necessary transformations we obtain (Irvine, 1981):

$x^* = x \sec\theta + z \sin\theta$, $z^* = z \cos\theta$, $L^* = L \sec\theta$, and $H^* = H \sec\theta$,

so that

$$\bar{z} = \frac{1}{2}\bar{x}(1-\bar{x})\left[1 - \frac{\bar{\varepsilon}}{3}(1-2\bar{x})\right]$$

where:

$$\bar{z} = \frac{z^*}{\dfrac{mg(L^*)^2\cos\theta}{H^*}} \ , \ \bar{x} = \frac{x^*}{L^*} \ , \ \text{and} \ \ \bar{\varepsilon} = \frac{mg(L^*)\sin\theta}{H^*}$$

Solving the equations of motion using the above transformed axes, the natural frequencies of the out-of-plane modes are given by:

$$\bar{\omega}_n = n\pi \quad , \qquad n = 1,2,3,\ldots$$

and those of the antisymmetric in-plane modes are:

$$\bar{\omega}_n = 2n\pi \quad , \qquad n = 1,2,3,\ldots$$

Frequencies of symmetric in-plane modes are given by the following transcendental equation:

$$\tan\frac{\bar{\omega}_n}{2} = \frac{\bar{\omega}_n}{2} - \frac{4}{(\lambda^*)^2}\left(\frac{\bar{\omega}_n}{2}\right)^3$$

For all of the above equations:

$$\bar{\omega}_n = \frac{(\omega_n^*)(L^*)}{\sqrt{\dfrac{H^*}{m}}} \quad , \quad (\lambda^*)^2 = \left(\frac{mg(L^*)\cos\theta}{H^*}\right)^2\left(\frac{L^*}{\dfrac{H(L_e^*)}{EA}}\right)$$

in which:

$$L_e^* = (L^*)\left[1 + \frac{1}{8}\left(\frac{mg(L^*)\cos\theta}{H^*}\right)^2\right]$$

is a quantity usually only slightly greater than the length of the cable chord itself. Substituting $\overline{\omega}_n$ into the transcendental equation yields the following equation, the roots of which are the natural frequencies in question:

$$f(\omega^*) = \left[\frac{(\omega^*)(L^*)}{\frac{\sqrt{\frac{H^*}{m}}}{2}}\right] - \frac{4}{(\lambda^*)^2}\left[\frac{(\omega^*)(L^*)}{\frac{\sqrt{\frac{H^*}{m}}}{2}}\right]^3 - \tan\left[\frac{(\omega^*)(L^*)}{\frac{\sqrt{\frac{H^*}{m}}}{2}}\right]$$

Equations shown are of general form and applicability. As special cases, they contain results for a horizontal cable ($\theta = 0^o$) and a vertical cable ($\theta = 90^o$).

Formulation Including Sag

More complicated expressions exist for cables with larger sag ratios such as the main cables of suspension bridges. For such cables, natural frequencies can be obtained by solving the following frequency equations (Irvine, 1981):

- For antisymmetric in-plane modes: $\tan\left(\overline{\omega}A + \frac{B}{\overline{\omega}}\right) = -\frac{C}{\overline{\omega}}$
- For symmetric in-plane modes: $\tan\left(\overline{\omega}A + \frac{B}{\overline{\omega}}\right) = \frac{\overline{\omega}}{D}$

Where

$$\overline{\omega}^2 = \frac{\omega^2 \ell}{2g\tan\psi_0}, \quad \tan\psi_0 = \frac{4\frac{s}{\ell}}{1-\left(2\frac{s}{\ell}\right)^2},$$

and $L = \frac{\ell(\text{asinh})(\tan\psi_0)}{\tan\psi_0}$, is the span of the cable, while ℓ is the length of the catenary hanging between the supports, and s is the cable sag. A, B, C, and D are parameters which depend on the value of ψ_0 .

Natural frequencies of cable stays with larger sag can be estimated using the following equation (Zui et al., 1996):

$$fn = \frac{\lambda}{\pi}\sqrt{\frac{g}{8s}}$$

where, for unsymmetric modes $\lambda = n\pi$, $n = 1,2,3\ldots$

for symmetric modes $\frac{\lambda - \tan\lambda}{\lambda^3} = \Gamma$, with $\Gamma = \frac{mL}{128EA\left(\frac{s}{L}\right)^3\cos^6\theta}$

Full-Scale Cable Properties

For many stay systems the term $\sqrt{T/m}$, is more or less constant as the cables are usually designed to a maximum working stress of 0.45 X GUTS (Guaranteed Ultimate Tensile Stress). The term, $\sqrt{T/m}$ **,** has been calculated for the stay cables of three bridges as listed in Table 17 and shown in Figure 114. The first two modes of vibration as a function of cable unstressed length (USL) are shown in Figure 115.

Table 17: Stay cable property comparison.

Bridge	**Cable Type**	**Average** $\sqrt{T/m}$
Alex Fraser	Helical Twist Parallel Wire	231
Maysville	Grouted 7 Wire Parallel Strand	188
Owensboro	Grouted 7 Wire Parallel Strand	201

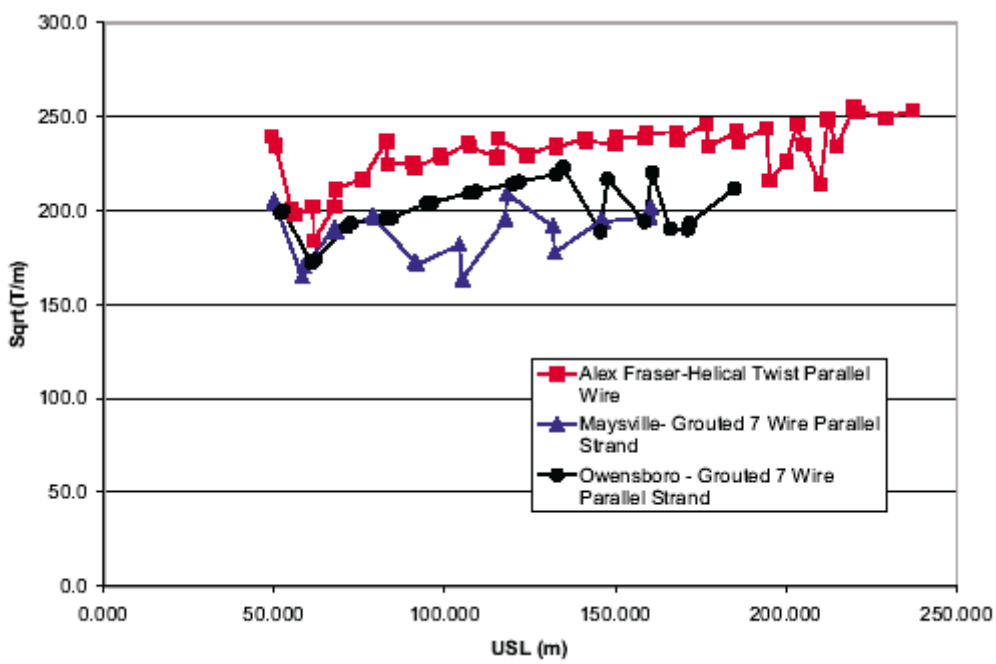

Figure 114: Cable $\sqrt{T/m}$ vs. Cable Unstressed Length, summary of Alex Fraser, Maysville, and Owensboro Bridges.

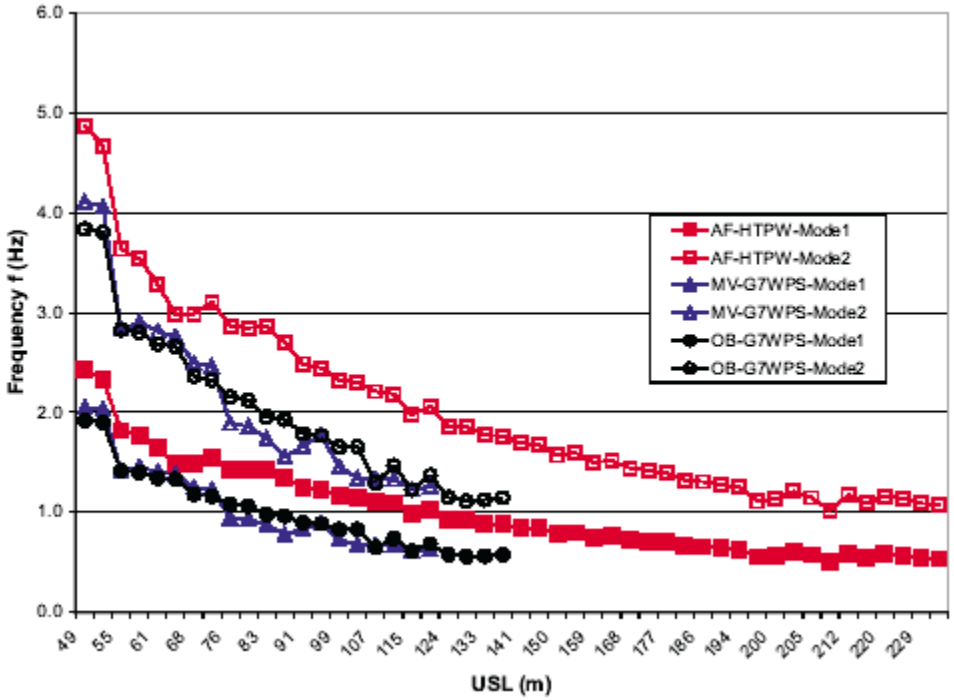

Figure 115: Cable Frequency vs Cable Unstressed Length, Summary of Alex Fraser, Maysville, and Owensboro Bridges.

APPENDIX D2: LIVE LOAD VIBRATION SUB-STUDY

D2.1 INTRODUCTION

This live load vibration sub-study was carried out by Buckland & Taylor Ltd. to assess the amount of vibration which is caused by live loading. To address this problem, a computer model of a cable-stayed bridge was used to model the dynamic effects of a moving train load. The vibrations of an individual set of cables were analyzed in detail. The cable tensions, displacements and anchorage rotations obtained from the dynamic time history analysis were compared to the results obtained from influence line calculation which are normally carried out during design. The engineering analyses were performed using in-house programs for nonlinear analysis (CAMIL) and live load analysis (MELL).

Example Bridge: Rama 8 Bridge in Bangkok, Thailand.

The RAMA 8 Bridge, shown in Figure 116, is a cable-stayed bridge over the Chao Phraya River in Bangkok, Thailand. The bridge has been designed by Buckland & Taylor Ltd. to carry four lanes of vehicle traffic and two pedestrian sidewalks on the main span and the back spans, and six lanes of traffic on the anchor span.

Total length of the main bridge is 475 m: main span -300 m, two backspans - 2 x 50 = 100 m, and anchor span -75 m. The 160 m high tower is a reinforced concrete inverted- Y type structure. There are two inclined cable-stay planes with 28 cables each for the main span and one cable-stay plane with 28 cables for the anchor span. Cable-stays are BBR Cona stays, consisted of seven-wire parallel strands, greased and sheathed. The main span superstructure has an effective depth of 2 m and consists of a 29.70 m wide deck which is made composite with two steel edge girders. The backspan girder is a continuous post-tensioned 2.5 m deep concrete box girder.

Figure 116: RAMA 8 Bridge – Artistic Rendering.

Rama 8 Bridge Computer Model

The RAMA 8 Bridge computer model, shown in Figure 117, was created to represent the global behavior of the bridge under static and dynamic loads. The complete bridge, with two approach spans, was modeled in three dimensions. The model has 1014 beam elements and 84 cable elements.

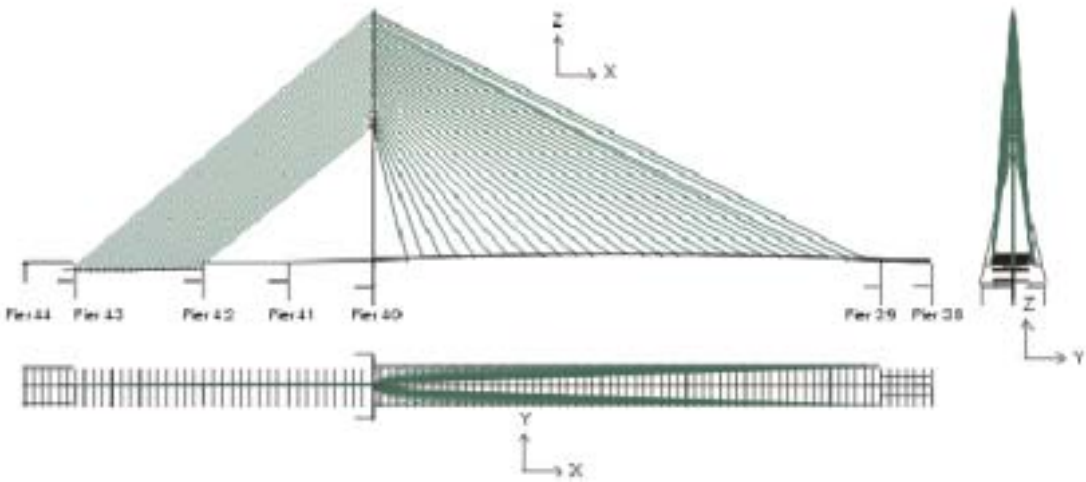

Figure 117: RAMA 8 Bridge computer model; XY, YZ & ZX views.

D2.2 FREE VIBRATION ANALYSIS

Description of Example Cable

The cable chosen to illustrate the effects of live loading on cable dynamics is the third longest cable of the main span of the RAMA 8 bridge -main span cable M26. The longest cable M28 was not chosen as it is close to the support and would not be excited as much by moving loads.

The example cable M26 has the following properties:

Unstressed length:	L = 299.140 m
Mass (per unit length):	m = 41.588 kg/m
Steel area:	A = 4350 mm2
Modulus of elasticity:	E = 195000 MPa
Outside cable diameter:	D = 0.16m
Dead load tension:	max T = 2801 kN (at tower)
	min T = 2745 kN (at deck)
	average T = 2773 kN
Horizontal component	H = 2471 kN
Ultimate capacity:	T_{ult} = 7700 kN (based on 1770 MPa)
Dead load D/C:	$\frac{\max T}{T_{ult}} = 0.362$

Cable geometry is defined with the following end points:

Cable anchor points at the tower: x = 1.247 m, y = 1.405 m, z = 184.326 m
Cable anchor points at the deck: x = 268.578 m, y= 11.447 m, z=48.293 m
Cable angles in the cable plane (to the horizontal plane):

At deck: $\alpha = 25.824°$

At tower: $\alpha = 28.068°$

Cable angle in horizontal plane: $\beta = 2.151°$ (to the x-axis)

where x is the longitudinal coordinate measured from the centerline of the tower towards pier P39, and y is the transverse coordinate measured from the bridge centerline -positive upstream (see Figure 117).

Single Cable Dynamics -Free Vibration

Theoretical solutions are based on the assumption that the cable is inextensible. (See Appendix D1 for a brief discussion of the cable vibration theory.) However, the numerical analyses, which were carried out using cable elements, modeled a "real" (extensible) cable. These results were then compared to the "theoretical" (inextensible) cable.

Extensible Cable Model

In order to capture the dynamic behavior of a single cable it is necessary to introduce additional degrees of freedom along the cable. (This is not typically required when the global dynamics of the bridge are evaluated.) Three computer models were built to simulate the behavior of the cable as an element independent of the structure (i.e. tower and the deck) and to investigate the convergence of the results. In these models, cable M26 was divided in 2, 10 and 20 segments of equal length. Figure 118 shows nodes and cable elements of the cable stay M26 in the 10-segment model. The cable was discretized in a similar manner in the 2- segment and the 20-segment models.

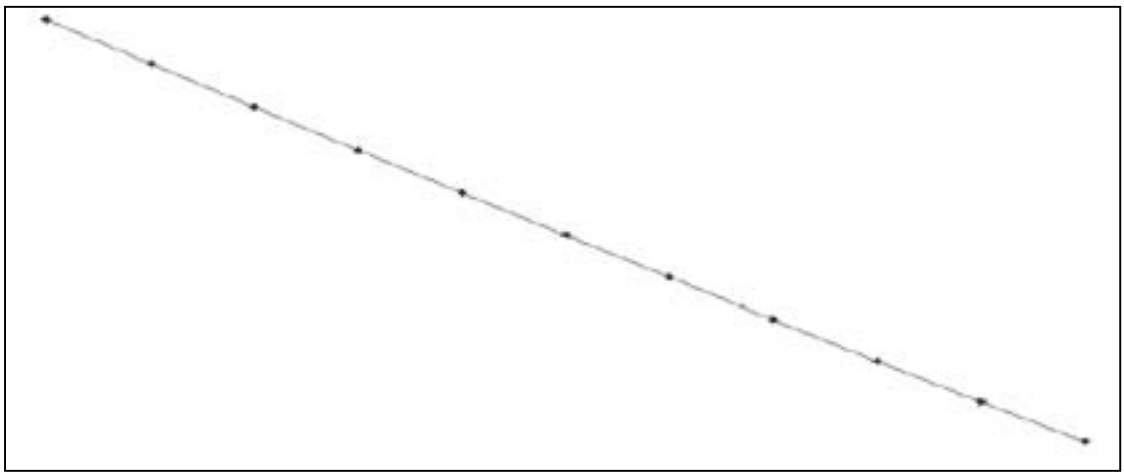

Figure 118: Independent Cable M26 discretization-10 segment model- XZ view.

Coordinates of cable nodes were defined using the cable parameters and the catenary equations for this cable (also see Figure 119):

$$y = \frac{T_H}{q_0}\cosh\left[\frac{q_0}{T_H} * x + K_1\right] + K_2$$

$$y' = \sinh\left[\frac{q_0}{T_H} * x + K_1\right]$$

where:

T_H - Horizontal component of the cable force
q_0 - Cable weight
K_1, K_2 - Constants obtained from boundary conditions at x = 0:

$$y' = \tan\theta \Rightarrow K_1 = \sinh^{-1}(\tan\theta) \qquad \text{and} \qquad y = 0 \Rightarrow K_2 = -\frac{T_H}{q_0} * \cosh(K_1)$$

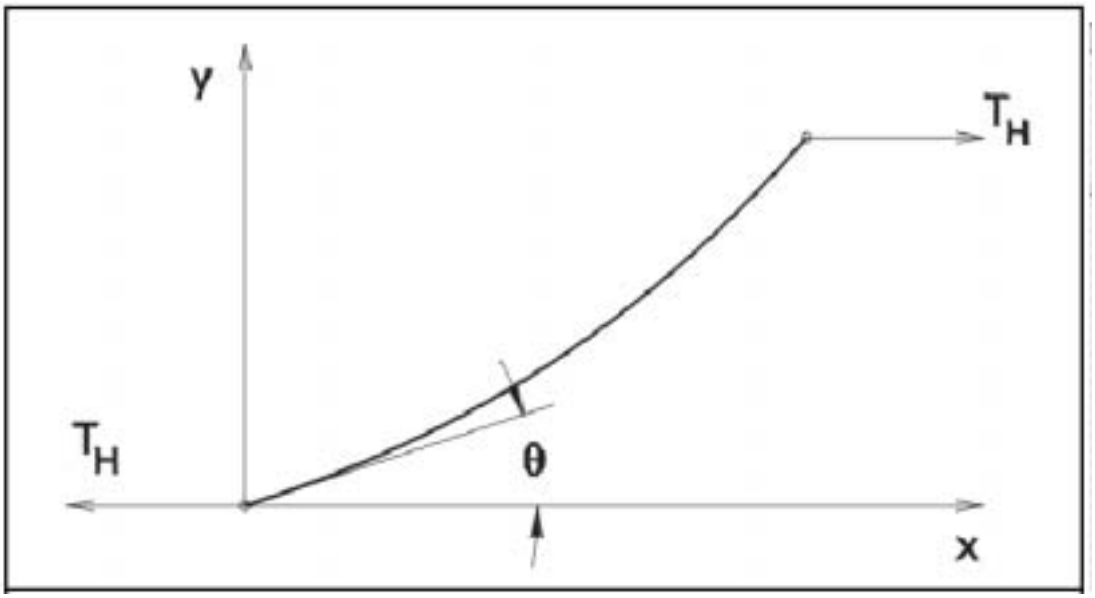

Figure 119: Cable catenary.

Only the cable end points are fixed, so the cable can vibrate spatially, not only in its plane. Free independent cable vibration periods obtained by analysis are shown in Table 18. Some typical cable modes for the 20-segment model are shown in Figure 120. All of these plots contain XY, YZ and XZ views of the cable and its mode shape.

Table 18: Free independent extensible cable vibration vs. theoretical inextensible.

Cable mode	Frequencies [Hz] (Periods are given in brackets [sec])				
	Theoretical inextensible		Analytical model (extensible)		
	Taut String	Inclined Cable	2-segment	10-segment	20-segment
1 OOP[a]	0.432 (2.31)	0.430 (2.33)	0.376 (2.66)	0.415 (2.41)	0.417 (2.40)
1 IP[b]	0.432 (2.31)	0.439 (2.28)	0.382 (2.62)	0.426 (2.35)	0.426 (2.35)
2 OOP	0.863 (1.16)	0.860 (1.16)	-	0.820 (1.22)	0.833 (1.20)
2 IP	0.863 (1.16)	0.860 (1.16)	-	0.820 (1.22)	0.833 (1.20)
3 OOP	1.295 (0.77)	1.290 (0.78)	-	1.205 (0.83)	1.235 (0.81)
3 IP	1.295 (0.77)	1.291 (0.78)	-	1.205 (0.83)	1.235 (0.81)

a. OOP - "Out-Of-Plane" -Refers to cable motion and vibrations in the plane that is perpendicular to the cable plane.
b. IP - "In-Plane" -Refers to cable motion and vibrations in the cable plane

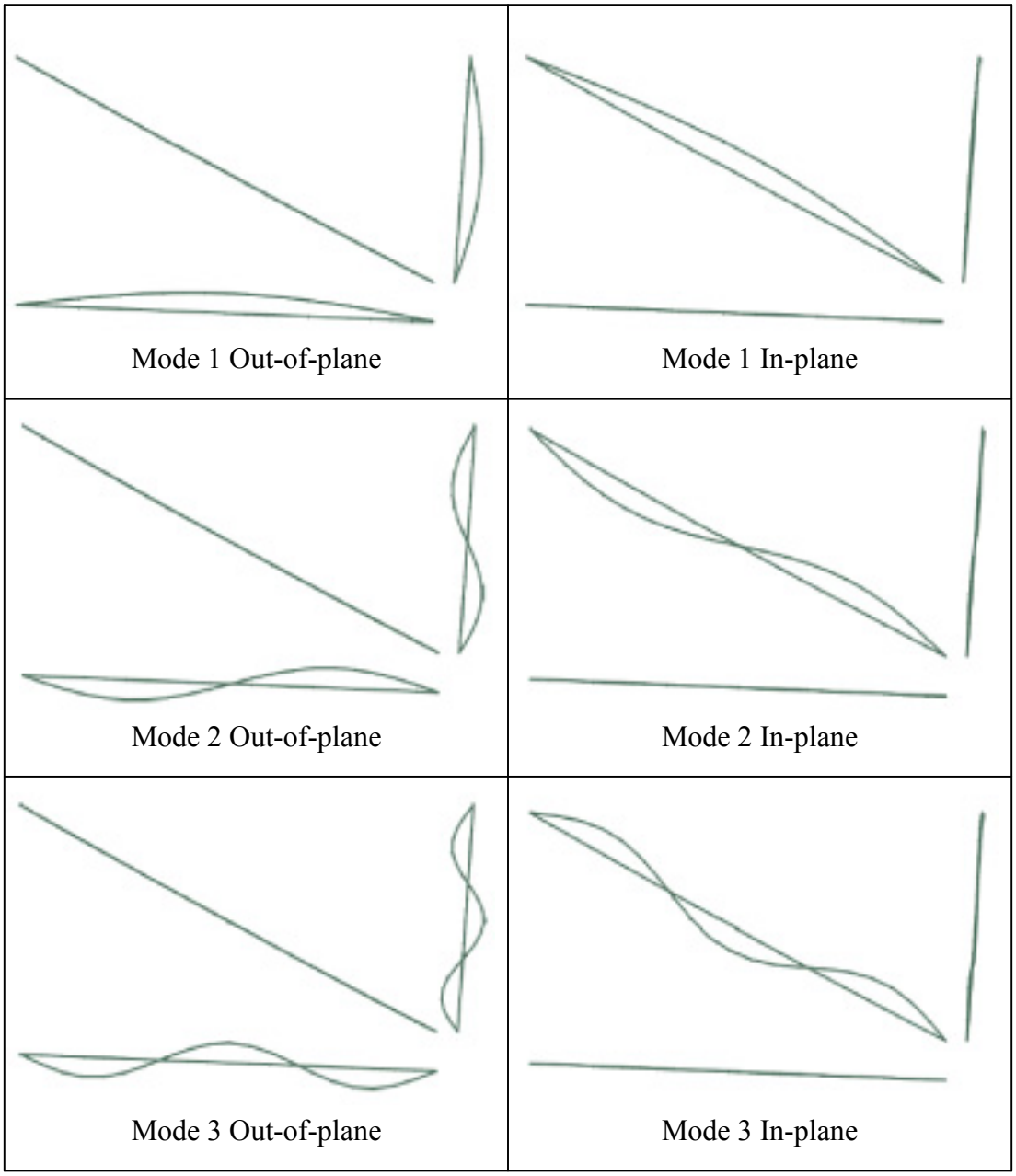

Figure 120: Cable modes; XZ, YZ, and XY views (as defined in Figure 117).

It can be seen that the cable vibrates only in its plane or perpendicular to its plane (out-of-plane vibration) for all modes. The vibration periods and frequencies are in fairly good agreement with theoretical values, and the error is 3.9% for the first mode and 5.2% for the third mode, for the 20-segment model.

The differences in natural frequencies are caused by several factors:

- The formula used to obtain the theoretical value is derived only for out-of-plane vibrations of a horizontal cable with small sag, neglecting the influence of cable extensibility due to existing tension in the cable, which is considered to be constant.

- The cable chosen is not horizontal, with varying tensile force along the cable (2% difference in tension between top and bottom), and is subjected to extension due to the tensile force.

The software used for analysis also accounts for cable extensibility, which is the most important factor causing differences in results.

It can also be seen that for symmetric modes, especially mode 1 (which carries most of the energy), the frequency for the in-plane mode is lower than for the out-of-plane mode. This is due to the fact that additional tension in the cable is generated in symmetric modes, so the cable becomes stiffer and, hence, the frequency increases (Irvine, 1981). The magnitude of the difference between the out-of-plane and in-plane frequencies depends on many parameters but the most influential factors are the magnitude of the cable tensile force and cable stiffness parameters (area and unstressed length).

Inextensible Cable

An "inextensible" cable model was used in order to achieve results closer to the theoretical values. The same model was used as for previous analyses, except that the cable area was increased to 100,000 mm^2. This caused the cable to be very stiff axially. Since no other parameters were changed, a high tensile force (T = 58,252 kN) was induced in the cable. In order to lower the force to the previous level, the cable unstressed length was increased to USL = 300.016 m. This resulted in an average tension of T=2776 kN, which was close to the value previously used (T = 2773 kN). With these parameters, free vibration periods obtained are given in Table 19:

Table 19: Free independent inextensible cable vibration periods – Theoretical values and values obtained by analysis.

Cable mode	Theoretical (sec)	Analytical 20-segment model (sec)
1 (OOP)	2.324	2.326
1 (IP)		1.698
2 (OOP)	1.162	1.167
2 (IP)		1.167
3 (OOP)	0.775	0.782
3 (IP)		0.777

The agreement between analysis values and theoretical values for out-of-plane vibrations is now excellent, with errors well below 1% .

Mode shapes are very similar to those shown in subsection “Extensible Cable Model” except for in-plane mode 1, which is shown in Figure 121. The period for this mode is much smaller (27%) than for the out-of-plane mode, which is due to a large increase in induced cable tension. Because of the great stiffness of the cable, any small differential movement induces large tensile forces in the cable, which has influence on the frequency increase. This effect is seen only in symmetric modes and diminishes as the mode number is increased.

The mode shape, as seen in Figure 1213, does not have a sine shape. It can be seen that inflection points exist in the vicinity of cable end points (Irvine, 1981).

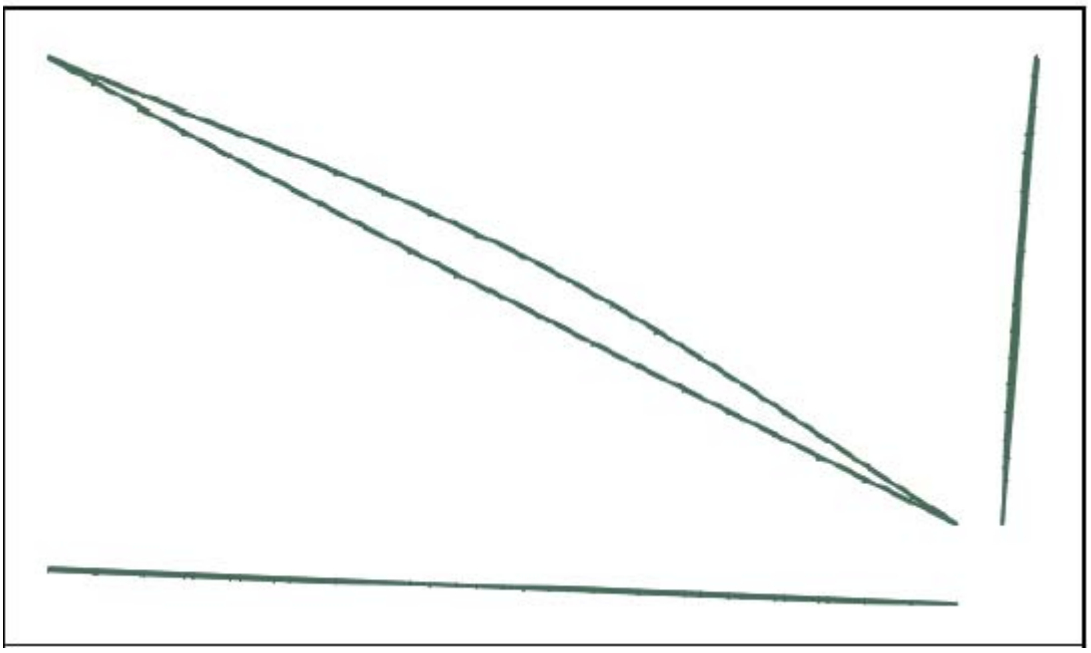

Figure 121: Inextensible cable mode 1 - In-plane; XY, YX & XZ views.

Cables Modeled as Part of the Structure

Modeling

Three computer models were again used to check the convergence of dynamic behavior of cable elements connected to the bridge deck and the tower. In these models, cable M26 was, as with the independent cable, divided in 2, 10 and 20 segments of equal length. Both the upstream and downstream cables in the main span were modeled. Figures 122 and 123 show nodes and cable elements of cable stay M26 for the 10-segment model. The cable was discretized in a similar manner in the 2-segment and the 20-segment model. Coordinates of cable nodes were defined using the catenary equation for this cable.

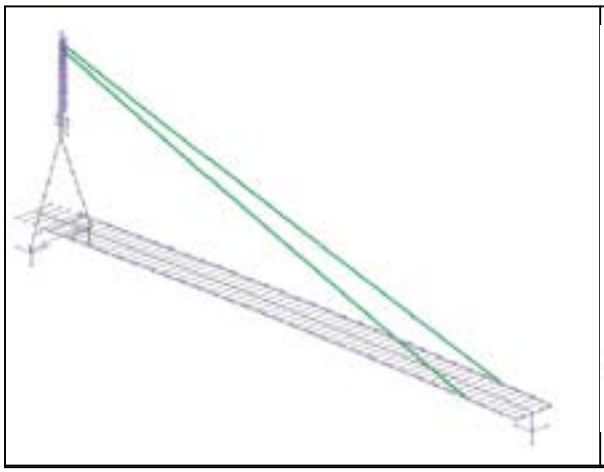

Figure 122: Cable M26 discretization - 10-segment model. View: Isometric. Only cables M26 are shown. Other cables not shown for clarity.

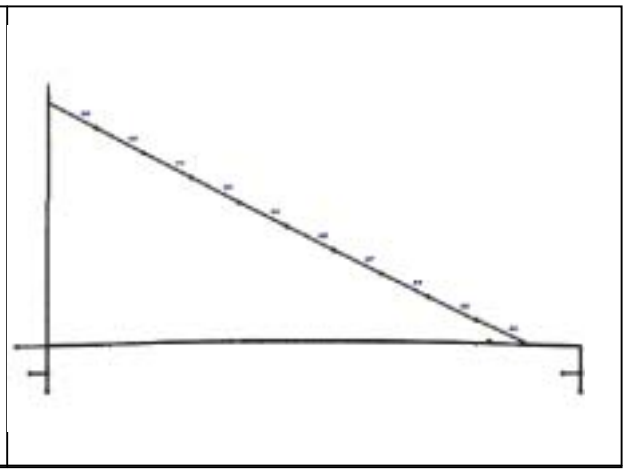

Figure 123: Cable M26 discretization - 10-segment model -XZ view. Other cables not shown for clarity.

Global Bridge Modes

The global modes of the bridge are shown in Figure 124 and 125. The fundamental vertical, longitudinal and transverse modes are shown in Figure 124. The second vertical and transverse and functional deck torsional modes are shown in Figure 125. It can be seen from these modes that the cables participate in these global modes. (Note: Since only the M26 cables were discretized in detail, the vibration of the other cables is not visible). Therefore the global modes will be reflected in the cable's response to the moving load.

Cable Modes

The natural vibration periods for the cables obtained from the analysis are given in Table 20 and the mode shapes are shown in Figures 126 to 128.

Because the cables now form part of the overall structure, the modes of the two identical M26 cables become weakly coupled. This means the cables either move in-phase or out-of-phase with respect to each other and thus the number of modes is doubled. It can be seen that pure in-plane and pure out-of-plane vibration of the cable is present only for the first fundamental cable mode. Higher modes are spatial (i.e. they involve complicated 3D motions), which is a further consequence of the interaction with the deck and tower. However, the vibration periods and frequencies are in good agreement with theoretical values, especially for the 10-segment and 20-segment cable models, for which the error in period for the first mode is less than 1 % .

Table 20: Cable vibration periods and frequencies –
Theoretical values and values obtained by analysis.

Cable mode	Theoretical		2-segment model		10-segment model		20-segment model	
	Sec.	Hz.	Sec.	Hz.	Sec.	Hz.	Sec.	Hz.
1 (OOP)	2.31	0.43	2.57	0.39	2.33	0.43	2.32	0.43
1 (IP)			2.53	0.40	2.28	0.44	2.27	0.44
2	1.16	0.86	-		1.18	0.85	1.17	0.86
3	0.77	1.30	-		0.80	1.25	0.78	1.28

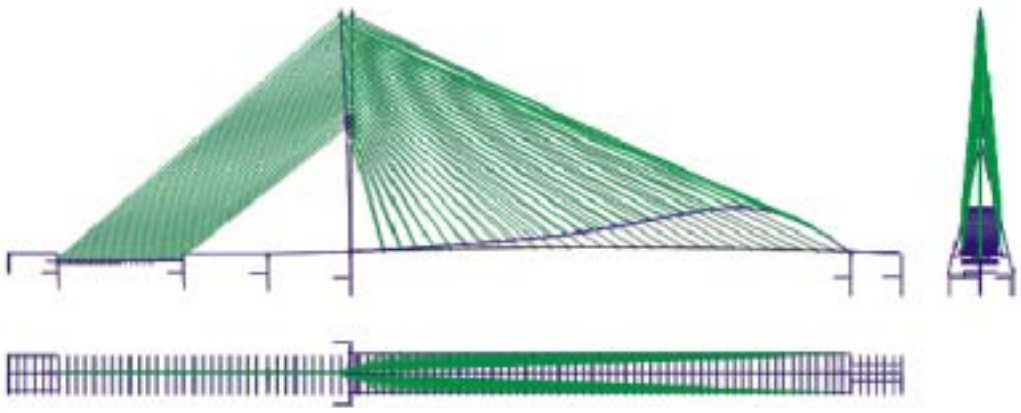

1st Vertical Mode (T=3.397 sec, f =0.294 Hz)

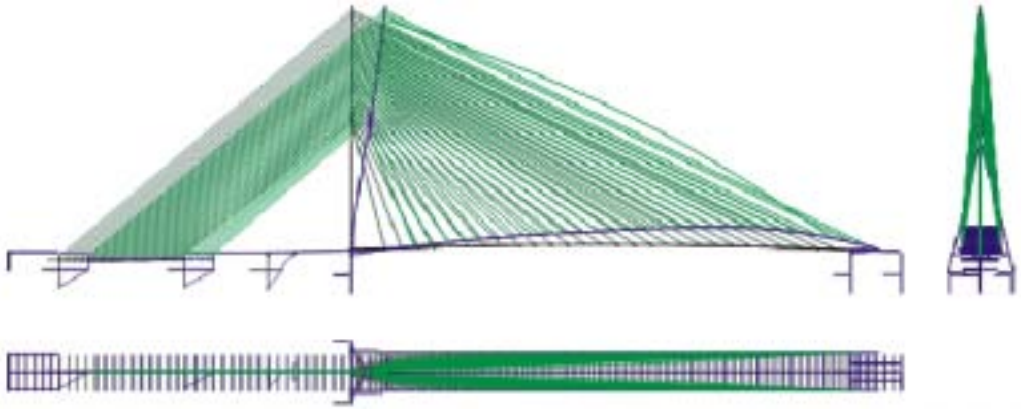

1st Longitudinal Mode (T= 2.774 sec, f =0.360 Hz)

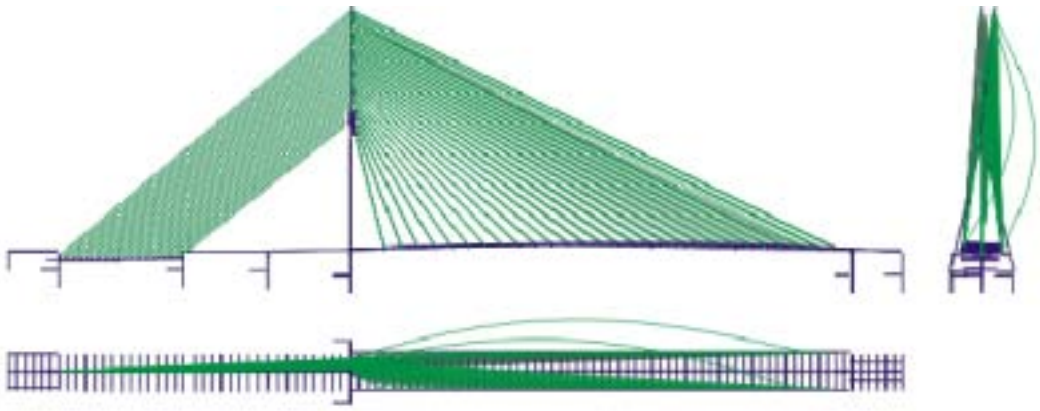

1st Transverse Mode (note tower top movement, T=2.562 sec, f =0.390 Hz)

Figure 124: Fundamental bridge modes.

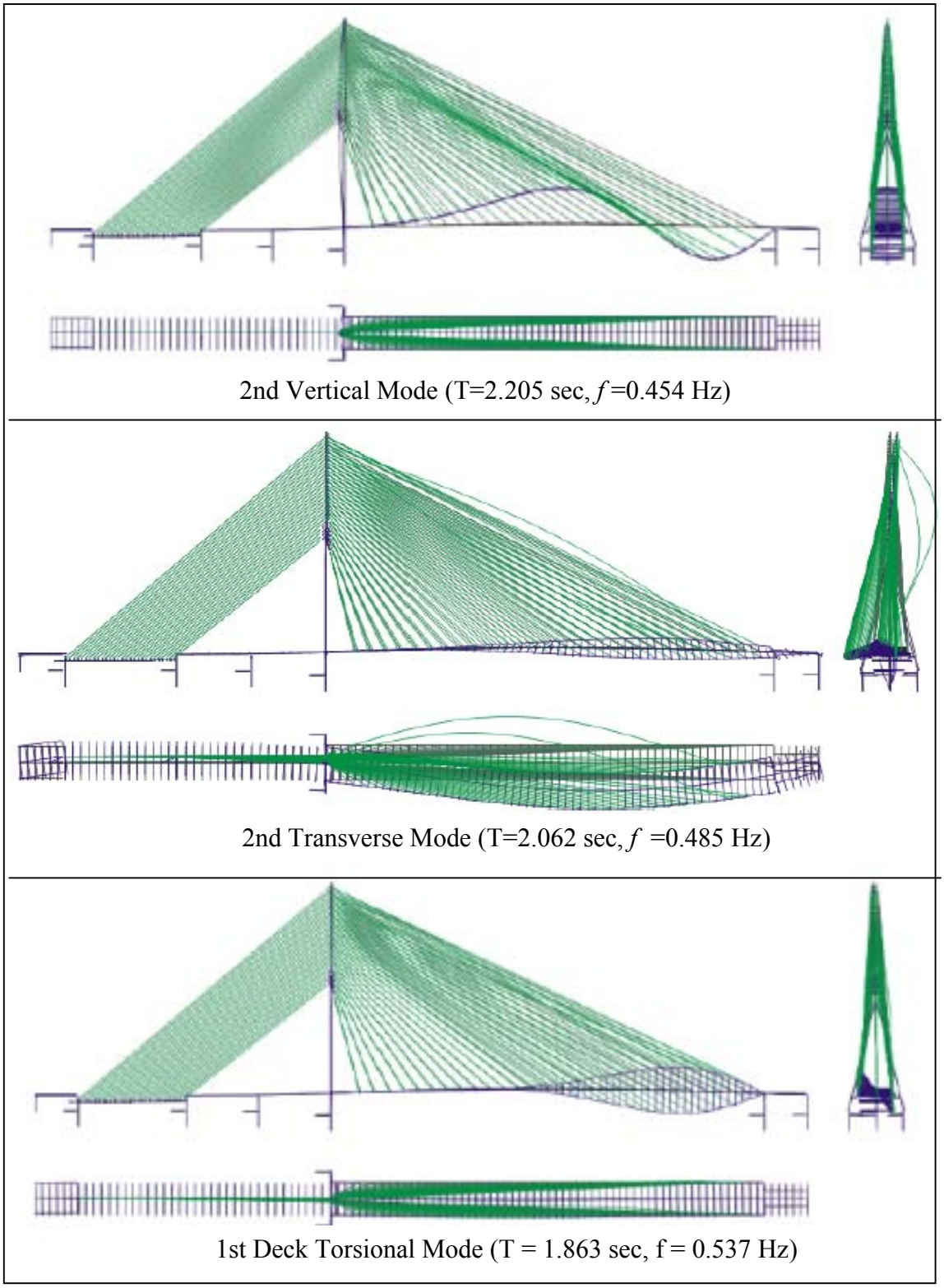

Figure 125: Additional bridge modes.

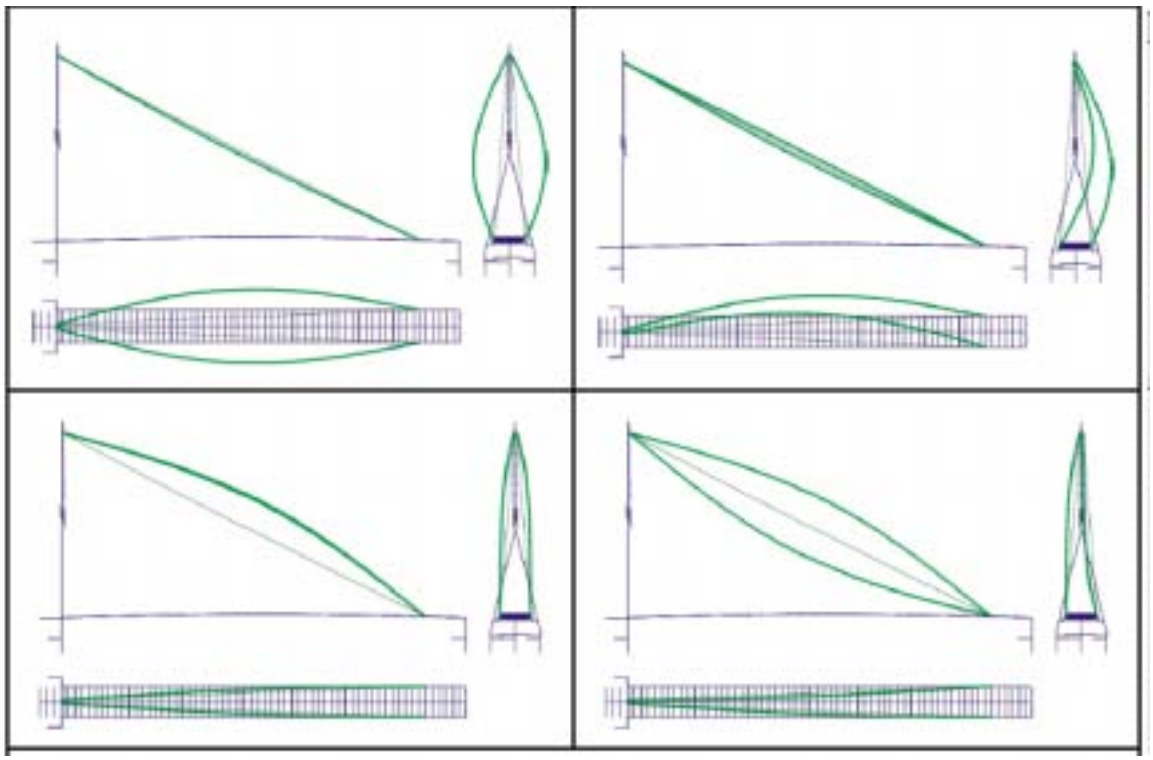

Figure 126: Four 'first' modes of the cables; XY, YZ & XZ views.

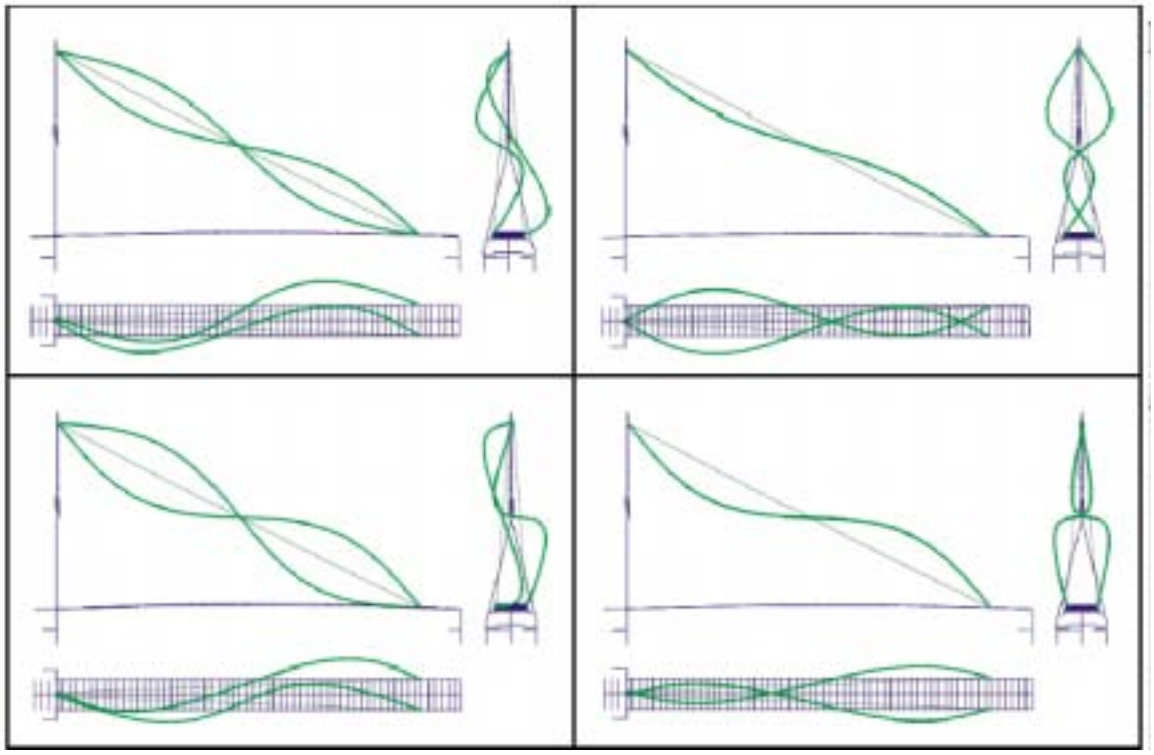

Figure 127: Four ‘second' modes of the cables; XY, YZ & XZ views.

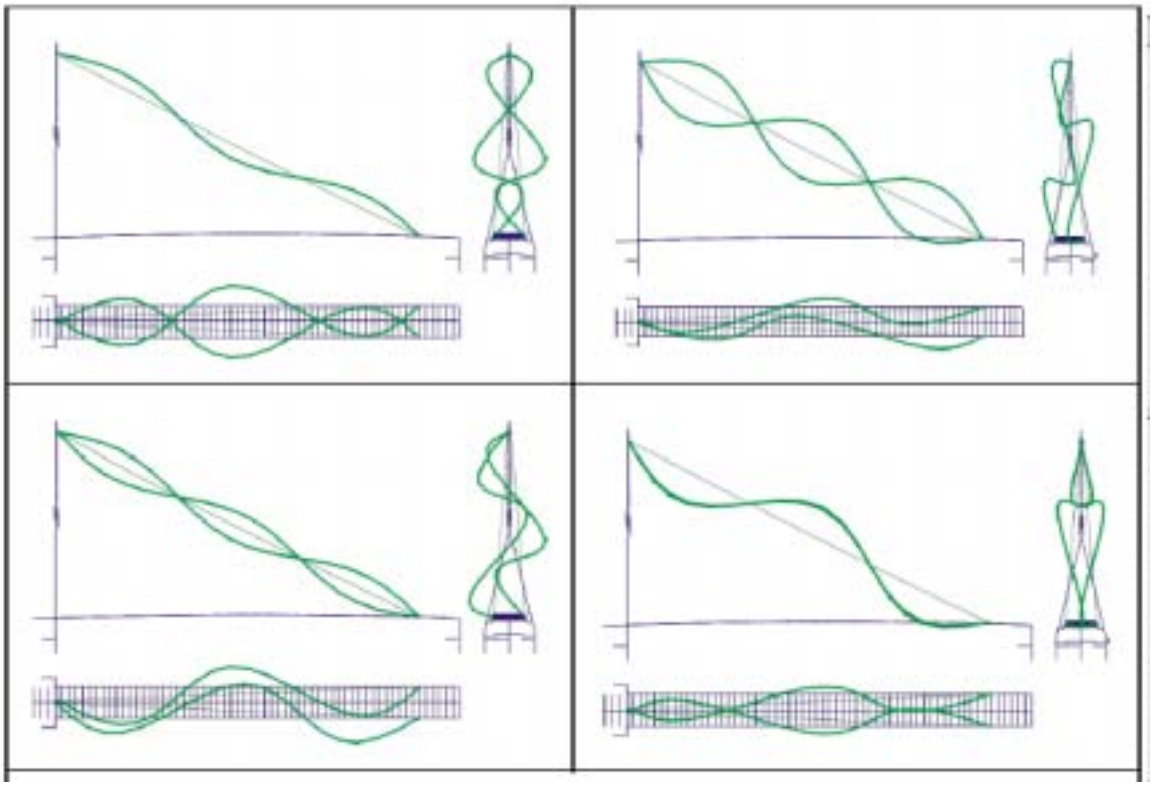

Figure 128: Four ‘third’ modes of the cables; XY, YZ & XZ views.

D2.3 STATIC LIVE LOAD ANALYSIS

Static live load analyses were performed using the influence line based program MELL and the train passage option of the bridge analysis program CAMIL, neglecting any dynamic properties of the train. For the latter program, the train live load was considered as a series of concentrated loads moving along the bridge over selected nodes. The train was treated as a static load and bridge dynamics were ignored so the bridge only responded statically to the train loading.

The live load used was a 5-car transit train. (A transit train was used because it represents a large moving load. Furthermore, the dynamic model for a transit train was used because it is more readily defined than a highway truck model, for which there are a large number of dynamic configurations). Each car weighed 369.5 kN, and thus the total weight of the train was 1847.5 kN. The train load was applied along the main span girder line. The dynamic allowance was taken as zero. Influence line analyses were performed using 200 (design accuracy) and 5000 (academic accuracy} steps (iterations) in the longitudinal positioning of the live load along the influence line to find the minimum and maximum effects due to live load. Computed results were tabulated for nodal deformations, girder member effects and main span cable forces and rotations at several locations, as identified in Figure 129.

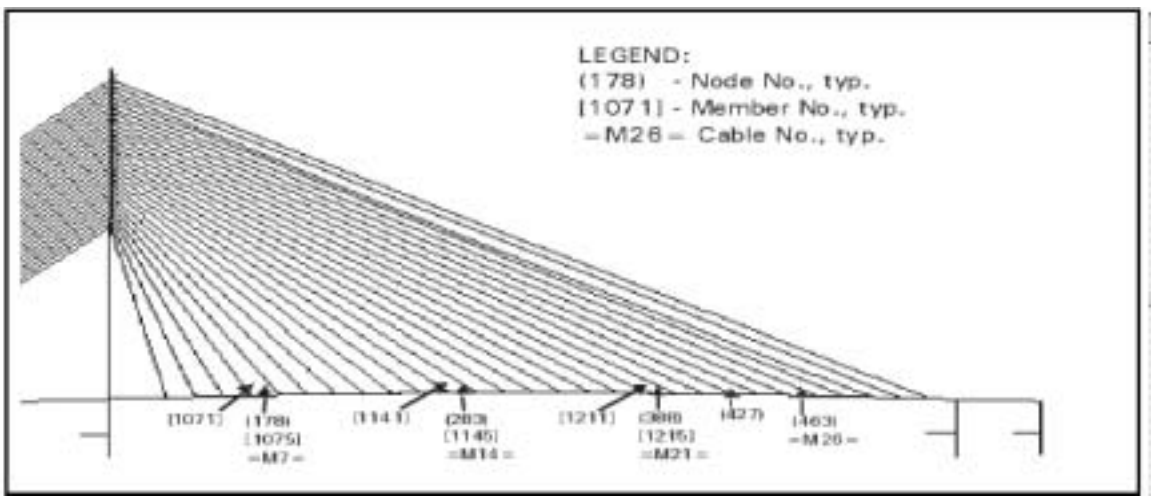

Figure 129: Nodes, members, and cables for comparison of results.

Displacements

Vertical displacement results are summarized in Table 21. Differences in results for displacements from analyses using 200 and 5000 calculation steps are practically nil. The differences between MELL's results and CAMIL's static train results are a maximum of 2.5%.

Table 21: Vertical displacements due to live load.

Vertical Displacements [mm]			
	Influence Line Analysis / Steps		TRAIN
NODE	200	5000	STATIC
178	-98	-98	-98
283	-183	-183	-186
388	-303	-303	-311
427	-332	-332	-340
463	-261	-261	-267

Bending Moments

Bending moment results are summarized in Table 22. Differences in results for bending moments from analyses using 200 and 5000 calculation steps are a maximum of 0.45%. The differences between MELL's results and CAMIL's static train results are a maximum of 3.4%.

Table 22: Bending moments due to live load.

Bending Moment (Strong Plane) [kNm]				
		Influence Line Analysis / Steps		TRAIN
	MEMB.	200	5000	STATIC
Max	1071	2845	2849	2900
	1075	2610	2646	2680
	1141	3984	3998	4010
	1145	3866	3883	3920
	1211	4564	4579	4650
	1215	4491	4511	4610
Min	1071	-2452	-2452	-2470
	1075	-2549	-2554	-2570
	1141	-3261	-3261	-3320
	1145	-3375	-3376	-3430
	1211	-1625	-1625	-1570
	1215	-1295	-1298	-1290

Cable Tensions

Cable force results summarized are in Table 23. Differences in results for cable forces from analyses using 200 and 5000 calculation steps are very small. The differences between MELL's results and CAMIL's static train results are a maximum of 0.55%.

Table 23: Cable forces due to live load.

Max Cable Force T1 [kN]				
		Influence Line Analysis / Steps		TRAIN
	MEMBER	200	5000	STATIC
Max	M7	269	269	270
	M14	322	322	324
	M21	391	391	393
	M26	230	230	230
Min	M7	-24	-24	-24
	M14	-14	-14	-14
	M21	-8	-8	-7
	M26	-20	-20	-20

Cable End Rotations

Cable end rotations, deck rotations and the relative differences between the two are summarized in Table 24. Differences in results from analyses using 200 and 5000 calculation steps are again practically zero. The differences in cable deck and relative rotations between MELL and CAMIL results are also very small.

Some differences exist between MELL's results and CAMIL's static train results for cable end rotations. The cable end rotations are not directly generated by the programs. Therefore they have to be computed according to the formula:

$$\Delta\theta_{LL} = \theta_{DL+LL} - \theta_{DL} = \text{atan}\left[\frac{V_{DL} + V_{LL}}{H_{DL} + H_{LL}}\right] - \text{atan}\left[\frac{V_{DL}}{H_{DL}}\right]$$

<u>where:</u>

- $\Delta\theta_{LL}$ - cable end rotation due to Live Load
- θ - cable angle to the horizontal plane
- V, H - Vertical and horizontal component of the cable force
- DL - Dead Load
- LL - Live Load

Since the cable end rotations are very small numbers, any small difference in calculating the V_{LL} and H_{LL} using MELL and CAMIL leads to small numbers that are close to each other in actual value but very different if expressed in percentages.

Table 24: Cable end rotations and deck rotations.

	ROTATIONS [deg]				
			Influence Line Analysis / Steps		TRAIN
	NODE	CABLE	200	5000	STATIC
Max Cable End Rotation	178	35	0.1319	0.1318	0.0917
	283	42	0.1894	0.1895	0.1423
	388	49	0.2458	0.2458	0.1907
	463	54	0.1572	0.1571	0.1369
Min Cable End Rotation	178	35	0.0065	0.0065	0.0000
	283	42	0.0017	0.0015	-0.0004
	388	49	0.0020	0.0020	0.0000
	463	54	-0.0048	-0.0047	-0.0044
Max Deck Rotation	178	35	0.1292	0.1293	0.1300
	283	42	0.1914	0.1915	0.1948
	388	49	0.2478	0.2478	0.2505
	463	54	0.0026	0.0027	0.0009
Min Deck Rotation	178	35	-0.0503	-0.0504	-0.0507
	283	42	-0.0971	-0.0971	-0.0975
	388	49	-0.1496	-0.1498	-0.1520
	463	54	-0.3446	-0.3447	-0.3536
Max (Cable - deck) Rotation	178	35	0.1822	0.1822	0.1015
	283	42	0.2865	0.2866	0.1841
	388	49	0.3954	0.3957	0.2635
	463	54	0.5018	0.5018	0.4802
Min (Cable- deck) Rotation	178	35	-0.1227	-0.1227	-0.0700
	283	42	-0.1897	-0.1899	-0.1073
	388	49	-0.2457	-0.2458	-0.1190
	463	54	-0.0074	-0.0074	-0.0003

D2.4 DYNAMIC LIVE LOAD ANALYSIS

Dynamic live load analyses were performed using the train option in the bridge analysis program. In this option, the train is considered as a dynamic moving load with its appropriate stiffness and damping parameters. Each train car is modeled as a mass (consisting of the car mass and the passengers mass) supported by springs and dampers that are fixed to bogies. Each bogie has its own unsprung mass and is supported by two axles. The axles transfer train load to nodes specified in the input file (usually main girder nodes). The dynamic response of the bridge due to the dynamic train loading was calculated using the Newmark's direct integration procedure.

Damping

For the structure's damping matrix calculation, the Rayleigh damping coefficients α and β were determined using frequencies of the 1st and the 15th bridge natural mode. The damping ratio at those two frequencies was set at 0.75% of critical. The variation of damping with frequency corresponding to the above criteria is shown with a heavily solid line in Figure 130. This figure also shows the damping distributions which would have resulted from picking 1st and 2nd or the 1st and 22nd modes to define the damping. The figure clearly indicates that for the frequency range of interest an acceptable damping distribution is achieved.

$\rho = 0.75\ \%$, $\omega_1 = 1.850$ rad/s, $\omega_{15} = 5.389$ rad/s

$$\alpha = 2\rho\frac{\omega_1 \quad \omega_{15}}{\omega_1 + \omega_{15}} = 0.02066 \qquad \text{and } \beta = \frac{2\rho}{\omega_1 + \omega_{15}} = 0.00207$$

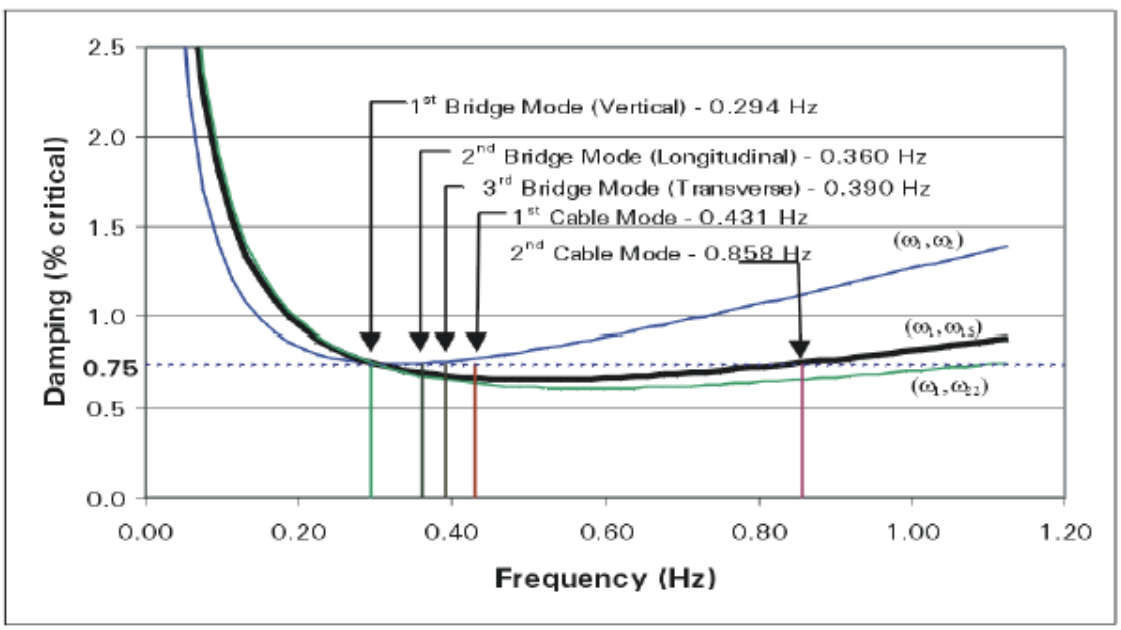

Figure 130: RAMA 8 Bridge Model Damping vs. Frequency.

Results for Train speed of 80 km/hr

The results obtained for a train speed of 80 km/hr are discussed in this section. The results for other train speeds are outside the scope of this study.

Deck Displacement Time Histories

The displacement time histories for both the static and dynamic load cases for node 427 (near the 3/4 span location of the main span) are shown in Figure 131. (This load case ignores dynamic effects and only captures the effect of the moving load position.) This figure shows that the dynamic displacement was only slightly larger than the static displacement. Furthermore, the bridge deck oscillations, which occurred after the train had left the bridge (the train has completely left the bridge at 20 seconds into the time history), were small in comparison to the static response. This figure also displays the velocity and acceleration records corresponding to the displacement time history.

The velocity record shows some higher frequency oscillations in the 15 second range which correspond to the individual cars leaving the bridge. As the first set of bogies left the bridge by moving across the pin joint at the end of the main span, the slope discontinuity set up pitching motions that were fed back to the structure via the second set of bogies. This phenomena can also be observed in the acceleration time history, which shows a base line acceleration corresponding to the static displacement and the accelerations due to the train superimposed until the train left the bridge.

Deck Girder Bending Moment Time History

The static and dynamic bending moment time histories for a deck girder member are shown in Figure 132. This figure shows that there was very little amplification due to dynamic effects. Both the static and dynamic time histories show oscillations in the maximum bending moment due to the passing of individual train cars. The dynamic moments after the train had left the bridge are negligible when compared to the static moments.

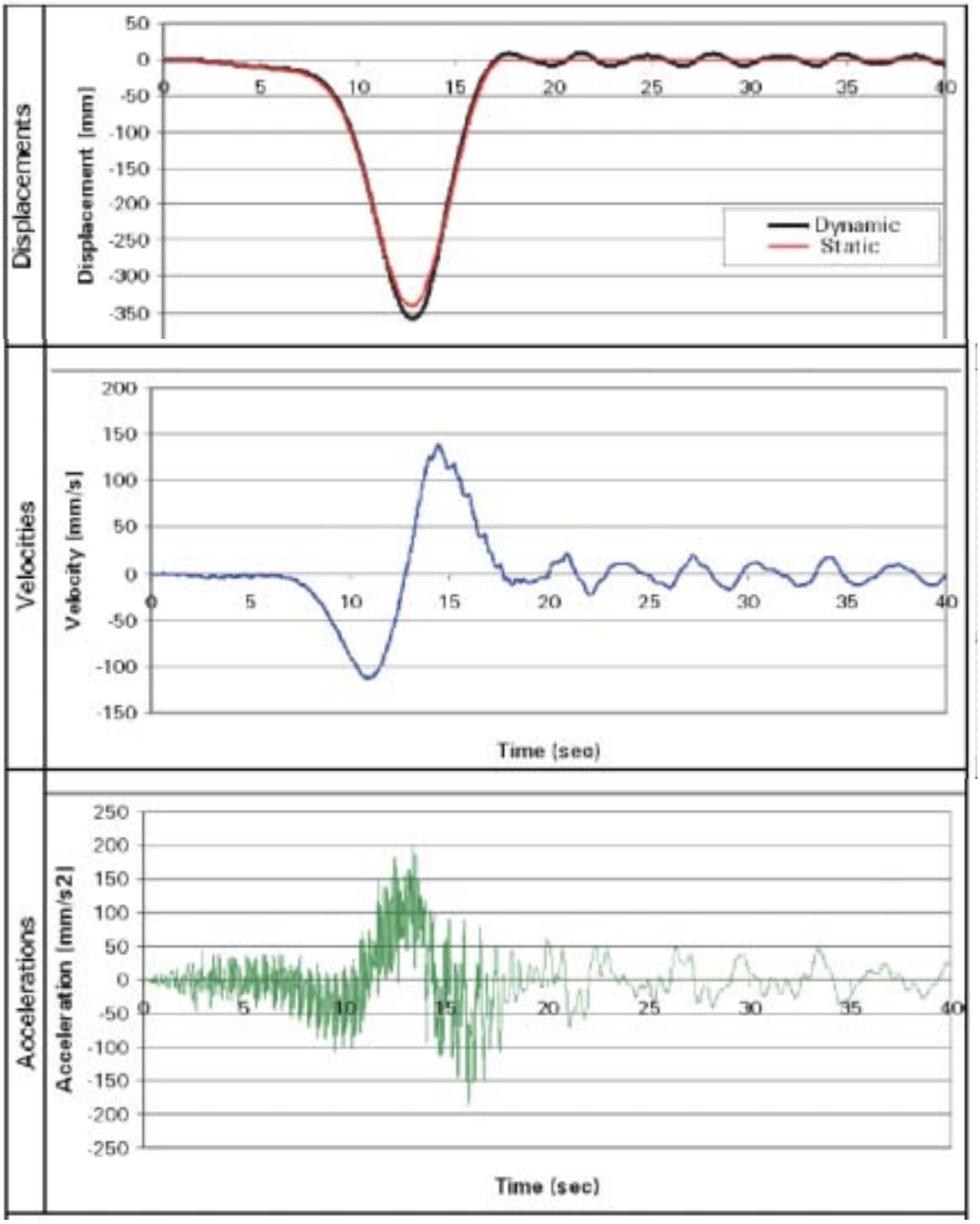

Figure 131: Vertical Displacements, Velocities, and Accelerations of Node 427 vs. Time. Train speed 80 km/h.

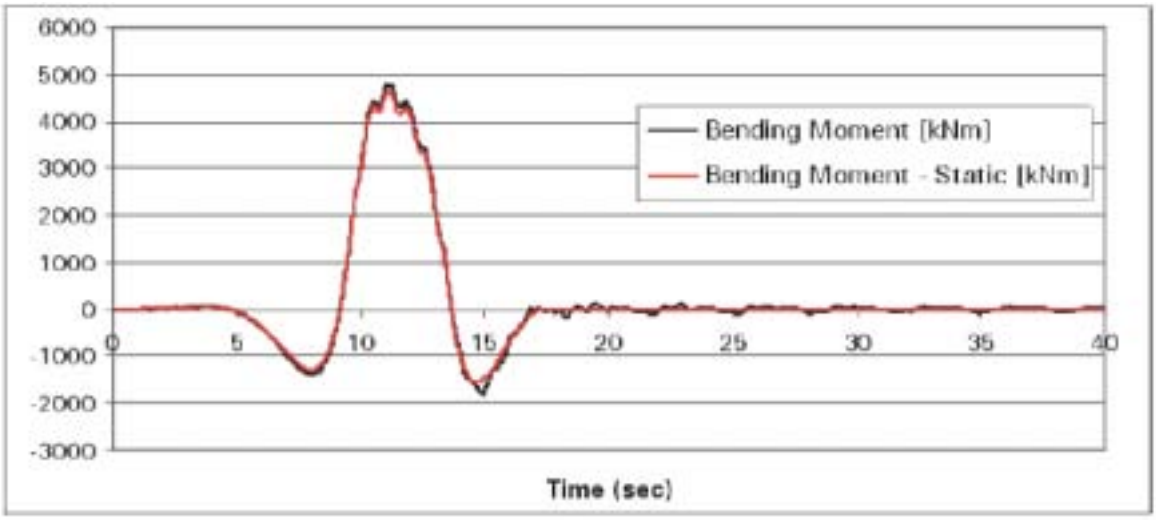

Figure 132: Member 1211; Bending Moment vs. Time. Train speed 80km/h.

Cable Tension Time Histories

The total cable force versus time diagram for a train speed of 80 km/hr is shown in Figure 133. The dynamic time history has the same shape as the static time history, but there are slightly larger maxima and minima due to dynamic effects. This figure also shows the maximum and minimum obtained from the influence line analysis.

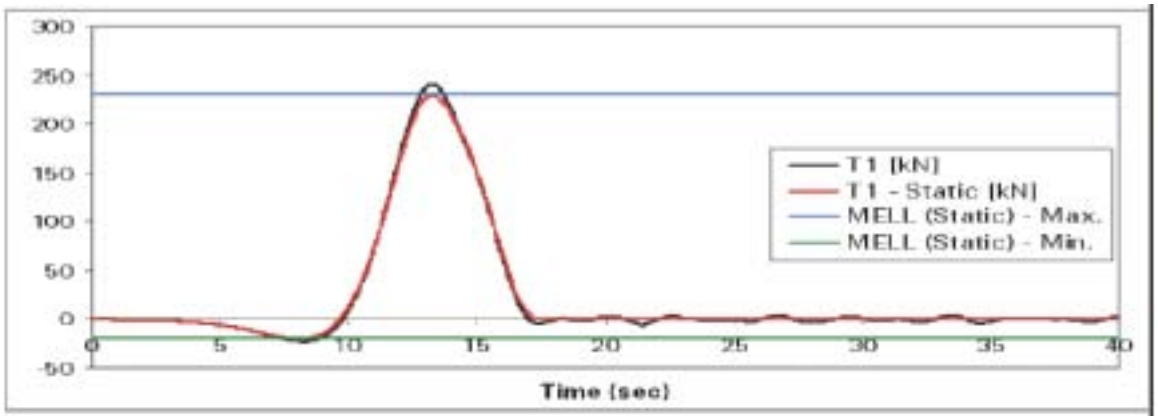

Figure 133: Cable M26, Tension vs. Time. Train speed 80 km/hr.

The difference in cable tension for cable M26 between the dynamic train load case and static train load case, for train speed 80 km/h, is shown in Figure 134.

The tension spectrum for cable M26 is shown in Figure 135. This spectrum was generated from the part of the cable tension time history which corresponds to the time after the train has crossed

the bridge, i.e. to the cable tension time history due to free bridge vibration, 20 seconds of elapsed time.

The two dominant peaks in the cable tension spectrum are at 0.3 Hz and 0.44 Hz. The first peak corresponds to the first vertical deck mode (0.294 Hz) which is the dominant mode in the structure's response. The second peak corresponds to a mixture of the second deck mode (0.454 Hz) and the first cable modes (in-plane and out-of-plane) at 0.44 Hz. Since these two modes are closely spaced, it is not possible to clearly separate them with the relatively short displacement time history obtained from the dynamic analysis.

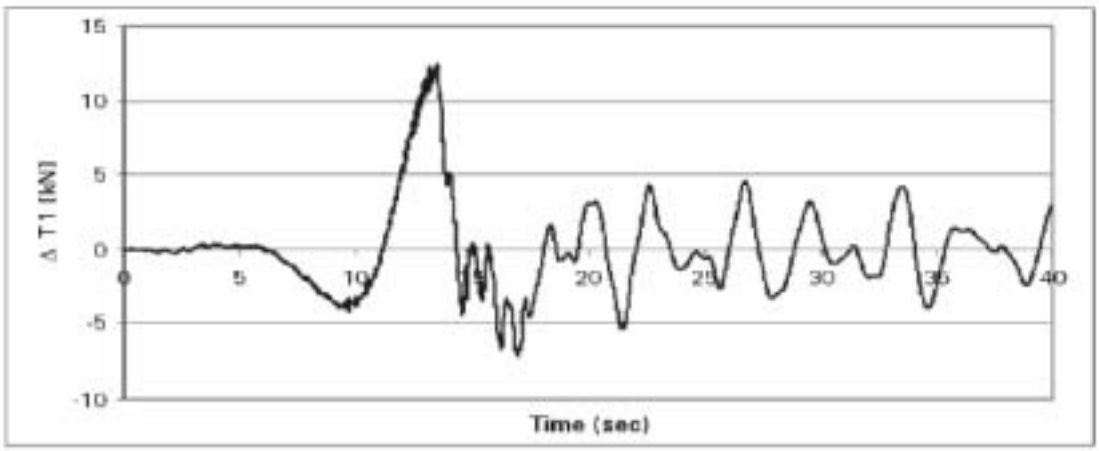

Figure 134: Difference in cable tension for cable M26 between the dynamic train load case and static train load case vs. Time. Train speed 80 km/h.

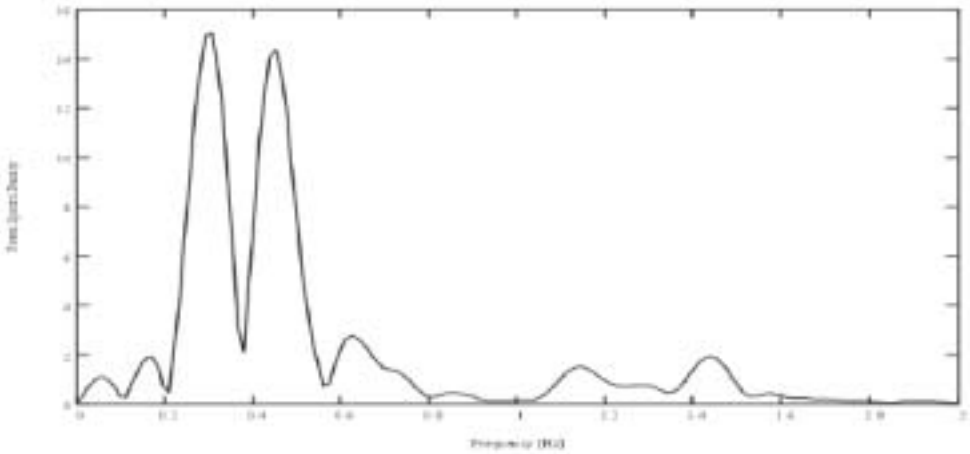

Figure 135: Cable M26 Tension Spectra. Train speed 80 km/h.

Cable Displacement Time Histories

Displacements in Global Coordinates

The displacements of the cable were obtained at the following five locations:

- tower end
- 1/4 span, close to the tower end of the cable
- 1/2 span, mid span of the cable
- 3/4 span, close to the deck end of the cable
- deck end

The x, y, z (x = along the bridge axis, y = transverse and z = vertical) displacement time histories are shown in Figure 136. The x and z displacements clearly show one dominant displacement cycle corresponding to the 'static' deformation of the deck followed by a series of vibration cycles, which are an order of magnitude smaller. Only the transverse displacement, which is much smaller to start with, shows free vibration oscillations that are comparable to the static deformations. However, the free vibration oscillations in this direction are not significantly larger than the free vibration oscillations in the other two directions. To study the cable vibrations in more detail, the records were transformed into the cable's local coordinate system as outlined in the next section.

Displacements in Local Coordinates

The cable displacements computed from the dynamic analysis were transformed from global x, y, z coordinates to local cable coordinates u, v, w, (u = along the cable, v = normal to the cable plane, w = orthogonal to both u and v). The transformation of coordinates systems (as depicted in Figure 137) was carried out using the following formulation:

Given that $\alpha = 2.15124$ deg is the cable angle in horizontal plane and $\beta = 26.95322$ deg is the cable chord angle to horizontal plane the transformation of displacements into cable plane is

$$\xi = x * \cos\alpha - y * \sin\alpha \qquad \text{and} \qquad \eta = x * \sin\alpha - y * \cos\alpha$$

and finally the transformation to displacements along and perpendicular to the cable is:

$$u = \xi * \cos\beta - z * \sin\beta, \qquad v = \eta \qquad \text{and} \qquad w = \xi * \sin\beta - z * \cos\beta$$

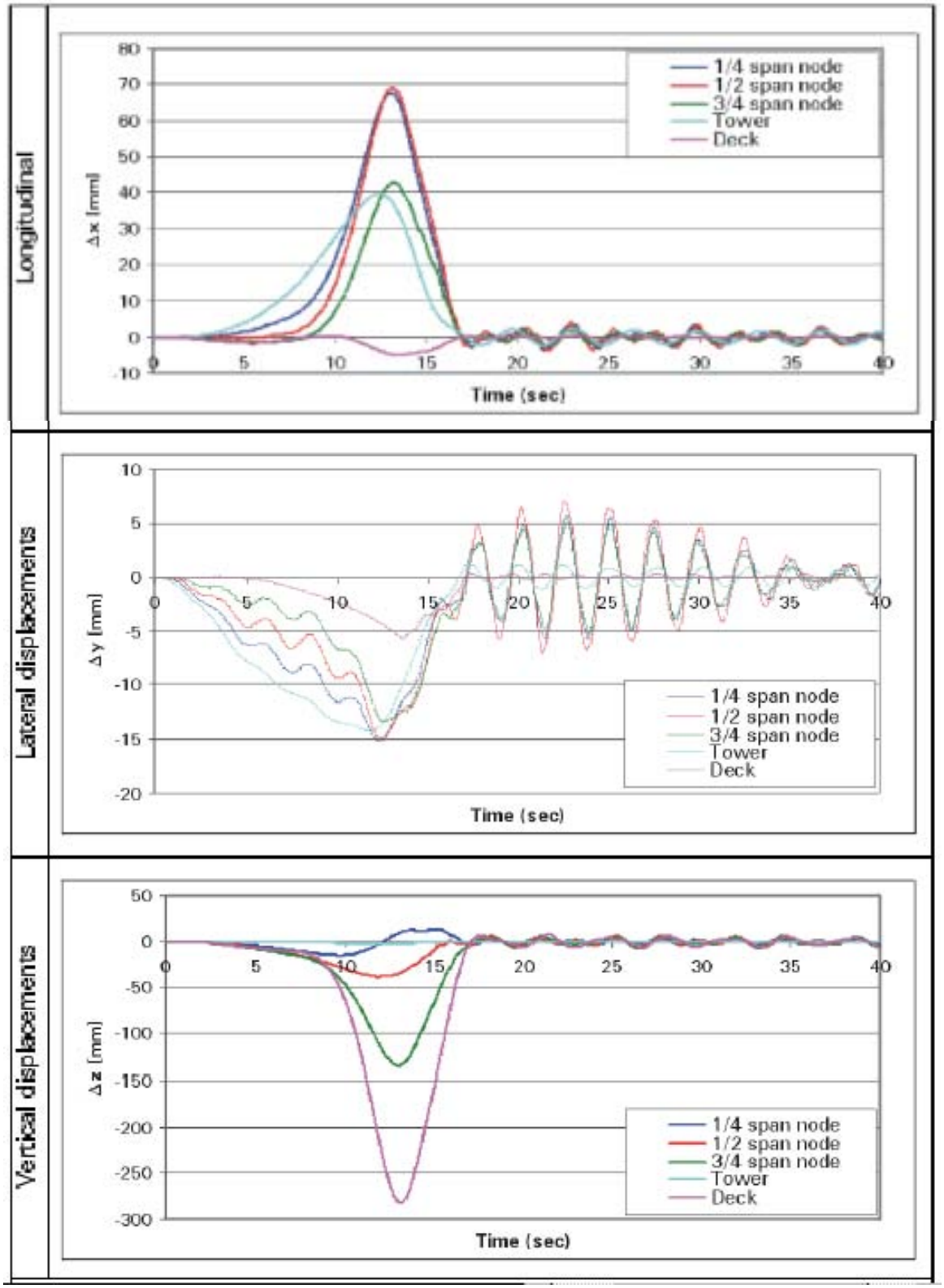

Figure 136: Global Coordinate Displacements of Cable M26 Nodes [mm] vs. Time. Train speed 80 km/hr.

The displacement records of the cable corresponding to the following three locations were analyzed:

- 1/4 span, close to the tower end of the cable
- 1/2 span, mid span of the cable
- 3/4 span, close to the deck end of the cable

These converted displacement records were plotted in both the cable plane (in- plane) and in a plane normal to the cable cord line (out-of-plane), These displacement traces are shown for the three cable locations in Figure 138. The out-of-plane deformation shows that the top of the cable actually moves up as the sag is reduced, while the bottom of the cable moves down with the deck and the center of the cable shows little movement as the deck deformation and sag reduction cancel each other. The transverse motion, which can be clearly observed in all three out-of-plane traces, results from the transverse movement of the bridge tower and deck. The in-plane movements also reflect this interaction of sag reduction and tower and deck deflection.

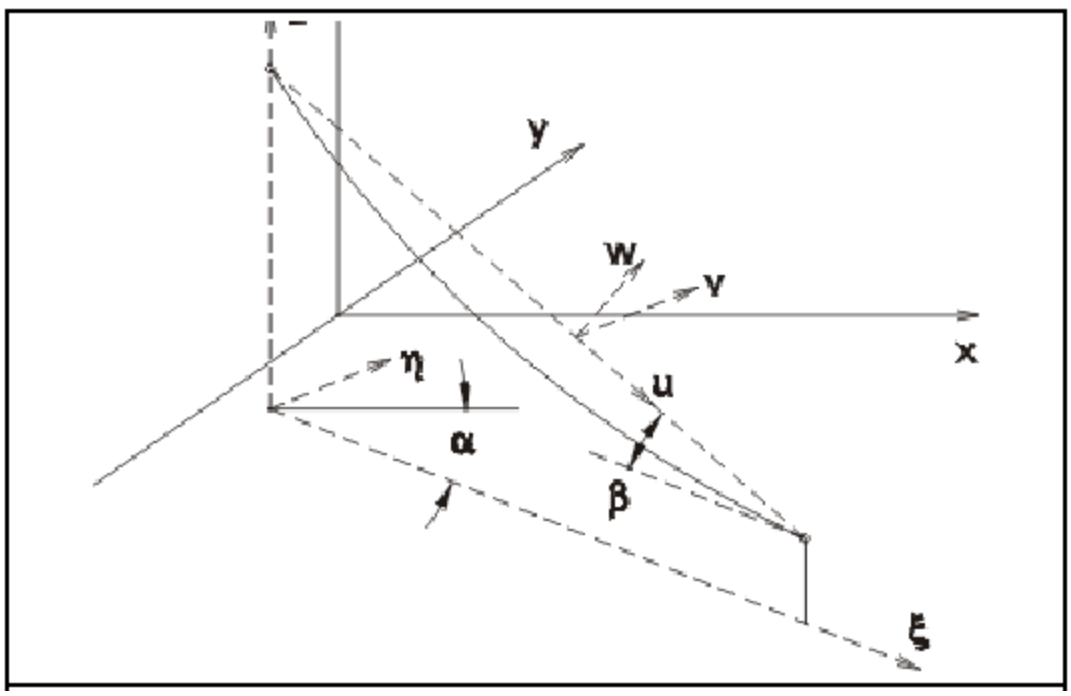

Figure 137: Transformation from global coordinates to coordinates along the cable.

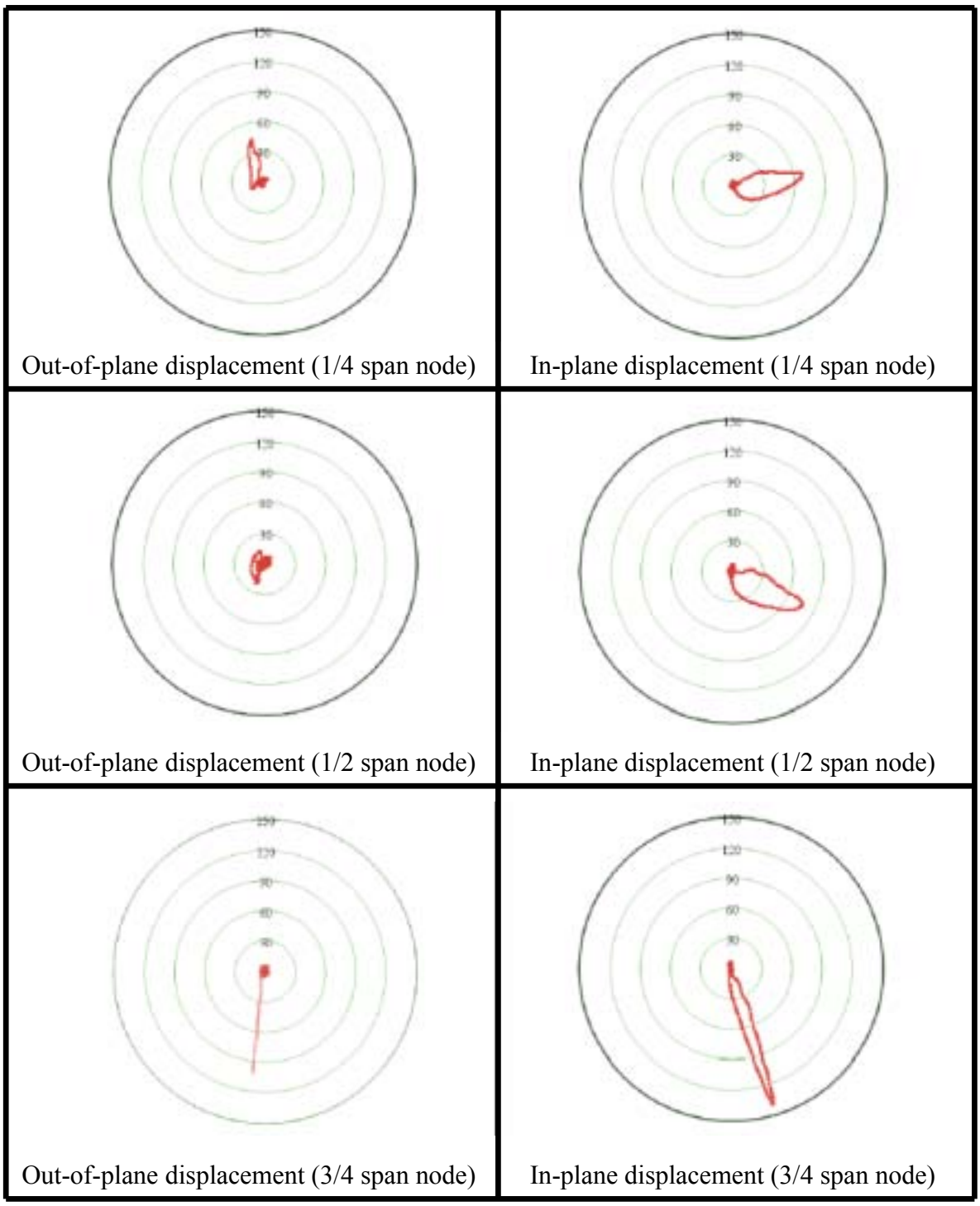

Figure 138: Local Coordinate Displacements of nodes of cable M26 [mm]. Displacements are shown for 3 nodes of the cable: at 1/4 span (closer to the tower), 1/2 span and 3/4 span (closer to the deck). Train speed 80 km/h.

Frequency Content of the Cable Displacement:

The portion of the displacement time history which corresponds to free vibration (after the train has left the structure), was used to generate Fourier spectra in order to assess the frequency content of the displacement. Since the time histories were not periodic within the record, they were windowed using a combination of a extended cosine and exponential window, in order to minimize spectral leakage. This means that the resulting spectra can not readily be used to estimate the damping in the individual modes. (This is of little concern because the damping value corresponding to 0.75% of critical damping was derived and used in the analysis). The resulting spectra for the cable displacement in the u, v, and w coordinates are shown in Figure 139.

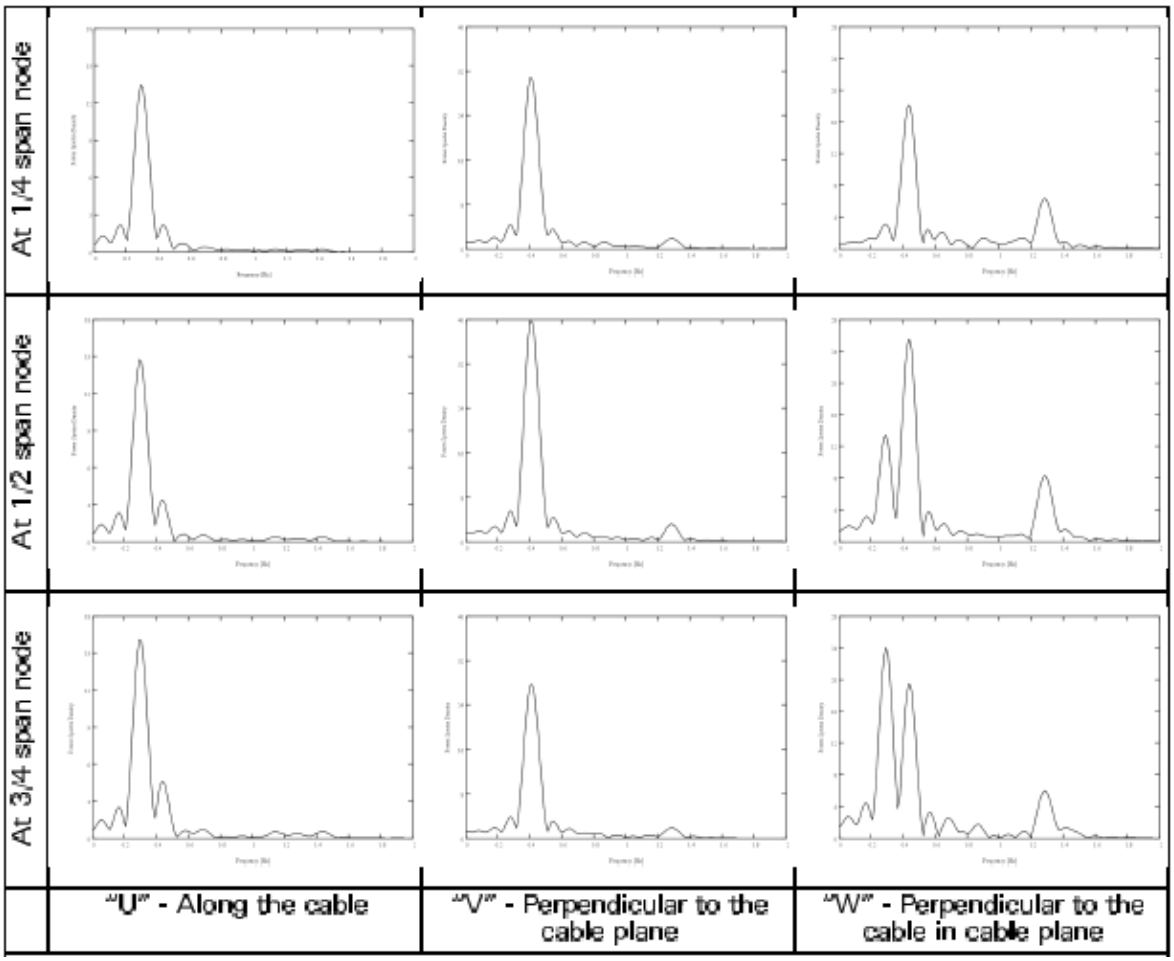

Figure 139: Spectra for movements of cable M26 nodes: at ¼ span (closer to the tower), ½ span, and ¾ span (closer to the deck). Frequency range 0 – 2 Hz, train speed 80 km/h.

The modes of vibration which are reflected by the spectral peaks shown in Figure 139 are:

- 0.29 Hz, first vertical mode
- 0.39 Hz, first transverse mode {with tower dominant motion)
- 0.43 Hz, out-of-plane modes of cables M26
- 0.44 Hz, in-plane modes of cables M26
- 0.45 Hz, second vertical mode of the deck
- 0.86 Hz, second mode of vibration of M26 cables
- 1.26 Hz, sixth vertical mode of the deck
- 1.28 Hz, third mode of vibration of M26 cables

The spectra for the u displacements (along the cable) at all three cable locations are dominated by the first vertical mode of the deck. The spectra for the v displacements (out of the cable plane) at all three cable locations are dominated by the first transverse mode of the structure. The spectra for the w displacements (perpendicular to the cable in the cable plane) at all three cable locations show a significant peak at 0.43 Hz. The mid span and 3/4 span (near the deck) location also exhibit a strong peak at 0.29 Hz corresponding to the first vertical mode of the bridge deck. Furthermore, all three locations show a spectral peak corresponding the sixth vertical mode of the deck at 1.26 Hz or the third mode of vibration of the cable at 1.28 Hz.

Cable End Rotations

Cable end rotations are often of interest in fatigue studies as they influence the bending stress ranges in the anchorage zones. These rotations are comprised of two components: the rotation of the cable end due to changes in sag as a result of increased or decreased load, and the cable anchorage rotations which are a caused by deck deflections. Both of these rotation components do not typically achieve their maximum amplitude at the same time. The individual rotation components as well as the total relative rotation (heavy solid line) between the cable and the anchorage are shown for Cable M26 in Figure 140. This figure also shows the maximum rotations computed using the influence line approach, which corresponds relatively well to the results obtained from the dynamic analysis. In contrast, the cable end rotations and deck rotation obtained for Cable M21, shown in Figure 141, display quite a different pattern and clearly show that the maximum relative rotation (heavy solid line) can not be approximated reliably by simply adding the maxima of the individual components.

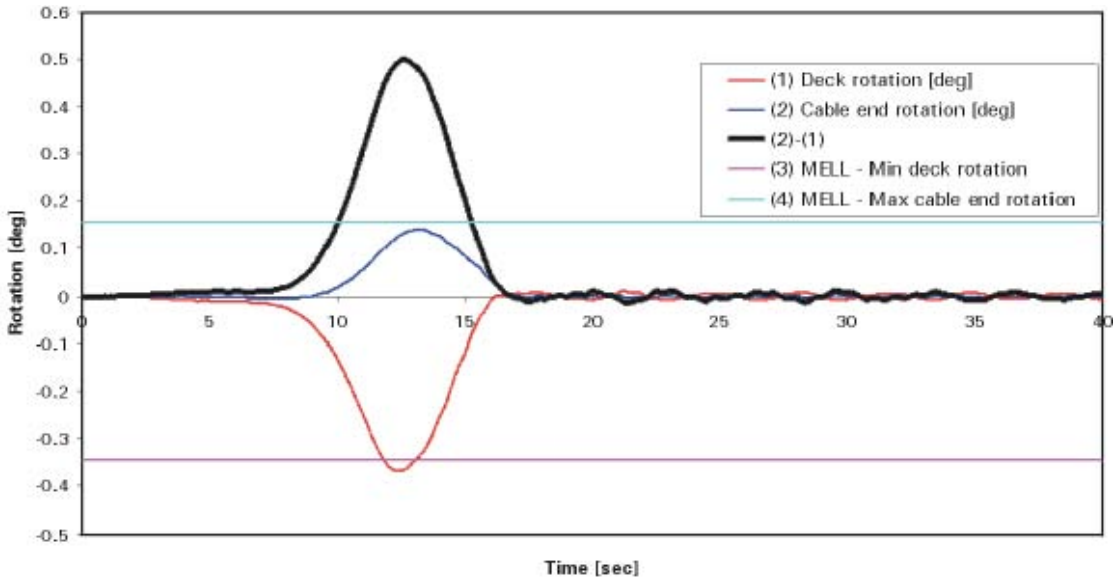

Figure 140: Deck rotations and cable end rotations for cable M26 – dynamic (train speed 80 km/h) and static

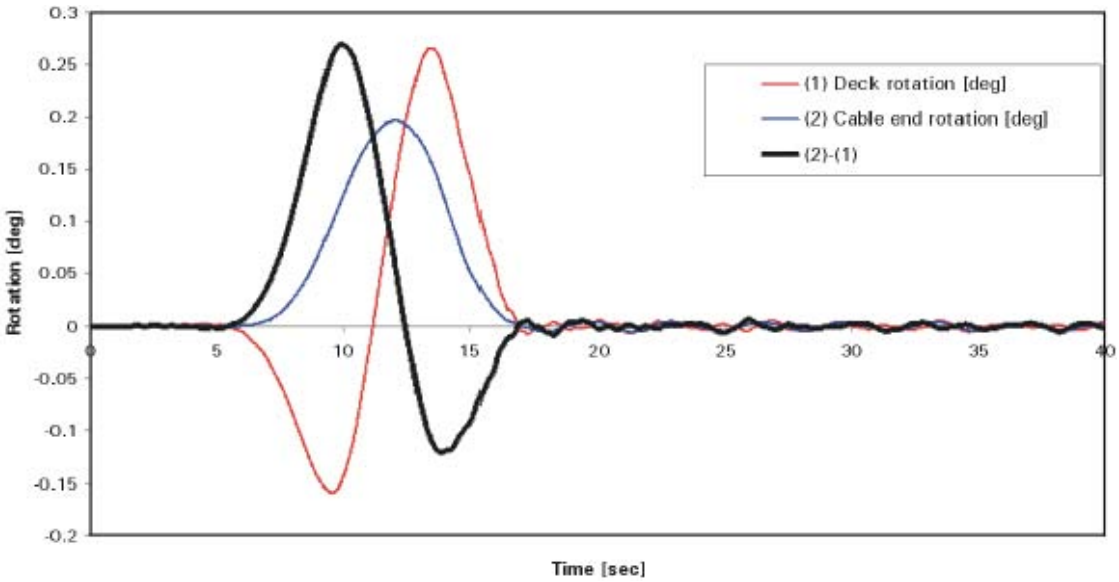

Figure 141: Deck rotations and cable end rotations for cable M21 – dynamic (train speed 80 km/h) and static.

D2.5 CONCLUSIONS

Using the model of an actual cable-stayed bridge, the cable vibration and moving live load analysis carried out as part of this study indicate that:

- A stay-cable which is discretized with twenty element accurately predicts the free vibration characteristics of a stay-cable.

- Once the cable is modeled as part of the complete structure with the tower and the deck providing realistic end conditions, the cable frequencies only change slightly but the mode shapes become spatial rather than being purely in-plane or out-of-plane.

- The cable tensions, displacements and end rotations are dominated by the 'static' deformation response associated with the moving load's passing and subsequent dynamic oscillations are typically an order of magnitude smaller than the static maximum.

- The increase in maximum cable tension due to dynamic effects is less than 10% for the 80 km/hr passing speed.

- The dynamic response of the cable, during the train passage and in the sub- sequent free vibration phase, is driven by the vibration of the bridge deck.

APPENDIX D3: STUDY OF USER COMFORT

Overview

In addition to the concerns regarding fatigue and other stress related issues due to cable vibration, it may also be important that the users of the bridge feel comfortable with any visible cable movements. A design criterion set forth by these factors would be independent of those required by the structural effects involved, similar in nature to existing codes limiting deflection in bridges or drift in tall buildings.

A survey was performed to determine at what limits users will no longer feel comfortable crossing a bridge either as a pedestrian or as a driver. Video models were created using 3D Studio to simulate various cable vibration scenarios. These videos were shown to fifty users who were asked to indicate their comfort level with crossing the bridge under these circumstances. The parameters varied in the models were mode of vibration, amplitude, and velocity of oscillations.

The following charts will demonstrate the results of the survey. User comfort was rated from 1 to 5, with 1 being the most comfortable and 5 being the least comfortable. The breakdown of the ratings was described to the users as follows:

1 - Vibrations are not noticeable or barely noticeable, I have no concerns with the safety of the bridge.
2 - Vibrations are noticeable, but I have little or no concern about the safety of the bridge.
3 - Not sure
4 - Vibrations are very noticeable, I have some concern about the safety of the bridge, but I would probably still cross it.
5 - Vibrations are excessive, I have major concerns about safety and will not cross the bridge.

Mode Shape

The following chart shows the effect of mode shape on user comfort. Users were shown videos with constant amplitude and frequency, with the mode shape varying from first to third. It was largely determined that mode shape does not play a significant role in affecting the user's comfort level.

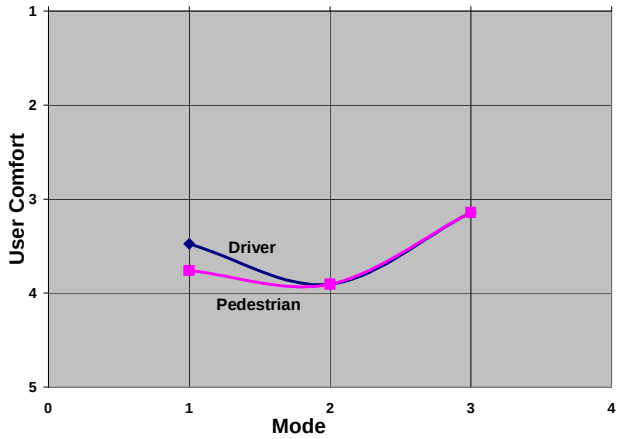

Figure 142: Effect of mode (constant amplitude and velocity).

Velocity

The next parameter tested was velocity. The amplitude and mode shape of the vibrations were held constant while the frequency was varied from 0.5 Hz to 2 Hz. The results indicate that users had strong reservations when frequencies were higher than 1 Hz, but they quickly became more comfortable when the frequency dropped below 1 Hz. It should be noted that the high level of concern demonstrated across all the simulations for this parameter is most likely due to the fact that too high of an amplitude was chosen as the constant. Nevertheless, this should have little effect on the shape of the distribution, just where it is located on the Y axis.

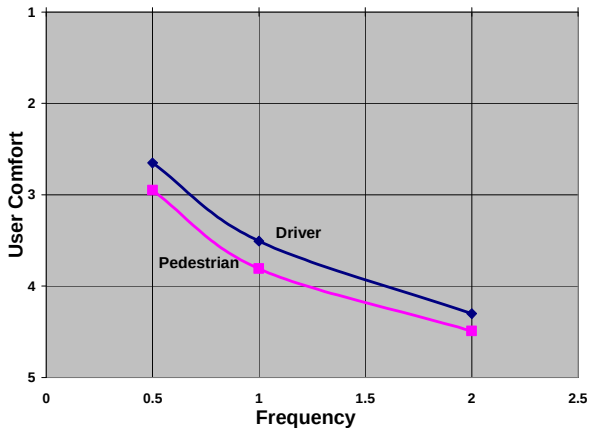

Figure 143: Effect of velocity (constant amplitude).

Amplitude

The final parameter tested was amplitude. Videos were shown that simulated vibrations with a constant velocity and constant mode shape, while amplitude was varied from 0.5 diameters to 2 diameters. The results indicate that at a point near 1 diameter vibration amplitude, the user begins to feel uncomfortable crossing the bridge. Below 1 diameter, this concern trails off quickly. The graph below does indicate that users were more comfortable with oscillations of 2 diameters than those of 1 diameter. This was dismissed as an anomaly caused by the number of videos that had been shown at this point in the survey, and the order in which the videos were shown.

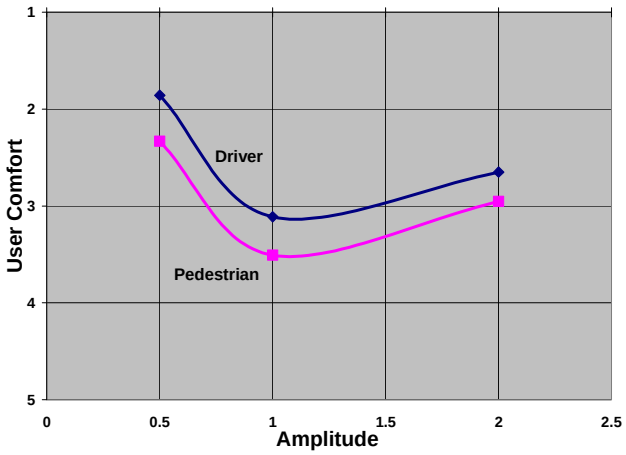

Figure 144: Effect of amplitude (constant velocity).

Conclusion

The two most important factors affecting user comfort are the amplitude of the vibration and the velocity. As the frequency range is somewhat limited, it would stand to reason that the comfort criteria could be based on the amplitude. According to this study, a reasonable recommendation of a limit on vibration amplitude would be 1 cable diameter. Ideally, further reducing this to 0.5 diameters or below has the effect of making the vibrations virtually unnoticeable. This study is preliminary, and based on a relatively small sample size, therefore further investigation should be performed to refine any design criteria based on user comfort. Also, while the above charts indicate that there isn't a significant difference in the perception of safety for a pedestrian and for a driver, this is probably not accurate and the difference could be established by producing a "driver" video that includes a moving viewpoint and other roadway distractions. This difference is important in that it would establish tighter criteria for bridges in urban areas or with pedestrian walkways compared to a more liberal criteria for rural locations with no pedestrians.

REFERENCES

Abdel-Ghaffar, A. M., & Khalifa, M. A. (1991). Importance of cable vibration in dynamics of cable-stayed bridges. *Journal of Engineering Mechanics, ASCE, 117*(11), 2571-2589.

Blevins, R. D. (1977). *Flow-induced vibration*, John Wiley and Sons.

Bosdogianni, A., & Olivari, D. (1996). Wind- and rain- induced oscillations of cables of stayed bridges. *Journal of Wind Engineering and Industrial Aerodynamics, 64*, 171-185.

Caracoglia, L. & Jones, N. P. (2002a). In-plane dynamic behavior of cable networks. I: Formulation and closed-form solutions. *Journal of Sound and Vibration* (in review).

Caracoglia, L. & Jones, N. P. (2002b). In-plane dynamic behavior of cable networks. II: Prototype prediction and validation.. *Journal of Sound and Vibration* (in review).

Carne, T. G. (1981). Guy cable design and damping for vertical axis wind turbines. *SAND80-2669,* Sandia National Laboratories, Albuquerque, NM.

Connors, H. J. (1970). Fluidelastic vibration of tube arrays excited by cross flow. Winter Annual Meeting of the ASME, New York.

Cooper, K. R. (c.1985). A note on the wind induced vibrations of bundled bridge stay cables. National Research Council of Canada, Note provided to RWDI..

Davenport, A. G. (1995). The dynamics of cables in wind. *Proceedings of Symposium on Cable Dynamics*, Liege, Belgium, Oct. 1995.

Davis, D. A., Richards, D. J. W., & Scriven, R. A. (1963). Investigation of conductor oscillation on the 275 KV crossing over the River Severn and Wye. *Proc I.E.E.* (110), pp.205-219.

Dean, D. L. (1962). Static and dynamic analyses of guy cable.s *Transactions, Paper 3375, Volume 127, Part II*, American Society of Civil Engineers.

Den Hartog, J. P. (1932). Transmission line vibration due to sleet. AIEE Transaction (51), pp. 1074-1076.

Ehsan, F., & Scanlan, R. H. (1990). Damping stay cables with ties. *Proceedings of the 5th US-Japan Bridge Workshop*, 203-217.

Ehsan, F., Scanlan, R. H. & Bosch, H. R. (1990). Modeling spanwise correction effects in the vortex-induced response of flexible bridges. *Journal of Wind Engineering and Industrial Aerodynamics, Vol. 36*.

Flamand, O. (1994). Rain-wind induced vibration of cables. *Proceedings of the International Conference on Cable-stayed and Suspension Bridges (AFPC)*, Deauville, France, Oct. 1994, 2, 523-531.

Geurts, C., Vrouwenvelder, T., Staalduinen, P., & Reusink, J. (1998). Numerical modeling of rain-wind-induced vibration: Erasmus Bridge, Rotterdam. *Structural Engineering International, SEI 8*(2), 129-135.

Gimsing, N.J. (1983). *Cable supported bridges - concept and design.* New York: John Wiley & Sons.

Gimsing, N.J. (1997). *Cable supported bridges – concept and design. 2nd ed.*, John Wiley & Sons.

Hardy, C., & Bourdon, P. (1979). The influence of spacer dynamic properties in the control of bundle conductor motion. IEEE PES Summer Meeting, Vancouver, British Columbia, Canada, July 1979.

Hardy, C., Watts, J. A., Brunelle, J., & Clutier, L. J. (1975). Research on the dynamics of bundles conductors at the Hydro-Quebec Institute of Research. Trans. E.&O. Div., CEA, Vol.14, Part 4.

Hikami, Y. (1986). Rain vibrations of cables of cable stayed bridge. *Journal of Wind Engineering*, JA WE, No.27 (in Japanese).

Hikami, Y., & Shiraishi, N. (1987). Rain-wind induced vibrations of cables in cable stayed bridges. Seventh International Conference on Wind Engineering, Aachen, Germany, 1987, 293-302.

Hikami, Y., & Shiraishi, N. (1988). Rain-wind induced vibrations of cables in cable-stayed bridges. *Journal of Wind Engineering and Industrial Aerodynamics, 29*, 409-418.

Hirsch, G. (1991). Cable vibration overview. *Proceedings of the 8th International Conference on Wind Engineering* (ICWE8 - July 1991), The University of Western Ontario, London, Canada, 453-464.

Hirsch, G. (1992). Recent advances in control of wind-induced vibrations of guyed masts. *Journal of Wind Engineering and Industrial Aerodynamics, 43*(3), 2113-2123.

Hirsch, G. (1994). Cable vibration overview. *Proceedings of the International Conference on Cable-stayed and Suspension Bridges (AFPC)*, Deauville, France, Vol. 2, 453-464.

Hjorth-Hansen, E., Strømmen, E., Myrvoll, F., Hansvold, C., & Ronnebrant, R. (2001). Performance of a friction damping device for the cables on Uddevalla cable-stayed bridge. *Proceedings of 4th International Symposium on Cable Dynamics*, A.I.M, Liège, Belgium, 179-186.

Irvine, H. M. (1981). Cable structures. Dover Publications, 94-97.

Irwin, P. A. (1997). Wind vibrations of cables on cable-stayed bridges. *Proceedings of Structural Congress XV*, Portland, Oregon, 383-387.

Irwin, P. A., Nedim, A., & Telang, N., (1999). Wind induced stay cable vibrations -A case study. *Proceedings of 3rd International Symposium on Cable Aerodynamics*, Trondheim, 1999, 171- 176.

Irwin, P. A., Lankin, J. B., & Garber, J., (2002). Wind tunnel investigation of inclined stay-cable galloping. *Proceedings of the 2002 ASCE Structures Congress*, Denver, Colorado.

Iwan, W. D., & Jones, N. P. (1984). NATFREQ Users Manual – a Fortran IV program for computing the natural frequencies, mode shapes, and drag coefficients for taut strumming cables with attached masses and spring-mass combinations. Naval Civil Engineering Laboratory Report Number CR 94.026.

Johnson, E. A., Spencer, B. F., Jr., & Fujino, Y. (1999). Semiactive damping of stay cables: a preliminary study. *Proceedings 17th International Modal Analysis Conference*, Society for Experimental Mechanics, Inc., Bethel, Connecticut, 417-423.

Jones, N. P., & Main, J. A. (2002). Evaluation of mitigation strategies for stay-cable vibration. *Proceedings of the 2002 ASCE Structures Congress*, Denver, Colorado.

Kobayashi, H., Minami, Y., & Miki, M. (1995). Prevention of rain-wind induced vibration of an inclined cable by surface processing. *Proceedings of the 9th International Conference on Wind Engineering*, New Delhi, India, 753- 758.

Kovacs, I. (1982). Zur frage der seilschwingungen und der seildämpfung. *Die Bautechnik, 10*, 325-332 (in German).

Kovacs, I., Strømmen, E., & Hjorth-Hansen, E. (1999). Damping devices against cable oscillations on Sunningesund Bridge. *Proceedings of 3rd International Symposium on Cable Dynamics*, A.I.M, Liège, Belgium, 145-150.

Krenk, S. (2000). Vibrations of a taut cable with an external damper. *Journal of Applied Mechanics, 67*, 772-776.

Kumarasena, T. (1999). Design considerations for new bridges. *HNTB Presentation at Workshop of Rain/Wind Vibrations in Cable-Stayed Bridges*, Atlanta, Georgia.

Langso, H., & Larsen, O. (1987). Generating mechanisms for cable-stay oscillations at the Faro Bridge. *Proceedings of the International Conference on Cable-stayed Bridges*, Bangkok, 1023-1033.

Larose, G. L., & Smitt, L. W. (1999). Rain/wind induced vibrations of the parallel stay cables for the Oresund High Bridge. *Proceedings of the 1999 IABSE Conference*, Malmo, Sweden.

Larose, G. L., & Zan, S. J. (2001). The aerodynamic forces on the stay cables of cable-stayed bridges in the critical Reynolds number range. *Proceedings of 4th International Symposium on Cable Aerodynamics*, Montreal, Canada.

Leblond, A. & Hardy, C. (1999). On the estimation of a (J ~ 45°) complex matrix of symmetric Stockbridge-type dampers. *Proceeding of the 3rd International Symposium on Cable Dynamics*, Trondheim, 139-144.

Lilien, J. L. (1997). Galloping of overhead electrical lines, mechanisms, wind tunnel experiments -field measurements. *Proceeding of the 2nd International Seminar on Cable Dynamics*, Tokyo, 37-48.

Main, J. A., & Jones, N. P. (1999). Full-scale measurements of stay cable vibration. *Proceedings of the 10th International Conference on Wind Engineering*, Balkema, Rotterdam, Netherlands, 963-970.

Main, J. A., & Jones, N. P. (2000). A comparison of full-scale measurements of stay cable vibration. *Proceedings of Structures Congress 2000, ASCE*.

Main, J. A., & Jones, N. P. (2001). Stay-cable vibration in cable-stayed bridges: Characterization from full-scale measurements and mitigating strategies. *Journal of Bridge Engineering. ASCE, 6*(6), 375-387.

Main, J. A., & Jones N. P. (2002a). Free Vibrations of a Taut Cable with Attached Damper. I: Linear Viscous Damper. *Journal of Engineering Mechanics, ASCE, 128*(10), 1062-1071.

Main, J. A., & Jones N. P. (2002b) "Free Vibrations of a Taut Cable with Attached Damper. II: Nonlinear Damper." Journal of Engineering Mechanics, ASCE, 128(10), 1072-1081.

Matsumoto, M., Shiraishi, N., & Shirato, H. (1989). Inclined-cable aerodynamics: Structural design, analysis & testing proceedings. *Proceedings of the ASCE Structures Congress*, San Francisco.

Matsumoto, M., Shiraishi, N., Kitazawa, M., Knisely, C., Shirato, H., Kim, Y, & Tsujii, M. (1990). Aerodynamic behaviour of inclined circular cylinders-cable aerodynamics, *Journal of Wind Engineering and Industrial Aerodynamics, 33*, 63-72.

Matsumoto, M., Shirashi, N., & Shirato, H., (1992). Rain-wind induced vibration of cables of cable-stayed bridges. *Journal of Wind Engineering and Industrial Aerodynamics: Proceedings of the 8th International Conference on Wind Engineering*, London, Ontario 1991, 44.

Matsumoto, M., Shirato, H., Saitoh, T., Kitazawa, M., & Nishizaki, T. (1993). Response characteristics of rain-wind induced vibration of stay-cables of cable-stayed bridges. *Wind Engineering: 1st European and African Regional Conference (IAWE)*, Cook, N .J. (ed.), 411- 420.

Matsumoto, M., Daito, Y., Kanamura, T., Shigemura, Y, Sakuma, S, & Ishizaki, H., (1997). Wind-induced vibration of cables of cable-stayed bridges. *Proceedings of 2 EACWE,* Genova, Italy, 1791-1798.

Matsumoto, M. (1998). Observed behaviour of prototype cable vibration and its generation mechanism. *Bridge Aerodynamics*, Larsen & Esdahl (eds), Balkema, Rotterdam, 189-211.

Meirovitch, L. (1970). *Methods of analytical dynamics*. New York: McGraw-Hill.

Mesarovich S., & Gasparini, G. A. (1990). Dynamic behavior of nonlinear cable system (I and II). *Journal of Engineering Mechanics ASCE 118*(5), 890-920.

Miyasaka, Y., Ohshima, K., & Nakabayashi, S. (1987). Experimental study on Ajikawa Bridge cable vibration. Hanshin Express-way Public Corp. Eng. Report No.7.

Miyata, T., & Yamada, H., (1995). On aerodynamically stable PE stay cables with decreased drag force by introduction of newly developed lumped surface roughness. *Proceedings of Symposium on Cable Dynamics*, Liege, Belgium, Oct. 1995.

Miyata, T., Yamada, H. & Hojo, T. (1994). Aerodynamic response of PE stay cables with pattern-indented surface. *Proceedings of the International Conference on Cable-stayed and Suspension Bridges (AFPC)*, Deauville, France, 2, 515-522.

Novak, M., & Tanaka, H. (1974). Effect of turbulence on galloping instability. *Journal of Engineering Mechanics, ASCE*, (100) EM1, February, 27-47.

Novak, M., Davenport, A.G., & Tanaka, H. (1978). Vibrations of towers due to galloping of iced guy cables. *Journal of Engineering Mechanics, ASCE*, (104) EM2, April, 457- 473.

Ohashi, M. (1991). Cables for cable-stayed bridges. *Cable-stayed Bridges: Recent development and Their Future*, Ito, M. et al. (eds), 125-150.

Ohshima, K., & Nanjo, M. (1987). Aerodynamic stability of the cables of a cable-stayed bridge subject to rain (A case study of the Aji River Bridge*). Proceedings of the US-Japan Joint Seminar on Natural Resources*.

Ozkan, E., Main, J. A., & Jones, N. P. (2001). Full-scale measurements on the Fred Hartman Bridge. *Proceedings of the Asia-Pacific Conference of Wind Engineering*, October 2001, Kyoto University, Japan.

Ozkan, E., Main, J. A., & Jones, N. P. (2001). Long-term measurements on a cable-stayed bridge. *Proceedings of the IMAC-XIX Conference*, February 2001, Orlando, FL.

Ozkan, E., Main, J. A. & Jones, N. P. (2001). Investigation of cable-deck interaction using full-scale measurements on a cable-stayed bridge. *Proceedings of the 1st Americas Conference on Wind Engineering 2001 – American Association for Wind Engineering (AAWE)*, Clemson University, SC.

Pacheco, B. M., Fujino, Y., & Sulekh, A. (1993). Estimation curve for modal damping in stay cables with viscous damper. *Journal of Structural Engineering, ASCE, 119*(6), 1961-1979.

Poston, R. W. (1998). Cable-stay conundrum. *Civil Engineering, ASCE, 68*(8), 58-61.

Pinto da Costa, A., Martins, J. A. C., Branco, F., & Lillen, J. L. (1996). Oscillations of bridge stay cables induced by periodic motions of deck and/or towers. *Journal of Engineering Mechanics, 122*(7), 603-612.

PTI Guide Specification (2001). Recommendations for stay cable design, testing and installation. Post-Tensioning Institute Committee on Cable-Stayed Bridges, 4th ed.

Rayleigh, J. W. S. (1877). *The Theory of Sound – Volume I.* Dover Publications, Inc., New York, NY, (1945 reprint).

Ruscheweyh, H., & Hirsch, G. (1974). Vibration measurements at the cable stayed Koehlbrand Bridge in Hamburg. Technical Report, Institute for Lightweight Structures, RWTH Aachen (in German).

Ruscheweyh, H., & Verwiebe, C. (1995). Rain-wind-induced vibrations of steel bars. *Proceedings of the International Symposium on Cable Dynamics*, Liege, Belgium, 469-472.

Ruscheweyh, H. (1999). The mechanism of rain-wind-induced vibration. *Wind Engineering into the 21st Century,* Larsen, Larose & Livesey (eds), Balkema, Rotterdam, 1041-1047.

Saito, T., Matsumoto, M., & Kitazawa, M. (1994). Rain-wind excitation of cables on cable-stayed Higashi-Kobe Bridge and cable vibration control. *Proceedings of the International Conference on Cable-stayed and Suspension Bridges (AFPC)*, Deauville, France, 2, 507-514.

Scruton, C. (1981). An introduction to wind effects on structures. Published for the Design Council, British Standards Institution and Council of Engineering Institutions.

Sergev, S. S. & Iwan, W. D. (1981). The natural frequencies and mode shapes of cables with attached masses. *Journal of Energy Resources Technology, 103*(3), 237-242.

Simiu, E. & Scanlan, R. H. (1996) *Wind effects on structures, 3rd edition*. Wiley Interscience.

Stiemer, S. F., Taylor, P., & Vincent, D. H. C. (1988). Full-scale dynamic testing of the Annacis Bridge. *I.A.B.S.E. Proceedings P-122*.

Strouhal,V. (1898). Uber eine besondere Art der Tonerregung. *Annl. Phys., Vol. 5*.

Stubler, J., Ladret, P. , Domage, J. B. & Peltier, M. (1999). An introduction to wind effects on structures. Pub1ished for the Design Council, British Standards Institution and Council of Engineering Institutions.

Tabatabai, H. & Mehrabi, A. B. (2000). Design of mechanical viscous dampers for stay cables. *Journal of Bridge Engineering, ASCE, 5*(2), 114-123.

Verwiebe, C., & Ruscheweyh, H. (1997). Recent research results concerning the exciting mechanisms of rain-wind induced vibrations. *Proceedings of the 2 EACWE,* Genova, Italy, 1783-1789.

Verwiebe, C., & Ruscheweyh, H. (1998). Bridge stay cable vibration: Phenomena, criteria and damper technology. *Proceedings of the 3rd International Symposium on Cable Dynamics*, Troudheim, 163-170.

Virlogeux, M. (1998). Cable vibrations in cable-stayed bridges. *Bridge Aerodynamics*, Larsen & Esdahl (eds), Balkema, Rotterdam, 213-233.

Wardlaw, R. L., Cooper, K. R. & Scanlan, R. H. (1973). Observations on the problem of subspan oscillation of bundled power conductors. DME/NAE Quarterly Bulletin No.(1).

Whitlock, Dalrymple, Poston & Associates, Inc. (1998). Evaluation and Repair of stay-cable vibrations of Fred Hartman Bridge and Veterans Memorial Bridge, Report 1, January 8, 1998, Texas Department of Transportation.

Wianecki, J. (1979). Cables wind excited vibrations of cable-stayed bridges. *Proceedings of the 5th International Conference of Wind Engineering*, Colorado, 1381-1393.

Xu, Y. L., Ko, J. M., & Yu, Z. (1997). Modal damping estimation of cable-damper systems. *Proceedings of 2nd International Symposium on Structures and Foundations in Civil Engineering*, China Translation and Printing Services Ltd., Hong Kong, China, 96-102.

Yamada, H. (1997). Control of wind-induced cable vibrations from a viewpoint of the wind resistance design of cable-stayed bridges. *Proceedings of the 2nd International Seminar on Cable Dynamics*, Tokyo, 129-138.

Yamaguchi, H. & Fujino, Y. (1998). Stayed cable dynamics and its vibration control. *Proceedings International Symposium on Advances in Bridge Aerodynamics*, Balkema, Rotterdam, Netherlands, 235-253.

Yamaguchi, H., & Jayawardena, L. (1992). Analytical estimation of structural damping in cable structures. *Journal of Wind Engineering and Industrial Aerodynamics,* 41-44, 1961-1972.

Yamaguchi, H., & Nagahawatta, H. D. (1995). Damping effects of cable cross ties in cable-stayed bridges. *Journal of Wind Engineering and Industrial Aerodynamics*, 54/55, 35-43.

Yoneda, M. & Maeda, K. (1989). A study on practical estimation method for structural damping of stay cable with damper. *Proceedings of Canada-Japan Workshop on Bridge Aerodynamics*, Ottawa, Canada, 119-128.

Yoshimura, T., Inoue, A., Kaji, K. & Savage, M. G. (1989). A study on the aerodynamic stability of the Aratsu Bridge. *Proceedings of Japan-Canada Joint Workshop on Bridge Aerodynamics,* 41-50.

Yoshimura, T., Savage, M., & Tanaka, H. (1995). Wind-induced vibrations of bridge stay-cables. *Proceedings of the International Symposium on Cable Dynamics*, Liege, Belgium, 437-444.

Zingoni, A. (1996). An efficient computation scheme for the vibration analysis of high tension cable nets. *Journal of Sound and Vibration, 189*(1), 55-79.

Zui, H., Shinke, T., & Namita, Y. (1996). Practical formulas for estimation of cable tension by vibration method. *Journal of Structural Engineering*, June 1996, 651-656.